Sensitivity of the retrosplenial cortex to distal damage in a network associated with spatial memory:

Evidence from lesion and gene expression studies in the rat.

GUILLAUME POIRIER

Thesis submitted to Cardiff University

For the Degree of Doctor of Philosophy

September 2006

ProQuest LLC
789 East Eisenhower Parkway
P.O. Box 1346
Ann Arbor, MI 48106-1346

Sensitivity of the retrosplenial cortex to distal damage in a network associated with spatial memory:

Evidence from lesion and gene expression studies in the rat.

Table of contents

Acknowledgments

I would like to thank my supervisor, John Aggleton, a wonderful mentor, for taking a chance on me. I am grateful that you made me part of your research group and for the lengths you have gone to help me along the way.

Very special thanks go to Laura Peronace, without whom I probably would not have made it in one piece. I am grateful for your understanding, especially when the research came first.

I would also like to express my gratitude to Dave Mumby, who set the ball in motion. I wish to thank Melissa Glenn for teaching me the basics, and to Trisha Jenkins for the work that laid the foundations for my thesis. Numerous people have provided invaluable assistance towards the completion of this thesis and related work, and Dave Carter, Kerrie Thomas, Jon Erichsen, Leslie-Anne Strabel, Matthew Mundy, Anthony McGregor, Peter Jones, Jeff Lewis, and Val Pearce deserve particular mention. Eman Amin deserves credit for never being daunted by the crazy schemes and mountains of work I created. I particularly wish to thank Kate Shires, for constant support during the course of this thesis, and other friends and colleagues who made me enjoy life in and out of the lab. Alex Johnson and Steve Chambers, amongst others, certainly deserve a few pints for their antics, as does Rachel Kyd for introducing me to surf in the Gower. The encouragement and reassurances provided by Elsa Pioli and Helen Pothuizen were well appreciated in the last stretch. The humour and enthusiasm of Mathieu Albasser, contrary to what he may think, have been great in helping me stay focused.

Finally, I wish to acknowledge the guidance of my family who has demonstrated the value of hard work. Most of all, I would like to acknowledge the unrelenting support of my parents, Carole Marcoux and Michel Poirier, who have always believed in me and encouraged me to reach for my dreams.

Summary

This thesis explores the influence of brain regions in the extended hippocampal system on the activity of the retrosplenial cortex in the rat. The primary motivation of the experiments presented in this thesis is to improve the understanding of the vulnerability of the retrosplenial cortex, especially in the context of diencephalic amnesia and Alzheimer's disease.

Using molecular imaging, it is shown that discernible networks of brain regions are active even at different training levels of the same spatial memory task, not just between different tasks. I provide evidence that multiple brain regions exhibit a relationship with memory. Importantly, these regions display associations with different memory components, which change according to the experience and the performance level of the subjects.

The lesion studies provide information about the vulnerability of granular b retrosplenial cortex to distal damage in certain regions. The pattern of the terminations of the projections from each region to the retrosplenial cortex does not appear to be predictive of the impact that damage to each will have on immediate-early gene activity in the latter. In addition to the anterior thalamic nuclei, the retrosplenial cortex is vulnerable to damage in the entorhinal cortex and in the hippocampus, but not in the laterodorsal thalamic nucleus. I show that retrosplenial cortex dysfunction can occur as early as one week after anterior thalamic nuclei lesions. Evidence is also shown to suggest that both granular and dysgranular subregions of the retrosplenial cortex are affected as a result of anterior thalamic nuclei lesions.

Finally, the presence of hormonal alterations in dysfunctional retrosplenial cortex tissue and evidence from a microarray analysis suggest that this region exhibits widespread alterations in cellular function after anterior thalamic nuclei lesions. The effects presented and the mechanisms that are proposed contribute to our understanding of the vulnerability of the retrosplenial cortex to neurological insults.

Publications

Poirier G., Thomas K.L., Mundy M.E., McGregor A. Jones P.M., & Aggleton J.P. (2006). Retrosplenial cortex immediate-early gene reactivity after lesions to its afferents: Selective vulnerability to distal damage. Abstract. Federation of European Neuroscience Societies, Vienna.

Poirier G., Albasser M., & Aggleton J.P. (2006). Immediate-early gene hypoactivity in the rat retrosplenial cortex after different lesions: An evaluation of the retrosplenial vulnerability to afferent damage. Abstract. Molecular and Cellular Cognition Society, Vienna.

Albasser M., Warburton E.C., Poirier G., & Aggleton J.P. (2006). Hippocampal lesions in rats markedly reduce retrosplenial cortex activity as measured by c-Fos gene expression. Abstract. Federation of European Neuroscience Societies, Vienna.

Poirier G. & Aggleton J.P. (2005). The retrosplenial cortex and immediate-early gene reactivity following deafferentation in the rat. Abstract. Experimental Psychology Society, London.

Poirier, G., Bloom, Z., & Aggleton, J.P. (2005). Temporal characterization of the effect of anterior thalamic nuclei lesions on immediate-early gene activation in retrosplenial cortex in the rat. Abstract. European Brain & Behaviour Society, Dublin.

Poirier G, Shires KL, Carter DA, & Aggleton JP. (2004). Transcriptome analysis of granular retrosplenial tissue following anterior thalamic excitotoxic lesions in the rat reveal a distal effect. Abstract. Soc Neurosci, San Diego.

Poirier G, Jenkins TA., Amin E, & Aggleton JP. (2003). Comparison of the concurrent expression of Fos and Zif268 proteins in temporal lobe of the rat: Effective connectivity and spatial learning during the performance of two different tasks in a radial arm maze. Abstract. 6th IBRO Congress of Neuroscience, Prague.

Abbreviations

Neuroanatomy

AD	anterodorsal nucleus
AM	anteromedial nucleus
AP	antero-posterior
ATN	anterior thalamic nuclei
AV	anteroventral nucleus
DG	dentate gyrus
DV	dorso-ventral
HIP	hippocampus
LD	lateral dorsal nucleus
lENT	lateral entorhinal cortex
mENT	medial entorhinal cortex
ML	medio-lateral
MTL	medial temporal lobe
PeRh	perirhinal cortex
PoRh	postrhinal cortex
Rdg	retrosplenial cortex, dysgranular subregion
Rgb	retrosplenial cortex, granular b subregion
rRSP	rostral retrosplenial cortex

Genes

Adcyap1	Adenylate cyclase activating polypeptide 1
Adrb3	adrenergic receptor beta 3
Adrbk1	adrenergic receptor kinase, beta 1
AP-1	activating protein 1
BDNF	brain-derived neurotrophic factor
Chgb	chromogranin B
COX1	cyclooxygenase 1
CRE	calcium cyclic AMP response element
CREB	calcium cyclic AMP response element binding protein
EST	expressed sequence tag
Fra1	Fos related antigen 1
Fra2	Fos related antigen 2
GFR	growth factor receptors
Git1	G protein-coupled receptor kinase-interactor 1
Hsd11b1	Hydroxysteroid dehydrogenase 11 beta type 1
IEG	immediate early gene
Klf5	kruppel-like factor 5
KMO	kynurenine 3-monooxygenase
MAPK	mitogen-activated protein kinase
NTR	neurotransmitter receptors
PKA	protein kinase A
RXRγ	retinoic X-receptor gamma
SRE	serum-responsive element
VIP	vasoactive intestinal peptide
VSCC	voltage-sensitive calcium channel

Pharmacology and chemistry

AMPA	alpha-amino-3-hydroxy-5-methyl-4-isoxazolepropionic acid
DAB	diaminobenzidine
DEPC	Diethylpyrocarbonate
GABA	gamma-aminobutyric acid
LTD	long term depression
LTP	long term potentiation
NMDA	*N*-methyl-D-aspartic acid
PBS	phosphate buffered saline
PBST	PBS with 0.2% Triton-X
PFA	paraformadehyde

Others

ANOVA	analysis of variance
CFI	comparative fit index
GFI	goodness of fit index
EEG	electroencephalogram
fMRI	functional magnetic resonance imaging
MCI	mild cognitive impairment
MLE	maximum likelihood Estimation
p	statistical probability
PET	positron emission tomography
r	Pearson product-moment correlation coefficient
R^2	squared multiple correlation
RAM	radial arm maze
RMSEA	root mean square error of approximation
SEM	structural equation modelling
TLI	Tucker-Lewis coefficient
ULS	Unweighted Least Squares
χ^2	chi squared

Chapter 1

General introduction

1.1: Overview

In this thesis, I will describe the use of a particular form of molecular functional imaging. I propose that the use of this approach will refine our understanding of a particular brain region, the retrosplenial cortex, both in the normal brain and in pathological conditions. It is currently known that the retrosplenial cortex is involved in spatial memory abilities in rodents, and in a wider array of episodic-type memory abilities in humans. One goal will be to investigate retrosplenial cortex activity within an interconnected network of regions. As a first step, I will examine the reactivity of the rat retrosplenial cortex during the acquisition of a spatial memory task using a non-invasive, molecular imaging approach. Following this investigation into the role of the retrosplenial cortex in spatial memory, I will seek to delineate further the sensitivity of this region to the loss of its afferents. There are numerous reasons to suppose that the retrosplenial cortex is unusually sensitive to brain insults, and that this sensitivity might contribute to neurological conditions. The goal will be to characterise the full breadth of molecular changes within the retrosplenial cortex following a distal lesion. Using molecular imaging, I will next examine the development of the retrosplenial dysfunction over time as a result of distal damage. I will then verify the selectivity of the retrosplenial vulnerability by testing the effects of damage in a number of afferents to the retrosplenial cortex. Finally, I will interpret these findings in light of the role of the retrosplenial cortex in spatial memory abilities and in clinical disorders involving cognitive dysfunction and memory deficits.

1.2: The need for a network analysis of brain structures supporting memory

A better understanding of the mechanisms necessary for successful learning and memory is a widely sought goal, one that has the potential to improve the fate of those afflicted with debilitating deficits in these cognitive domains. Great strides have been made in the characterisation of the role of specific brain regions in memory functions. One of the regions of the brain that has stimulated enormous energies in research over the last several decades is the medial temporal lobe. Since the report of Scoville and Milner now almost fifty years ago (1957), studies on other patients and on animal models has promoted the widely accepted belief that damage to the medial temporal lobe (MTL) can cause permanent memory impairments in humans and other mammals. This has led to the influential notion that a group of closely connected MTL structures form a memory system that is critical for declarative memory (Squire and Zola-Morgan,

1991). These structures comprise the hippocampal formation and adjacent cortex, including the entorhinal cortex, the perirhinal cortex, and the parahippocampal cortex (homologous to the postrhinal cortex in the rat).

The majority of the memory models that have been developed (e.g. Teyler and DiScenna, 1985; Damasio, 1989; Squire and Zola-Morgan, 1991; McClelland and Goddard, 1996; Murre, 1996; Nadel and Moscovitch, 1997) have concentrated on the various mnemonic abilities of the structures within this part of the brain. The role of individual components within this system has been debated, but most have agreed on the primary importance of the hippocampus. Attention has generally been focused on the hippocampus and other regions of the medial temporal lobe, without the integration of other regions other than in references to neocortical areas as the resting place of memory traces. The focus on the medial temporal lobe has persisted in spite of considerable evidence of the importance for memory of various other brain regions, including neocortical and diencephalic regions (Horel, 1978; Gaffan, 1994, 2001; Simons and Spiers, 2003).

In contrast to models such as the "medial temporal memory system" proposed by Squire and Zola-Morgan (1991), an alternative view emphasises the notion of functional diversity within the medial temporal lobe, in conjunction with the contribution of additional brain areas (e.g. Tulving and Markowitsch, 1997). Aggleton and Brown (1999), proponents of such a view, suggested the incorporation into an extended system of a number of brain regions beyond the medial temporal lobe. There are a number of key differences between the models of Squire and Zola-Morgan (1991) and of Aggleton and Brown (1999), and one of these is the inclusion by the latter of specific diencephalic and additional neocortical structures into this extended hippocampal memory system.

In order to evaluate and characterise further the neural substrates of memory, it could prove of great value to be able to visualise the activity of multiple regions as induced by a certain learning task. Such information could, for example, have a direct bearing on the debate over the extent of the medial temporal lobe memory system. As a complement to the traditional lesion approach or more recent inactivation approaches, such an imaging technique could help immensely in the direct investigation of the existence of the networks or specific brain structures involved in the performance of tasks requiring learning and memory. The obvious candidate technique for this type of

approach is high field imaging. High field imaging techniques such as positron emission tomography, functional magnetic resonance imaging and their derivatives use information about metabolism and blood circulation to make inferences about brain activity. These techniques have provided astounding insights into the dynamic workings of the brain. The spatial resolution of these techniques, however, remains limited to the regional level. An alternative approach is to use the knowledge of cellular mechanisms associated with learning and memory to provide imaging techniques that enable the visualisation of relevant activity at the cellular level. The use of such a technique could provide the opportunity to identify brain networks brought into play by specific behavioural tasks in conjunction with the visualisation of a cellular plasticity signal. The use of a marker of plasticity enables the localisation of areas and cells that are active and putatively exhibiting plasticity changes in reaction to the performance of a behaviour. This is an advantage over conventional high field imaging techniques that can only permit the visualisation of areas of tissue that are simply metabolically active during a task, without providing information about the potential plasticity changes that may underlie different brain responses induced by behavioural learning. One such approach, consisting of immediate-early gene imaging, affords a very high spatial resolution visualisation of putative plasticity. While this approach is inherently limited in its temporal resolution, its advantages on other dimensions make it an invaluable technique. The immediate-early gene imaging approach will be presented below.

1.3: Immediate-early gene mapping

1.3.1: Cellular mechanisms and the immediate-early genes

One of the fundamental questions in neuroscience is the nature of the neural substrate of memory. Major advances are made continuously to answer this question. Learning and memory, as observed at the behavioural level, is the result of changes at the molecular level. As shown in Figure 1.1, it is believed that memory storage requires brain structural changes that are reliant upon protein synthesis to subserve these long-term modifications for long term memory (Davis and Squire, 1984; Matthies, 1989; Bailey and Kandel, 1993). While protein synthesis is necessary for long-term memory, it may not be required for short-term memory (e.g. Mizumori et al., 1985; Meiri and Rosenblum, 1998).

The early reports of protein synthesis-dependent memory processes led to the examination of the mechanisms leading to this protein synthesis, such as gene transcription and translation, as well as the identification of candidate genes. Long term changes are made possible by alterations in gene expression in order to permit, guide, prepare and maintain functional and structural alterations (Goelet et al., 1986) or neurotransmitter plasticity (Black et al., 1987). For this to occur, environmental stimuli and depolarization are assumed to be transduced by gene expression into longer lasting events.

Short-term memory is thought by many to rely on modifications of existing proteins, whereas long-term memory necessitates the synthesis of new proteins, and thus is dependent on gene expression (Goelet et al., 1986). Protein synthesis results from the transcription and the subsequent translation of mRNA. The transcription of mRNA itself is induced by the convergence of a multitude of stimuli, with a requirement for protein synthesis. Thus, studies looking into the molecular basis of long-term memory have often focused on the pathways that control the transcription of mRNA.

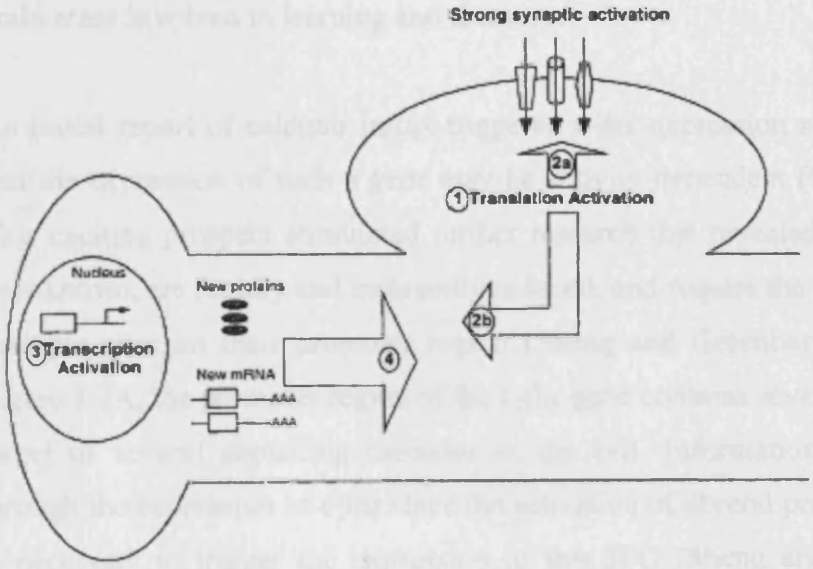

Figure 1.1: Synaptic activity-dependent gene transcription

1) Activation of synapse leads to translation of pre-existing mRNA;

2) Protein synthesis can affect synaptic activity (a) and lead signalling to the nucleus that will generate gene expression (b);

3) Newly produced mRNA and proteins are transferred to the synapse;

4) Modification or stabilisation of synaptic response.

(taken from Wells and Fallon, 2000).

Immediate-early genes (IEGs) are those genes that are first expressed following cell stimulation, their induction requiring no prior protein synthesis (Tischmeyer and Grimm, 1999). There are in fact numerous reasons why it is of interest to examine the expression of these particular genes and their role in memory processes. IEGs exhibit regulatory properties that make them suitable candidates for mechanisms underlying learning processes. Whilst their swift expression distinguishes them from other proteins, IEGs themselves can be grouped into different, orthogonal categories based on their expression and the type of function they subserve. The distinction can be made between constitutive and inducible IEGs. Inducible IEGs exhibit low baseline levels and an activity-dependent induction that is dependent on the pre-existence of constitutive IEGs present in quiescent cells (Herdegen and Leah, 1998). Additionally, IEGs can be divided into transcription factors and effector proteins. The former, as their name implies, by returning to the nucleus will modulate the transcription of other genes. In contrast, effector proteins will directly produce changes in the cell. One of the first and now most widely studied IEGs is c-*fos*, an inducible transcription factor. We will now focus mostly on this IEG as it will be used as a marker in all of our studies. The next section will underline why c-*fos* is a logical candidate to use for the visualisation of brain areas involved in learning and memory.

An initial report of calcium influx-triggered c-*fos* expression suggested to the authors that the expression of such a gene may be activity-dependent (Greenberg et al., 1986). This exciting prospect stimulated further research that revealed that IEGs, as they are now known, are rapidly and transiently induced, and require the concurrent activation of multiple sites on their promoter region (Sheng and Greenberg, 1990). As shown in Figure 1.2A, the promoter region of the c-*fos* gene contains several elements that are the target of several signalling cascades in the cell. Information integration can occur through the expression of c-*fos* since the activation of several promoter elements at once is necessary to trigger the expression of this IEG (Sheng and Greenberg, 1990), as depicted in Figure 1.2B. The c-*fos* protein product is a transcription factor that forms part of the AP-1 DNA binding complex that dictates the expression of target genes (see Figure 1.2B). The convergence of signals upon its promoter region in combination with its ability to regulate other genes suggests a role of the c-*fos* gene in transducing extra- and intracellular signals into long-term responses (Sheng and Greenberg, 1990; Morgan and Curran, 1991).

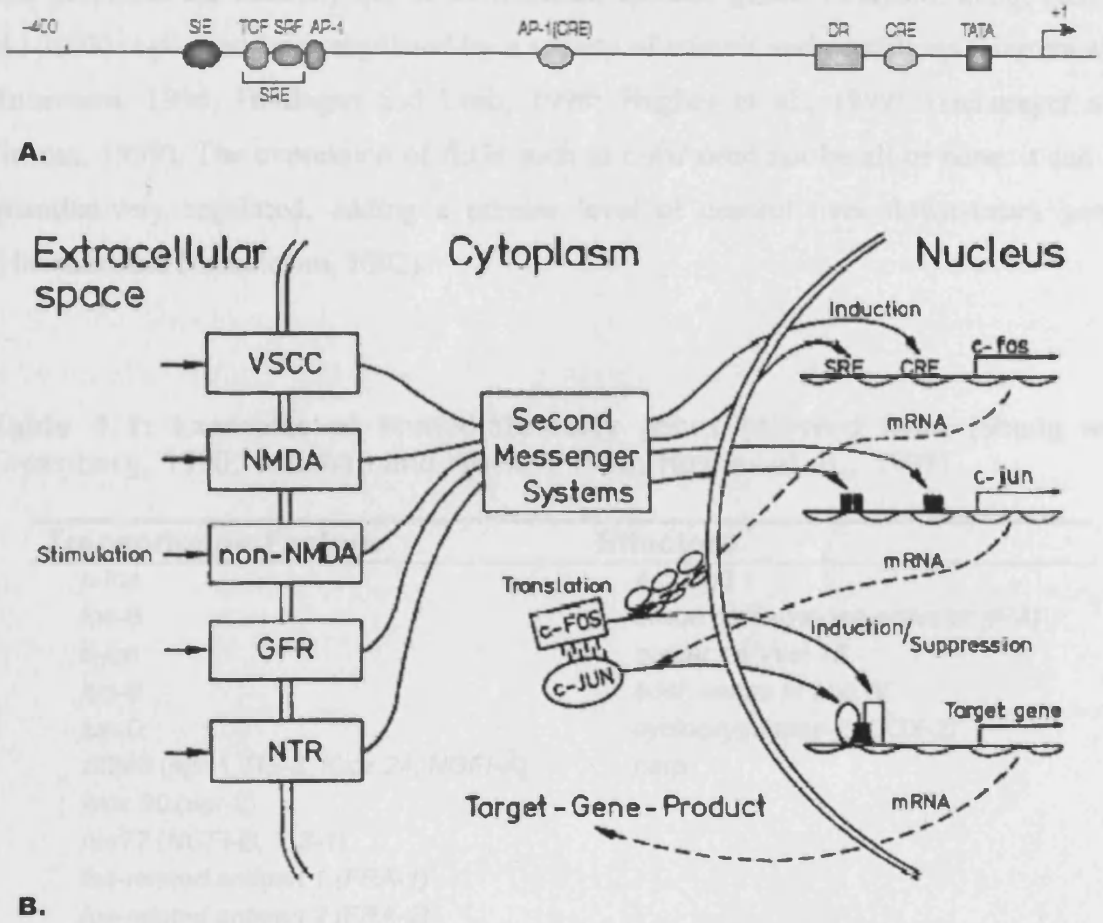

Figure 1.2: The c-*fos* gene is the target of many cellular cascades.
A) Some of the binding elements on the promoter region of the c-*fos* gene. These are the target of different second messenger systems (taken from Hazzalin and Mahadevan, 2002). B) Signal-transcription coupling: Stimulus integration by the c-*fos* promoter results in effector protein activation (taken from Gass and Herdegen, 1995).

The rapid and transient induction of IEGs during early acquisition of a task has suggested that they are plausible candidates for a role in the processes leading from short-term to long-term memory. IEGs, however, can be portrayed as being on standby; their induction being protein neosynthesis independent, it is thus very rapid. Lanahan and Worley (1998) have estimated that 30 to 40 genes are neuronal IEGs, and of those, 10 to 15 are regulatory genes, the rest being effector genes (cf. examples in Table 1). c-*fos* is one of the IEGs the activity of which was proposed to result in increased efficacy of synaptic response to subsequent stimuli (Morgan and Curran, 1991). It is now known that the rapid induction of IEGs following cell stimulation regulates neuroplastic processes by starting or even stopping gene transcription in order, for example, to

modulate synaptic support directly via effector IEGs or indirectly, via regulatory genes that modulate the transcription of downstream effector genes. (Clayton, 2000; Fass et al., 2003). c-*fos* can be upregulated by a variety of stimuli and conditions (Herrera and Robertson, 1996; Herdegen and Leah, 1998; Hughes et al., 1999; Tischmeyer and Grimm, 1999). The expression of IEGs such as c-*fos* need not be all or none, it can be quantitatively regulated, adding a precise level of control over downstream genes (Hazzalin and Mahadevan, 2002).

Table 1.1: Examples of immediate-early genes (derived from (Sheng and Greenberg, 1990; Lanahan and Worley, 1998; Hughes et al., 1999).

Transcription Factors	Effectors
c-*fos*	*arc/arg3.1*
fos-B	*tissue plasminogen activator (tPA)*
c-*jun*	*homer 1a/Vesl 1S*
jun-B	*bdnf, exons III and IV*
jun-D	*cyclooxygenase-2 (COX-2)*
zif268 (egr-1,TIS-8, Krox 24, NGFI-A)	*narp*
krox 20 (egr-2)	
nur77 (NGFI-B, TIS-1)	
fos-related antigen 1 (FRA-1)	
fos-related antigen 2 (FRA-2)	

1.3.2: c-fos expression and pattern of stimulation

The activity of the IEG c-*fos* need not be equated with metabolic activity, and thus cellular activity. While there can be an overall correspondence of local cerebral glucose utilisation and of c-*fos* activity, there are also several instances where discrepancies occur between c-*fos* and metabolic activation or expression of other IEGs (Morgan and Curran, 1991; White and Price, 1993; Clayton, 2000; Hoffman and Lyo, 2002). It must be emphasised that it is not depolarisation or metabolic activity *per se*, but rather signalling changes that induce c-*fos* (Clayton, 2000; Hoffman and Lyo, 2002). This is an important point that augments the value of this IEG for mapping purposes. This realisation suggests that it is cells that are changing their activity—cells that are undergoing change—that can be identified by visualising c-*fos* expression, not cells that are merely *active*.

Electrical stimulation results in the expression of certain transcription factors, without inducing a generalized enhancement of gene expression (Pazmany et al., 1995). c-*fos* mRNA expression is induced by a single electrical pulse in cell culture (Pazmany et al., 1995). The type of depolarisation has implications for the extent of c-*fos* expression. Phasic and chronic stimulation induce gene expression via distinct signalling cascades—different types of calcium channels and different kinases (Brosenitsch and Katz, 2001). Thus, it is not surprising that different stimulation patterns preferentially trigger c-*fos* expression. As shown in Figure 1.3, *c-fos* induction levels have been found to be proportional not to the size of the action potential after individual stimulations but rather the stimulus frequency, and inversely correlated with inter-train interval. Furthermore, the levels of this IEG are also correlated with the net calcium increase but not the concentration or peak of calcium increase (Sheng, 1993; Chergui et al., 1996; Chergui et al., 1997; Fields et al., 1997). Therefore meaningful but not random variations in activity may elicit a c-*fos* response.

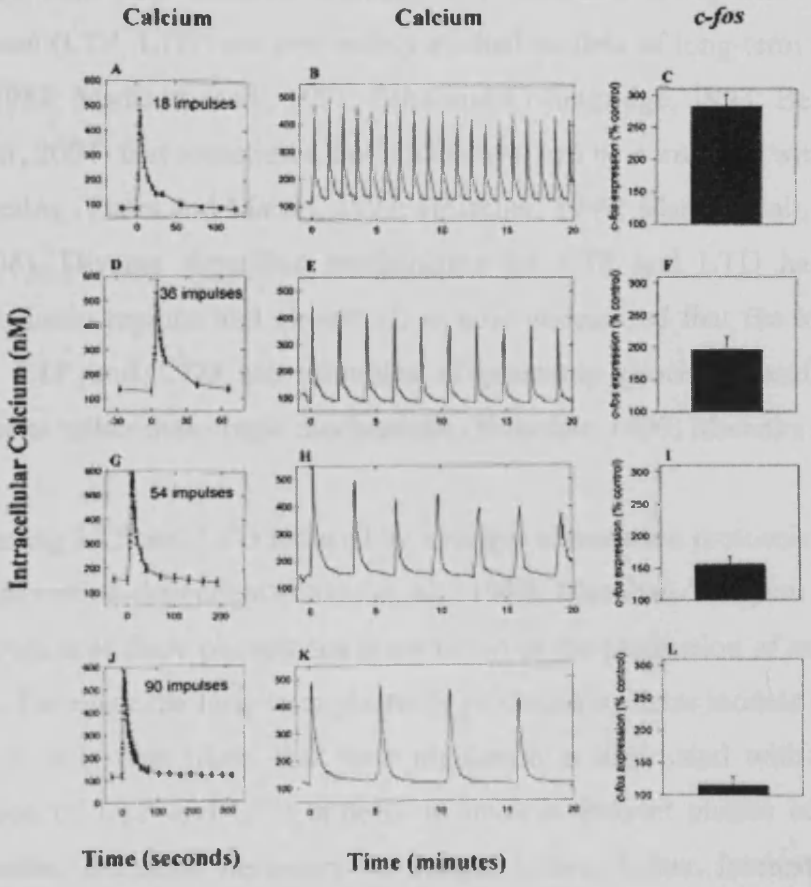

Figure 1.3: The effect on c-*fos* expression of temporal convergence of stimulation (Fields et al., 1997)

In addition to temporal convergence, spatial convergence also boosts c-*fos* induction (Miyachi et al., 2005), thus further emphasising a role for c-*fos* activity in directing plastic changes as a result of stimulus coincidence detection.

Calcium oscillations are known to be ubiquitous to cell signalling. It has been reported that these oscillations, by reducing the calcium threshold necessary to induce immediate-early gene expression, can thus increase the detection of meaningful signals even at low levels of stimulation (Dolmetsch et al., 1998). In light of this finding, it is plausible that in addition to acting as a molecular coincidence detector, the activity of c-*fos* can extract relevant signals from noise and couple this electrical activity with gene expression to produce long lasting modifications.

1.3.3: Neuroplasticity and c-fos

Artificially induced long-term plasticity is used as a model to study activity-dependent plasticity that may underlie learning and memory. Long-term potentiation and depression (LTP, LTD) are two widely studied models of long-term plasticity (Cotman et al., 1988; Madison et al., 1991; Bliss and Collingridge, 1993; Bear, 2003; Malenka and Bear, 2004) that sometimes, but not always, can be correlated with memory abilities and learning (Shors and Matzel, 1997; Hölscher, 1999; Martin et al., 2000; Whitlock et al., 2006). Diverse signalling mechanisms for LTP and LTD have been found in different brain regions and circuits. It is now understood that the long-term plasticity models LTP and LTD are examples of plasticity processes and themselves label phenomena rather than single mechanisms (Hölscher, 1999; Malenka and Bear, 2004).

Long lasting LTP and LTD induced by stronger stimulation protocols are translation but not transcription-dependent (Otani et al., 1989; Manahan-Vaughan et al., 2000). The long duration of these phenomena is anchored in the production of new proteins but not mRNA. Therefore the long-term plasticity produced by these models depends on protein synthesis. It is thus likely that their regulation is associated with IEG activity. The generation of LTP and LTD appears to involve distinct phases of induction and of stabilisation, the latter necessary for longer lasting forms. Interestingly, using these models, no relation or negative correlations have been reported between the induction of long-term plasticity and IEG activation (e.g. Schreiber et al., 1991). Some IEGs appear to play an active role in regulating the duration and stabilisation of LTP. Fos, like some other IEGs, has been found to be upregulated by stimuli that produce LTP (Nikolaev et

al., 1991; Kasahara et al., 2001). Like c-*fos*, *zif268* (also known as Egr-1, krox24, Tis8, NGFI-A) is also an IEG that is involved in regulation of genes by excitatory stimuli. Its expression pattern can be similar to that of c-*fos* (e.g. Zangenehpour and Chaudhuri, 2002). However, Zif268 but not Fos seems to display the most robust expression and correlations with the persistence of LTP and LTD (Dragunow et al., 1989; Jeffery et al., 1990; Wisden et al., 1990; Abraham et al., 1993; Demmer et al., 1993; Abraham et al., 1994; Lindecke et al., 2006).

The use of different LTP and LTD protocols, in conjunction with the apparent heterogeneity of plasticity mechanisms in different regions (Nikolaev et al., 1991), may be responsible for some inconsistencies in reports evaluating the association of Fos and LTP. Additionally, *in vitro* studies have revealed in cell culture that compared to other IEGs, c-*fos* exhibited a higher stimulation threshold for induction (Pazmany et al., 1995). In accord with these *in vitro* findings, c-*fos* may require stronger or more extensive stimulation protocols than necessary for LTP induction and for the expression of other IEGs (Worley et al., 1993; Waltereit et al., 2001). Importantly though, a c-*fos* CNS knockout has been found to display impaired LTP induction, emphasising a role for c-*fos* in neuroplasticity (Fleischmann et al., 2003).

1.3.4: c-fos, memory and behaviour

Importantly, it has been contended that the variation of c-*fos* mRNA following natural cell stimulation (e.g. with olfactory stimulation and learning as opposed to electrical stimulation) is more reliable and follows regional activity patterns more closely than various other IEGs, including *zif*268 and c-*jun* (Gall et al., 1998).

Memory processes have been revealed to be time-dependent and involve distinct cellular populations at different time points (Igaz et al., 2002). Cellular imaging using IEG labelling allows us to visualise these changes. Since the proposal that Fos could play a role in learning and memory (e.g. Robertson, 1992; Kaczmarek, 1993), the use of c-*fos* as a marker for neuronal activity has become widespread. It has been used to uncover the selective role of brain regions in multiple tasks. These include associative and non-associative paradigms, involving all sensory modalities, using such approaches as cellular imaging, or blocking and knocking out IEG expression. Although this topic has been extensively reviewed (Herrera and Robertson, 1996; Herdegen and Leah,

1998; Hughes et al., 1999; Stork and Welzl, 1999; Tischmeyer and Grimm, 1999), I will discuss those findings most relevant to the research described in this thesis.

It has repeatedly been found that novel stimulus exposure and behavioural training can induce increases in Fos expression (Tischmeyer and Grimm, 1999). For example, compared to a control group, exploration of a novel environment for 20 or 30 min elicited in the retrosplenial cortex the upregulation of c-*fos* expression (Hess et al., 1995; Nagahara and Handa, 1997; Ons et al., 2004). The retrosplenial c-*fos* expression was not significantly correlated with movement of the rat in the open field (Nagahara and Handa, 1997). In contrast to these findings, Duncan and colleagues (1996) reported no difference in retrosplenial Fos immunoreactivity when sampling the tissue under 30 min after the behaviour. This absence of significant Fos upregulation may possibly be explained by the fact that the exposure to the novel environment took place under dim lighting, but is most likely due to the short delay after the exposure. Since c-fos mRNA in general peaks 30-45 min after stimulation and protein expression follows that of mRNA, it is possible that the type of stimulus was insufficient to induce signigicant levels of Fos protein in such a quick period.

The upregulation of expression of c-*fos* triggered by novel stimuli is generally transient; it first increases, then declines with continued stimulus exposure as the novelty fades (e.g. Greenberg et al., 1986; Jeffery et al., 1990; Sharp et al., 1991). Within specific brain circuits, this effect appears to be independent of the nature and modality of the stimuli. For example, neurotransmitter receptor stimulation (Greenberg et al., 1986), electrophysiological stimulation (Jeffery et al., 1990), hypertonic saline (Sharp et al., 1991) and sensory stimulation through exposure to a novel environment (Anokhin et al., 1991) all elicit an upregulation of c-*fos* that subsides with repeated stimulation.

The induction of c-*fos* by novelty appears to be more than a simple reflection of the stress of a novel experience. Stimuli deemed "stressors" also elicit c-*fos* expression that subsides with repeated experience (cf. review by Tischmeyer and Grimm, 1999). The general dissociation between stress and c-*fos* is supported by the lack of effect of adrenalectomy on the c-*fos* expression pattern in multiple brain regions following acute and repeated restraint stress (Melia et al., 1994). The novelty of the stimulus appears to matter most. For example, Fos immunoreactivity was found to be upregulated after repeated open field exposure, each in a novel environment (Wirtshafter, 2005).

Similarly, c-*fos* levels that were reduced after repeated restraint stress were upregulated by exposure to a different stressor, in this case swim stress (Melia et al., 1994). In contrast to these findings, it was reported that unlike other brain regions, the locus coeruleus maintained upregulated levels of expression c-*fos* with repeated footshock stress (Smith et al., 1992). This pattern was found to be correlated with the corticosterone surge that accompanied the stressful experience, and may reflect the direct involvement of this region in the stress response and the different adaptation dynamics of this system (Smith et al., 1992). The distinctive response of certain brain regions, as exemplified above, highlights the fact that different brain regions and circuits may differentially respond to the same experience.

Exposure to novel stimuli can induce c-*fos* expression in a stimulus, modality, and brain region-dependent fashion. For example, compared with exposure to novel objects, familiar objects elicit least electrical activity from neurons in the perirhinal cortex, and to a lesser extent from hippocampal neurons. Similarly, use of the same paradigm produced a lower amount of Fos immunoreactive cells in a few select areas including the perirhinal cortex, but not in the hippocampal formation (Zhu and Brown, 1995; Zhu et al., 1995; Zhu et al., 1996). In contrast to the Fos expression pattern elicited by novel individual stimuli, novel of arrangements of familiar stimuli elicited a different pattern (Wan et al., 1999). Using a "paired-viewing" procedure, exposure to novel pictures of individual objects triggered greater Fos expression than exposure to familiar pictures in the perirhinal cortex but not the hippocampus (Wan et al., 1999). In contrast, pictures of novel arrangements of familiar stimuli elicited a differential activation of Fos expression in the hippocampal subfields but not in the perirhinal cortex (Wan et al., 1999).

The relevance of c-*fos* in relation to learning mechanisms is particularly striking in light of paradigms evaluating the induction of this IEG at different levels of task acquisition. In contrast to the upregulation observed during acquisition of a task, Fos expression was found to be reduced in many brain regions when the acquisition reached an asymptote (Anokhin et al., 1991; Hess et al., 1995; Bertaina-Anglade et al., 2000; He et al., 2002a; He et al., 2002b). Throughout acquisition of learning, Fos levels are positively associated with the level of mastery of the task (e.g. Bertaina-Anglade et al., 2000), and it was concluded that such findings support a role of c-*fos* expression in the acquisition

and memory of a task, not simply performance (Anokhin et al., 1991; Bertaina-Anglade et al., 2000). We can thus think of c-*fos* activity as a learning derivative.

As described below, findings using a conditional fear conditioning paradigm have provided further insight into the nature of the IEG induction, leading some to suggest that the notion of IEGs as novelty-triggered may be insufficient to capture the essence of the nature of the IEG induction. It was found that whilst repeated exposure to a context led to a reduction in the resultant Fos expression, pairing context exposure with a shock led to an increased Fos induction upon re-exposure to this context alone (Campeau et al., 1991; Beck and Fibiger, 1995). It is the subsequent potentiation of IEG induction that has led Clayton (2000) to suggest a re-interpretation of extant results in terms of salience of stimuli for an adaptive response, rather than simple novelty response.

1.3.5: Lesion studies and the contribution of c-fos imaging

Recent investigations applying cellular imaging with c-*fos* have extended previous findings originally investigated through traditional lesion methods. Whilst the lesion approach has generated valuable information and founded the basis for multiple theories and models, there exist some inherent limitations in this approach that may hinder the study of memory abilities and their substrates. This view will next be discussed.

Attempts to understand the separate contributions of brain structures to memory have often focused on the effects of circumscribed lesions. The fact that circumscribed lesions result in impaired performance on different tasks is deemed to reflect the importance of a particular structure for the normal performance of a task. Thus, the lesion approach has been helpful in determining how vital certain structures might be for processing particular types of information. While widespread and ubiquitous to neuroscience, this approach is constrained by inherent limitations (cf. discussion in Grobstein, 1990; Lomber, 1999). For example, lesions can encroach upon adjacent structures and produce diffuse damage not specific to the target. Compensation may also occur, via spared routes, or through the use of alternate behavioural strategies. The outcome of lesions can be misleading if the target region is heterogeneous. For example, the role of the entorhinal cortex may be misinterpreted if lesions leave intact a small subregion with grid cells that code spatial elements of the environment (Hafting et al., 2005).

An underlying limitation of the lesion approach is that the dysfunction can only be indirectly attributed to the site of overt damage. The dysfunction reflects the activity of the spared tissue. Lesions to one structure may alter the dynamics of connected structures, complicating the direct evaluation of the role of individual structures (cf. review by Schoenfeld and Hamilton, 1977; Grobstein, 1990). Moreover, the permanence of lesions precludes the assessment of temporal dynamics. This is problematic as memory abilities are essentially time-dependent (Izquierdo and Medina, 1997; Ambrogi Lorenzini et al., 1999). Finally, lesion studies always examine the result of an abnormally functioning brain, as opposed to one that is normally functioning, but simply deprived of the functions of the region targeted by the lesion (Aggleton et al., 2000).

Lesion studies have sometimes produced contrasting views on the role of brain regions in various learning and memory abilities (Bachevalier and Mishkin, 1989; Mumby et al., 1996; Aggleton et al., 2000; Harker and Whishaw, 2002; Aggleton and Vann, 2004; Vann and Aggleton, 2004b; Aggleton and Brown, 2005). For example, studies evaluating the contribution of the retrosplenial cortex in behavioural tasks requiring spatial memory abilities have produced either no or only slight deficits (Neave et al., 1994; Aggleton et al., 1995; Warburton et al., 1998), or substantial deficits (Sutherland et al., 1988; Markowska et al., 1989; Whishaw et al., 2001; Harker and Whishaw, 2002; Vann and Aggleton, 2002; Vann et al., 2003). These inconsistencies seem to be due primarily to the irregular extent of the damage produced, and the integrity of neighbouring fibre bundles. It appears that extensive retrosplenial lesions that include the caudal part yet spare the cingulum bundle produce deficits similar to lesions that are smaller but interrupt the cingulum bundle. In other words, damage to the cingulum bundle may have the same effect as complete retrosplenial lesions. Both of these patterns of lesions produce larger deficits than small retrosplenial lesions that spare the cingulum bundle (Aggleton and Pearce, 2001; Vann and Aggleton, 2002; Vann and Aggleton, 2004b). This example shows the ambiguities that can arise when comparing studies where the lesions are of different sizes or nature. These ambiguities reflect the extent of lesions and the potential sufficiency of the remaining tissue to support the mnemonic task at hand, as well as the vulnerability of fibres of passage. The effect of fibre tract interruption underlines the importance of communication between brain

areas, and it is this latter point that will be discussed next, again in relation to the lesion approach.

The use of lesions to study the function of brain regions has often been fruitful in identifying regions that are necessary for normal cognitive function. However, in many instances the effects of lesions may be best considered as changes in the activity between networks of regions and their connections (Schoenfeld and Hamilton, 1977). Lesion studies attempting to identify the components of networks important for spatial memory have sometimes been complicated by the many different ways that information can be transmitted. This is another level of complexity and is reflected in the nature of central nervous tissue wiring, as illustrated in the example that follows. As demonstrated below, it has become apparent that multiple systems and multiple connections exist that can sustain the performance of a task (Aggleton et al., 2000). Instances abound highlighting the importance of cooperation of brain regions in the service of memory abilities and behaviour, and the examples that follow illustrate the notion that brain regions can act in concert and that information can be transmitted several ways. Certain regions may be involved in transmitting information, but in their absence, remaining routes may suffice. A region that seemed unimportant for the performance of a task can be found to be crucial under some circumstances where the network is affected.

An example comes from the finding that bilateral anterior thalamic nuclei lesions in monkeys can spare an object-in-place type of visuospatial task (Ridley et al., 2002), yet testing monkeys with anterior thalamic nuclei lesions crossed with inferotemporal lesions revealed a deficit (Ridley et al., 2004). In the latter study, monkeys with ipsilateral unilateral lesions of the anterior thalamic nuclei and the inferotemporal cortex did not produce a deficit in this task, highlighting the importance of interaction between these two regions to perform that particular task (Ridley et al., 2004). In these studies by Ridley and collaborators (Ridley et al., 2002; Ridley et al., 2004), damage to two regions on their own did not produce performance decrements, suggesting that their integrity was not crucial for the task tested. However, the importance of these regions was revealed when they were damaged together to produce a deficit. Independent damage to each of these two structures did not prevent the remaining tissue from sustaining the performance of that particular task. The lesion studies however revealed the detrimental effect of damaging these two nodes in a manner that prevented serial

communication from occurring in parallel pathways in each hemisphere, as revealed by the lack of effect of ipsilateral lesions.

Similarly, other studies have revealed the existence of parallel networks of regions that work together to contribute to a task. Crossed lesions of the anterior thalamic nuclei and of the hippocampus produced greater deficits on spatial memory tasks than unilateral lesions alone (Warburton et al., 2001). Another example of greater spatial memory deficit was found after crossed lesions of the hippocampus and of the entorhinal cortex in an object-in-place paradigm (Parron et al., 2006). Finally, Sutherland and Hoesing (1993) found that crossed lesions of the retrosplenial cortex with either the hippocampus or anterior thalamic nuclei both produced larger deficits than ipsilateral lesions in a spatial memory version of the water maze. These examples of potentiated deficits through the explicit disruption of connected regions highlight the synergistic nature of brain networks underlying substrates of memory abilities. They also typify the notion that in the presence of parallel connections, certain lesions may fail to produce significant deficits (Aggleton et al., 2000).

While the studies just described above highlighted the role of parallel connections, Warburton and colleagues (2000) found that the effects of lesions can be complicated by the existence of both parallel and crossed connections. In order to evaluate the joint activity of the anterior thalamic nuclei and the fornix (hippocampus), ipsilateral and crossed lesions were produced. These crossed lesions, however, failed to produce substantial impairments in a T-maze alternation task (Warburton et al., 2000). Only when additional damage was added that prevented both parallel and crossed connections did the rats display a marked deficit (Warburton et al., 2000). It can be deduced from such results that in order to appreciate the extent of region interaction, an impractical number of crossed lesions would need to done, depending on the target. A final limitation of the lesion method is that it does not inform us about the underlying mechanisms of memory function at the cellular level (Izquierdo and Medina, 1998).

The IEG imaging approach allows an unbiased, whole-brain analysis of extensive, potentially parallel circuits, without having to damage multiple regions to see the result of their interaction. The benefit of the IEG approach is that it actually combines whole, intact brain imaging with the visualisation of mechanisms of plasticity, at high, cellular resolution. In an attempt to help clarify some inconsistencies between lesion studies and

predicted performance abilities based on anatomical connections (Aggleton et al., 2000; Aggleton et al., 2004; Aggleton and Brown, 2005), efforts were made to investigate the activity of Fos protein elicited by the performance of tasks requiring the use of spatial memory abilities in brain regions that are part of a proposed extended hippocampal system (Aggleton and Brown, 1999). This allowed researchers to visualise within a single preparation the potential contribution of regions throughout the whole brain. Studies have been done using rodents with intact brains to look at the contribution of the hippocampal formation and extra-hippocampal regions to working memory abilities in the radial arm maze (Vann et al., 2000a; Vann et al., 2000b), as well as contrasting tasks requiring allocentric reference and non-allocentric abilities in the water maze (Jenkins et al., 2003; Teather et al., 2005). Other studies have compared the expression of different IEGs in the hippocampus for such types of tasks (Guzowski et al., 2001), as well as the contribution of novel compared to familiar stimuli arrangements in a radial arm maze task (Jenkins et al., 2004b). In spite of the benefits of this approach, important limitations to the IEG imaging approach remain. Of particular concern is that the temporal resolution is poor in comparison to some other techniques. Furthermore, activity-dependent Fos induction in a brain region does not automatically mean that this region is necessary for the performance of that task. The use of methods to block IEG activity provides a way of confirming the importance of these molecules for learning and memory (cf. review by Chiasson et al., 1997).

1.3.6: Lesions, injury, pathological dysfunction and c-fos

While we cannot establish how vital a brain region is for the performance of a task based on the fact that Fos is upregulated there, in combination with a lesion approach this type of imaging could inform us about potential effects distal to the site of a lesion. This could allow researchers to infer about the effects of compromises to the integrity of certain structures upon the function of other, intact structures within a network. We will next discuss the merits of using IEG imaging to evaluate the network dysfunction.

Motivated by inconsistencies in the lesion literature and the numerous observations of temporary deficits, Izquierdo and Medina have contended that lesion approaches may lead to "overinterpretation" of the results (1998). They suggested the prevalence in the literature of exaggerated attribution of responsibility of behavioural deficits to the intended target of lesions. In accord with this view, there are clinical examples of alterations in regions distal to those exhibiting overt pathology (Fazio et al., 1992; Reed

et al., 1999). Such distal effects have also been found in animal models, where assays after certain lesions revealed in subsets of connected regions a long-lasting reduction in glucose utilisation, nitric oxide synthase or immediate-early gene activity (Beck et al., 1996; Meguro et al., 1999; Liu et al., 2003; Glenn et al., 2005).

In light of the existence of such covert pathology, that is, pathology that is not overt, i.e. observable using traditional means such as Nissl stains or structural imaging, immediate-early gene imaging has been used to delineate the consequence of lesions in anatomically defined circuits. Building on the potency of IEG imaging, this line of research seeks to relate behavioural performance to the extent and distribution of dysfunction after brain damage. This imaging approach has been used to assay behavioural performance in relation to cellular IEG activity after various forms of injury, such as after ischemia (Puurunen et al., 2001) or with ageing (Touzani, 2003). While c-*fos* can be triggered by a wide array of phenomena, we will next discuss more specifically the ways in which the activity of this IEG can be directly induced by pathology.

In response to brain injury, there is no apparent universal IEG pattern. The type and the location of lesion can have a differential effect on the regional distribution of Fos immunoreactivity, as different circuits are activated and different transynaptic networks trigger IEG expression. Axotomy is associated with selective and persistent expression of immediate-early genes. After axotomy, c-Jun and weakly zif268, but not c-*fos*, are expressed in the axotomised neurons (Hughes et al., 1999). The induction of c-Jun is prolonged, it has been observed up to 100 days later (Hughes et al., 1999). This effect can be observed in neurons that neither regenerate nor undergo apoptosis. Transient c-Jun expression has been reported in neurons until they re-connect or undergo apoptosis. In a review of the literature, Hughes and colleagues (Hughes et al., 1999) suggest that apart from c-Jun, and to a lesser extent JunD, other IEGs do not play a role in axotomised neurons.

Alternatively, kindling, prolonged seizure activity, spreading depression, ethanol-withdrawal seizures, mechanical injury including saline infusion and fluid-percussion, and also hypoxia-ischemia result in early peaks of c-*fos* induction (in minutes to a couple of hours) that can then last between 12 and 72 hours, depending on the paradigm. Degeneration is associated with transient c-*fos* and *zif268* but prolonged c-

Jun expression. In apoptotic neurons that display a condensed chromatin, c-*fos* is strongly expressed. It may be neuroprotective against apoptosis (Herrera and Robertson, 1996; Herdegen and Leah, 1998; Hughes et al., 1999). Paradigms that lead to cell death can produce c-*fos* superinduction due to the inhibition of protein synthesis by mechanisms associated with cell death, the resultant lack of Fos precluding the negative autoregulatory feedback. The inhibition of Fos protein translation in what may be irreversibly injured neurons can last for a week after hypoxia-ischemia (Gass and Herdegen, 1995; Herrera and Robertson, 1996; Hughes et al., 1999). The induction of c-*fos* by mechanical, chemical or ischemic brain injury might at least, in part, be the result of spreading depression (Herrera and Robertson, 1996). It is important to note that c-*fos* mRNA, but not protein, is associated with deleterious cellular mechanisms. That is, pathological processes are generally not associated with persistent Fos protein expression. Overall, if c-*fos* is induced by an insult to the brain, this upregulation will be short, and that as long as sampling time is consequently appropriate, c-*fos* upregulation should be a reflection of plasticity, not pathology.

As an example, immediate-early gene imaging has been used to delineate the consequence of lesions in circuits that are part of the proposed extended hippocampal system (Aggleton and Brown, 1999). For example, the impact of lesions on distal IEG activity has been related to performance in rats with fornix (Vann et al., 2000c), hippocampal (Jenkins et al., 2003; Jenkins et al., 2006) and anterior thalamic nuclei lesions (Jenkins et al., 2002a; Jenkins et al., 2002b; Jenkins et al., 2004a). This form of imaging has helped further characterise the neural substrates of spatial memory processes and the response of interconnected regions to damage to one of the nodes. Importantly, molecular approaches such as cellular imaging of Fos have helped inform discrepancies between lesion studies and predicted performance patterns based on anatomical connections (Aggleton et al., 2000; Glenn et al., 2005).

1.3.7: Advantages and disadvantages of using IEGs for mapping

Certain properties of IEGs make them particularly appealing to identify networks. Interestingly, action potentials are not sufficient to effectively trigger c-*fos*. They must be accompanied by receptor activation to trigger maximal c-*fos* induction (Luckman et al., 1994). This potentiation through concurrent membrane activity suggests that transynaptic modulation via receptor activity of neuronal activity is a more efficient means of inducing c-*fos* (Luckman et al., 1994). Furthermore, it has been reported that

after electrical stimulation, c-*fos* can be found both in pre- and post-synaptic cells (Nikolaev et al., 1991). These two findings highlight the transynaptic nature of c-*fos* activation, and make it an appealing candidate to visualise the activity of cells that are not simply metabolically active, for example, but rather are especially active within a network.

It is important to consider the basal activity of IEGs, in order to better interpret the results of a study. Fos activity is low under basal conditions, enabling sensitive detection of increased signal activity. In contrast Zif268 is high, facilitating detection of reductions in activity (Hughes et al., 1992). Furthermore, timing of sampling is not trivial. Given the vast influence of diverse stimuli of an organism, Dragunow and Faull (1989) have cautioned that the history of the organism in the preceding 1-12 hours may influence Fos levels at the time of sampling. This caution highlights the uttermost importance of appropriate controls in an experiment.

There exist differential spatial and activity-induced expression patterns of c-*fos* and *zif268* expression. For example, electrical stimulation or a stressor will produce differential mapping of Fos and Zif268 (Cullinan et al., 1995; Luckman, 1997). The problem posed by these heterogeneous patterns of IEG activity induced by various stimuli is compounded by the fact that some regions do not express specific IEGs, at least under some conditions. It is thus important to recognise that IEG changes reflect plasticity involving these particular IEGs rather than necessarily absolute levels of plasticity.

1.4: Memory, underlying neural circuits, and retrosplenial cortex function

It has been claimed that knowing the site and the identity of molecular mechanisms associated with memory is insufficient, that only an analysis of these mechanisms throughout a network of brain regions will actually reveal the nature of the memory (Thompson and Krupa, 1994). As discussed previously, IEG imaging can be a powerful tool to visualise network activity (Anokhin et al., 1991; Hess et al., 1995; Aggleton et al., 2000; Bertaina-Anglade et al., 2000; Guzowski et al., 2001; He et al., 2002a; He et al., 2002b; Jenkins et al., 2003; Aggleton et al., 2004; Aggleton and Brown, 2005). The application of a technique such as IEG imaging can be informed by extant data on anatomical substrates of memory.

This thesis will describe an experiment where molecular imaging was used to visualise brain regions where plasticity was induced by the performance of a spatial memory task. The use of this approach should first be guided by current knowledge about the potential substrates of spatial task performance and memory. While at first it would seem reasonable to consider that brain activity in response to spatial contextual information should apply to various sorts of events that involve spatial context, there are reasons to believe that not all spatial-related memory abilities are equivalent, nor are they mediated by the same substrates. For example, spatial memory in a maze task is not necessarily equivalent to other forms of contextual information in a fear conditioning paradigm, and the brain regions necessary for the performance of these tasks are not necessarily the same (cf. Phillips and LeDoux, 1995; Good and Honey, 1997; Richmond et al., 1999). The performance of tasks that depend upon a diversity of spatial allocentric memory abilities is deemed to be largely subserved by the hippocampal formation, in conjunction with the anterior thalamic nuclei, the mammillary bodies, and cortical structures such as the entorhinal, perirhinal, postrhinal, parietal, prefrontal, and retrosplenial cortices (Redish and Touretzky, 1997; Steckler et al., 1998; Aggleton et al., 2000; Mizumori et al., 2000; Vann and Aggleton, 2004a). The use of IEG mapping to identify regions of importance for spatial memory abilities adds a plausible molecular mechanism that could orchestrate the underlying plasticity changes occurring with learning and memory. IEG mapping lends itself to the concurrent evaluation of the importance of multiple regions at once, providing a powerful tool to characterise the conjoint work of brain regions. Most importantly, the mapping of functional activity can be done in an intact system. In contrast to the lesion approach, focusing on one region with IEG mapping does not lead to dysfunction in other regions. Furthermore, IEG mapping can help distinguish different categories of spatial tasks based on different cues. Finally, unlike permanent lesions, we can look at temporal changes in function using IEG imaging. The dynamic interactions between regions can be evaluated throughout different stages of learning, distinguishing between regions that are necessary for acquisition but not once the task is established, or during consolidation, or simply for the execution of the task.

My research focus will be on the retrosplenial cortex (see Figure 1.4). This region was selected because of its likely vulnerability to brain insults and its intimate relationship

with both the anterior thalamic nuclei and the hippocampus. I will first provide an overview of the functions of the retrosplenial cortex.

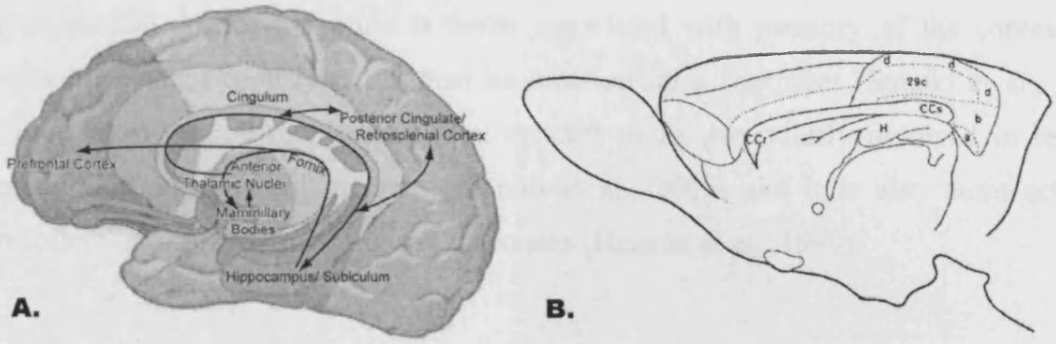

Figure 1.4: The location of the human (a, Aggleton and Brown, 2006) and rat (b) retrosplenial cortex, here labelled 29 a-d (Vogt et al., 1981).

1.4.1: Functions of the human retrosplenial cortex

In primates, the retrosplenial cortex comprises areas 29 and 30. These areas are within the posterior cingulate region, which also includes areas 23 and 31. In rats, there are no areas 23, 30 and 31. As such, in rodents but not primates the terms posterior cingulate and retrosplenial cortex (area 29) are equivalent (Vogt, 1993). Widespread evidence exists of retrosplenial cortex dysregulation in disorders that involve memory impairment. These disorders include Alzheimer's disease (Desgranges et al., 1998; Nestor et al., 2003), vascular dementia (Martinez-Bisbal et al., 2004), Wernicke-Korsakoff syndrome (Aupée et al., 2001; Reed et al., 2003), hypoxia-induced amnesia (Reed et al., 1999; Aupée et al., 2001), and epilepsy (Archer et al., 2003). Furthermore, damage that is mainly focused on the retrosplenial cortex due to haemorrhage or infarct has been found to result in amnesia (Maguire, 2001a), amnesia accompanied by temporal order judgment impairment (Valenstein et al., 1987; Bowers et al., 1988), amnesia with topographic disorientation (Yasuda et al., 1997) and topographic disorientation without episodic memory impairment (Takahashi et al., 1997).

The role of the human retrosplenial cortex appears to span diverse memory abilities as exemplified by functional imaging reports. For example, the retrosplenial cortex appears to be involved in novel image detection (Tulving et al., 1994) and paired word associate learning (Fletcher et al., 1995). The retrosplenial cortex is believed to be of importance for the processing of episodic more than semantic memory (Wiggs et al., 1998). This brain region was found to be consistently activated in autobiographical memory studies

in a review (Maguire, 2001b) and a meta-analysis (Svoboda et al., 2006) of the literature. In another review of the literature, Maguire (2001a) found that the retrosplenial cortex is found to be activated by most navigation-type tasks. Similarly, retrosplenial cortex activation is better associated with memory of the context of a stimulus (which room?) rather than its location on a computer (Suzuki et al., 2005). Furthermore, the retrosplenial cortex appears to be particularly involved in retrieval more than encoding of memory (Kondo et al., 2005) and it is also more active in recollection rather than familiarity responses (Henson et al., 1999).

1.4.2: Retrosplenial cortex function, dysfunction, and the impact of anterior thalamic nuclei damage

The anterior thalamic nuclei and the retrosplenial cortex share strong reciprocal connections (Vogt et al., 1981; van Groen et al., 1993). The anterior thalamic nuclei are vulnerable to both vascular (Chung et al., 1996; Schmahmann, 2003) and non-vascular insults including Alzheimer's Disease (Braak and Braak, 1991), Wernicke-Korsakoff syndrome (Harding et al., 2000), schizophrenia (Sharp et al., 2001), and infectious agents (Bentivoglio, 2004). There is evidence from clinical studies and from animal models that damage to thalamic nuclei produces diaschisis, dysregulation of activity in diverse, remote brain regions (Pappata et al., 1990; Rousseaux et al., 1991; Makela et al., 1998; Jenkins et al., 2002b; Caulo et al., 2005). The extent of the diaschisis produced by thalamic damage can be related to the cognitive performance of the patient (Baron et al., 1992). While no such analysis has been done with patients that have selective anterior thalamic nuclei damage, pathology that includes the anterior thalamic nuclei is associated with amnesia (Aggleton and Sahgal, 1993; Harding et al., 2000; Van der Werf et al., 2000; Van der Werf et al., 2003), and anterior thalamic nuclei damage has been found to be associated with diaschisis (Kim et al., 1994). It remains to be confirmed whether the distal dysfunction is also related to cognitive deficits in patients with selective anterior thalamic nuclei damage.

It appears that the posterior cingulate, and maybe more specifically the retrosplenial cortex, may be an important site of dysfunction following anterior thalamic nuclei pathology. Damage due to an infarct that was relatively selective for anterior thalamic nuclei produced autobiographic memory deficits and was accompanied by long-lasting and selective posterior cingulate hypometabolism (Clarke et al., 1994). Similarly, patients that have suffered amnesia as a result of acute hypoxia were found to exhibit

selective thalamic hypometabolism accompanied only by retrosplenial hypometabolism (Reed et al., 1999). As previously mentioned, the retrosplenial cortex is dysfunctional in patients suffering from Alzheimer's disease. There is currently conflicting evidence about the state of the connections between the retrosplenial cortex and the thalamic nuclei in this neurodegenerative disorder. For example, recent analyses of the brains of AD patients found a reduction in the integrity of white matter fibre tracts in thalamo-cortical and cortico-thalamic connections in some studies (e.g. Medina et al., 2006; Xie et al., 2006) but not others (e.g. Bozzali et al., 2002). There is reason to believe that the retrosplenial cortex involvement in clinical disorders may be associated with its vulnerability to anterior thalamic lesions. The sensitivity of the retrosplenial cortex to anterior thalamic nuclei damage has been evaluated in animal models.

Immediate-early gene (IEG) immunoreactivity in retrosplenial cortex is markedly depressed in rats with anterior thalamic nuclei lesions when assayed after behavioural treatment or in rats taken from their home cage (Jenkins et al., 2002b). The protein products of the IEGs Fos and Zif268 display a striking reduction in expression, which is stable, and unaccompanied by overt neuronal degeneration (Jenkins et al., 2004a). This effect is observed in spite of the numerous remaining connections, and is not observed after postrhinal cortex lesions, suggesting that the retrosplenial cortex is selectively susceptible to disconnection from its afferents (Jenkins et al., 2004a). It is worth noting that the cells that are affected are in the same laminae that display dendrite disorganisation with age in rats (Wyss, 1992)

As discussed above, there has been some controversy over the importance in rats of retrosplenial cortex integrity for the performance of tasks that require spatial abilities (Harker and Whishaw, 2002; Aggleton and Vann, 2004). Recent findings and observations by Aggleton and colleagues (Aggleton and Pearce, 2001; Vann and Aggleton, 2002; Vann and Aggleton, 2004b) appear to explain the lack of substantial deficits in a number of reports (Neave et al., 1994; Aggleton et al., 1995; Warburton et al., 1998). There is thus agreement that extensive retrosplenial cortex lesions can induce substantial deficits in performance of tasks including spatial reference memory version of the water maze, working memory in a radial arm maze, idiothetic and allothetic homing on a circular platform, non-matching-to- place alternation, object-in-place exploration (Sutherland et al., 1988; Whishaw et al., 2001; Harker and Whishaw, 2002; Vann and Aggleton, 2002; Vann et al., 2003). In contrast, egocentric performance of a

T-maze type task and object identity recognition appear to be spared (Vann and Aggleton, 2002).

In a study involving relatively small lesions that spared the rostral portion of the retrosplenial cortex, Alexinsky (2001) reported, not unexpectedly one might think in light of issues discussed above, no deficit in a version of the radial arm maze task involving both reference and working memory. This result is consistent with other experiments where a portion of the retrosplenial cortex was spared (Neave et al., 1994; Aggleton et al., 1995). Rats with retrosplenial lesions have been found to perform differentially on spatial memory tasks depending on the time of the lesion, either pre- or post-training (Cain et al., 2006). While the restricted size of the lesion may explain the null effects obtained on a reference and working memory task, the protocol used by Alexinsky (2001) also included pre-training of the rats, contrary to other studies outlined above where an effect of retrosplenial lesions was found. This methodological difference may also have mitigated the effect of the lesion.

In spite of the small size of the retrosplenial lesions in this study (Alexinsky, 2001), the surgery appeared to leave the rats insensitive to the movement of a distal cue. This insensitivity to a landmark change was interpreted as a failure to attend to the contextual change, and an overriding of spatial strategies by cue-based strategies (Alexinsky, 2001). Alternatively, this result could simply reflect a reduction in allocentric information processing. This could happen as a result of malfunction or the absence of the head direction cells found in the retrosplenial cortex (Chen et al., 1994b). These cells are associated with heading vector-based orientation, and their activity can be anchored to landmarks (Chen et al., 1994a; Chen et al., 1994b), just like head direction cells found in the anterior thalamic nuclei (Goodridge and Taube, 1995). Based on the idea that these cells can integrate a landmark into an "allocentric directional coordinate" (Chen et al., 1994a), their absence or dysfunction may explain the lack of effect of the movement of a landmark in the study by Alexinsky (2001), as the rats may have relied more heavily on other information to perform the task. This interpretation is consistent with recent findings in the monkey that visual attention generates a signal in posterior cingulate that agrees better with allothetic than idiothetic processing (Dean and Platt, 2006). It is also in accord with the finding that lesions of the dysgranular subregion of the retrosplenial cortex resulted in rats using an egocentric rather than an allocentric strategy in a radial arm maze task (Vann and Aggleton, 2005).

In spite of the disruptive effect of retrosplenial lesions on allocentric spatial abilities, some Fos imaging studies of spatial memory did not find differential upregulation in this region. In contrast to exploration of a new environment (Hess et al., 1995; Nagahara and Handa, 1997; Ons et al., 2004) and performance of tasks dependent upon allocentric spatial memory abilities (Jenkins et al., 2003), performing a well-learned working memory version in a radial arm maze in a novel environment did not elicit greater Fos expression in the retrosplenial cortex (Vann et al., 2000a). This is an unexpected finding given the purported role of the retrosplenial cortex in spatial memory abilities. Performance of the same working memory task did however induce greater retrosplenial Fos expression than obtaining rewards for running up and down only one of the arms of the radial arm maze (Vann et al., 2000a). While at first the lack of difference in induced Fos expression between performance of the radial arm maze task in a novel and a familiar environment may seem surprising, this may be a reflection of the underlying dynamics. Fos studies using other versions of radial arm maze tasks revealed that compared to thalamic nuclei, several neocortical areas (the retrosplenial cortex was not evaluated) exhibited a peak in Fos expression with further training (He et al., 2002a; He et al., 2002b). Thus the nonsignificant upregulation of Fos that was observed in the study by Vann and colleagues (2000a) may have become significant with further training.

There is converging evidence from lesion (Bussey et al., 1996; Bussey et al., 1997) and electrophysiological studies (Gabriel, 2000) that is coherent with a slower learning rate or a preferential role of the retrosplenial cortex in later stages of task acquisition. Similar to the peaking pattern of Fos in radial arm maze studies described above (He et al., 2002a; He et al., 2002b), in avoidance and approach conditional discrimination the anterior thalamic and retrosplenial cortex develop a discriminatory firing pattern respectively early and late in training (Gabriel, 2000; Smith et al., 2002). Importantly, as discussed next, thalamic nuclei lesions can prevent the acquisition of the conditional firing ability of retrosplenial neurons.

Anterior thalamic nuclei lesions can disrupt the training-induced neuronal activity of a conditional auditory discrimination response in retrosplenial cortex (Gabriel et al., 1989; Kubota and Gabriel, 1995). In turn, learning-induced unit activity is disrupted in anterior cingulate cortex after lesions in the retrosplenial cortex (Gabriel and

Sparenborg, 1987). In this paradigm, the later peaking activity in retrosplenial cortex was deemed to be relevant for retrieval of the conditional association (Kubota and Gabriel, 1995). Retrosplenial cortex, anterior thalamic and hippocampal neuronal activity can discriminate between conditional stimuli for both avoidance and approach behaviour, and can also do so in a context-specific fashion (Freeman et al., 1996), and this retrosplenial cortex context-specific firing is disrupted by entorhinal lesions (Freeman Jr. et al., 1997). I will next discuss the timing and duration of plasticity in relation to spatial memory abilities.

1.5: Time to learn

Several authors have evaluated the changing role of brain regions after the complete acquisition of a spatial memory task. For example, in addressing the potentially time-limited role of the hippocampus in certain mnemonic functions, Bontempi and colleagues (1999) found that increasing the retention time after acquisition of a spatial discrimination resulted during subsequent testing in decreased hippocampal but increased neocortical metabolic activity. This change in the balance of hippocampal and neocortical function is in accord with other studies, and is part of a debate over the nature of the temporal role of hippocampal function that I will not further discuss here (for recent reviews of the topic, cf. Squire et al., 2004; Wiltgen et al., 2004; Moscovitch et al., 2005).

In accord with numerous lesion studies, inactivation studies by Ambrogi Lorenzi and colleagues (1999), where electrical communication was inhibited without damaging the tissue, have emphasised that memory abilities, including spatial memory abilities, are essentially time-dependent. The permanent nature of the manipulation made via a lesion precludes the use of this approach for the direct assessment of temporal dynamics, a problematic constraint as memory abilities are essentially time-dependent (e.g. Ambrogi Lorenzini et al., 1999). Commendable efforts have been made into characterising these temporal dynamics. Most of the studies have investigated the time-dependent nature of the brain functions in avoidance tasks. For example, Izquierdo and colleagues (1997) have evaluated the role of numerous molecular mechanisms at multiple points after acquisition of an inhibitory avoidance task. In terms of spatial memory, several groups have evaluated the activity of brain regions shortly after acquisition of a task compared to after a long period (weeks), i.e. after longer term consolidation. This approach has been used to look at glucose utilisation in several brain regions (Bontempi et al., 1999)

as well as IEG imaging in the anterior cingulate using a spatial water maze task (Teixeira et al., 2006). There exist few reports assessing the temporal dynamics of IEGs in relation to the level of mastery of a spatial task. For example, data were reported on the hippocampal expression of IEGs induced at different levels of training by the acquisition of a spatial and a non-spatial memory task in the water maze (Guzowski et al., 2001; He et al., 2002a), and several brain regions after performance in a radial arm maze task using version with fixed or a variable set of baited arms (He et al., 2002b).

Guzowski and colleagues (2001) tested rats in a water maze task. In their first experiment, one condition consisted of training to find a platform in a fixed position, the other to a cued moving platform. The expression of the IEGs c-*fos*, *zif268* and *arc* was evaluated by taking tissue punches from the brain after the last trial. The animals were trained in one session consisting of six trials over ~ 8-10 minutes. In comparison to cage controls, levels of all three IEGs were found to be elevated in the dorsal hippocampus by water maze training. There were no differences between the training groups. In order to more closely relate IEG expression to the level of learning, the authors of this study correlated the performance of the rats to their IEG expression levels. When looking at the last three trials, during which performance was more stable, they found a negative correlation between all IEGs and escape latency for the spatial tasks (i.e. better performance associated with higher IEG levels), but only *arc* analyses reached statistical significance. No correlations were found for the cued version.

Another group of rats in this same study (Guzowski et al., 2001) was trained in three different versions of the water maze task. One group of rats was trained to asymptote to find a platform in a fixed position. Another group of rats was trained in the same way but on the last day the platform position changed. These rats learned the new location of the platform rapidly and their performance was similar to the fixed position group by the second trial. The last group consisted of rats tested for only one session in the fixed position version of the task. All IEG levels from the dorsal hippocampus samples were lower in the group tested at asymptote compared to the group that only just started acquiring the task. In this brain region, levels of *arc*, c-*fos* and *zif268* were higher in the group trained to a new position when compared to the group at asymptote, but again only differences in *arc* levels achieved statistical significance. c-*fos* levels were not different between asymptote level and novel position groups in entorhinal or primary visual cortex sample tissue. In contrast, *arc* levels were higher in the group at asymptote

level compared to the novel position group in the entorhinal but not the visual cortex. *zif268* levels, in contrast to those in the hippocampal sample, were not different between any of the tasks in the entorhinal nor the primary visual cortex. Finally, c-*fos* levels were higher for the one session training group in all three brain regions sampled. Overall, these results suggest that the ability to find a fixed platform in a new location was best associated with *arc*, compared to c-*fos* and *zif268*, especially in the hippocampus but also in the entorhinal cortex.

I will address two points regarding the findings of Guzowski and colleagues (2001): the tissue sampling method and the use of the correlation analyses. It is possible that the roles of c-*fos* and *zif268* are not as directly associated with learning mechanisms as *arc*. However, several issues may confound the results reported above. First, the tissue of sampling method precluded a fine grain analysis, and as such, prevented from evaluating the separate contribution of different hippocampal subfields. This is important as the different components do not necessarily act in concert or subserve the exact same functions. For example, when rats performed fixed platform and cued platform versions of a water maze similar to those described by Guzowski and colleagues (2001), Fos visualisation revealed that the function of subcomponents of the hippocampal formation was heterogeneous (Jenkins et al., 2003). Similarly, water maze performance of a fixed platform task also induced hippocampal subfield-specific changes in *arc* expression (Gusev et al., 2005). These findings reinforce the idea that subregion-specific functions within the sampled tissue may have affected the analyses of the findings reported by Guzowski and colleagues (2001).

Second, it must be kept in mind that in the study by Guzowski and colleagues (2001), correlations were calculated between IEG levels and the mean escape latency of the rats on the last three trials. This was done because it was deemed that the performance of the rats on the last three trials, as it was stabilising, was a better reflection of their learning ability. The authors, in fact, chose to correlate IEG activity with a performance measure that varied very little as it was at or close to asymptote. It could be argued that using the mean latency in the asymptotic trials actually only addresses a small part of the learning process, i.e. that part during optimising or fine tuning. Obtaining an actual learning rate by calculating the slope of individual performance may better reflect learning. Correlating such a learning rate with IEG expression could have proven to be a more sensitive measure. Intriguingly, Kelly and Deadwyler (2002) found using an operant

conditioning paradigm that arc levels were negatively correlated to the performance of the rats. Their result is the opposite to the water maze findings of Guzowski and colleagues (2001). The slow learning rats expressed the highest levels of this IEG. This may reflect different network dynamics induced by the task used. In any case, in reference to the positive correlation reported by Guzowski and colleagues (2001), Kelly and Deadwyler (2002) proposed the analysis of trials preceding asymptotic performance, as these exhibit the greatest learning increments, in order to clarify the contribution of this IEG to learning mechanisms.

Another research group evaluated IEG expression in relation to the learning level of tasks dependent upon spatial memory (He et al., 2002a; He et al., 2002b). Using different variations of radial arm maze tasks requiring working and/or reference memory, they found, as mentioned previously in section 1.3.4, that IEG expression was lower when behavioural performance was close to asymptote than during early acquisition. For the version combining working and reference memory (He et al., 2002a), they found that the hippocampal subfield CA3, but not CA1 nor the dentate gyrus, showed changed levels of Fos expression with learning. In addition to the CA3, Fos levels were also upregulated by learning the task in the anterior cingulate cortex and the motor cortex. However, only blocking of Fos by antisense injections into the dorsal hippocampus, but not cingulate or motor cortex, produced reference and working memory deficits (He et al., 2002a). In another experiment where they compared the standard reference/working memory version to a variable position version of the radial arm maze, they also found reductions in Fos upregulation with further training. They also again found that only in the CA3 region of the hippocampus was Fos upregulated when rats were trained to find pellets in rewarded arms that remained in fixed positions. However, in the version where the position of the reward was changed every session, the CA1 and the dentate gyrus now also exhibited an upregulation in Fos expression (He et al., 2002b). As the authors emphasised, performance of the variable position version was not affected by altering extra-maze or intra-maze cues, suggesting that it was independent of spatial cues (He et al., 2002b). Hippocampal lesions produced deficits in the variable version and working but not reference deficits in the fixed position version (He et al., 2002b). The authors concluded that the hippocampus may thus also play an important role in non-spatial memory (He et al., 2002b). The findings of He and colleagues (2002a; 2002b) and Guzowski and colleagues (2001) highlight subtle differences in network dynamics in different types of spatial memory tasks, but

especially, they indicate a dynamic role of plasticity mechanisms during the acquisition of these tasks.

1.6: Conclusion

The use of immediate-early gene imaging not only provides a form of functional imaging within normal tissue, it also allows the measurement of processes that may have a direct involvement in mnemonic processes. The analysis of immediate-early genes combines a cellular-level resolution with the mapping of activity through a marker that is actually itself involved in the induction of long-lasting modifications. Evaluating the cellular immunoreactivity of specific structures can be more powerful than the assessment of blocks of brain containing many structures, such as in PCR. Perhaps most importantly, analyses using an immunohistochemical approach can be highly localised and thus can identify heterogeneity of function within a given brain area. In contrast, a more global approach that evaluates relatively large brain areas may preclude subregion-specific findings (Alder et al., 2002).

By using IEG imaging, I propose to examine the following questions: 1) Does the expression of the IEGs Fos and Zif268 vary within the MTL at different stages of learning? 2) Are there relative changes in different MTL structures?

Based on the striking effect of anterior thalamic nuclei lesions on retrosplenial cortex Fos immunoreactivity, I also intend to determine: 3) How quickly do anterior thalamic nuclei lesions produce Fos immunoreactivity in retrosplenial cortex? 4) Do lesions in other afferent regions produce such a dramatic impact on Fos reactivity in the retrosplenial cortex?

5) Having qualified in more detail the IEG changes in retrosplenial cortex after distal lesions, I next propose to seek a better understanding of the underlying cause. This goal involves characterising the broad array of molecular changes that might occur in retrosplenial cortex following anterior thalamic nuclei damage.

Chapter 2

Spatial memory, regional plasticity and limbic network interactions

2.1: Introduction

The role of brain regions in memory functions appears to change with time. For example, the importance of the hippocampus may decrease with the passage of time, as memories relying on the function of the hippocampus become reliant on neocortical function (reviewed by Teyler and DiScenna, 1985; Alvarez and Squire, 1994). Studies evaluating the temporal dynamics of the neural substrates of spatial memory have often tested different periods *after* the acquisition of a task, either a short (days) or long (weeks) time after acquisition, i.e. after different durations of consolidation. While the evidence for a time-dependent role of brain regions in mnemonic functions was largely derived from lesion studies, recently there has been converging evidence from other types of approaches. For example, researchers have reported time-dependent roles of certain brain regions in tasks relying on spatial memory in studies using transgenic mice (Frankland et al., 2001), metabolic imaging (e.g. Bontempi et al., 1999), and immediate-early gene imaging (e.g. Teixeira et al., 2006). Bontempi and colleagues (1999) demonstrated the existence of time-limited regional metabolic activity in mice tested on a spatial reference memory task in a radial arm maze. Mice tested after acquisition of the spatial task five days post-training exhibited high metabolic activity in the hippocampus, the subiculum, the entorhinal cortex, and rostral retrosplenial cortex, but low metabolic activity in frontal, anterior cingulate, and temporal cortex. The opposite pattern was observed in mice tested 25 days post-acquisition.

Studying transgenic mice heterozygous for a null mutation of α-calcium-calmodulin kinase II, Frankland and colleagues (2001) also found a time-related impairment in memory. They reported that these mice were impaired in contextual fear conditioning and a spatial reference water maze task at long ($\geq$ 10 days) but not short ($\leq$ 3 days) delays after acquisition of the tasks. These mice were found to exhibit deficient cortical but not hippocampal long-term potentiation (Frankland et al., 1998), thus highlighting a role for cortical function only at later time point after the acquisition of the tasks.

Using a combination of Fos immediate-early gene imaging and functional inactivation, Texeira and colleagues (2006) found that the anterior cingulate cortex appeared to be relatively more active after performance of a probe test in the water maze one month than one day after training, and that AMPA receptor blockade in that region resulted in an impairment only at the longer delay after the initial acquisition. They did not find a difference in Fos counts in CA1, CA3, or dentate gyrus between probe tests in the water

maze between the two retention intervals, and hippocampal receptor inactivation produced a deficit at both time points.

The change in balance of hippocampal and neocortical function observed in some but not all spatial tasks is part of a debate over the nature of the temporal role of hippocampal function (for recent reviews of the topic, cf. Squire et al., 2004; Wiltgen et al., 2004; Moscovitch et al., 2005). Very little is known about the role of medial temporal lobe regions *during* the acquisition of a spatial task, and the current study sought to address the nature of time-dependent processes by evaluating the role of hippocampal and extra-hippocampal regions at different performance levels.

In a review of inactivation studies, where electrical communication was inhibited, without damaging the tissue, it was emphasised that memory abilities, including spatial memory abilities, are time-dependent even on a short time scale quantified in minutes (Ambrogi Lorenzini et al., 1999). Studies investigating the role of regional activity on a shorter time-scale and at different stages (i.e. pre-training, training, post-training) using approaches other than lesions have explicitly investigated the time-dependent nature of brain functions generally by focusing on avoidance (Izquierdo and Medina, 1997) or object recognition tasks (e.g. Barker et al., 2006). While several studies in rats have compared the role of brain regions after the acquisition of a task to the performance of that task weeks later, few studies have investigated brain dynamics at different levels of learning, i.e. not after asymptotic levels were reached or after a long period deemed to reflect consolidation. In the domain of spatial tasks, it has been reported that the initial (5-min post-test) metabolic activation does not change with training, but that the dynamic time course of metabolic activation (1,3h post-test) is modified in several regions, including hippocampal regions, the entorhinal cortex, and the retrosplenial cortex (Bontempi et al., 1996). More directly related to plasticity, data relating to task mastery have been obtained for hippocampal expression of IEGs induced by different levels of training in a spatial and a non-spatial memory task in the water maze (Guzowski et al., 2001; He et al., 2002a). Likewise, IEG activity has been examined in several brain regions after performance in a radial arm maze task using a variant with fixed or a variable set of baited arms (He et al., 2002b), with the hippocampus playing a crucial role in the performance of the spatial tasks.

The current study sought to extend the findings of these studies by using a pre-training step, and the use of refined controls, and evaluating different brain regions. Furthermore, the current study capitalized on the sensitivity of the correlational approach to explore the relationships between regional immediate-early gene cell counts and task performance measures of spatial reference and working memory. The use of this method was based on a similar approach taken by Bertaina-Anglade and colleagues (2000), where the role played by different brain regions in relation to various levels of performance was considered with regards to the acquisition of an appetitive operant task.

Fos and Zif268 immediate-early gene protein products were visualised. Both of these immediate-early genes display patterns of expression that are associated with neural activity patterns and spatial memory formation (Herdegen and Leah, 1998; Hughes et al., 1999; Tischmeyer and Grimm, 1999; Guzowski, 2002; Davis et al., 2003). The brain regions that were selected for study are involved in episodic-like memory (reviewed by Aggleton and Pearce, 2001) and are anatomically connected, forming pathways that communicate and process information from neocortical polysensory areas (perirhinal and postrhinal cortices), via the lateral and medial entorhinal cortices to the hippocampus (dentate gyrus, CA1, CA3) and then to the retrosplenial cortex (Burwell and Amaral, 1998b; Witter et al., 2000; van Groen and Wyss, 2003). The present study tested the hypothesis that regional immediate-early gene activation patterns change with different levels of pre-asymptotic training.

The type of approach that compares experimental conditions by subtracting or normalising the signal can yield information about the topography of regions associated with a particular behavioural event. A specific goal of the present study was to evaluate, in an intact brain, the *interaction* of a group of regions. Thus, going beyond the identification of regions that play a role in specific memory functions (topography), where regions that are active at the same time are deemed to play similar roles (functional connectivity), the direct effects of interacting regions on each other as a function of a behavioural event can be addressed (effective connectivity). One statistical method used to estimate effective connectivity is covariance-based structural equation modelling. This approach has gained favour in human functional imaging studies (Horwitz et al., 1999). Since its introduction to the neurosciences in 1991 (McIntosh and Gonzalez-Lima), covariance-based structural equation modelling and related

developments have enabled the investigation of brain network dynamics in a manner that was not possible before from the observation of clinical cases or from lesions in animal models.

In the present study, the use of immediate-early gene imaging in an intact brain afforded the possibility of quantifying at a molecular level the activity of a subset of brain regions. In particular, an objective of the study was to evaluate the nature of regional interactivity at two different levels of mastery of the same task dependent on spatial memory. For the current study, simple, anatomically informed models that included a subset of limbic regions were used. Taking advantage of the fact that immediate-early gene imaging affords a form of functional imaging, analyses were conducted to obtain not only measures of simultaneous activation, but more specifically of the effective connectivity of the brain regions studied (cf. Jenkins et al., 2003). In other words, by defining an anatomically derived model and using structural equation modelling to produce path analyses, the current study addressed causal relations in a network of brain regions that are known to play a role in spatial memory. These analyses estimated the strength of the connections between the regions tested and their effective connectivity. The strength of the path coefficients that were obtained yield an estimation of the influence that one neural system exerts over another (Friston et al., 1993). Friston and colleagues, active proponents of the study of dynamic interactions between brain regions, have argued that the measure of effective connectivity is a reflection of synaptic connectivity and that changes in effective connectivity represent Hebbian or associative plasticity (Friston et al., 1993).

On the basis of previous Fos immediate-early gene studies using the radial arm maze, it was hypothesised that especially CA3, but also CA1 and the dentate gyrus, would yield important associations with performance parameters in the Trained groups (He et al., 2002a; He et al., 2002b). Corresponding information about mastery of a spatial reference task and IEG activity was not available for the remaining regions tested. Nevertheless, in light of the presence of head-direction cells in retrosplenial cortex (Chen et al., 1994), and of the important anatomical link this region provides between the hippocampus and cortical regions (van Groen and Wyss, 2003), it was hypothesised that the retrosplenial cortex would be found to play a pervasive role in the performance of the tasks tested. The postrhinal cortex receives substantially more visuospatial input than the perirhinal cortex (Burwell and Amaral, 1998a), and cells in the postrhinal

cortex can also exhibit stronger positional firing properties (Burwell and Hafeman, 2003) than those in the perirhinal cortex (Burwell et al., 1998). The perihinal and the postrhinal cortices have stronger connections with the lateral and the medial divisions of the entorhinal cortex, respectively, and these regions form two routes of communication into the hippocampus (Burwell and Amaral, 1998b; Witter et al., 2000). It has been shown that the medial but not the entorhinal cortex appears to carry a spatial signal (Hargreaves et al., 2005). Accordingly, it was hypothesised that the postrhinal and the medial entorhinal cortices would display more important associations with task performance than would the perirhinal and the entorhinal cortices.

I, therefore, propose to examine the following questions. 1) Does the expression of IEGs within the medial temporal lobe vary at different stages of learning? 2) Are there relative changes in different MTL structures? 3) By conducting correlational analyses, is it possible to identify more precisely the type of memory function that is associated with particular regions? 4) By using structural equation modelling is it possible to derive different patterns of associations within the MTL at different stages of learning?

2.2: Methods

2.2.1: Subjects

The subjects were 32 Dark Agouti male rats (Harlan, UK) that were food restricted and maintained at 85% of their free-feeding weight throughout the experiment. Animals were caged in pairs, one experimental rat with its yoked control, under a standard laboratory lighting regime (L:D, 13:11, lights on at 07.00). All rats were habituated to handling prior to start of the experiment.

2.2.2: Apparatus

The apparatus consisted of an elevated radial maze based on that originally described by Olton and Papas (1979). Eight arms (87 cm long x 10 cm wide) were symmetrically arranged around an octagonal central platform (34 cm diameter). The floor of the maze was made of laminated wood and the arms of clear Perspex were 24 cm high. Each arm contained at its end a 2-cm diameter food well that was 0.5 cm deep. The walls of the central platform were formed by eight Perspex doors connected to a pulley system, thus enabling the experimenter control of the rat's access to the arms.

The testing took place in two rooms, each with a radial arm maze of the same dimensions. Both rooms were distinctive in shape and size, and salient cues (such as posters on the walls). The luminance of each room was similar.

2.2.3: Behavioural training

The rats received some of the sucrose pellets used as food reward in their home cage a few days prior to start of the experiment. The animals were next habituated to the testing environment and underwent performance shaping to lead them to seek sucrose pellets at the end of the arms, prior to training of the experimental task. Pairs of animals (an experimental animal with its yoked control) underwent two 15 min habituation sessions in the apparatus, followed the next day by another two sessions where the animals individually explored the apparatus until all the sucrose pellets had been retrieved.

The rats were next trained on a standard reference memory task (Olton and Papas, 1979). At the start of a trial, four of the eight arms were baited. A rat was placed in the central platform and the arms were opened simultaneously to allow the rat to explore the arms and retrieve the sucrose pellets. An arm was considered selected when both hind paws of the rat passed the threshold of the door into the arm. The doors were then all closed, that of the currently explored arm being reopened the moment the rat reached the end of the arm. Upon return of the rat to the central platform, after having eaten the food reward, the doors were kept closed for 10 s. Training was continued until all four baited arms had been visited, or 10 min had elapsed. The same four arms were baited throughout the pre-training, while different sets of arms were chosen for each pair of rat. Additionally, in order to try to minimise the use by the rats of intramaze cues to guide their performance, these cues were made irrelevant by rotating the maze one arm after each trial. Daily training sessions consisted of four trials, and the animals were trained for a maximum number of 14 sessions.

Pre-training has been used to help dissociate different components of spatial task performance (discussed in Cain, 1998). The use of task pre-training has resulted in the observation that the performance of a task is dependent on many components, such as acquisition of the task demands, and the acquisition and use of a strategy, all of which do not necessarily rely on the same anatomical structures or molecular cascades (e.g.

(e.g. Whishaw, 1989; Bannerman et al., 1995). In order to assess the molecular anatomical mapping of allocentric spatial memory, the rats in the current experiment were first trained on the same task in a separate room, so that once in the second room, the influence of learning the task demands on brain region activation would be minimised and any difference could be attributed to learning and using the allocentric spatial cues in relation to the position of the baited arms in the new environment. In this new room, the rats were trained for five daily sessions, again comprising four trials per session, each lasting until all 4 rewards had been retrieved, or otherwise of a maximal duration of 10 min.

In order to compare immediate-early gene activity during early and late acquisition, animals in the experimental group were paired with an animal undergoing the same training scheme, but staggered by three sessions. All four animals within a running cohort (two Trained—early and late; two Yoked, early and late) were killed on the same day. The staggered animals underwent the same training scheme, except that they only had two sessions in the second maze. Each experimental cohort consisted of a rat from each group (Trained for 2 and 5 sessions, and Yoked for 2 and 5 sessions). The design of the study is represented in Figure 2.1.

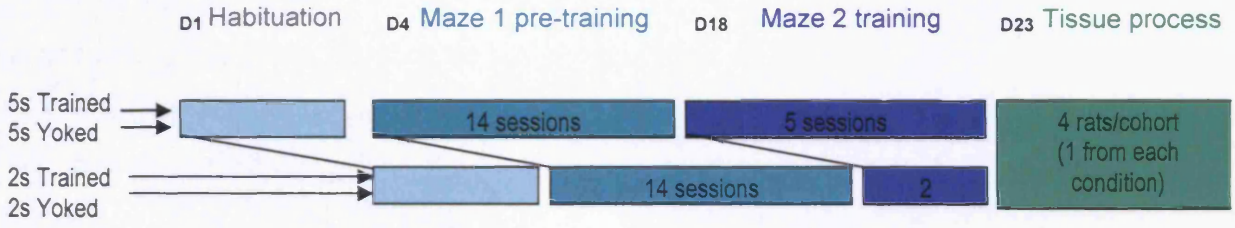

Figure 2.1: The design of the study. Each cohort consisted of one rat from each condition, i.e. 2- and 5-session experience, and Trained and Yoked. Rats were habituated to a maze in a first room, and then trained to perform a concurrent spatial discrimination. After acquisition of the task, the rats were next trained in a new maze in a second room. Two groups of rats were trained for a different number of sessions (two and five) in the second maze. Additionally, each rat was yoked to a control rat (see text for details).

2.2.4: Behavioural parameters

Two main types of parameters were used to characterise the learning and the performance of the rats, time and arm entry errors. The latter type of parameter comprised of three measures: 1) Reference memory errors, as defined by an entry into a non-rewarded arm; 2) Working memory errors, as defined by re-entry into an arm previously visited during the current trial. Working memory errors were further divided into errors committed by a re-entry into a previously rewarded arm, here labelled "working (non-reference)" errors, and those committed by re-entry into a never-rewarded arm, labelled "working (reference)" errors.

Performance measurements were compiled, for the second maze, separately for each type of error. These measurements consisted of the total number of errors committed, the number of errors committed only in the last test session, and the rate of learning. In order to obtain a value for the rate of learning, a linear function was fitted to the data points and the value of the slope was used as a representation of the rate of learning.

2.2.5: Sham-conditioning protocol

Each animal was paired with a yoked control that was also food restricted. This yoked control rat was only allowed to explore one pre-determined arm at a time, and only four different arms per session. The number of arm entries was equal to that of the rat to which it was yoked. Furthermore, working memory errors produced by the experimental animal were controlled for by presenting the yoked control with an unbaited arm for each working memory error made. Rarely, in order to prevent the trials from exceeding 10 m, when deemed necessary an animal was guided in and out of the pre-selected arms by the experimenter. Overall, it was intended that the experience of the yoked rats would be matched as closely as possible for the number of arms explored, for rewarded and non-rewarded arm explorations, duration of the exploration in the maze, and also, especially in the final test session, with the number of different arms explored. The choice of the four arms visited by the yoked control rats changed each session, and was the same as the experimental rats on the final session. Thus, for the final session, the relative movement of a pair of experimental and yoked rats in the room was intended to be very similar in terms of distances and places traversed, the time spent in the maze as well as the number of rewarded excursions in the maze.

2.2.6: Immunohistochemistry

Ninety minutes after the onset of the last test session, the rats were irreversibly anaesthetised with sodium pentobarbital (140 mg/kg, Euthatal, Rhone Merieux, UK) and perfused transcardially with 0.1 M PBS followed by 4% paraformaldehyde in 0.1 M PBS. The brains were removed and post-fixed in 4% paraformaldehyde for four hours and then transferred to 25% sucrose overnight. Sections were cut at 40 μm on a freezing microtome in the coronal plane. Adjacent series were collected in 0.1 M PBS for Nissl staining and in 0.1 M PBS containing 0.2% Triton X-100 (PBST) for immunohistochemical visualisation of Fos and Zif268 proteins.

A single experimental cohort was processed together, each Trained rat in the same container as its Yoked control to minimise confounds due to immunohistochemical artefacts. Endogenous peroxidase activity was blocked by washing the sections with 0.3 % hydrogen peroxide in PBST for ten minutes, and then four times with PBST alone for the same duration. Sections were incubated at 4°C for 48 hours in PBST with rabbit polyclonal antibody for Fos (1:5000, Ab-5, Oncogene Science) and Zif268 (1:3000, C-19, Santa Cruz). Sections were then rinsed for ten minutes in PBST, four times. Next they were incubated in biotinylated secondary antibody, and then avidin-biotinylated horseradish peroxidase complex in PBST (Elite Kit, Vector Laboratories). Sections were next rinsed in Tris non-saline buffer (pH 7.4). Finally, immunoreactivity was visualised with diaminobenzidine (DAB Substrate Kit, Vector Laboratories) chromogen incubation. Sections were then mounted on gelatinised slides. These slides and another series of cresyl violet stained tissue were dehydrated through a series of alcohol gradients and coverslipped.

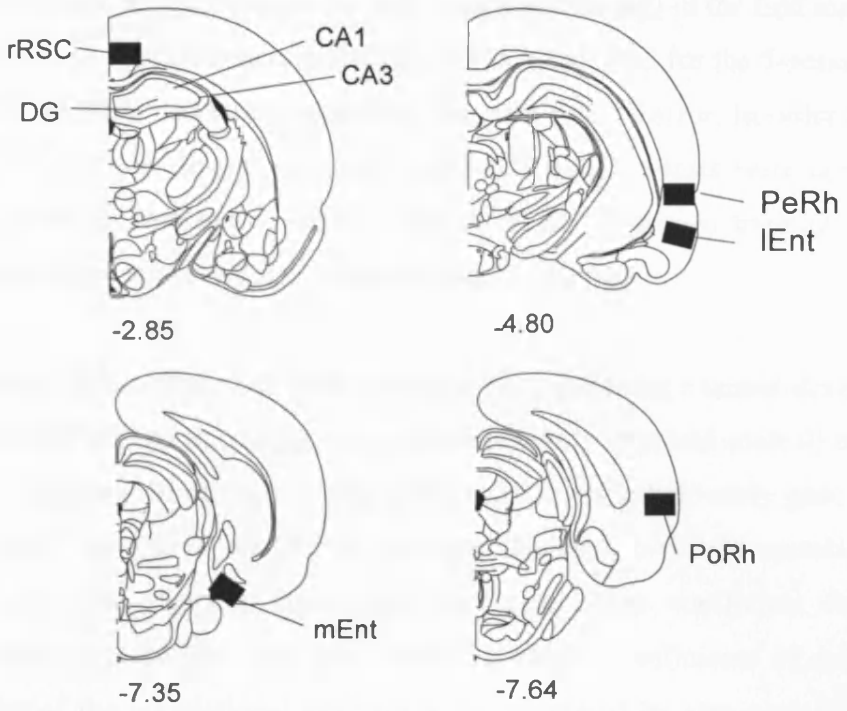

Figure 2.2: Regions of interest were immediate-early gene cell counts were obtained (PeRh=perirhinal cortex; PoRh= postrhinal cortex; lEnt= lateral entorhinal cortex; mEnt= medial entorhinal cortex; rRSC=rostral retrosplenial cortex; DG=dentate gyrus; CA1,3=Cornus Ammoni, subregion 1 and 3.

2.2.7: Cell counts

Sections were scanned using a Leitz Dialux 20 microscope equipped with a Dage MTI CCD72S camera interfaced to a PC computer by a Scion LG-3 frame-grabber board. After image processing, counts of the stained nuclei were obtained using the public domain NIH Image program. Cortical areas were assessed using counts above threshold in a standard frame sample area (0.78 x 0.55 mm) using a 10x objective. The regions of interest are depicted in Figure 2.2. For hippocampal subfield counts (dentate gyrus, CA3, and CA1), the entire extent of the target region within the selected coronal sections was assessed (see Figure 2.2). Counts were typically taken from three consecutive sections from both hemispheres for all regions, and these counts were averaged to produce a mean.

2.2.8: Statistical analyses

Mixed-design analyses of variance (ANOVA) were conducted to evaluate the performance of both training groups (2- and 5-session training) in the first maze. For the second maze only a repeated measures analysis was conducted for the 5-session training group. ANOVAs were conducted separately for each type of error. In order to evaluate performance at the two crucial sessions, sessions 2 and 5, t-tests were compared the mean error numbers between sessions 2 and 5 for the 5-session training group, and between session 2 of the 2- and the 5-session training groups.

Immediate-early gene cell counts were evaluated by conducting a mixed-design analysis of variance (ANOVA) on normalised cell counts (training to yoked control) between the two levels of training. In order to evaluate the role of immediate-early gene activity in individual brain regions in relation to task performance, bivariate correlations were calculated using the Pearson product-moment correlation coefficient for regional immediate-early gene activity and performance metrics. Coefficients of determination for the results of the correlational analyses were calculated by obtaining the square of the r values. The SPSS 14.0 (Chicago) statistical package was used for the analyses described above.

Path analyses were obtained by using structural equation modelling based on the Maximum Likelihood Estimation (MLE), using the statistical package Amos 6.0 (Chicago). It is recommended that when using this method with samples smaller than 500, the ratio of the chi-square to the degrees of freedom should be less than 2. The MLE method is the most frequently used, but may be more dependent than other methods on the assumption of multivariate normality when sample sizes are small (Tabachnik and Fidell, 1996, p. 747). Another estimation method, Unweighted Least Squares (ULS), was used to confirm the results. This method is less dependent on multivariate normality and is not affected by sample numbers. The ULS method produced similar results, but since its use is less widespread because it does not generate a significance level index, only the MLE results are reported. Furthermore, in order to remain conservative because of inconsistencies yielded by the numerous fit indices available, in addition to the MLE significance chi-square, several measures of model fit were reported, as recommended by Tabachnik and Fidell (1996, p. 752). These fit indices will be discussed next.

Two types of models were tested against the models derived in the current study. One model is "saturated", and all the regions are interconnected. A saturated model provides the most fit, and the goodness of fit index (GFI) compares the similarity of this particular model to the tested model by providing an index of the variance. In contrast, the comparative fit index (CFI) compares the tested model to an independent model. An independent model has the least fit, and a good CFI means that the tested model is opposite to the independent model. The CFI was chosen because it penalises for small samples sizes. Using a different approach for the same comparison as the CFI, the Tucker-Lewis coefficient (TLI) is less affected by sample size. Finally, another index is the Root Mean Square Error of Approximation (RMSEA). This index estimates lack of fit compared to the saturated model, but based on the residuals. Good fitting models either have a GFI $\geq$ 0.9, CFI $\geq$ 0.90-0.95, TLI $\geq$ 0.95, or RMSEA $\leq$ 0.05.

First, simplex models were tested, based only on the serial, unidirectional, anatomical connections between each node of the network (Figure 2.3a). Each model only considered five regions, because the number of degrees of freedom precluded an inclusive analysis of all the regions tested. Two complementary models were tested for each condition, evaluating two streams of communication (Burwell and Amaral, 1998b; Witter et al., 2000). Based on the origin of information transmission, these were designated as caudal and rostral routes into the hippocampus and out to the retrosplenial cortex (Figure 2.3b).

a.

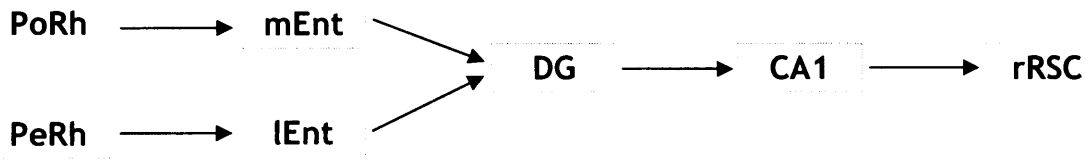

b.

Caudal route

PoRh ⟶ mEnt ⟶ DG ⟶ CA1 ⟶ rRSC

Rostral route

PeRh ⟶ lEnt ⟶ DG ⟶ CA1 ⟶ rRSC

Figure 2.3: Anatomical pathways (a), and the simplex models tested (b).

While attempts were made to integrate the CA3 into the models, the inclusion of this region generated a substantial reduction in the fitness of the models. The independent function of CA3 and CA1 under various conditions has been recently emphasised (Manns and Eichenbaum, 2005). It is plausible that the CA3 region may play a more independent role relative to the models tested and in the behavioural context of the current study. The CA3 region may, for example, exhibit more robust activity patterns with other efferents such as the septum (e.g. Swanson and Kohler, 1986). Alternatively, it is also plausible that the failure to integrate this region in the models stemmed from the fact that this structure displays auto-associative characteristics as a result of recurrent connections from the CA3 to itself (reviewed in Amaral and Witter, 1989). It is possible that reverberating activity particular to the CA3 may make it difficult to integrate it into a model based on covariance analyses. As such, as can be seen in Figure 2.3, this region was omitted from the analyses.

Next, anatomically plausible paths between regions were freely estimated to obtain increases in the fit of the model. No more paths were added when the model reached a satisfactory fit level in order to maintain the most parsimonious model. Thus, final models were anatomically derived and tested against statistical assumptions; they were not simply connectional models that were purely fitted to the data.

2.3: Results

2.3.1: Behavioural analyses

In terms of the analyses for task performance of the 5-session training group in the second maze, some rats did not explore four arms or more in each of the trials during the first session, and only the remaining rats (n=5) were included in that particular session. The other analyses included all the subjects (n=8 per group).

2.3.1.1: Reference memory errors

The mean number of reference errors per session is presented in Figure 2.4. A mixed-design ANOVA revealed that the number of reference errors in the first maze significantly decreased with training [F (9,108) = 16.64, $p<0.0001$]), and there was no difference in the rate of acquisition of reference memory between the 2-session and the 5-session groups [F (1,12) = 0.15, $p=0.707$]), nor was there any interaction between the two groups [F (9,99) = 1.41, $p=0.193$]).

The rats in the 5-session group committed a reduced number of reference errors with training in the second maze [F (4,16) = 4.13, $p=0.017$]). A paired-samples t-test (one-tailed) revealed that the mean number of reference errors committed by the 5-session group was significantly higher during the second session (M=10.0, SD=3.5) than the fifth session (M=3.9, SD=3.7, $p=0.007$). Additionally, an independent samples t-test (two-tailed) revealed that the mean number of reference memory errors committed by the 2- and 5-session training groups in their respective second session was not significantly different (2-session, M=10.0, SD=3.9; 5-session, M=10.0, SD=3.5, $p=1.000$).

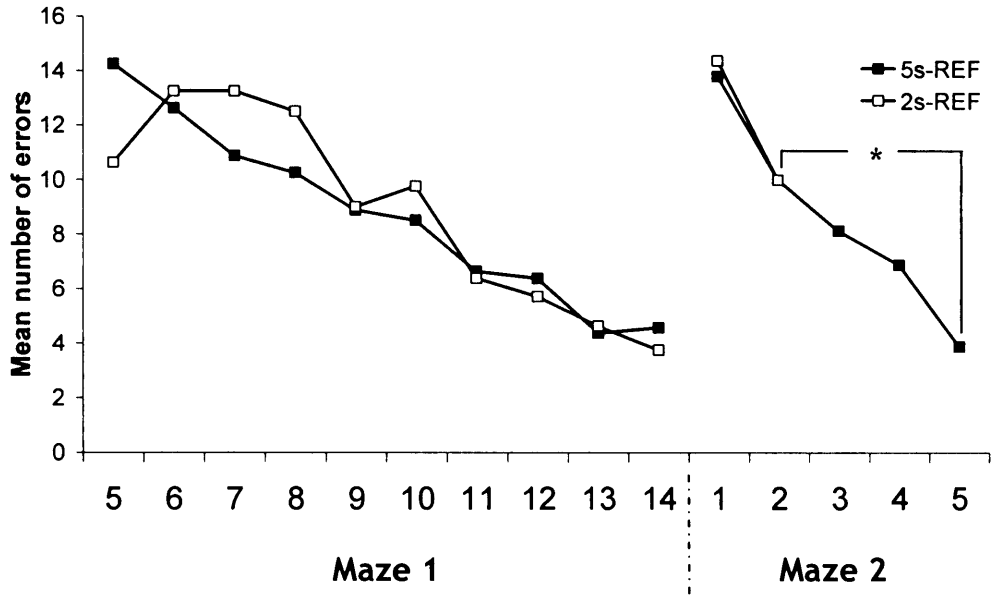

Figure 2.4: Mean number of reference memory errors per session. Sessions prior to 5 are not presented because they comprise a disproportionate number of incomplete trials, where often fewer than four arms were visited. Performance was significantly different between the two levels of training, i.e. between the second and the fifth training sessions in the second maze. (2,5s=2,5-session training; REF= reference memory) *p<0.05.

2.3.1.2: Working memory errors

2.3.1.2.1: Working memory (non reference) errors

The mean number of working memory errors per session is presented in Figure 2.5. As shown in Figure 2.5a, a mixed-design ANOVA revealed that the number of working (non reference) errors committed by the rats in the first maze significantly decreased with training [F (9,108) = 3.18, p<0.0001]), and that there was no difference in the rate of acquisition of working (non reference) memory between the 2-session and the 5-session groups [F (1,12) = 0.55, p=0.818]), nor was there any interaction between the two groups [F (9,108) = 1.23, p=0.287]). In the second maze, working (non reference) memory performance initially improved but then stabilised, and there was no significant effect overall of training session on working (non reference) errors for the rats in the 5-session group in the second maze [F (4,16) = 1.72, p=0.194]).

In order to verify the crucial comparison of means between the second and the fifth sessions, a paired-samples t-test (one-tailed) revealed that the mean number of working

(non reference) errors committed by the 5-session group was significantly higher during the second session (M=2.4, SD=1.2) than the fifth session (M=1.1, SD=0.8, p=0.025). Additionally, an independent samples t-test revealed that the mean number of errors of working (non reference) errors committed by the 2- and 5-session training groups in their respective second session was not significantly different (2-session, M=2.1, SD=2.4; 5-session, M=2.4, SD=1.2, p=0.793).

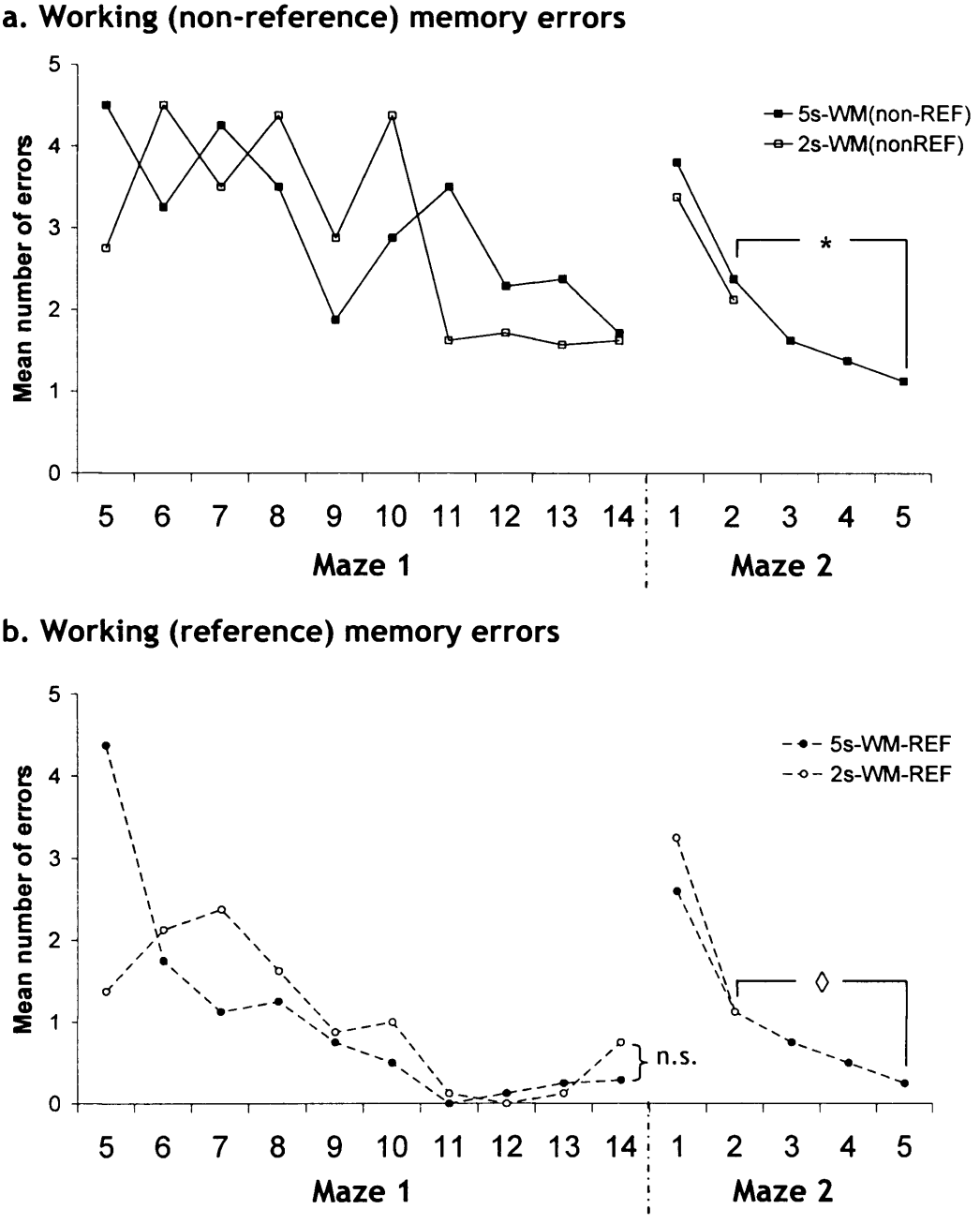

Figure 2.5: Mean number of working (non reference, a) and working (reference, b) memory errors per session. Sessions prior to 5 are not presented because they comprise a disproportionate number of incomplete trials, where often fewer than four arms were visited. Performance was significantly different between the two levels of training, i.e. between the second and the fifth training sessions in the second maze.(2,5s=2,5-session training; WM= working memory; WM-REF=re-entry into a non-rewarded arm; nonREF=re-entry into a rewarded arm). *p<0.05; ◊p=0.056.

2.3.1.2.2: Working memory (reference) errors

As shown in Figure 2.5b, a mixed-design ANOVA revealed that the number of working (reference) errors committed by the rats in the first maze significantly decreased with training [F (9,108) = 8.09, $p<0.0001$]), and that there was no difference in the rate of acquisition of working (reference) memory between the 2-session and the 5-session groups [F (1,12) = 0.007, $p=0.932$]). There was an interaction between training session and group [F (9,108) = 2.88, $p=0.004$]), but importantly, an independent samples t-test (two-tailed, equal variances not assumed) revealed that the mean number of working (reference) memory errors was not different between the two groups on the last test session in the first maze (2-session, M=0.75, SD=1.16; 5-session, M=0.29, SD=0.76, $p=0.372$).

The rats in the 5-session group committed a reduced number of working (reference) errors with training in the second maze [F (4,16) = 3.22, $p=0.040$]). A paired-samples t-test (one-tailed) revealed that the mean number of working (reference) errors committed by the 5-session group was marginally higher during the second session (M=1.1, SD=1.3) than the fifth session (M=0.25, SD=0.46, $p=0.056$). Additionally, an independent samples t-test (two-tailed) revealed that the mean number of working (reference) errors committed by the 2- and 5-session training groups in their respective second session was not significantly different (2-session, M=1.13, SD=2.10; 5-session, M=1.13, SD=1.25, $p=1.000$).

2.3.1.1: Time

The amount of time the subjects spent in the maze is presented in Figure 2.6. A univariate ANOVA on the time data revealed that the total duration of time spent in the last test session was not significantly different between any of the conditions. There was no significant effect of condition (i.e. training or forced choice, [F (1,28) = 0.00, $p=0.983$] or of extent of maze experience [F (1,28) = 2.37, $p=0.135$], and there was only a marginally significant interaction between condition and maze experience [F (1,28) = 0.49, $p=0.078$]. Additionally, an independent samples t-test (two-tailed) revealed that the total duration of time spent in the second maze did not differ between experimental and yoked subjects in the 2-session (Trained, M=2786.0, SD=858.1; Yoked, M=3060.8, SD=1429.6, $p=0.648$) or 5-session experience groups (Trained, M=6005.6, SD=2532.1; Yoked, M=6045.3, SD=2175.2, $p=0.974$).

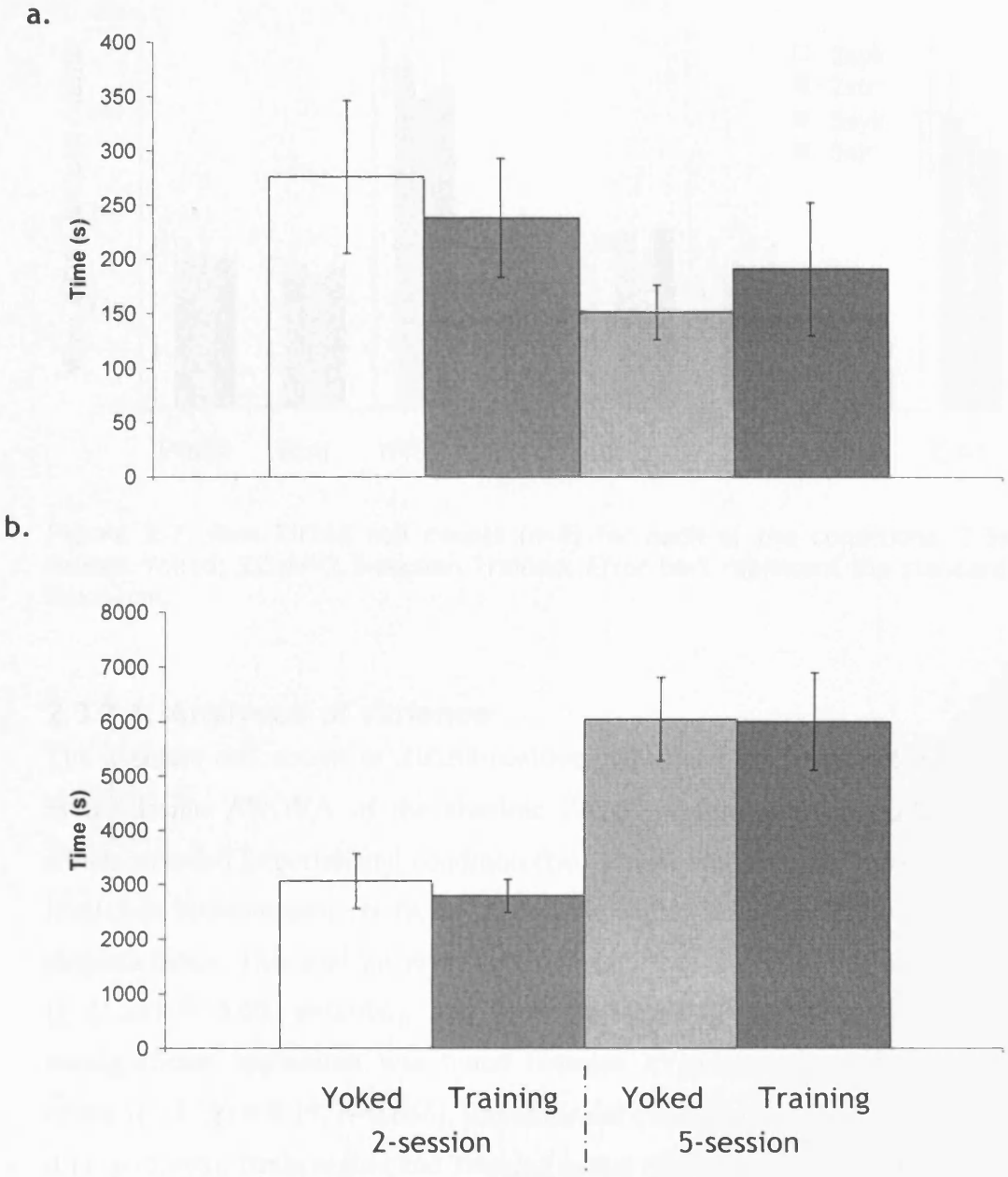

Figure 2.6: Time spent in the second maze during the final session (a) and in total (b). There were no significant differences in time spent in the maze between groups on the last session or overall between trained and yoked subjects in either the 2-session or 5-session experience groups. Error bars represent the standard error of the mean.

2.3.2: Immunohistochemical results

In light of unsuccessful labelling of Fos-positive because of technical reasons (faulty antibodies), data for this IEG were only obtained for half of the subjects, i.e. four subjects per group. Because of the resulting low numbers per group, these data have reduced power and so it was thus decided not to present them. The data for Fos-positive cell counts can, however, be found in Appendix A for the sake of comparison.

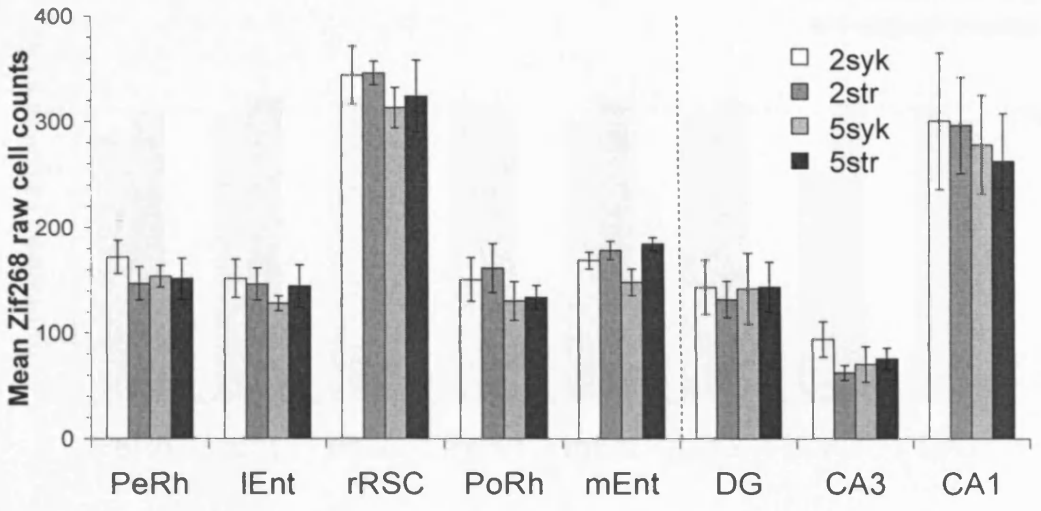

Figure 2.7: Raw Zif268 cell counts (n=8) for each of the conditions. 2,5syk= 2,5-session Yoked; 2,5str=2,5-session Trained. Error bars represent the standard error of the mean.

2.3.2.1: Analyses of variance

The absolute cell counts of Zif268-positive cell nuclei are presented in Figure 2.7. A mixed-design ANOVA of the absolute Zif268-positive cell counts was conducted, which included Experimental condition (two levels) and Training extent condition (two levels) as between-subjects factor, and Brain region condition (8 levels) as a within-subjects factor. This analysis revealed a nonsignificant effect of Experimental condition [F (1,28) = 0.00, p=0.996], and Training extent [F (1,28) = 0.70, p=0.409]. A nonsignificant interaction was found between Experimental condition and Training extent [F (1,28) = 0.19, p=0.666], Experimental condition and Brain region [F (7,196) = 0.11, p=0.998], Brain region and Training extent [F (7,196) = 0.10, p=0.998]. There was no significant three-way interaction between Experimental condition, Training extent and Brain region [F (7,196) = 0.05, p=1.000].

The IEG Zif268-positive cells counts in both Trained groups were next normalised to the counts of their Yoked controls. As shown in Figure 2.8, the results of the two-way ANOVA on these normalised Zif268-positive cell counts revealed that there was no statistically significant main effect of brain region [F (7,98) = 1.07, p=0.39], nor of training extent [F (1,14) = 3.29, p=0.091], neither was there a significant interaction between brain region and extent of training [F (7,98) = 1.53, p=0.165].

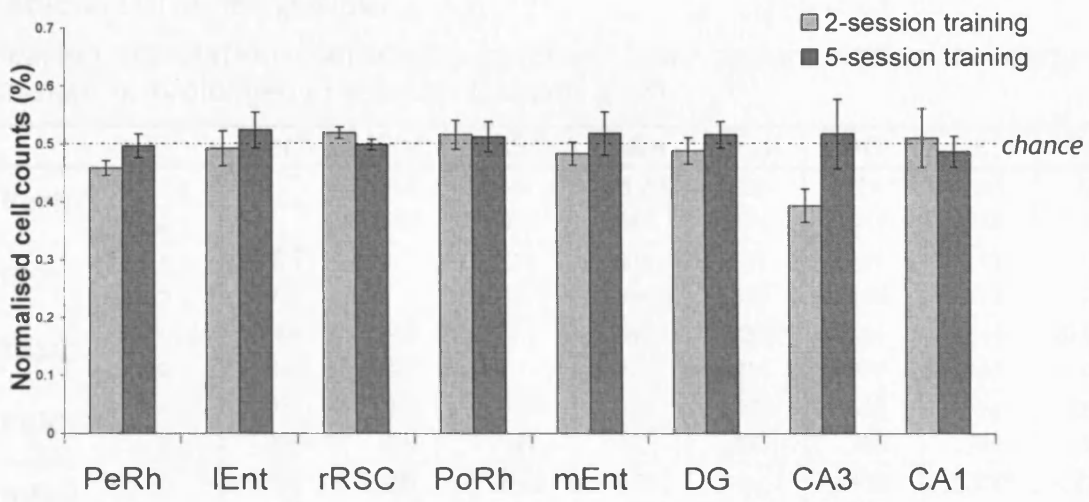

Figure 2.8: Average Zif268 cell counts, normalised for each trained subject to its yoked control (n=8 per condition). No overall difference was found in normalised Zif268 cell nuclei cell counts as a result of longer training in the radial arm maze. Error bars represent the standard error of the mean.

2.3.2.2: Structural equation modeling

The previous analyses of variance were based on the normalisation of cell counts from one behavioural group to another. The results of such analyses can yield information about differences in regional activation between groups, but cannot address the issue of network dynamics directly. This particular issue is especially relevant in light of the objectives and the design of the present study, where the two experimental groups that were compared performed exactly the same task, only the average level of mastery of the task distinguished them. One of the goals of the current study was to obtain information on the nature of the interaction between the regions tested, not only whether or not these regions differentially exhibited Zif268 active cells between the two levels of performance of the task. In order to obtain this information, path analyses were conducted.

2.3.2.2.1: Inter-regional Zif268 count correlations

First, before presenting the estimated influence of the brain regions on each other (effective connectivity), concurrent activation measures (functional connectivity) will be presented in the form of Pearson correlation coefficients (Tables 2.1 and 2.2).

Table 2.1: Trained groups.

Pearson correlation coefficients between brain regions during the early (2-session) or prolonged (5-session) training (n=8).

		Perh	lEnt	rRSC	PoRh	mEnt	DG	CA3	CA1
Perh	*r*	-	.645	.697	**.717***	-.365	**.721***	-.098	.544
	p		*.084*	*.055*	*.045*	*.374*	*.044*	*.818*	*.163*
lEnt	*r*	**.791***	-	.315	.628	.181	.301	.213	.133
	p	*.019*		*.447*	*.096*	*.668*	*.468*	*.613*	*.754*
rRSC	*r*	.084	.315	-	.486	**-.830***	.654	-.545	**.919****
	p	*.843*	*.447*		*.222*	*.011*	*.079*	*.163*	*.001*
PoRh	*r*	.007	.389	.515	-	-.078	.553	.114	.264
	p	*.987*	*.341*	*.192*		*.855*	*.155*	*.789*	*.527*
mEnt	*r*	.449	.267	-.642	-.455	-	-.419	**.811***	**-.791***
	p	*.264*	*.523*	*.086*	*.257*		*.302*	*.014*	*.019*
DG	*r*	-.164	.094	.539	.125	-.527	-	.110	**.724***
	p	*.697*	*.825*	*.168*	*.768*	*.180*		*.795*	*.042*
CA3	*r*	.488	-.109	-.102	-.566	.304	-.315	-	-.376
	p	*.220*	*.797*	*.810*	*.143*	*.464*	*.447*		*.358*
CA1	*r*	-.520	-.209	**.752***	.251	**-.712***	.459	-.314	-
	p	*.187*	*.619*	*.031*	*.549*	*.048*	*.252*	*.449*	

The upper diagonal matrix is based on data from the early Training condition; the lower diagonal matrix is based on data from prolonged Training condition. *p*=statistical probability. *r*=Pearson product-moment coefficient. Correlation (two-tailed) is significant at the 0.05 (*) or 0.01 level (**).

Table 2.2: Yoked groups.

Pearson correlation coefficients between brain regions during the early (2-session) or prolonged (5-session) yoked experience (n=8).

		Perh	lEnt	rRSC	PoRh	mEnt	DG	CA3	CA1
Perh	*r*	-	.289	.025	.306	-.146	.352	.225	-.024
	p		*.487*	*.953*	*.461*	*.730*	*.393*	*.592*	*.955*
lEnt	*r*	.109	-	.423	.516	-.079	.462	.004	.267
	p	*.797*		*.297*	*.190*	*.852*	*.250*	*.992*	*.523*
rRSC	*r*	-.457	.396	-	.643	-.696	**.807***	.187	**.791***
	p	*.255*	*.332*		*.085*	*.055*	*.015*	*.657*	*.020*
PoRh	*r*	.295	.349	.423	-	-.479	**.868****	.628	.325
	p	*.478*	*.396*	*.296*		*.229*	*.005*	*.096*	*.432*
mEnt	*r*	.647	.204	**-.729***	.006	-	-.491	-.053	-.689
	p	*.083*	*.628*	*.040*	*.989*		*.217*	*.901*	*.058*
DG	*r*	-.425	.222	.649	-.333	-.597	-	.649	.360
	p	*.294*	*.597*	*.082*	*.420*	*.118*		*.082*	*.380*
CA3	*r*	.096	.282	.386	.010	-.065	.609	-	-.317
	p	*.820*	*.498*	*.345*	*.981*	*.879*	*.109*		*.444*
CA1	*r*	-.649	.242	**.899****	.038	**-.847****	**.804***	.229	-
	p	*.082*	*.563*	*.002*	*.929*	*.008*	*.016*	*.585*	

The upper diagonal matrix is based on data from the early Yoked condition; the lower diagonal matrix is based on data from the prolonged Yoked condition. Correlation (two-tailed) is significant at the 0.05 (*) or 0.01 level (**).

As seen in Tables 2.1 and 2.2, the only significant correlation for both Trained or Yoked rats was between the retrosplenial cortex and CA1. There were some regional associations that were unique to both the Trained and the Yoked groups. Irrespective of the number of sessions in the maze, the Trained groups exclusively showed positive correlations between the perirhinal cortex and the postrhinal cortex, the lateral entorhinal cortex, as well as the dentate gyrus. Additionally, a positive correlation was also found between the medial entorhinal cortex and the CA3 hippocampal subfield. In terms of the Yoked groups, the only exclusive significant correlations were between the dentate gyrus and both the postrhinal cortex as well as the retrosplenial cortex.

In spite of the low sample sizes, the significant correlations all indicated a strong relationship between the variables, as the lowest coefficient was >0.71, which is beyond the value considered for a large effect (i.e. 0.10 = small, 0.30 = medium, 0.50 = large effect, cf. Cohen, 1992). The brain regions for which Zif268 cell counts were significantly associated with each other shared a minimum of 50 % of their variance (i.e. based on r^2, the coefficient of determination). It may be reasonable to assume that if Type I errors were committed, the significant associations yielded would have been found to range from small to large effect sizes. On the contrary, only relationships of high strength were found. Furthermore, the correlational analyses for the functional connectivity of brain regions revealed significant correlations that were almost exclusively between regions known to be directly anatomically connected. The only exception was the positive association between the postrhinal cortex and the dentate gyrus in the 2-session Yoked group, while the links are deemed to be poly-synaptic via the medial entorhinal cortex (Naber et al., 2001). Curiously, this group did not exhibit a significant correlation between the postrhinal cortex Zif268 and medial entorhinal cortex cell counts, in spite of their dense interconnections.

It is important to note that the stronger the correlations between the brain regions, the more power structural equation modelling has to detect an incorrect model (Tabachnik and Fidell, 1996). The results of structural modelling analyses are presented next. Again, it is emphasised that the modelling analyses were anatomically driven.

2.3.2.2.2: Path analyses

2.3.2.2.2.1: Best-fit model and condition comparisons

The path analyses were conducted according to two different approaches. The first approach presented was based on finding the absolute best fit for a putative network underlying performance in the radial arm maze task tested in the current study. The best fit was obtained for the caudal route of the Trained rats in the 5-session condition. The analyses for the network in the 5-session caudal route in the Trained group yielded a model with consistently very high fit indices (see Figure 2.9b). This best-fitting model was then used as a template and tested in the other conditions for the caudal routes (see Figures 2.9 and 2.10). A homologous model was also tested for the rostral route in all conditions (see Figures 2.11, and 2.12).

The results of these analyses revealed that the model did not fit all conditions well. In the Trained groups, for example, while the model exhibited high fit indices in the caudal route for the 5-session group, for the 2-session group the level of fit appeared to be only marginal. In effect, because the ratio of the chi square to the degrees of freedom was larger than 2 (see Method section), the null hypothesis that the model fit the data could not be accepted. Therefore, the model did not fit the data for the trained group in the 2-session condition.

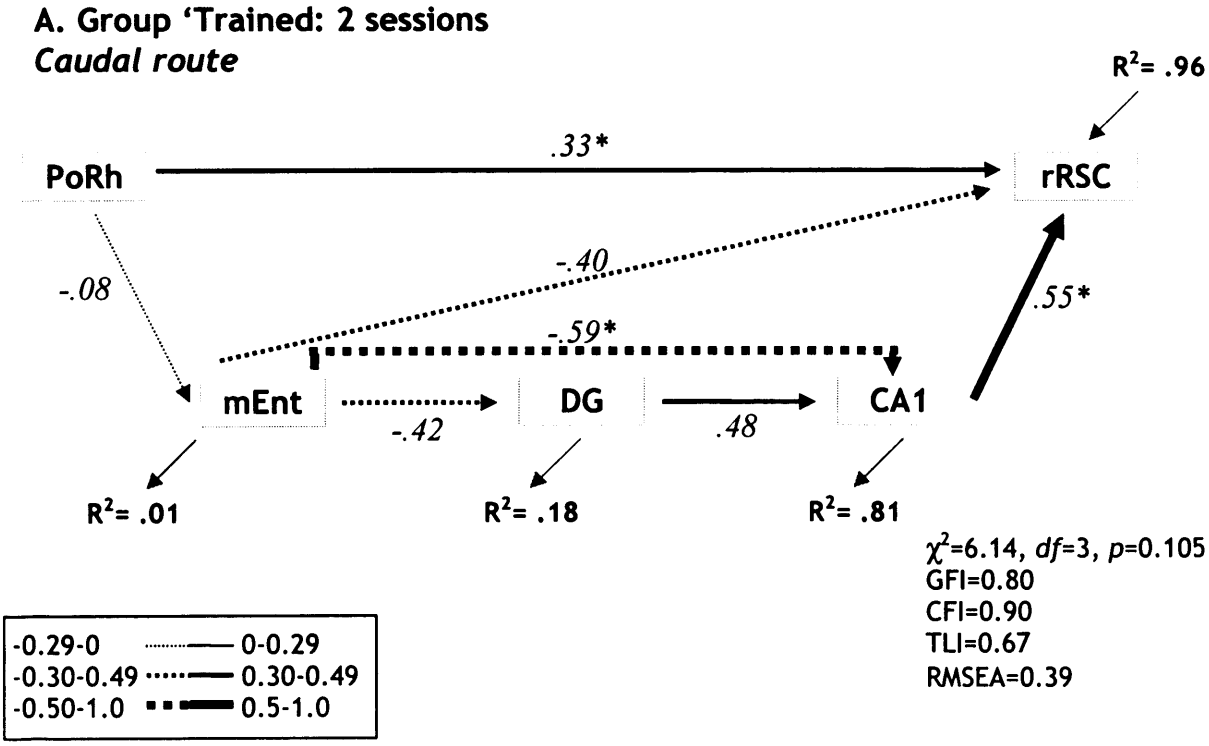

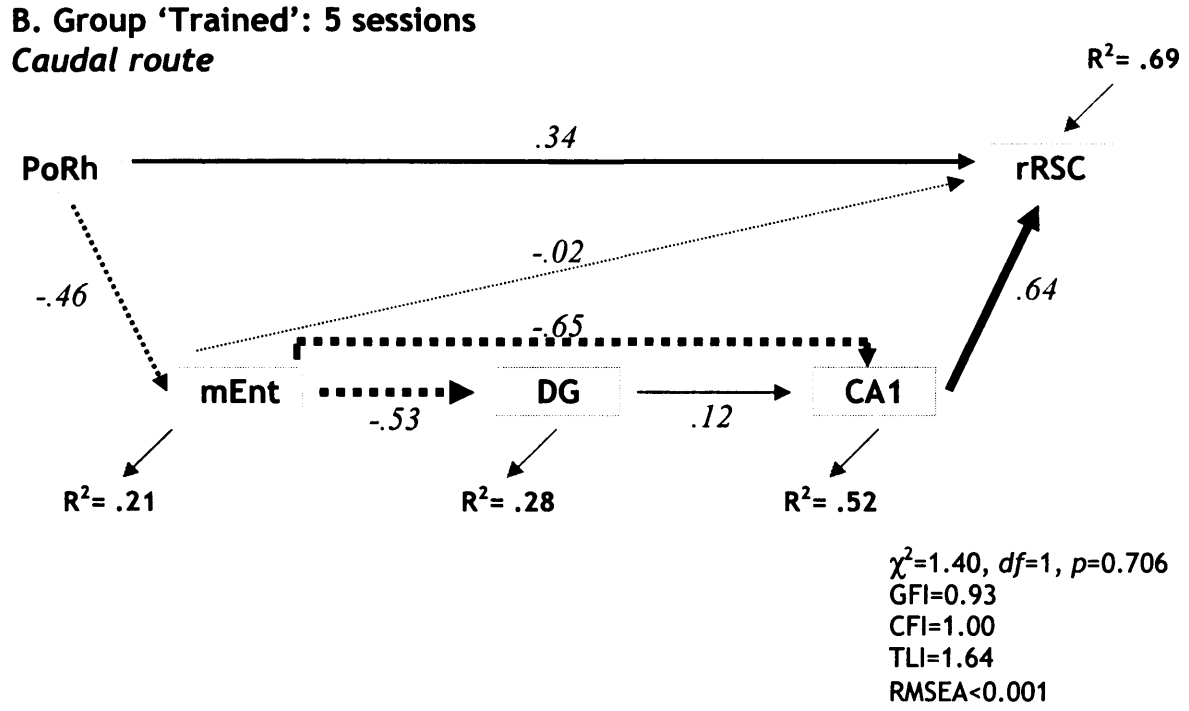

Figure 2.9: Representation of the path analyses of the caudal route for the Trained subjects in the two-session (A) and five-session groups (B).

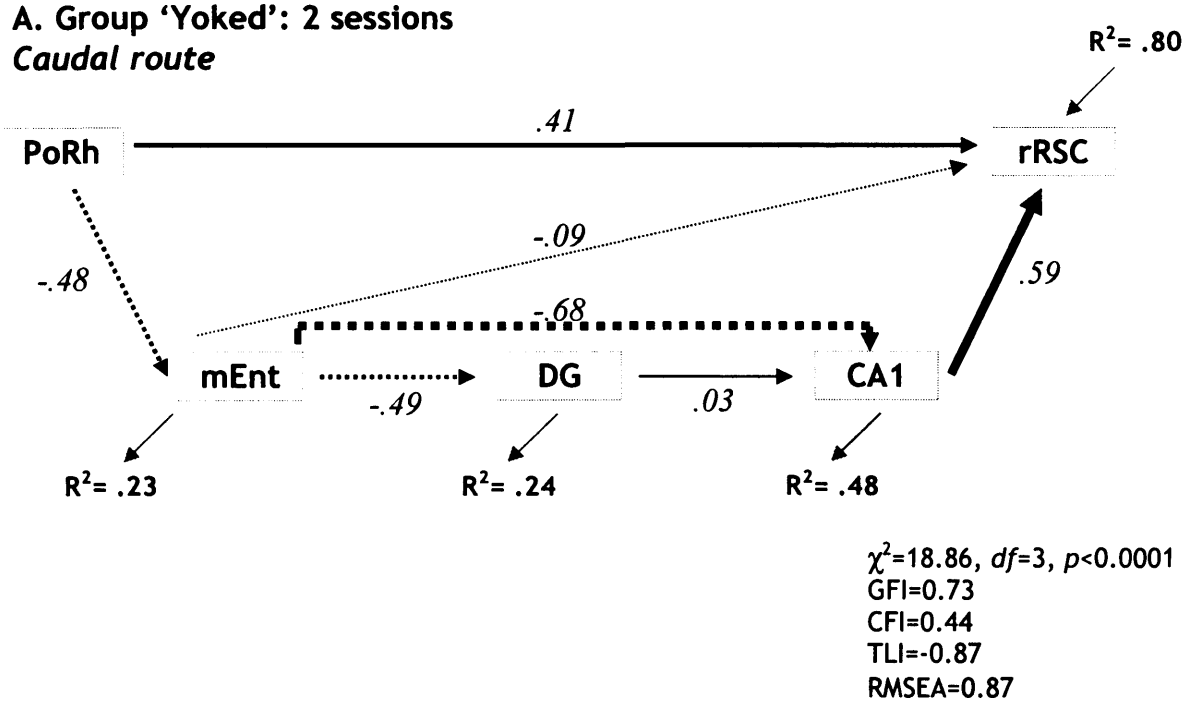

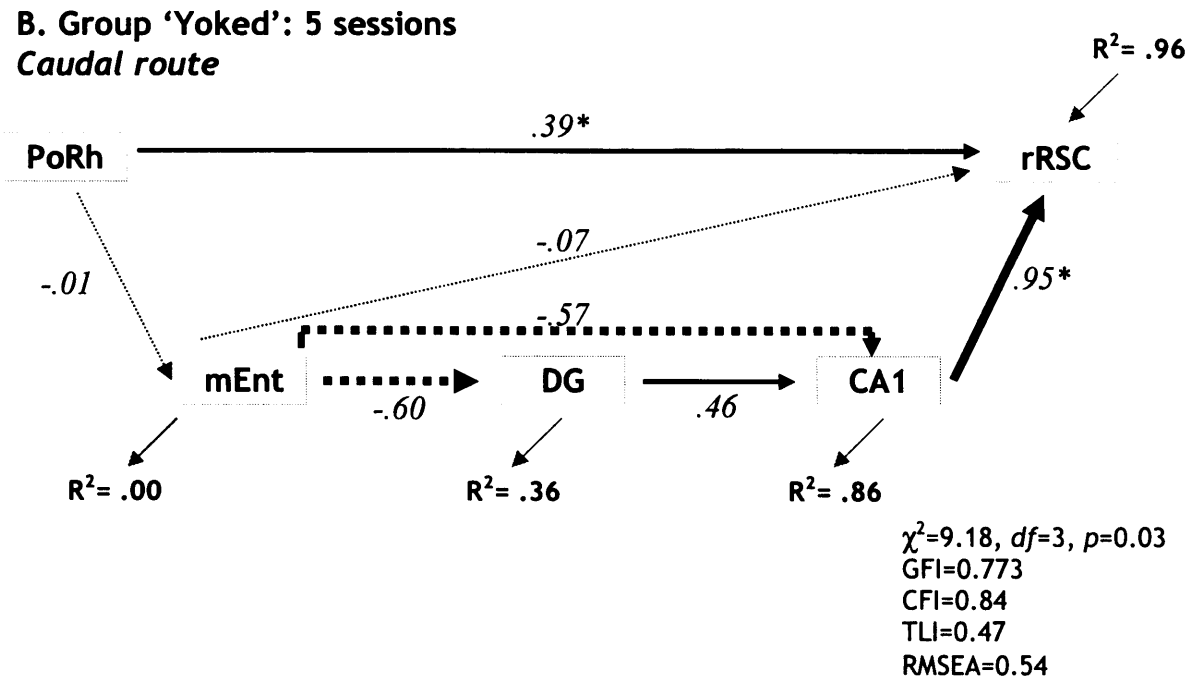

Figure 2.10: Representation of the path analyses of the caudal route for the Yoked subjects in the two-session (A) and five-session groups (B).

For the rostral route, the model did not fit the data of the 2-session group, but displayed low levels of fit for the 5-session group (see Figure 2.11). In contrast, the model did not fit the data of the Yoked groups for any condition or route (see Figures 2.10 and 2.12). Overall, it can be concluded that the networks activated appear to be different for the Trained and Yoked conditions. In reference to the particular model tested, a better fit was only apparent with prolonged training. For the caudal route, while overall fit was better with prolonged training, the latter was associated with a reduction in the number of significant paths. In contrast, prolonged maze exposure yielded increases in the number of significant paths in the Yoked group. For the rostral route, the number of significant paths increased in both the Trained and the Yoked groups. It may be noted that, amongst the regions tested, the retrosplenial cortex always exhibited the largest R^2, representing the amount of correlation with all the other regions.

A. Group 'Training: 2 sessions
Rostral route

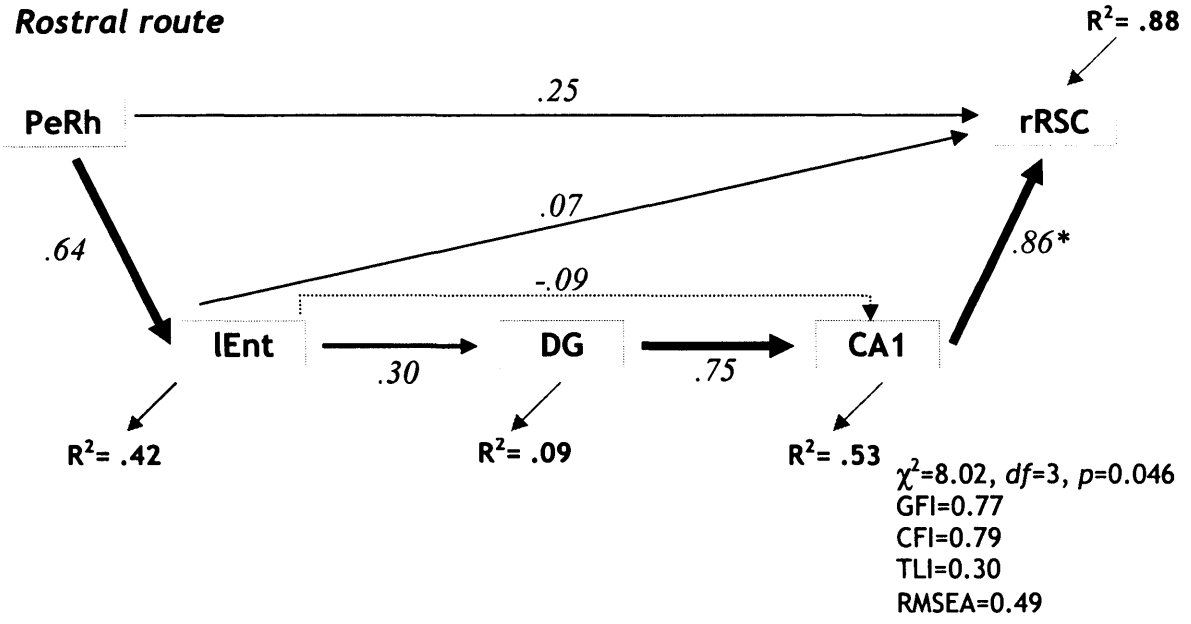

B. Group 'Training: 5 sessions
Rostral route

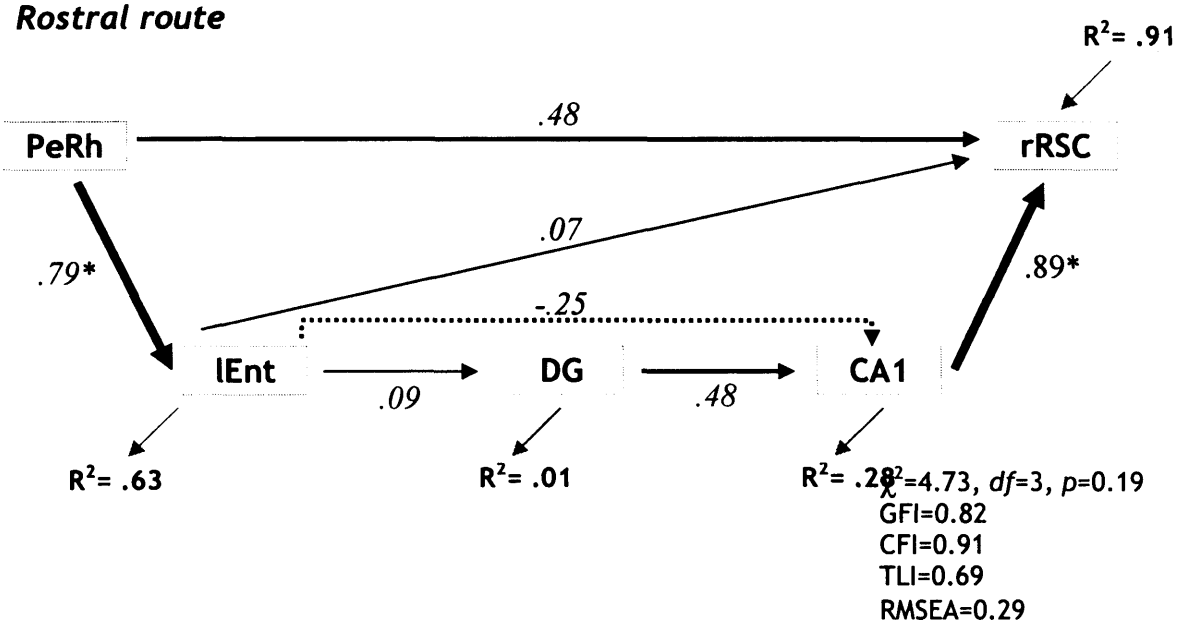

Figure 2.11: Representation of the path analyses of the rostral route for the Trained subjects in the two-session (B) and five-session groups (B).

A. Group 'Yoked: 2 sessions
Rostral route

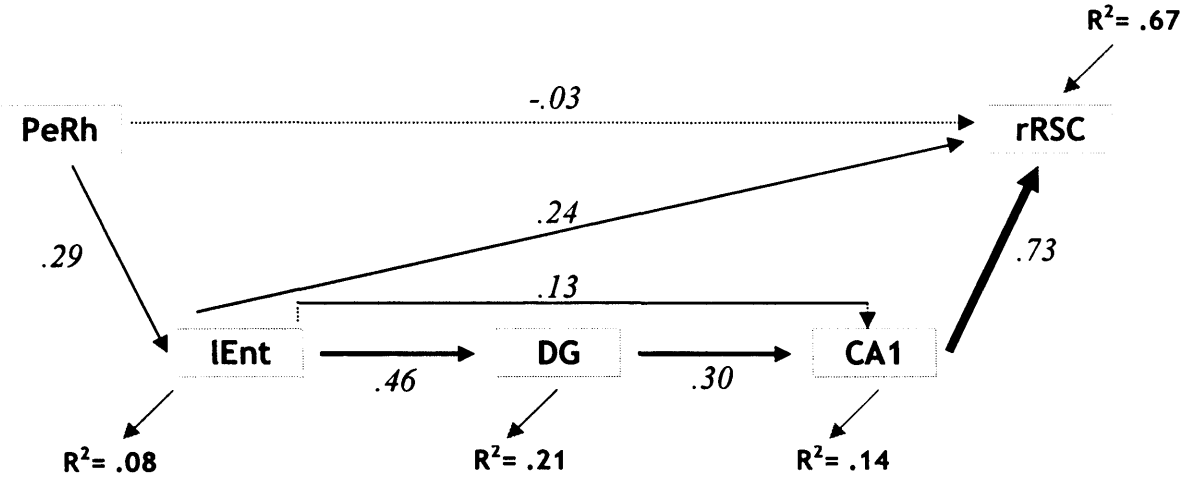

χ^2=18.44, *df*=3, *p*<0.0001
GFI=0.73
CFI=0.21
TLI=-1.62
RMSEA=0.86

B. Group 'Yoked: 5 sessions
Rostral route

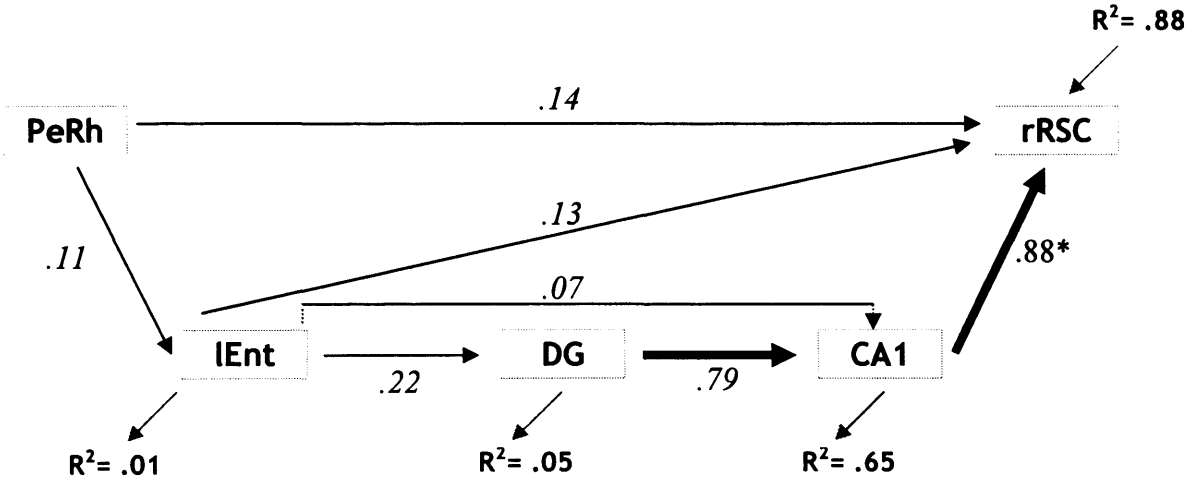

χ^2=6.37, *df*=3, *p*=0.10
GFI=0.79
CFI=0.81
TLI=0.363
RMSEA=0.40

Figure 2.12: Representation of the path analyses of the rostral route for the Yoked subjects in the two-session (A) and five-session groups (B).

2.3.2.2.2.2: Optimal route fit for each individual group

The results of the analyses in the previous section suggested that the model tested may not have been optimal for each condition, and each route. Based on this finding, the models that are now presented are those that yielded the best, most parsimonious fit for each group and each route (see Figures 2.13-16).

Different models were derived for the caudal and the rostral routes for both Trained and Yoked groups. Models with a satisfactory fit were obtained for both routes in the Trained groups, for both early and prolonged training conditions. For the caudal route of the Trained group in the 5-session group, freeing three paths yielded a more parsimonious model that still retained a good level of fit (see Figure 2.13B). The model specific to the caudal route for the Trained group in the 2-session condition now yielded an acceptable level of fit (see Figure 2.13A), which remained weaker than that of the 5-session group.

In terms of the rostral route, satisfactory models were obtained for both training conditions of the Trained groups. In contrast to the models for the caudal route, the models for the rostral route did not rely on mediation by the entorhinal cortex (see Figures 2.15). Comparisons between the caudal and rostral routes in the Trained groups revealed that the strength of the connection between the postrhinal cortex and the retrosplenial cortex was reduced with prolonged training in the caudal route, whereas the strength of the connection between the perirhinal cortex and the retrosplenial cortex increased with prolonged training in the 5-session group.

In terms of the Yoked groups, models were not found that provided a good fit for either the rostral or the caudal route in the 2-session condition (see Figures 2.14A and 2.16A). However, in the 5-session condition a good fitting model was obtained for the rostral route (see Figure 2.16B), and a weakly fitting model was obtained for the caudal route (see Figure 2.14B).

A. Group 'Trained: 2 sessions
Caudal route

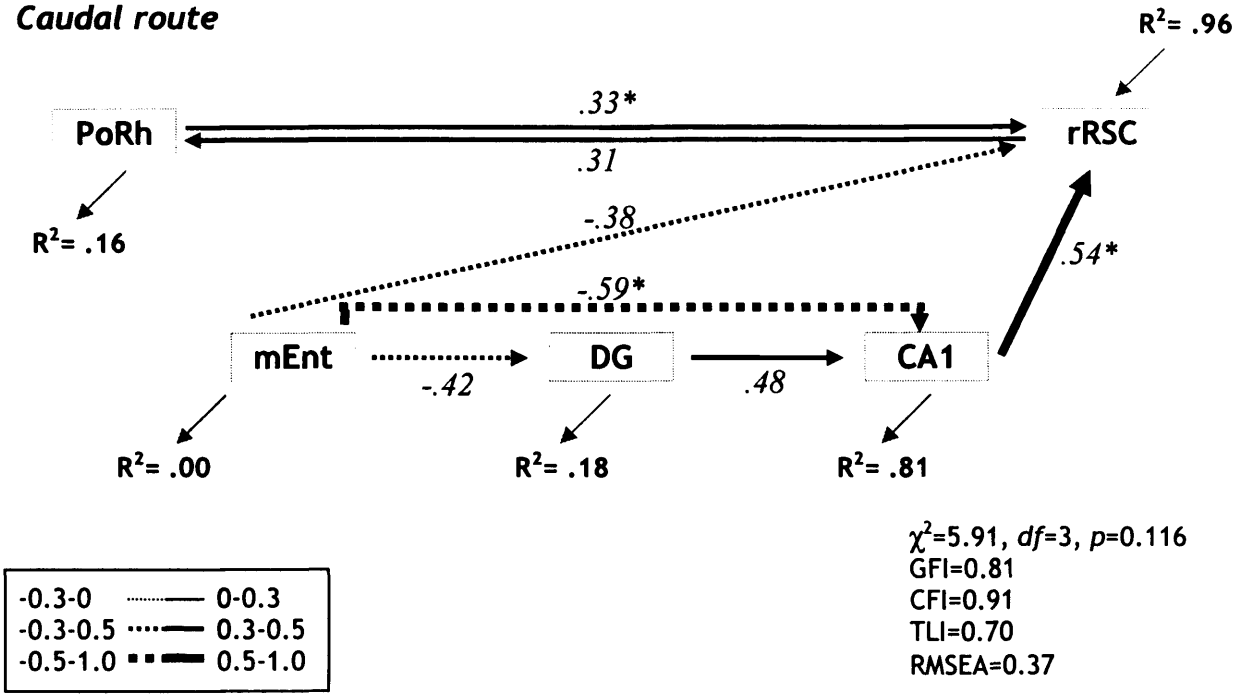

χ^2=5.91, *df*=3, *p*=0.116
GFI=0.81
CFI=0.91
TLI=0.70
RMSEA=0.37

B. Group 'Trained': 5 sessions
Caudal route

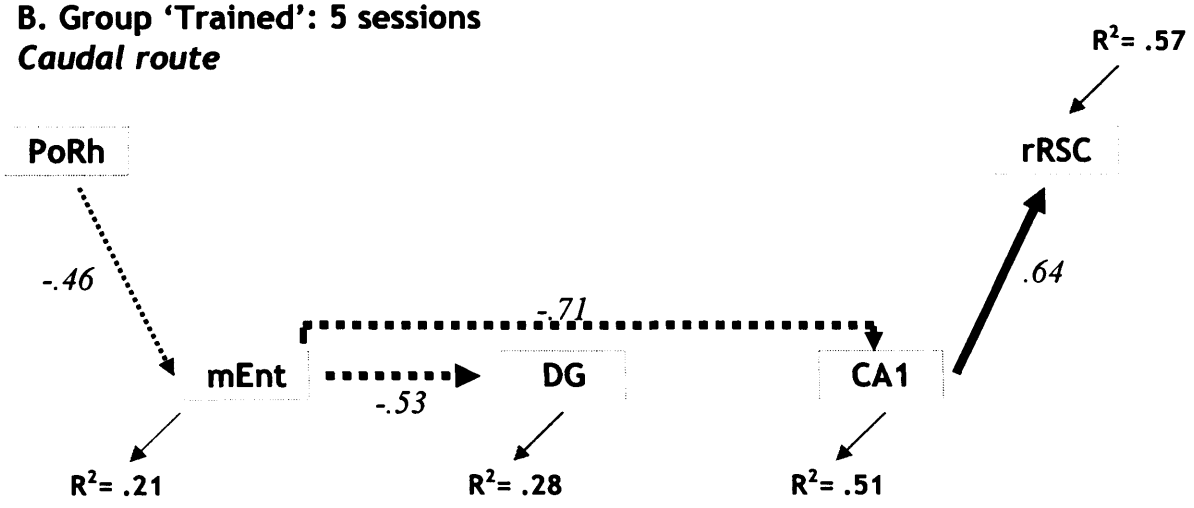

χ^2=3.67, *df*=6, *p*=0.721
GFI=0.86
CFI=1.00
TLI=1.47
RMSEA<0.001

Figure 2.13: Representation of the path analyses of the caudal route for the Trained subjects in the two-session (A) and five-session groups (B).

A. Group 'Yoked': 2 sessions
Caudal route

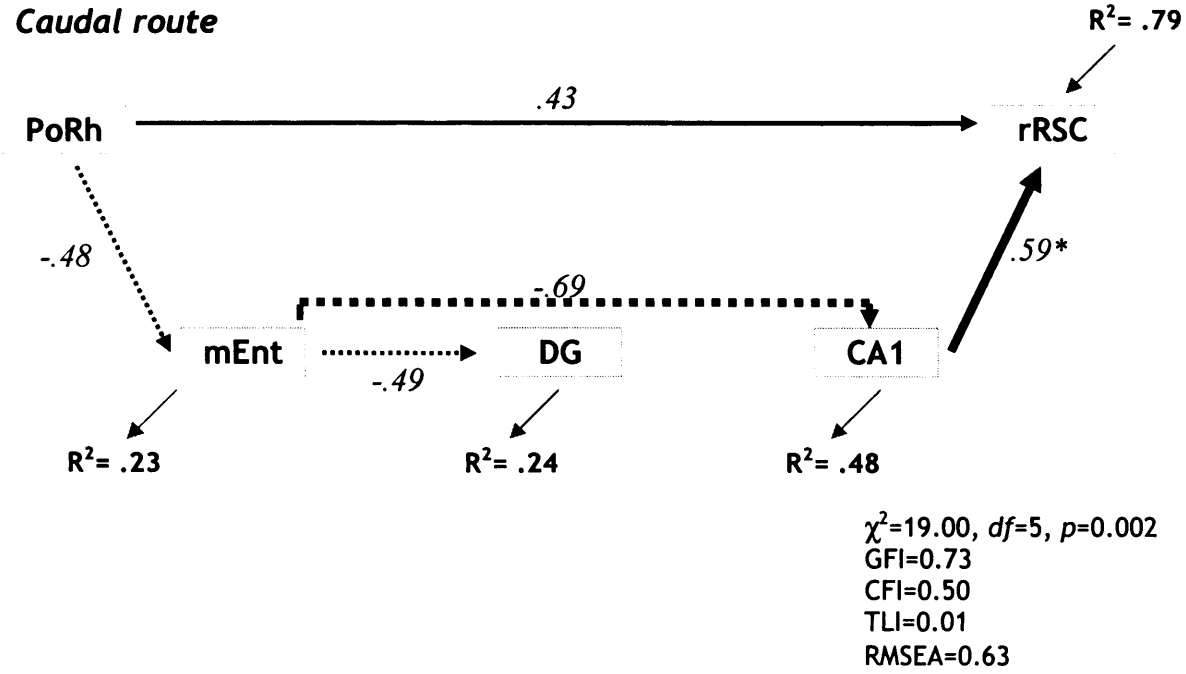

B. Group 'Yoked': 5 sessions
Caudal route

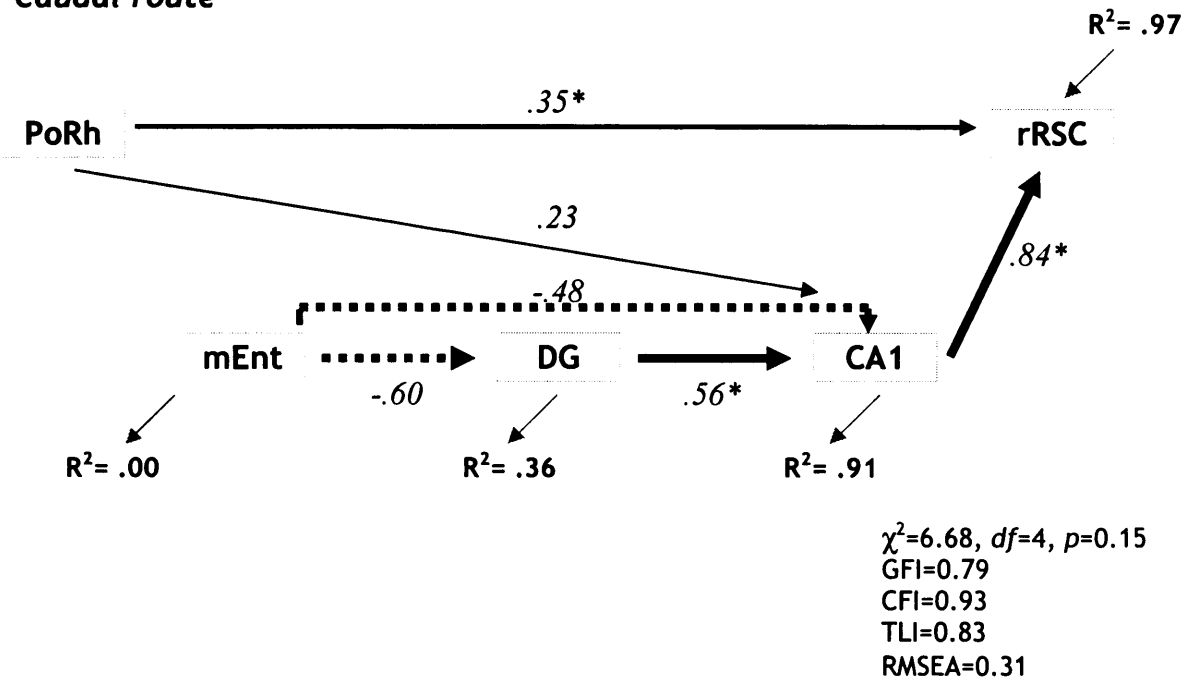

Figure 2.14: Representation of the path analyses of the caudal route for the Yoked subjects in the two-session (A) and five-session groups (B).

A. Group 'Training: 2 sessions
Rostral route

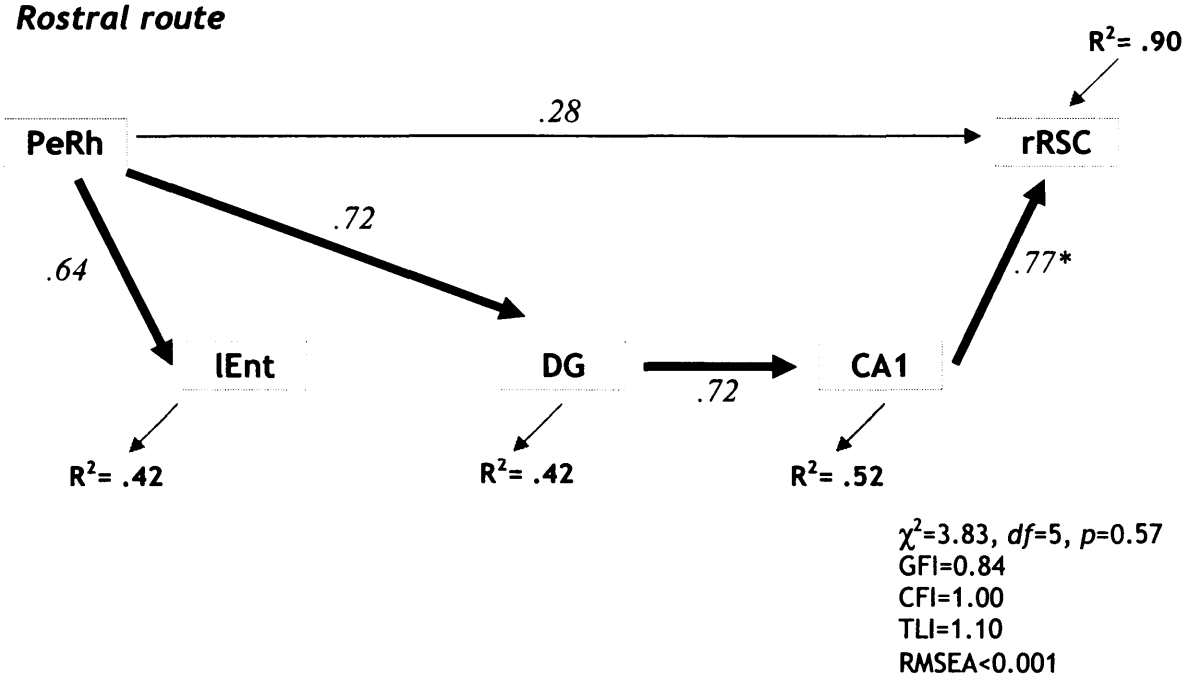

B. Group 'Training: 5 sessions
Rostral route

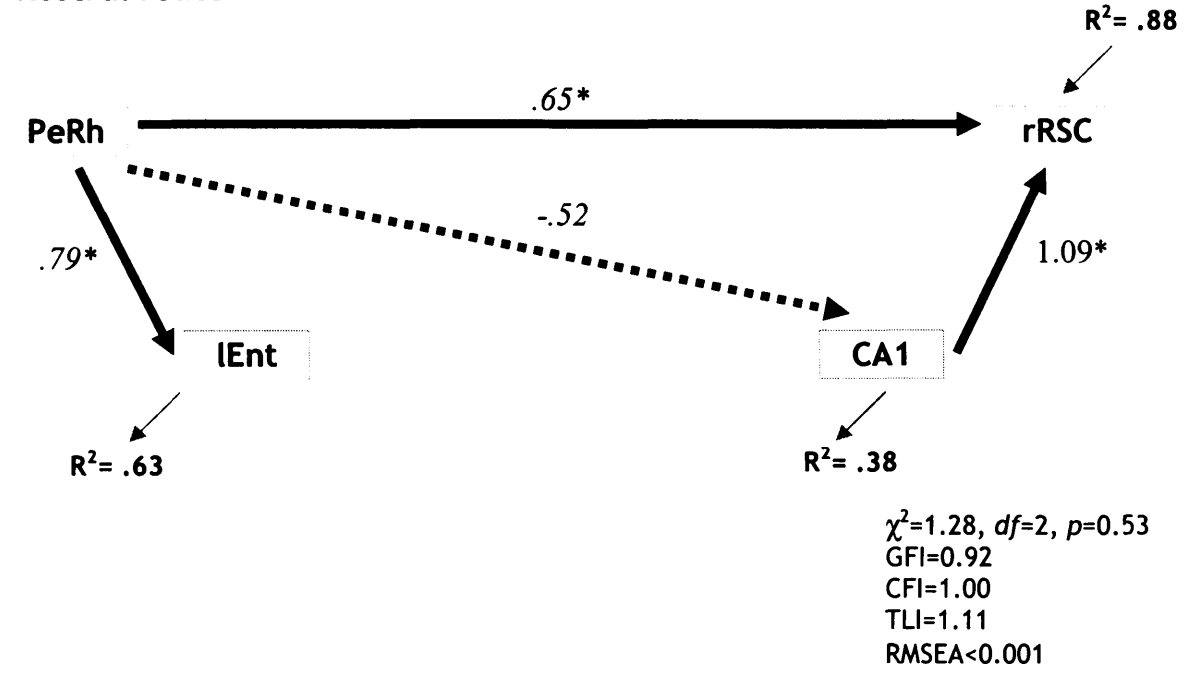

Figure 2.15(A, B): Representation of the path analyses of the rostral route for the Trained subjects in the two-session group (A) and the five-session group (B). In (B), particularly high multicollinearity is present (see explanation in text), where rRSC and CA1 are almost identical. Because of this, another model was evaluated (see Figure 2.15C, next page).

C. Group 'Training: 5 sessions
Rostral route (extreme multi-collinearity problem addressed, cf. text)

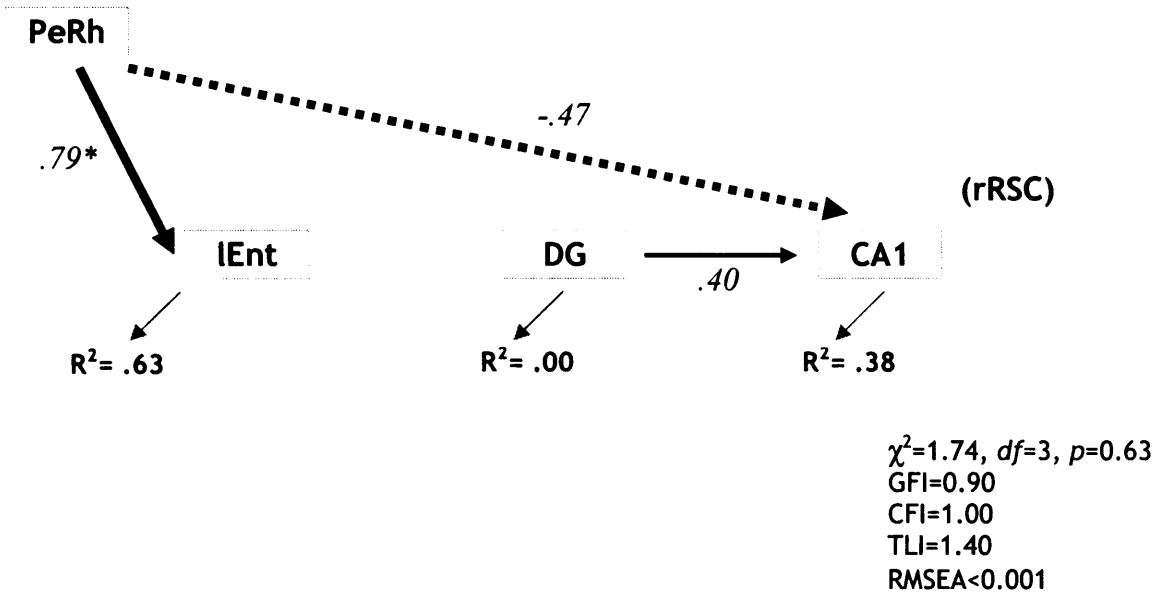

Figure 2.15C: There was particularly high multicollinearity in the caudal route of Trained group, 5-session level, where rRSC and CA1 were almost identical. Because of this, here another model was evaluated, where rRSC was removed, not because of weak connections, but since both it and CA1 exhibited activity patterns suggestive of a single 'unit'. In this model, DG, while unnecessary for a satisfactory fit, was reinstated.

Both modelling approaches, i.e. highest fit for all regions tested and optimal fit per condition per route, yielded some high path coefficients. Except for any models pertaining to the caudal route of Trained subjects, there was an apparent multicollinearity issue between the retrosplenial cortex and CA1. That is, in cases where the path coefficients are close to 1 or beyond 1, or where the squared multiple correlation (R^2) is close to 1, the two variables are close to being identical (Tabachnik and Fidell, 1996, p. 641). In the model exhibiting the most extreme example of multicollinearity (5-session rostral route of Trained subjects), the rostral retrosplenial cortex was removed because it appeared that the CA1 and it were functioning as a single 'unit'. The dentate gyrus was reinstated, even though the presence of that particular region was not necessary for the overall fit.

A. Group 'Yoked: 2 sessions
Rostral route

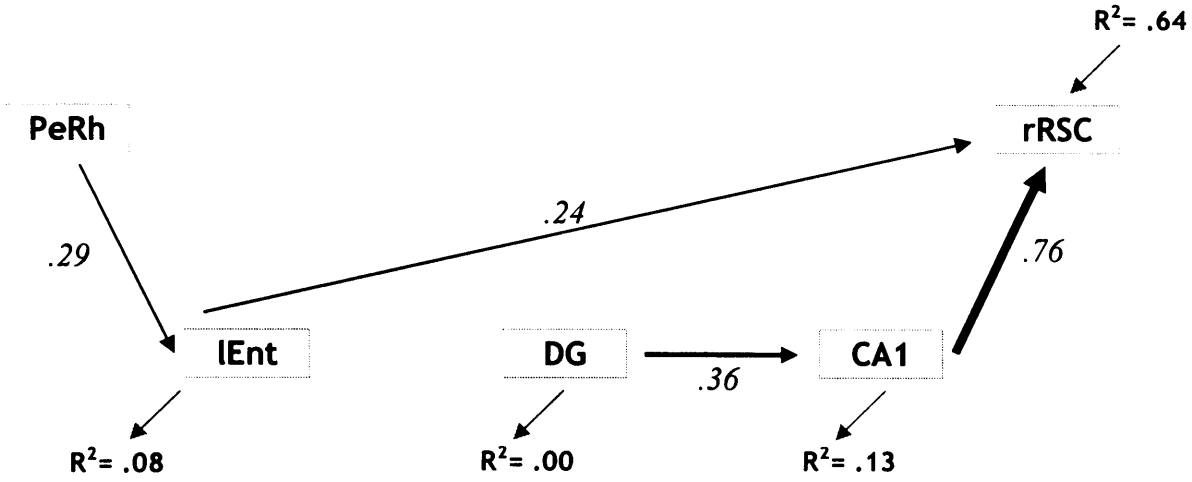

χ^2=20.23, *df*=6, *p*=0.003
GFI=0.72
CFI=0.28
TLI=-2.07
RMSEA=0.58

B. Group 'Yoked: 5 sessions
Rostral route

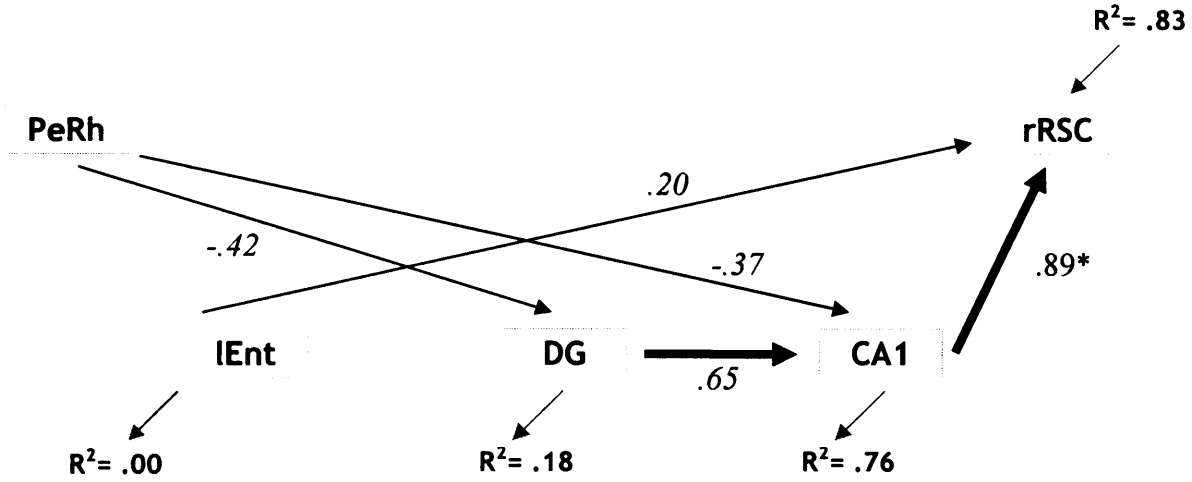

χ^2=3.26, *df*=5, *p*=0.66
GFI=0.86
CFI=1.00
TLI=1.20
RMSEA<0.001

Figure 2.16: Representation of the path analyses of the rostral route for the Yoked subjects in the two-session (A) and five-session groups (B).

Overall, the level of fit generally seemed to improve with further experience in the maze for both Trained and Yoked groups. This increase in model fit was achieved differently for the Trained and the Yoked groups. Whereas from two to five sessions the models for the Trained groups tended to exhibit more reductions than increases in the strength of paths, the opposite was apparent for the Yoked groups.

For the Trained subjects, a common pattern emerged in both the rostral and the caudal routes, whereby the influence of the dentate gyrus and the strength of its connections were reduced with prolonged training (see Figures 2.13 and 2.15). In contrast to the apparent disengagement of the dentate gyrus with prolonged training in the Trained groups, for the Yoked groups the strength of dentate gyrus paths increased with prolonged maze experience.

2.3.2.3: Correlational analyses for brain regions and behaviour

Correlational analyses were next conducted for a fine grain analysis of regional immediate-early gene activity in relation to the various aspects of behaviour, including measures of working and reference memory, in addition to the duration of each subject's experience in the final maze. A summary of these correlational analyses is presented for Zif268 in Tables 2.3-6. The multiple comparison adjustment according to the Bonferroni method reduces the chance of Type I error but severely limits the power of an individual test when a high number of tests are conducted. As recommended by Perneger (1998), the correlations obtained in the current study were not subjected to a multiple correction adjustment. These analyses served to generate new hypotheses, and further work will be necessary to validate the findings. It should be noted that the significant results that were found exhibited high correlations (>0.7), suggesting that the variables tested shared over 50% of their variance. Such a strong effect would be unlikely to arise as a result of chance.

The results of the correlational analyses for Zif268 activity in the 2-session training group revealed several strong associations between task performance and Zif268 activity in the tested brain regions (see Figure 2.17). A positive association was found between non reference-related working memory errors in the final testing session and counts of Zif268 in the dentate gyrus [r= 0.82, n=8, p<0.05] and the perirhinal cortex [r= 0.75, n=8, p<0.05].The improvement in working memory for rewarded arms (as

obtained by the learning curve) was found to be positively associated with Zif268 activity in the perirhinal cortex [r= 0.83, n=8, p<0.05] and the rostral retrosplenial cortex [r= 0.75, n=8, p<0.05], whereas the improvement in working memory for rewarded arms (based on the number of errors in the final session) was positively associated with Zif268 activity in the dentate gyrus [r= 0.78, n=8, p<0.05]. The total number of reference memory errors was negatively associated with counts of Zif268-positive cell nuclei [r= -0.74, n=8, p<0.05], while the reference memory learning curve was positively associated with Zif268 activity in the dentate gyrus [r= 0.85, n=8, p<0.01] and in the postrhinal cortex [r= 0.75, n=8, p<0.05].

a.

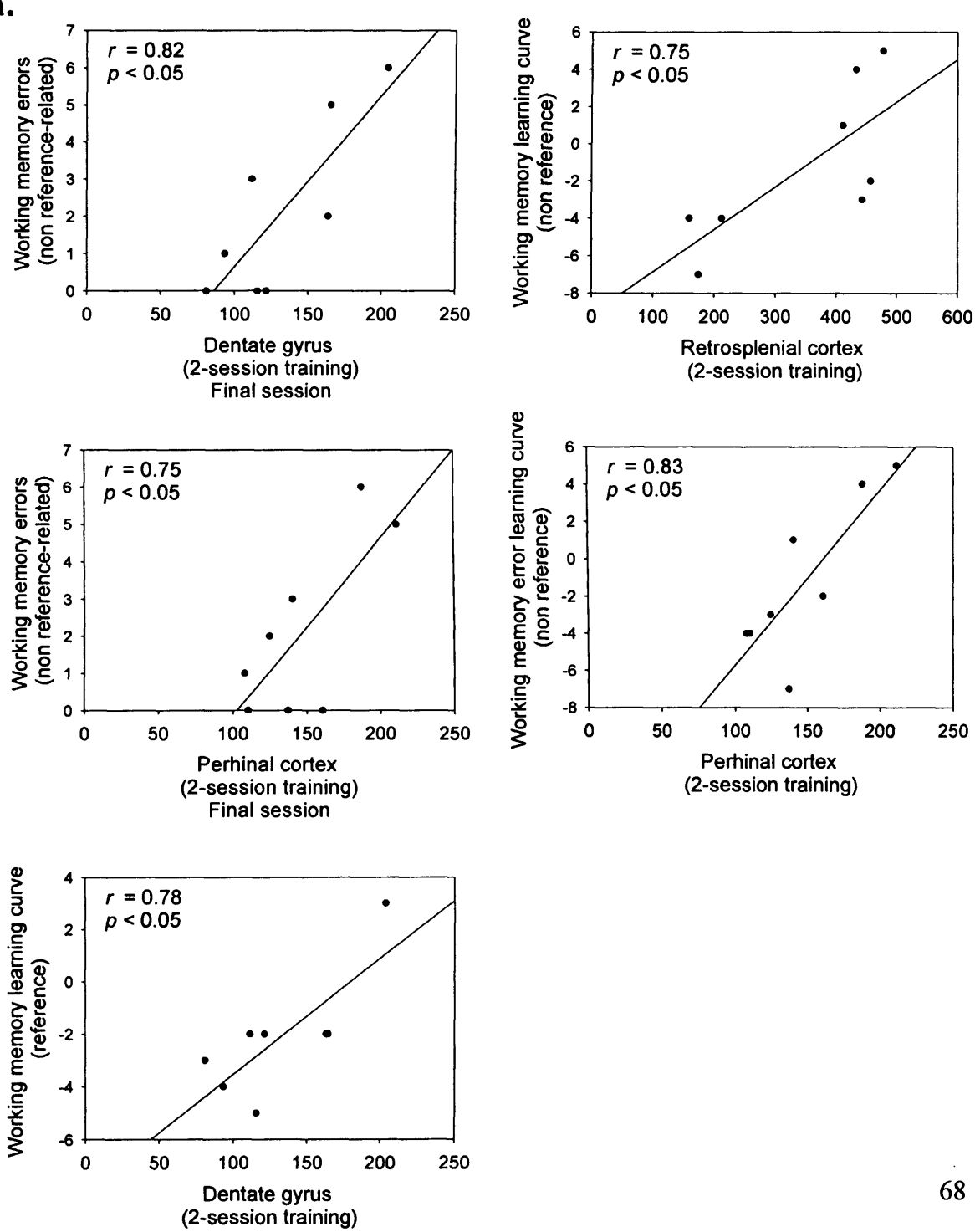

b.

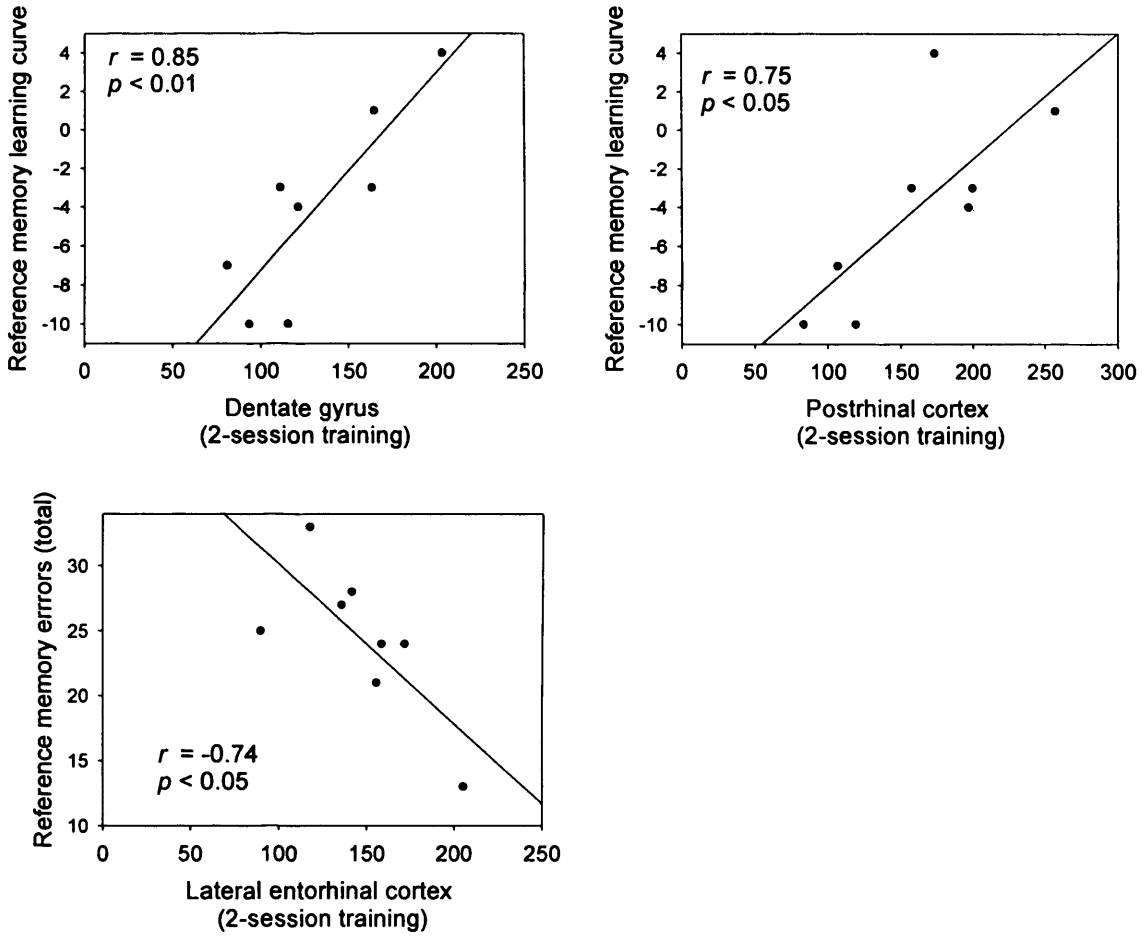

Figure 2.17: Scatter plots of the significant correlations found for the 2-session training group of Zif268 activity with working (a) and reference memory errors (b).

In contrast to the associations found in subjects trained only for two sessions in the new maze, a different set of associations was found for the subjects trained for five sessions (see Figure 2.18). The only commonality was found for the postrhinal cortex, for which Zif268-positive cell counts were positively associated with the total number of reference memory errors across the sessions [r= 0.80, n=8, p<0.05], similarly to the positive correlation it exhibited with the reference memory learning curve in the 2-session group. The other significant correlations all involved either different brain regions or the same brain regions but with a correlation to a different type of error.

The total number of reference memory errors across the sessions was also positively associated with Zif268 activity in the retrosplenial cortex [r= 0.72, n=8, p<0.05]. A

negative association was found between working memory errors for rewarded arms in the final test session and Zif268 activity in the CA3 hippocampal subfield [r= -0.94, n=8, p<0.01]. The improvement of the subjects in working memory for rewarded arms across sessions was positively associated with Zif268 activity in the CA1 hippocampal subfield [r= 0.72, n=8, p<0.05]. Zif268 activity in this particular region was also positively associated with reference memory errors in the last session [r= 0.72, n=8, p<0.05].

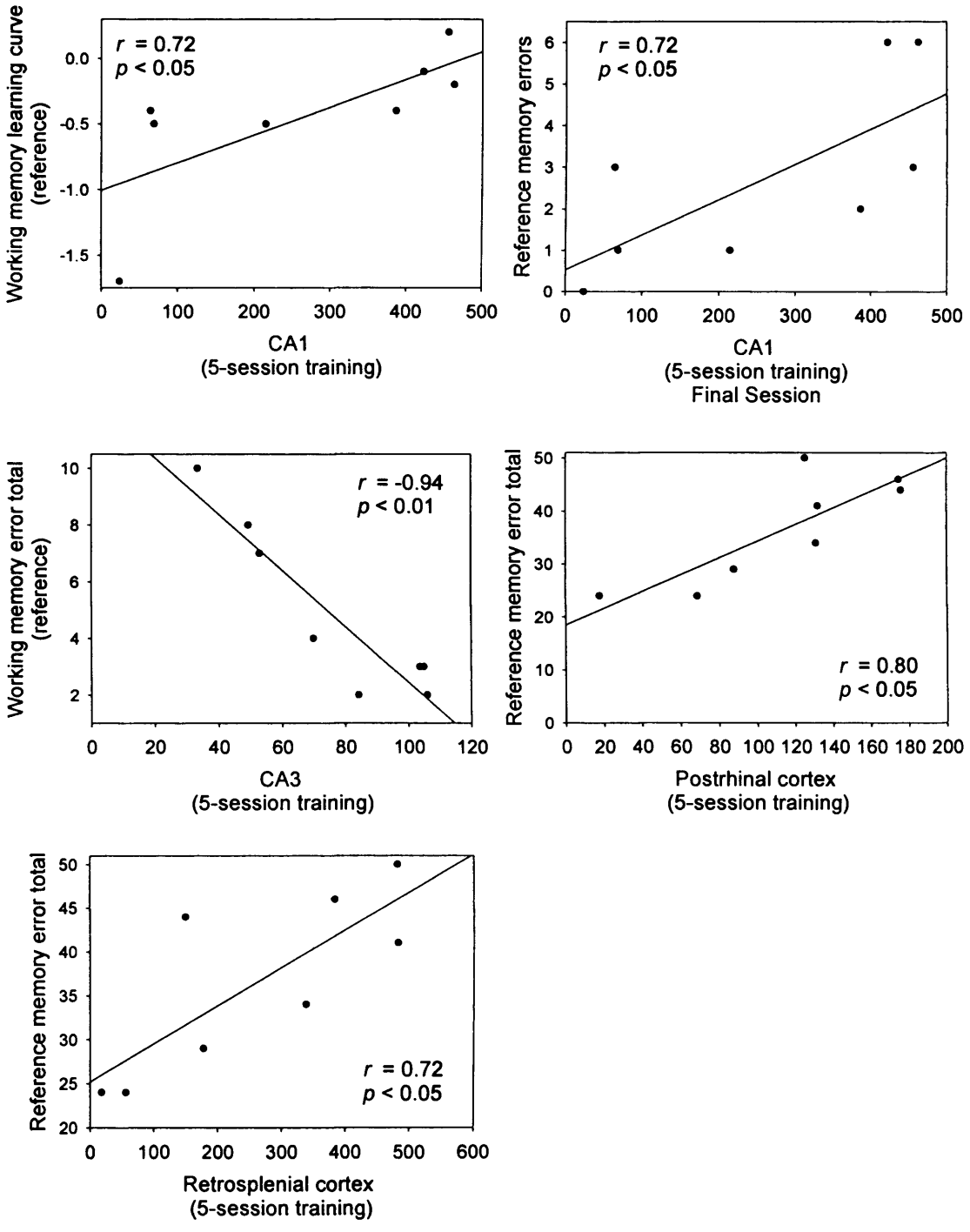

Figure 2.18: Scatter plots of the significant correlations found for the 5-session training group with Zif268 activity.

Table 2.3: Correlations for Zif268-positive cells, conducted using the Pearson-product moment coefficient for behaviour in the final maze for the 2-session training group.

Region	Measure	WMnr (fs)	WMnr (t)	WMnr (curve)	WMref (fs)	WMref (t)	WMref (curve)	REF (fs)	REF (t)	REF (curve)
PeRh	*r*	**.746***	.025	**.826***	.401	.260	.458	.197	-.402	.690
	p	*.034*	*.953*	*.012*	*.325*	*.534*	*.253*	*.641*	*.323*	*.058*
lEnt	*r*	.156	-.192	.263	-.133	-.315	.073	-.223	**-.741***	.373
	p	*.713*	*.649*	*.530*	*.753*	*.447*	*.863*	*.596*	*.036*	*.363*
rRSC	*r*	.608	-.147	**.750***	.237	.157	.267	.386	-.001	.495
	p	*.110*	*.728*	*.032*	*.572*	*.711*	*.522*	*.345*	*.998*	*.212*
PoRh	*r*	.608	.262	.562	.216	-.039	.423	.364	-.252	**.754***
	p	*.110*	*.530*	*.147*	*.608*	*.928*	*.297*	*.375*	*.547*	*.031*
mEnt	*r*	-.541	.179	-.689	-.179	-.191	-.130	-.306	-.196	-.233
	p	*.166*	*.671*	*.059*	*.672*	*.651*	*.759*	*.461*	*.641*	*.578*
DG	*r*	**.816***	.570	.655	.622	.331	**.782***	.567	-.030	**.854****
	p	*.013*	*.140*	*.078*	*.100*	*.423*	*.022*	*.142*	*.944*	*.007*
CA3	*r*	-.221	.564	-.507	.075	-.063	.196	-.039	-.128	.100
	p	*.598*	*.145*	*.199*	*.860*	*.882*	*.642*	*.927*	*.763*	*.815*
CA1	*r*	.506	.016	.561	.320	.256	.318	.454	.176	.418
	p	*.200*	*.971*	*.148*	*.439*	*.541*	*.442*	*.259*	*.677*	*.303*

Correlation is significant (2-tailed) at the 0.05 (*) or 0.01 level (**). N=8. WMref =Working memory errors (rewarded arms); WMnr = working memory errors (non-rewarded arms); fs = final session; REF = reference memory errors; t = total for all sessions in the final maze; curve = slope of improvement based on a linear trend line fitted to errors committed across sessions in the final maze.

Table 2.4: Correlations for Zif268-positive cells, conducted using the Pearson-product moment coefficient for behaviour in the final maze for the 5-session training group.

Region	Measure	WMnr (fs)	WMnr (t)	WMnr (curve)	WMref (fs)	WMref (t)	WMref (curve)	REF (fs)	REF (t)	REF (curve)
PeRh	*r*	-.159	.367	-.365	-.677	-.326	-.259	-.144	-.003	-.562
	p	*.706*	*.371*	*.374*	*.065*	*.430*	*.535*	*.733*	*.994*	*.147*
lEnt	*r*	-.243	.655	-.593	-.483	.196	-.348	.103	.499	-.586
	p	*.561*	*.078*	*.121*	*.225*	*.642*	*.398*	*.808*	*.208*	*.127*
rRSC	*r*	-.035	.114	-.152	.131	-.101	.454	.588	**.716***	.164
	p	*.934*	*.787*	*.720*	*.757*	*.811*	*.258*	*.125*	*.046*	*.698*
PoRh	*r*	-.307	.558	-.611	.286	.463	-.248	.167	**.796***	-.057
	p	*.460*	*.150*	*.107*	*.492*	*.248*	*.554*	*.692*	*.018*	*.894*
mEnt	*r*	-.145	-.069	-.130	-.345	-.143	-.322	-.300	-.527	-.338
	p	*.733*	*.871*	*.759*	*.403*	*.736*	*.437*	*.470*	*.179*	*.413*
DG	*r*	-.341	.318	-.281	-.327	.147	-.056	.020	.500	-.286
	p	*.409*	*.443*	*.500*	*.429*	*.728*	*.895*	*.963*	*.207*	*.492*
CA3	*r*	.085	-.411	.311	-.307	**-.939****	.328	-.205	-.674	-.009
	p	*.841*	*.312*	*.453*	*.460*	*.001*	*.427*	*.626*	*.067*	*.983*
CA1	*r*	.253	-.251	.300	.572	.069	**.716***	**.722***	.502	.564
	p	*.546*	*.550*	*.470*	*.138*	*.870*	*.046*	*.043*	*.205*	*.145*

Correlation is significant (2-tailed) at the 0.05 (*) or 0.01 level (**). N=8. WMref =Working memory errors (rewarded arms); WMnr = working memory errors (non-rewarded arms); fs = final session; REF = reference memory errors; t = total for all sessions in the final maze; curve = slope of improvement based on a linear trend line fitted to errors committed across sessions in the final maze.

In terms of potential associations with the duration of the exploration, the correlational analyses (Tables 2.5 and 2.6) revealed a strong, positive association between Zif268 cell counts in the dentate gyrus and the total amount of time spent in the maze for the 2-session training group [r= 0.72, n=8, p<0.05], and between Zif268 cell counts in the CA1 hippocampal subfield and the amount of total amount of time spent in the maze for the 5-session yoked control group [r= 0.72, n=8, p<0.05]. These results are presented in Figure 2.19.

Table 2.5: Correlations for Zif268-positive cells, conducted using the Pearson-product moment coefficient for time spent in the final maze for the 2-session trained and yoked control groups (n=8 per group).

		Measure	Region	Perh	lEnt	rRSC	PoRh	mEnt	DG	CA3	CA1
2 sessions	Trained	Last session	*r*	.427	-.182	.493	.347	-.469	.521	-.305	.464
			p	*.291*	*.667*	*.215*	*.400*	*.241*	*.185*	*.463*	*.247*
		Total	*r*	.624	.112	.653	.691	-.488	**.717***	-.228	.553
			p	*.098*	*.791*	*.079*	*.058*	*.219*	*.045*	*.587*	*.155*
	Yoked	Last session	*r*	.556	.602	.396	.488	-.524	.399	-.198	.430
			p	*.153*	*.114*	*.331*	*.220*	*.183*	*.328*	*.639*	*.288*
		Total	*r*	.151	.611	.434	.174	-.591	.148	-.471	.548
			p	*.721*	*.108*	*.282*	*.680*	*.123*	*.727*	*.239*	*.160*

Correlation is significant (2-tailed) at the 0.05 (*) or 0.01 level (**).

Table 2.6: Correlations for Zif268-positive cells, conducted using the Pearson-product moment coefficient for time spent in the final maze for the 5-session trained and yoked control groups (n=8 per group).

		Measure	Region	Perh	lEnt	rRSC	PoRh	mEnt	DG	CA3	CA1
5 sessions	Trained	Last session	*r*	-.536	-.366	.142	.438	-.361	-.371	-.371	.421
			p	*.171*	*.372*	*.738*	*.277*	*.380*	*.366*	*.366*	*.300*
		Total	*r*	-.633	-.341	.307	.358	-.494	-.150	-.477	.691
			p	*.092*	*.409*	*.460*	*.384*	*.213*	*.722*	*.232*	*.058*
	Yoked	Last session	*r*	-.546	.013	.453	.191	-.655	.035	-.517	.538
			p	*.162*	*.976*	*.260*	*.650*	*.078*	*.935*	*.189*	*.169*
		Total	*r*	-.476	-.109	.461	-.113	-.669	.441	-.371	**.718***
			p	*.233*	*.796*	*.250*	*.790*	*.070*	*.273*	*.366*	*.045*

Correlation is significant (2-tailed) at the 0.05 (*) or 0.01 level (**).

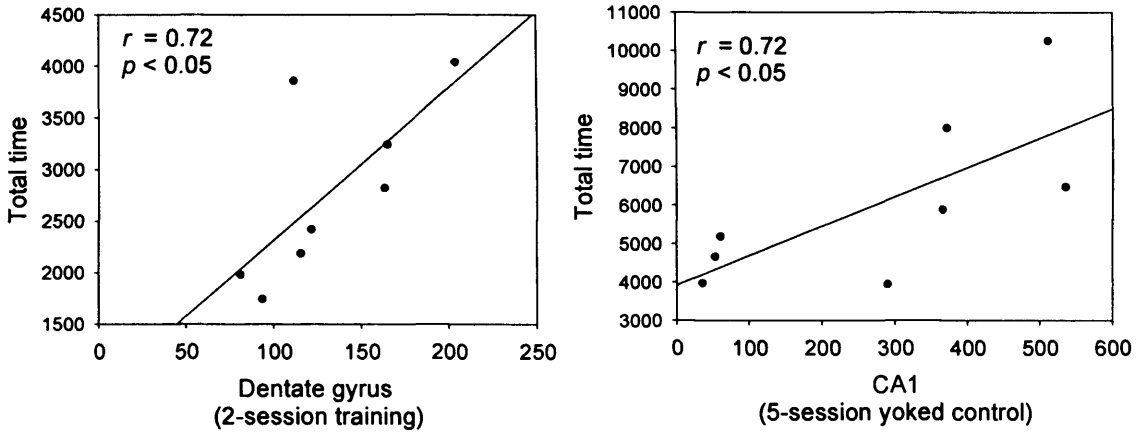

Figure 2.19: Scatter plots of the significant correlations found for time spent in the maze with Zif268 activity.

2.4: Discussion

The present study extended the findings of previous radial arm maze reference memory studies in a number of ways. It is the first IEG study of radial arm maze performance to use a pre-training phase to look at regional activity in relation to spatial reference and working memory performance. The use of a pre-training phase potentially increased the likelihood that the results obtained through training in the second maze were due to the use and learning of new spatial associations, and not confounded by the acquisition of other information such as the task demands. Second, the present study used improved controls that allowed a better comparison of the experimental groups to the control groups by yoking the number of arms explored by the subjects in the latter groups to that of subjects in the experimental groups. Third, it is the first study to use statistical path analysis to investigate the network dynamics of a subset of brain regions in relation to the performance level of a spatial reference and working memory task.

Extended training of the subjects for five days yielded significant improvements in the number of reference and working memory errors committed. The performance improvement was detectable without any significant reduction in the average duration of the last test session of each experimental group. While univariate analyses yielded no differences in the absolute and normalised counts of immunoreactive cells between the training conditions, multivariate analyses yielded dynamic patterns of network activity of brain regions according to the condition tested. Strong correlations were found

between regional immediate-early gene activity and performance measures, and just as effective connectivity differed according to training level, so did many of these correlations. The findings will now be discussed in greater detail.

2.4.1: Univariate analyses of regional Zif268 expression

The use of standard univariate analyses of normalised Zif268-positive cell counts did not reveal any significant effect of either the extent of training or of brain region. Meanwhile, the use of structural equation modelling provided information about the change in network dynamics, a perspective not possible using univariate techniques, revealing the direct effect of regions upon others within a network.

The present null results of the univariate analyses appear to contradict previous findings (Guzowski et al., 2001; He et al., 2002a; He et al., 2002b), obtained with regards to task mastery. It is possible that some differences between studies may reflect the different immediate-early genes used to evaluate regional activity, as the patterns of expression of these genes do not necessarily parallel each other (Guzowski et al., 2001). As discussed below, there also exist task and procedural differences between the studies, which may contribute to the different findings.

One difference that appears to be consistent between the current study on task mastery and others is the relative performance levels of the groups compared. In the current study, the behavioural analyses revealed that the performance levels were significantly different between the groups. Furthermore, the 5-session training group did not appear to be performing at asymptote. According to the results of He and colleagues (He et al., 2002a; He et al., 2002b), who used a similar paradigm and methods, Fos levels follow an inverted U-shape with training in regions also tested in the current study. If the difference between the performance levels of the two groups tested was either too small or too large, this may have yielded differences in Zif268 counts that were too small to be detected. As discussed in section 1.5, in an experiment comparing rats at different levels of training in a reference version of the water maze, Guzowski and colleagues (2001) found higher hippocampal and entorhinal expression of c-*fos*, *zif268*, and *arc* mRNA levels in the first session compared to the seventh-session group. In order to compare the results of the current experiment to those obtained by Guzowski and colleagues (2001), I will assume that protein levels, had they been obtained by the latter, would exhibit the same general patterns as seen with mRNA (Zangenehpour and

Chaudhuri, 2002). Keeping in mind that the task used in the present experiment was qualitatively different from that used by Guzowski and colleagues (2001)—i.e. locating a platform vs. performing repeated concurrent spatial discriminations, the two paradigms cannot easily be compared. Yet, two issues will be addressed in an attempt to clarify the results.

The first issue stems from the use of two different paradigms. The task used in the present study presumably imposed a greater spatial memory load, both in terms of reference and working memory, as multiple locations, instead of one single platform location (Guzowski et al., 2001), had to be learned and visited. The putative greater load on spatial memory may have played a role in role in maintaining Zif268 activity at more similar intensities between the two training levels. However, the experiment previously described by He and colleagues (2002b) also required reference and working memory for multiple locations, thus potentially invalidating this argument. Maybe more importantly, one particular difference in methodology may be emphasised. In the experiment of Guzowski and colleagues (2001), the seventh-session group appears to be performing at asymptotic levels, and had reached this level approximately half-way through the training regime. According to the inverted U-shape reported by He and colleagues (2002a; 2002b), it would seem that the results of Guzowski and colleagues (2001) reflect the fact that the seventh session was performed after reaching asymptotic levels. This contention is confirmed when verifying the performance levels of the subjects in that group, where it is apparent that they had reached asymptotic levels halfway through the training regimen.

The potential reduction in the immediate-early gene activation difference between the groups based on the separate locations on a hypothetical inverted U-shaped curve may have been compounded by the variability in performance within the groups. This variability may have contributed to yield the null results, as the criterion was the number of sessions in the maze, rather than actual performance level. Such a possibility was addressed by conducting correlational analyses between performance measures and regional Zif268 counts, and the results of these analyses will be discussed later.

The current results, based on Zif268 cell counts, are in agreement with those of Bontempi and colleagues (1996), as well as those of Ros and colleagues (Ros et al., 2005), based on metabolic function. Neither of these studies found any difference in

acute (5-min post-test) regional metabolic activity between training levels in the hippocampus or the retrosplenial cortex. The current findings however, supplemented these observations by providing evidence that, while the absolute activity may not significantly change, the level of interaction between regions appears to differ between the training levels. While no differences where found in metabolic activity immediately after testing, Bontempi and colleagues (1996) found differences in the ensuing regional metabolic activity one hour and three hours after testing. It is not clear how the changes in the dynamics of regional metabolic activity reported by Bontempi and colleagues (1996) as a function of training relate to the findings in the current study.

In subsequent reports, Bontempi and colleagues (Bontempi et al., 1999; Maviel et al., 2004), upon finding that longer post-acquisition delays lead to reductions in metabolic and immediate-early gene hippocampal measures, proposed that their findings reflect the existence of underlying consolidation processes that are independent of overt task practice. A similar conclusion has been offered by Freeman and Gabriel (1999), using a different system. They found in cingulothalamic areas that electrophysiological activity changes that arise with conditional tone discrimination training can also occur simply with the passage of time. Our findings suggest that any such transfer or consolidation process may take place after the acquisition of the task, as no differences are apparent between the training levels here.

2.4.2: Correlational analyses: Inter-regional Zif268 expression

The brain region correlational analyses suggested numerous associations between brain regions in the network tested. High bivariate correlations between factors become very low partial correlations when underlying processes that are simultaneously affecting several variables are present (Tabachnik and Fidell, 1996, p. 641). As such, certain significant correlations that were nonsignificant using the structural equation modelling analyses are likely reflecting the fact that in the current study, the two regions may not actually have a direct effect on each other but rather their correlated activity may be the result of the separate influence on each of another region. For example, the significant correlations between the medial entorhinal cortex and the retrosplenial cortex in the 2-session Training and the 5-session Yoked groups were not significant when the influence of other regions was considered, neither was the significant correlation found between the perihinal cortex and the dentate gyrus in the 2-session Trained group. The

significant correlations however held up between the perirhinal cortex and lateral entorhinal cortex (5-session Training group), as well between the medial entorhinal cortex and the CA1 (2- and 5-session Training groups), even when the influence of other regions was taken into account.

2.4.3: Correlational analyses: Behavioural parameters and regional Zif268 expression

While the number of subjects in the current study was relatively low, and in spite of the potential for Type I errors as a result of the multiple tests, the variance shared by the associated variables was of such a remarkable size that I believe the associations that were found to be of genuine interest and worth pursuing, and replicating.

Retrosplenial cortex Zif268-positive cell activity was significantly correlated with reference memory in the prolonged but not early training group. This finding is consistent with previous reports of a more important role of retrosplenial cortex in late than early learning found with conditional learning with lesions in rats (Bussey et al., 1996; Bussey et al., 1997) and electrophysiological recording in rabbits (Gabriel and Sparenborg, 1987; Smith et al., 2002). Interestingly, the Zif268 cell counts in the retrosplenial cortex also significantly correlated with working memory (non-reference) errors early in training.

The lateral entorhinal cortex was significantly correlated with reference memory errors in the Early but not the Late training group. Meanwhile, the medial entorhinal cortex was not significantly correlated with any behavioural measure. While the evidence for the importance in memory of the entorhinal cortex and its subdivisions is not consistent, it may cautiously be said that entorhinal cortex lesions often do not produce performance deficits (Bouffard and Jarrard, 1988; Galani et al., 2002), and when a deficit is observed it is likely to be more substantial in spatial reference than working memory (Cho and Jaffard, 1995; Jarrard et al., 2004). This view is not inconsistent with the current findings. However, in light of recent evidence of the distribution within the medial entorhinal cortex of cells (i.e. 'grid cells') that exhibit spatial correlates (Hafting et al., 2005), it appears that the location of the medial entorhinal lesions or IEG visualisation may be critical. Thus, the null finding for the medial entorhinal cortex may

also reflect the properties of the area sampled, and not be generalisable to medial entorhinal cortex in general.

Zif268 cell counts in the postrhinal cortex were significantly correlated with reference errors. The postrhinal cortex is the only region for which a significant correlation with the same behavioural measure was found in both Early and Late training groups. This finding is consistent with reports that the neuronal firing in the postrhinal cortex can exhibit spatial correlates (Burwell and Hafeman, 2003), and that postrhinal cortex lesions produce a reference deficits in a radial arm maze task (Liu and Bilkey, 2002).

There was an apparent shift in the site of Zif268 activity in the hippocampal subregions from the dentate gyrus in the Early condition to CA1 and CA3 subfields in the Late training condition. The dentate gyrus was significantly correlated with measures of the three types of memory [working (reference and non-reference) and reference], and even total time spent in the maze, but only in the Early training group. In contrast, the CA1 hippocampal subfield was significantly correlated with reference and working (reference) errors, and even total time spent in the maze for the Yoked group in the Late training group. The CA3 subfield was only associated with working (reference) errors in the Late training group.

Intriguingly, the CA3 subfield was negatively associated with working (reference) errors. CA3 and the lateral entorhinal cortex are the only regions to be negatively associated with errors. Whereas for the other regions rats exhibited plasticity in a proportional manner to the number of errors committed, for CA3 and the lateral entorhinal cortex, it was successful performance that was associated with increased plasticity.

The identity of specific functions of hippocampal subregions is still in debate, but general patterns appear to be emerging, based on lesion evidence and computational modelling. For example, the dentate gyrus appears to subserve the encoding of spatial information but not necessarily retrieval processes, whereas the CA3 region may be involved in both encoding and retrieval, including working memory processes, and the CA1 field is then only critical for retrieval processes (cf. reviews by McClelland and Goddard, 1996; Rolls and Kesner, 2006). The findings of the current study are not

contradictory with this view, as Zif268 activity in the dentate gyrus was found to be significantly associated with task performance only in the early training condition, whereas, in contrast, in the CA3 and CA1 regions it was only significantly associated with performance with prolonged training.

Finally, perirhinal cortex Zif268 cell counts were significantly correlated with working (non-reference) errors in the Early training group. It seems that the perirhinal cortex may be processing task performance-related information, yet, in light of evidence from lesion studies, it appears that Zif268 activity in the perirhinal cortex may not necessarily reflect a critical function of this region in the performance of the type of spatial task used in the current study (cf. recent reviews by Aggleton et al., 2004; Aggleton and Brown, 2005). Given this view, it appears unlikely that in the early Training group in the present study, the perirhinal cortex played a role in establishing conjunctions of objects and locations. The results relating to the perihinal cortex lead me to emphasise that the results of immediate-early gene studies require validation through alternate approaches to verify the importance of IEG activity in the performance of a task. In this particular instance, Zif268 activity in the perirhinal cortex was significantly correlated with a performance parameter in the spatial memory task tested, and further studies will be necessary to elucidate this finding.

2.4.4: Structural equation modelling

The observation of the absence of apparent absolute differences in absolute Zif268 activity levels, but of different network dynamics has a parallel in human metabolic imaging studies. For example, it was reported (Maguire et al., 2000) that equivalent cortico-hippocampal networks were activated by different memory tasks, however, the effective connectivity significantly differed for each of these tasks. This type of network dynamics has been referred to as neural context (McIntosh, 1999). This neural context hypothesis refers to the idea that learning and memory arise from the dynamics of large-scale neural networks, that regions may play a role in numerous functions, and, importantly, that the role played by an individual region is influenced by its interaction with anatomically connected regions. As such, a region may display equivalent patterns of activity between different tasks, but actually be integrated into different networks in these tasks (McIntosh, 1999). Along this vein, the models for the caudal route of the Trained groups provide a particularly salient example of effective connectivity changes in spite of similar levels of Zif268 activity between the conditions. For this particular

route, and in this particular experimental condition, prolonged training reduced the importance of the indirect effects, leaving only direct regional influences, as is especially apparent in Figure 2.13B. In other words, there was an apparent pruning of the connections. Similarly, it was apparent that a pattern consistently emerged in the Trained groups, whereby the strength of the connections with the dentate gyrus decreased with prolonged training. In effect, the mediation of the dentate gyrus on the influence of various regions on CA1 activity decreased with prolonged training. This finding was consistent with the results of the correlational analyses that suggested that the dentate gyrus was only involved in task performance in the 2-session condition.

In relation to the path coefficients, it should be noted that negative path coefficients should not necessarily be regarded as the reflection of inhibitory influences (McIntosh and Gonzalez-Lima, 1991). It is suggested that these coefficients should rather be understood in the same fashion as correlation coefficients, such that a negative coefficient would mean that each unit increase in a region would result in a proportional decrease in the regions to which it is connected (McIntosh and Gonzalez-Lima, 1991). The arguments levelled for the interpretation of structural modelling results based on 2-deoxyglucose data are also valid for immediate-early gene imaging. These authors claim that interpreting negative coefficients as inhibitory, in electrophysiological terms, is not directly warranted.

In combining structural equation modelling and immediate-early gene imaging, the results of the current study provided estimates of the direct influence of regions within a cortico-hippocampal network, with a candidate gene to orchestrate the putative plasticity changes associated with the acquisition of the task. The current study also underlined potential candidate regions that could subserve individual memory components of the spatial memory task tested. Overall, the findings of the current study yielded a multi-dimensional insight into the network dynamics associated with the acquisition of a spatial memory task by providing integrative molecular, behavioural, and systems information.

Appendix A:

Fos correlational analyses

The results of the correlational analyses for Fos activity in the 2-session training group revealed a number of strong significant associations in spite of the relatively low number of subjects. As presented in Table 2.3, these significant associations were only found for the final session of testing. A negative association was found between the number of working (non reference memory errors during the last test session) and both dentate gyrus [r= -0.96, n=4, p<0.01] and CA3 Fos activity [r= -0.95, n=4, p<0.01]. In the final test session as well, negative associations were found between the number of reference errors and Fos activity in the rostral retrosplenial cortex [r= -0.97, n=4, p<0.05] and the postrhinal cortex [r= -0.99, n=4, p<0.05]. There was also a negative association between the amount of time spent in the maze during the final session and Fos-positive cell counts in the CA3 region [r= 0.95, n=4, p<0.05]. As seen in Table 2.4, the only significant association in the 5-session training group for Fos activity was a positive one between working (non reference) memory errors Fos activity in the medial entorhinal cortex [r= 0.92, n=5, p<0.05].

Table 2.7: Correlations for Fos-positive cells, conducted using the Pearson-product moment coefficient for behaviour in the final maze for the 2-session training group.

Region	Measure	Time (fs)	Time (t)	WMnr (fs)	WMnr (t)	WMnr (curve)	WMref (fs)	WMref (t)	WMref (curve)	REF (fs)	REF (t)	REF (curve)
PeRh	*r*	-.362	-.579	-.267	-.898	.206	-.420	.167	-.790	-.848	-.540	-.475
	p	*.638*	*.421*	*.733*	*.102*	*.794*	*.580*	*.833*	*.210*	*.152*	*.460*	*.525*
lEnt	*r*	-.468	-.359	.186	-.607	.564	-.516	-.193	-.422	-.914	-.855	-.012
	p	*.532*	*.641*	*.814*	*.393*	*.436*	*.484*	*.807*	*.578*	*.086*	*.145*	*.988*
rRSC	*r*	-.648	-.474	.158	-.501	.471	-.687	-.375	-.402	**-.970***	-.916	.006
	p	*.352*	*.526*	*.842*	*.499*	*.529*	*.313*	*.625*	*.598*	*.030*	*.084*	*.994*
PoRh	*r*	-.850	-.745	-.115	-.467	.135	-.880	-.462	-.539	**-.989***	-.824	-.197
	p	*.150*	*.255*	*.885*	*.533*	*.865*	*.120*	*.538*	*.461*	*.011*	*.176*	*.803*
mEnt	*r*	-.133	-.357	-.136	-.910	.364	-.195	.315	-.694	-.727	-.476	-.383
	p	*.867*	*.643*	*.864*	*.090*	*.636*	*.805*	*.685*	*.306*	*.273*	*.524*	*.617*
DG	*r*	-.943	-.832	-.215	-.338	-.055	**-.962***	-.557	-.517	-.925	-.743	-.235
	p	*.057*	*.168*	*.785*	*.662*	*.945*	*.038*	*.443*	*.483*	*.075*	*.257*	*.765*
CA3	*r*	**-.954***	-.910	-.434	-.148	-.418	**-.955***	-.572	-.488	-.697	-.463	-.355
	p	*.046*	*.090*	*.566*	*.852*	*.582*	*.045*	*.428*	*.512*	*.303*	*.537*	*.645*
CA1	*r*	-.517	-.897	-.916	-.347	-.861	-.521	.031	-.737	-.281	.187	-.829
	p	*.483*	*.103*	*.084*	*.653*	*.139*	*.479*	*.969*	*.263*	*.719*	*.813*	*.171*

Correlation is significant (2-tailed) at the 0.05 (*) or 0.01 level (**). N=4. WMref =Working memory errors (rewarded arms); WMnr = working memory errors (non-rewarded arms); fs = final session; REF = reference memory errors; t = total for all sessions in the final maze; curve = slope of improvement based on a linear trend line fitted to errors committed across sessions in the final maze.

Table 2.8: Correlations for Fos-positive cells, conducted using the Pearson-product moment coefficient for behaviour in the final maze for the 5-session training group.

Region	Measure	Time (fs)	Time (t)	WMrew (fs)	WMrew (t)	WMrew (curve)	WMnr (fs)	WMnr (t)	WMnr (curve)	REF (fs)	REF (t)	REF (curve)
PeRh	*r*	.008	-.019	.571	.476	-.033	-.386	.270	-.380	.474	.711	-.130
	p	*.990*	*.975*	*.315*	*.418*	*.958*	*.521*	*.660*	*.528*	*.419*	*.178*	*.835*
lEnt	*r*	-.340	-.147	.539	.632	.206	-.445	.399	-.112	.439	.562	-.353
	p	*.576*	*.813*	*.349*	*.253*	*.740*	*.453*	*.506*	*.857*	*.459*	*.324*	*.561*
rRSC	*r*	-.216	-.398	.079	.680	-.489	-.525	-.282	-.598	-.043	.399	-.432
	p	*.728*	*.507*	*.899*	*.207*	*.403*	*.363*	*.646*	*.287*	*.945*	*.506*	*.467*
PoRh	*r*	-.649	-.344	.218	.609	.211	-.491	.297	.025	.178	.272	-.540
	p	*.236*	*.571*	*.725*	*.275*	*.734*	*.401*	*.628*	*.969*	*.774*	*.658*	*.347*
mEnt	*r*	.120	.345	.267	.056	.714	.653	.203	**.921***	.066	-.559	.155
	p	*.847*	*.570*	*.664*	*.929*	*.175*	*.232*	*.744*	*.026*	*.916*	*.328*	*.803*
DG	*r*	-.146	-.159	-.664	-.441	-.211	.073	-.307	.036	-.485	-.473	.003
	p	*.814*	*.798*	*.222*	*.457*	*.733*	*.908*	*.616*	*.954*	*.407*	*.421*	*.996*
CA3	*r*	-.369	-.279	-.664	-.219	-.112	.018	-.296	.170	-.534	-.567	-.191
	p	*.542*	*.650*	*.222*	*.723*	*.858*	*.977*	*.628*	*.784*	*.354*	*.319*	*.759*
CA1	*r*	-.591	-.436	-.565	-.020	-.163	-.311	-.168	-.040	-.404	-.265	-.385
	p	*.294*	*.463*	*.321*	*.974*	*.794*	*.611*	*.788*	*.949*	*.500*	*.667*	*.522*

Correlation is significant (2-tailed) at the 0.05 (*) or 0.01 level (**). N=5. WMref =Working memory errors (rewarded arms); WMnr = working memory errors (non-rewarded arms); fs = final session; REF = reference memory errors; t = total for all sessions in the final maze; curve = slope of improvement based on a linear trend line fitted to errors committed across sessions in the final maze.

Chapter 3

Retrosplenial cortex vulnerability to afferent damage: A Fos imaging study in the rat.

3.1: Introduction

The retrosplenial cortex forms part of a network that is involved in learning and memory in humans (Maguire, 2001a; Maguire, 2001b; Svoboda et al., 2006) and non-human animals (Vogt et al., 1992; Gabriel, 2000; Aggleton and Pearce, 2001). In the previous chapter, I have presented evidence that suggests a role for putative retrosplenial cortex plasticity in spatial reference memory performance (see section 2.3.2.3). Additionally, I have demonstrated that the retrosplenial cortex can exhibit dynamic effective connectivity patterns with training, and that it shares a strong connection with the CA1 hippocampal subfield (see section 2.3.2.2). Widespread evidence exists of retrosplenial cortex dysregulation in disorders that involve cognitive impairment. These disorders include Alzheimer's disease (Desgranges et al., 1998; Nestor et al., 2003), vascular dementia (Martinez-Bisbal et al., 2004), Wernicke-Korsakoff syndrome (Aupée et al., 2001; Reed et al., 2003), hypoxia-induced amnesia (Reed et al., 1999; Aupée et al., 2001), epilepsy (Archer et al., 2003), hypothyroidism (Krausz et al., 2004) and schizophrenia (Mitelman et al., 2003; Newell et al., 2005).

Interest in the retrosplenial cortex and its dysfunctions stems not only from direct evidence that this region, along with the hippocampus and the anterior thalamic nuclei work together to sustain memory abilities (Sutherland, 1993), but also from the ways which, in conjunction with its afferents, it might contribute to disorders characterised by cognitive deficits. In Alzheimer's disease, for example, pathology commences at an early stage not in retrosplenial cortex but in the entorhinal cortex and the anterior thalamic nuclei (Braak and Braak, 1991a, b), yet retrosplenial cortex is typically the first to show metabolic decreases (Minoshima, 1997; Nestor et al., 2003; Buckner, 2004). The mismatch between overt pathology and metabolic alterations suggests the possibility that damage to afferents may be responsible for retrosplenial dysfunction. In accord with this notion, Clarke and colleagues (1994) found that an anterior thalamic infarct resulted in retrosplenial hypometabolism.

Previous studies in the rat revealed that large unilateral thalamic lesions in rats decrease levels of metabolic enzymes and levels of presynaptic receptors in granular retrosplenial cortex (van Groen, 1993). Perhaps more striking is the recent discovery that selective anterior thalamic lesions cause a dramatic loss of the protein products of the immediate early genes (IEGs) c-*fos* and *zif268* in superficial granular retrosplenial cortex (Jenkins

et al., 2004). After anterior thalamic lesions, as many as 90% of the cells can stop producing Fos (Jenkins et al., 2004). This change may be an example of 'covert pathology' (i.e. a functional lesion where there is no overt pathology). This is because the effects seem persistent (Jenkins et al., 2004), and there is no evidence of cell death in retrosplenial cortex (Vogt, 1981b; Jenkins et al., 2004). Tests of covert pathology would include whether the loss of IEG expression is associated with changes in retrosplenial plasticity. This prediction was recently confirmed *in vitro* (Garden et al., 2006). Two months after anterior thalamic lesions, electrophysiological investigations of rat retrosplenial slices revealed abnormalities in the lesion side, including a loss of long-term depression (LTD) in the superficial but not the deep layers of the granular retrosplenial cortex (Garden et al., 2006). This dysfunction is arguably the most convincing demonstration of covert pathology as the slice experiments stimulated intact microcircuits yet their plasticity remained deficient.

These findings show that the impact of rostral thalamic damage could potentially be amplified via covert pathology in the retrosplenial cortex. Such an amplification would broaden our understanding of conditions such as diencephalic amnesia and Alzheimer's disease. For this reason, the present study sought to reveal other possible candidate regions where damage might result in retrosplenial dysfunction in the absence of cell death. For the first experiment, the target regions were the anterior thalamic nuclei (ATN), the laterodorsal thalamic nuclei (LD), and the contralateral retrosplenial cortex (RSC). These three regions were selected because they all have dense projections to the retrosplenial cortex (Vogt, 1981b; van Groen and Wyss, 1992a; van Groen and Wyss, 1995; van Groen et al., 1999; van Groen and Wyss, 2003). Because they differ in their pattern of lamina termination, it is possible that further information might be derived concerning the causes of the vulnerability of the retrosplenial cortex. In addition, discrete lesions were placed in the antero-dorsal hippocampus (adHIP), in order to provide a control group for the unintended presence of some hippocampal damage in the thalamic lesion groups. As the anterior (Tomitaka et al., 2000; Wang et al., 2001) and laterodorsal (van Groen and Wyss, 2003) thalamic projections to the retrosplenial cortex remain ipsilateral, within-subject comparisons were made after unilateral lesions in the target sites, i.e. across cortical tissue from the hemisphere ipsilateral to the lesion to the 'intact' hemisphere contrateral to the lesion.

For the second experiment, the target regions were the hippocampus (HIP) and the entorhinal cortex (ENT). In this experiment, using a different strain of rats, bilateral lesions were produced. The hippocampus and the entorhinal cortex both have reciprocal connections with the retrosplenial cortex, and their projections also display different patterns of lamina termination in the retrosplenial cortex (van Groen and Wyss, 1990a, b; van Groen and Wyss, 1990c; Insausti et al., 1997; van Groen and Wyss, 2003; Wiltgen et al., 2004). Fos cell counts were obtained for retrosplenial cortex granular b after each of the lesions. This subregion of retrosplenial cortex was selected because: 1) When anterior thalamic damage disrupts retrosplenial Fos expression, it is this subregion of the retrosplenial cortex that appears to be most sensitive (Jenkins et al., 2004); and 2) Lesion of granular b but not granular a retrosplenial cortex produce water maze deficits (van Groen et al., 2004); 3) The loss of retrosplenial cortex LTD after anterior thalamic nuclei damage was observed in the granular b subregion (Garden et al., 2006); 4) This subregion is easily identified, so improving experimental reliability. Thus, the findings of the present study will inform us about the importance of afferent damage for retrosplenial function, in relation to the location of the damage as well as the lamina of the terminations of the disrupted afferents.

3.2: Methods

Rats were housed in pairs under diurnal light conditions (14 h light/10 h dark) and after their arrival a period of at least a week was allowed before the rats received surgery. They were given unrestricted access to food and water in their home cages. All experiments were carried out in accordance with UK Animals (Scientific Procedures) Act, 1986 and associated guidelines.

3.2.1: Experiment 1: Anterior thalamic nuclei, laterodorsal thalamic nucleus, antero-dorsal hippocampus, and retrosplenial cortex unilateral lesions

3.2.1.1: Subjects

The subjects were 32 male pigmented rats (Dark Agouti strain) weighing between 200 and 225 g at the time of surgery.

3.2.1.2: Surgery

The rats were first anaesthetised with an intraperitoneal injection of pentobarbitone sodium (Sagatal, Rhône Mérieux, 75 mg/kg), and then placed in a stereotaxic frame (Kopf Instruments, CA) using atraumatic earbars, and with the incisor bar at +5.0. A craniotomy was created over the injection sites. Excitotoxic lesions were produced by injecting N-methyl-D-aspartate (NMDA; Sigma Chemicals UK; 0.12 M in phosphate buffered saline (PBS), pH 7.4) using a 1 µl syringe (Hamilton, Switzerland) that was attached to a moveable arm mounted on the stereotaxic frame. The stereotaxic coordinates relative to bregma were:

ATN group (n=6): 0.20 µl of 0.12 M NMDA was injected into two sites: anterio-posterior, -0.5; medio-lateral, ±1.0 and 1.7 from the midline, depending on the target hemisphere; dorso-ventral, -6.3 and -5.7 from dura for the medial and lateral injections, respectively.

LD group (n=9): 0.20 µl of 0.12 M NMDA was injected into one site: anterio-posterior, -1.4; medio-lateral, ±2.3 from the midline, depending on the target hemisphere; dorso-ventral, -5.1 from dura.

adHIP group (n=5): 0.07 µl of 0.12 M NMDA was injected into one site: anterio-posterior, -1.4; medio-lateral, ±2.3 from the midline, depending on the target hemisphere; dorso-ventral, -4.1 from dura.

Contralateral retrosplenial cortex (n=8): 0.3 µl, 0.3 µl, and 0.15 µl of 0.09 M NMDA was injected rostro-caudally into three sites: The final anterio-posterior coordinates relative to bregma were; -1.8, -3.3, -4.8 and inter-aural zero, +4.0, +2.5, +1.0, respectively. Medio-lateral coordinates were ±0.6, 0.6, and 0.8 from the midline, respectively, and dorso-ventral coordinates were -2.3, -2.3, and -2.1 from dura, respectively. Each injection was made gradually over a 4 min period, following which the needle was left *in situ* for a further 4 min before being withdrawn. The control for this condition was a group of normal rats (n=4) from the same cohort, that did not undergo any aspect of the surgical procedure.

At the end of surgical procedure, the scalp incision was sutured, antibiotic powder (Aureomycin, Fort Dodge Animal Health, Southampton, UK) was applied topically and all rats also received a 5 ml subcutaneous injection of glucose saline. The rats were then placed in a recovery box maintained at 40°C. Paracetamol was dissolved in the rats' drinking water, and the rats were observed daily until recovery. Rats were administered the respiratory stimulant Millophylline (0.02 ml, s.c., Arnolds Veterinary Products, Shropshire, UK) as needed. The immediate-early gene analysis for this group of rats was from 3.5 to 4.5 months post surgery.

3.2.2: Experiment 2: Hippocampal and entorhinal cortex bilateral lesions

For this experiment, tissue was obtained from cohorts of rats already involved in behavioural experiments. This allowed a reduction in the number of subjects used and the added benefit provided by sampling tissue from already behaviourally characterised subjects. Relatively higher numbers of subjects were tested in Experiment 2 than Experiment 1 as the lesions were bilateral and so required between-subjects comparisons. Rats with hippocampal lesions for Experiment 2A were provided by Anthony McGregor and Peter M. Jones (Jones, Pearce, Davies, Good, and McGregor, unpublished observations). Compared with sham rats, the rats with hippocampal lesions in that experiment were impaired on a water maze task that required the discrimination of local geometric features (i.e. short vs. long wall) to find the platform (Jones et al., submitted). The rats with entorhinal cortex lesions for Experiment 2B came from Mundy et al. (2005). These rats underwent conditioned aversion of drinking solutions according to a blocked or an intermixed presentation design. The rats with entorhinal cortex lesions exhibited the same pattern of response as sham subjects, displaying a preference for the solution that was presented in an intermixed fashion over the solution that was presented in a blocked fashion. In other words, the entorhinal cortex damage did not affect perceptual learning.

3.2.2.1: Subjects

The subjects were male Lister Hooded rats (Harlan, UK) weighing 280-400 g. Bilateral lesions were produced in the hippocampus (Experiment 2A, HIP n= 14, HIPsham=7) and the entorhinal cortex (Experiment 2B, ENT n=12, ENTsham n=8).

3.2.2.2: Surgery

3.2.2.2.1: Experiment 2A: Hippocampal lesions

Rats received bilateral lesions of the hippocampus or sham surgery. Each rat was deeply anaesthetized in an anaesthetic box with a mixture of oxygen and isoflurane. It was then placed into a stereotaxic frame (Kopf Instruments, CA) using atraumatic ear bars, and the anaesthetic was reduced to a maintenance concentration. The scalp was incised along the midline and a dental burr was used to remove the bone overlying the neocortex. A 2 µl Hamilton syringe, which was used to make infusions of ibotenic acid, was attached to a moveable arm which was mounted on the stereotaxic frame. The plunger of the Hamilton syringe was attached to an electronic microdrive (Model KDS 310, KD Scientific, New Hope, PA) which regulated the volume and rate of infusion of the neurotoxin. Ibotenic acid (Biosearch Technologies, San Rafael, CA) was dissolved in sterile phosphate-buffered saline (pH 7.4) to produce a 63 mM solution. Volumes of between 0.05 µl and 0.10 µl were infused in 28 sites (for stereotaxic coordinates of the injection sites, see Coutureau et al., 1999). Infusions were made at a rate of 0.03 µl/min, and the needle was left *in situ* for 2 min after completing each infusion. Rats in the sham-operated control groups underwent a similar surgical procedure to those in lesion groups in which the skin was incised, the neocortex exposed and the dura perforated with a 25 gauge Microlance3 needle (Becton Dickinson, Drogheda, Ireland), but no injection was made. At the end of both the lesion and sham procedures the scalp incisions were sutured and the rats were placed in a recovery box maintained at 40°C for 3 - 4 h. In addition, rats in the lesion groups received a sub-cutaneous 10ml injection of saline and glucose solution. Once the rats had recovered sufficiently, they were transferred back to their home cages. The immediate-early gene analysis for this group of rats was from 2 to 2.5 months past surgery.

3.2.2.2.2: Experiment 2B: Entorhinal cortex lesions

Rats received bilateral lesions of the entorhinal cortex or sham surgery. The procedures were the same as described above for the hippocampal lesions, except for the infusion site volumes and coordinates. Volumes of between 0.05 µl and 0.10 µl were infused in 14 sites. The details of these infusions have been described elsewhere (Mundy et al., 2005). The immediate-early gene analysis for this group of rats was approximately three months post surgery.

3.2.3: Behaviour and histology for Experiments 1 and 2

For Experiments 1 and 2, the rats were exposed to a novel environment to induce immediate-early gene activation above resting levels, and so avoid floor effects. The rats were placed for 15 minutes in a novel environment in a novel cage after which they were returned to their home cages. Ninety minutes after the onset of this exposure to a novel context, the animals were irreversibly anaesthetised with sodium pentobarbital (140 mg/kg, Euthatal, Rhone Merieux, UK) and perfused transcardially with 0.1 M PBS followed by 4% paraformaldehyde in 0.1 M PBS. The brains were removed and post-fixed in 4% paraformaldehyde for four hours and then transferred to 25% sucrose overnight. Sections were cut at 40 µm on a freezing microtome in the coronal plane for ATN, LD, adHIP and RSC, and horizontal plane for HIP and ENT groups. Adjacent series were collected in 0.1 M PBS for Nissl staining and in 0.1 M PBS containing 0.2% Triton X-100 (PBST) for immunohistochemical visualisation of Fos protein.

3.2.4: Immunohistochemistry for Experiments 1 and 2

Endogenous peroxidase activity was blocked by washing the sections with 0.3 % hydrogen peroxide in PBST for ten minutes, and then four times with PBST alone for the same duration. Sections were incubated at 4°C for 48 hours in PBST with rabbit polyclonal antibody for Fos (1:5000, Ab-5, Oncogene Science). Sections were then rinsed for ten minutes in PBST, four times. Next they were incubated in biotinylated secondary antibody, and then avidin-biotinylated horseradish peroxidase complex in PBST (Elite Kit, Vector Laboratories). Sections were next rinsed in Tris non-saline buffer (pH 7.4). Finally, immunoreactivity was visualised with diaminobenzidine (DAB Substrate Kit, Vector Laboratories) chromogen incubation. Sections were then mounted on gelatinised slides. These slides and another series of cresyl violet stained tissue were dehydrated through a series of alcohol gradients and coverslipped.

3.2.5 Cell counting

Sections were viewed on a Leica DMRB microscope, photographed using an Olympus DP70 camera, and transferred to a computer. Counts of the stained nuclei were carried out using the program analySIS^D (Olympus, UK). The threshold was set automatically, at the same level for all sections from a same processing batch. Counts were made in a frame area of 1768 x 1331 μm, using 5x magnification. The camera was positioned so that counts were taken across all layers of retrosplenial granular cortex b. Counts were typically taken from three consecutive sections from both hemispheres of the retrosplenial cortex (approximately between -2.56 and 3.14 from bregma), and these counts were averaged to produce a mean. These data were then analysed using the statistical package SPSS 14.0 (Chicago). For Nissl stain results, t-tests were used to compare the cell counts in 'Intact' or Sham retrosplenial tissue, respectively from rats with unilateral or bilateral lesions, to lesion-associated retrosplenial tissue (i.e. either from the contralateral hemisphere or from Lesion subjects). For immunohistochemistry results, analyses of variances were conducted, followed by t-tests. The effect sizes of main effects were reported in order to understand better the impact of the manipulations.

3.2.5.1: For Experiment 1, within-subjects comparisons were made to compare raw cell counts from each hemisphere for the ATN, LD, and adHIP(ctrl) groups. For the RSC group, since interhemisphere comparisons were inherently impossible, cell counts from the contralateral hemisphere were compared to counts from normal rat controls.

3.2.5.2: For Experiment 2, between-subjects tests were used to make comparisons between sham and lesion subjects for the HIP and ENT groups. The homogeneity of variances was verified using Levene's Test of Equality of Variances and the statistical results were selected appropriately.

The analyses of Fos-positive cell numbers were complemented by a qualitative analysis of the patterns of the effects of the lesions according to retrosplenial cortex laminae. For this purpose, the horizontal mean profile function of analySIS^D (Olympus, UK) was used. A representative section was chosen from each lesion group in order to produce laminar profiles of Fos activity. For each section, an area of equal size was selected in granular b retrosplenial cortex. A measure of the intensity of each pixel was made on a single horizontal plane, across all laminae (i.e. across the width of the image). Horizontal line profiles were made across the vertical axis, and averaged for that area,

thus producing a mean profile of the Fos activity in granular b retrosplenial cortex. The areas chosen contained laminae that appeared as parallel as possible, thus optimising the averaging of the horizontal profiles by keeping the laminae aligned.

3.3: Results

3.3.1: Lesion analyses

3.3.1.1: Experiment 1

In Figure 3.1 are depicted the largest and the smallest lesions for each of the four lesion groups in Experiment 1.

3.3.1.1.1: ATN: One rat that had minimal ATN damage was excluded. Typical lesions in the remaining rats (n=5), included most of anterodorsal and anteroventral nuclei, while sparing some of the anteromedial nucleus (see Figure 3.1a for the smallest and largest extent of the lesions in the ATN group). Damage was found in the most rostral portion of the laterodorsal nuclei (n = 5). There was some extension of the lesion damage into the immediately adjacent part of the CA3 region in two cases. The cell loss in CA3 was very restricted, so it amounts to only less than 20 % on one section -2.12 from bregma for one case, and about 40 to 80 % for those sections corresponding to -1.80 to -2.56 from bregma for the other case. There was some dentate gyrus damage in the latter case, amounting to 40-50 % cell loss in just those sections corresponding to -2.12 to -2.56 from bregma, and also in one other subject other where the cell loss comprised approximately one third of that subfield, just in tissue corresponding to -1.80 from bregma. Injection tracts passed through the fornix fimbria in all cases, and minor damage to the reticular nucleus of the thalamus was also observed in four subjects. In the subject with the largest lesion, some damage was also found contralaterally in the parataenial nucleus and the paraventricular thalamic nucleus. No damage was found contralaterally in the anterior thalamic nuclei.

3.3.1.1.2: LD: Three cases were discounted as the laterodorsal thalamic nuclei damage was minimal for two rats (< 50 %), and in another rat the damage only encompassed the caudal portion of the anterior thalamic nuclei. All remaining rats in the LD group (n = 6) exhibited substantial damage to the target nucleus throughout its entire extent (see Figure 3.1b for the smallest and largest extent of the lesions in the LD group). In four

cases, there was some CA3 damage immediately above the laterodorsal thalamic nucleus lesion (from less than 20 % up to 60 % on a section, for just those sections ranging at most from around -2.12 to -.3.80 from bregma). There was some tract damage in the fimbria fornix in four cases. In the largest lesion, some involvement of the most dorsal portion of reticular thalamic nucleus was also present.

3.3.1.1.3: Thalamic nuclei lesion control group (adHIP, n = 5): Lesions in this group were typically very localised (see Figure 3.1c for the smallest and largest extent of the lesions in this group). Tract damage was found in the fimbria fornix and the cell loss was restricted to the lateral part of the CA3 region, with the most largest area of damage extending approximately -1.40 to -3.14 mm from bregma.

3.3.1.1.4: Unilateral RSC (n = 8): Rats in this group exhibited damage that was confined to the rostral retrosplenial cortex, as intended. Typically, some dysgranular retrosplenial cortex was spared. Superficial retrosplenial granular b showed some restricted cell sparing. In spite of the proximity of the midline, damage generally appeared to be confined to the target hemisphere. However, without otherwise exhibiting obvious damage, Nissl stained sections showed that the contralateral retrosplenial tissue was often found to be bereft of cells in lamina II and the superficial part of lamina III.

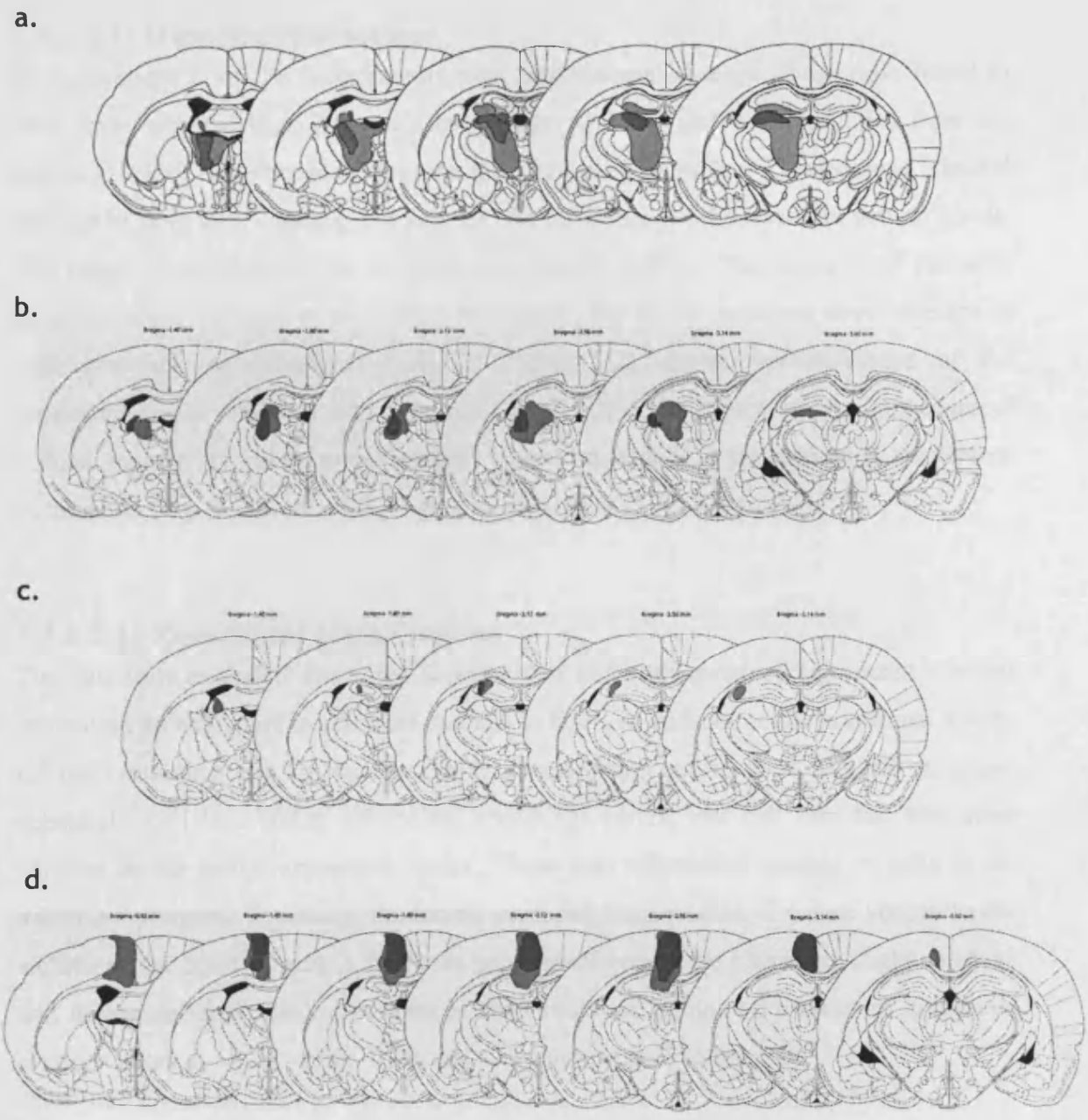

Figure 3.1: Extent of the damage for lesions to anterior thalamic nuclei (a), laterodorsal thalamic nuclei (b), control antero-dorsal hippocampus (c), and contralateral retrosplenial cortex (d). The numbers refer to the distance of the section from bregma (mm). The maximum and minimum extents of the lesions are shown in grey and black respectively.

3.3.1.2: Experiment 2

3.3.1.2.1: Hippocampal lesions

In Experiment 2, of the fourteen rats with hippocampal damage, three were found to have sustained less than 30% cell loss (range 10-30%) and were excluded from the analysis. All of the remaining rats with hippocampal lesions (n = 11) sustained bilateral damage to both the dentate gyrus and the CA subfields at all dorsal and ventral levels. The range of cell loss in the hippocampus was 60-100%. The majority of rats also sustained some cell loss in the ventral subiculum, but no rat sustained direct damage to post-subiculum or entorhinal cortex. Figure 3.2a shows reconstructions of the maximum (light shading) and minimum (dark shading) extent of the hippocampal lesions on a series of horizontal sections taken at distances in mm ventral to the surface of the brain (top to bottom: -3.1, -3.6, -4.6, -5.6, -6.6, -7.6, -8.4 mm).

3.3.1.2.1: Entorhinal cortex lesions

Two rats were excluded due to the fact that they had both sustained significant bilateral subiculum damage, and in one case damage to CA1, in addition to the entorhinal lesion. Of the remaining rats in the entorhinal cortex lesion group (n = 10), all sustained substantial cell loss within the medial entorhinal cortex, and cell loss that was more variable in the lateral entorhinal cortex. There was substantial sparing of cells in the subicular complex. Typically, the lesion extended from -4.6 to -7.6 mm ventral to the surface of the brain. Figure 3.2b shows reconstructions of the maximum (light shading) and minimum (dark shading) extent of the entorhinal lesions on a series of horizontal sections taken at -4.74, -5.60, -6.10, and -7.10 mm ventral to bregma.

2a.

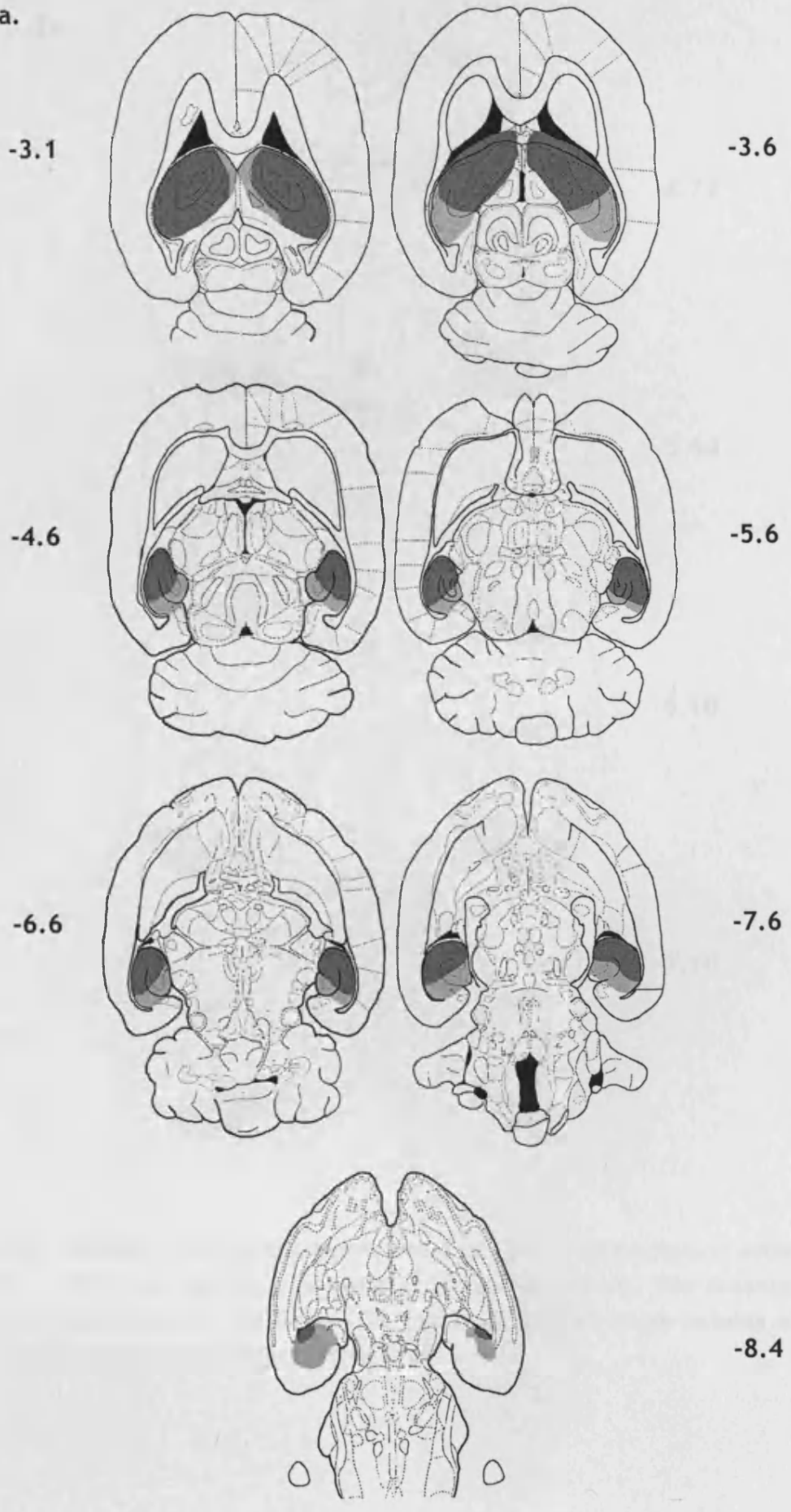

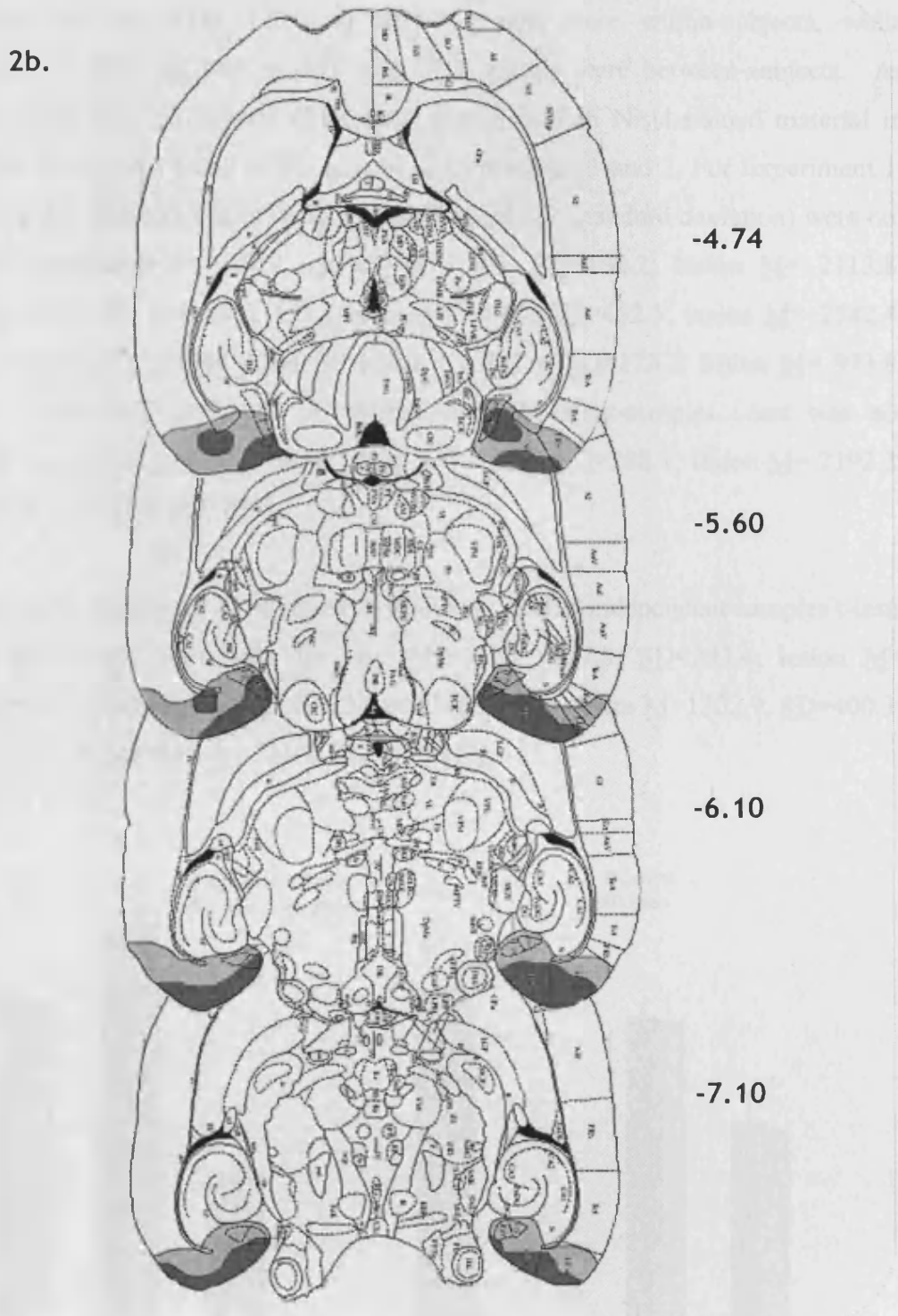

Figure 3.2: Reconstructions of the hippocampal (a, -3.1 to -8.4 mm) and entorhinal (b, -4.74 to -7.10 mm) lesions on a series of horizontal sections. The distances are relative to the surface of the brain. The maximum and minimum extents of the lesions are shown in grey and black respectively.

3.3.2: Nissl counts

Comparisons for the ATN, LD, and adHIP groups were within-subjects, while comparisons for RSC, as well as HIP and ENT groups were between-subjects. As shown in Figure 3.3, no overall differences were found in Nissl-stained material in retrosplenial cortex as a result of the lesions in Experiment 1 and 2. For Experiment 1, two-tailed paired-samples t-tests (where M=mean and SD=standard deviation) were not statistically significant for ATN (sham M=2109.1, SD=190.2; lesion M= 2113.8, SD=117.6, t(4)=1.82, p=0.885), LD (sham M=2549.9, SD=452.5; lesion M= 2582.4, SD=405.3, t(6)=1.99, p=0.849), adHIP (sham M=891.4, SD=173.3; lesion M= 973.8, SD=218.5, t(4)=1.167, p=0.308). A two-tailed independent-samples t-test was not statistically significant either for RSC (sham M=2153.5, SD=288.1; lesion M= 2192.3, SD=471.0, t(11)=0.185, p=0.857).

The results were similar for Experiment 2, where two-tailed independent-samples t-tests were not statistically significant for HIP (sham M=1977.8, SD=293.4; lesion M= 1952.1, SD=171.8, t(15)=0.228, p=0.823), or ENT groups (sham M=1302.9, SD=400.3; lesion M= 1251.4, SD=356.4, t(11)=0.242, p=0.813).

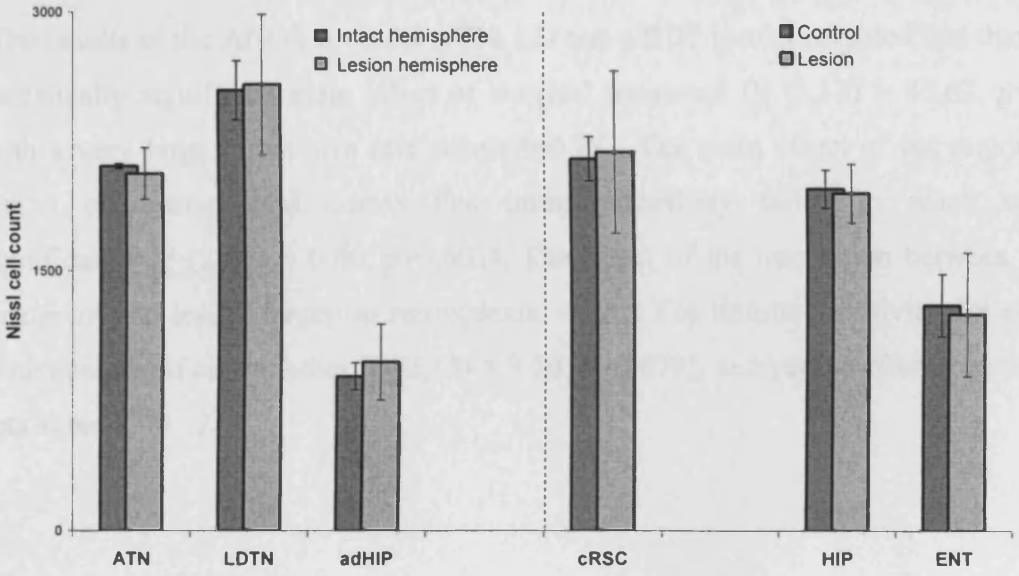

Figure 3.3: Relative to their respective controls, counts of Nissl-stained material revealed no differences as a result of each lesion (Experiment 1 on the left, Experiment 2 on the right). Error bars represent the standard error of the mean.

3.3.3: Retrosplenial cortex immunohistochemistry

For the hippocampal lesions, tissue was not obtained on an adequate plane for one rat that was thus excluded (remaining n =10). For all the other groups, tissue was obtained for each subject. Variances were not significantly different between the levels compared, and thus the statistical analyses were based on the assumption of equal variances.

3.3.3.1: Fos-positive cell count comparisons

3.3.3.1.1: Experiment 1: ATN, LD, adHIP and RSC lesions

In order to evaluate the effect of ATN, LD, and adHIP(ctrl) lesions, a mixed factorial design analysis of variance (ANOVA) was conducted on the raw Fos-positive cell counts, where surgical treatment was a within-subjects factor and lesion target was a between-subjects factor. Given the fact that interhemispheric comparisons could not be made for the RSC group and that for this group comparisons were made to normal control subjects, (i.e. between- rather than within-subjects comparison), a separate independent-samples t-test was conducted on the RSC data.

The results of the ANOVA on the ATN, LD and adHIP results revealed that there was a statistically significant main effect of surgical treatment [F (1,13) = 45.63, p<0.001], with a very large effect size (eta squared=0.78). The main effect of the region of the lesion on retrosplenial cortex Fos immunoreactivity failed to reach statistical significance [F (2,13) = 0.60, p=0.601]. The effect of the interaction between surgical treatment and lesion target on retrosplenial cortex Fos immunoreactivity did not reach statistical significance either [F (2,13) = 3.10, p=0.079], and yet the effect size was large (eta squared=0.32).

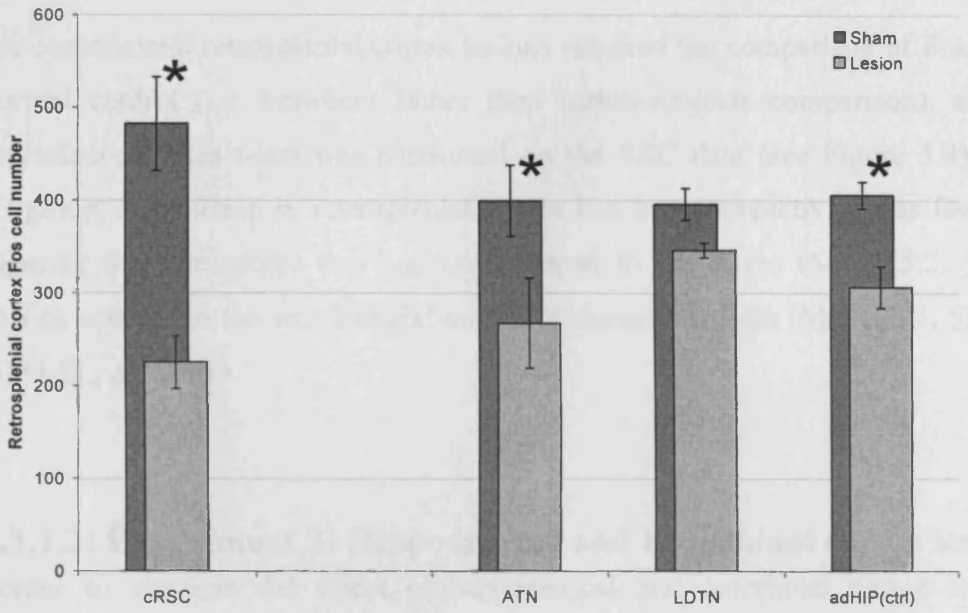

Figure 3.4: Effect of ATN, LD, adHIP(ctrl) and RSC lesions on Fos immunoreactivity in retrosplenial cortex granular b. Error bars represent the standard error of the mean. Note that the RSC comparisons are between-subjects, and ATN, LD, and adHIP(ctrl) comparisons are within-subject. Error bars represent the standard error of the mean, * $p<0.05$.

Follow-up tests to the significant main effect of surgical treatment conducted using paired-samples t-tests revealed the effect of surgical treatment for each lesion target (see Figure 3.4). There was a statistically significant decrease in retrosplenial cortex Fos immunoreactivity in the ATN group when comparing the 'intact' hemisphere (M= 399.7, SD=85.8) with the hemisphere that was ipsilateral to the lesion (M= 267.8, SD=108.8), $t(4)=5.28$, $p=0.006$). Similarly, in the adHIP(ctrl) group, a reduction in retrosplenial cortex Fos immunoreactivity was found when comparing the 'intact' hemisphere (M= 405.6, SD=31.8) with the hemisphere ipsilateral to the lesion (M= 306.2, SD=50.0), $t(4)=4.24$, $p=0.013$). However, the effect of surgical treatment was not statistically significant for the LD group, where no statistically significant reduction in retrosplenial cortex Fos immunoreactivity was found when comparing the 'intact' hemisphere (M= 395.8, SD=41.5) with the hemisphere ipsilateral to the lesion (M= 346.0, SD=19.6), $t(5)=2.14$, $p=0.085$). Consistent with the evidence of a stronger effect of anterior over laterodorsal thalamic nucleus damage on retrosplenial cortex Fos expression, the one rat within the LD group that exhibited some damage in the anterodorsal thalamic nucleus (i.e. part of ATN) was also the rat that displayed the greatest reduction in Fos immunoreactivity.

Since contralateral retrosplenial cortex lesions required the comparison of Fos levels to a normal control (i.e. between- rather than within-subjects comparison), a separate independent-samples t-test was conducted on the RSC data (see Figure 3.4). For the RSC group, a reduction in retrosplenial cortex Fos immunoreactivity was found when comparing the hemisphere that was contralateral to the lesion (M= 225.2, SD=85.4) with Fos activity in the retrosplenial cortex of normal subjects (M= 482.5, SD=123.1, t(13)=4.81, $p<0.001$).

3.3.3.1.2: Experiment 2: Hippocampal and Entorhinal cortex lesions

In order to evaluate the effect of hippocampal and entorhinal cortex lesions on retrosplenial cortex Fos immunoreactivity, a two-way ANOVA was conducted, where surgical treatment and lesion target were between-subjects factors. The results of the ANOVA revealed that there was a statistically significant main effect of surgical treatment [F (1,31) = 10.62, p=0.003], with a large effect size (eta squared=0.26). A statistically significant effect of lesion target was also found [F (1,31) = 11.90, p=0.002], again with a large effect size (eta squared=0.28). The effect of the interaction between surgical treatment and lesion target on retrosplenial cortex Fos immunoreactivity did not reach statistical significance [F (1,31) = 1.69, p=0.203], and the effect size was only moderate (eta squared=0.05).

Follow-up tests conducted using independent-samples t-tests (two-tailed) revealed the effect of surgical treatment for each lesion target. As shown in Figure 3.5a, there was a statistically significant decrease in Fos-positive cell count in retrosplenial cortex in the HIP group (M= 1056.5, SD=307.2) when compared to the sham lesions (M= 1526.8, SD=482.3, t(15)=2.47, p=0.026). Likewise, as shown in Figure 3.5b, there was a statistically significant decrease in retrosplenial cortex Fos-positive cell counts in the ENT group (M= 834.7, SD=148.3) when compared to sham lesions (M= 1036.8, SD=232.4, t(16)=2.25, p=0.039).

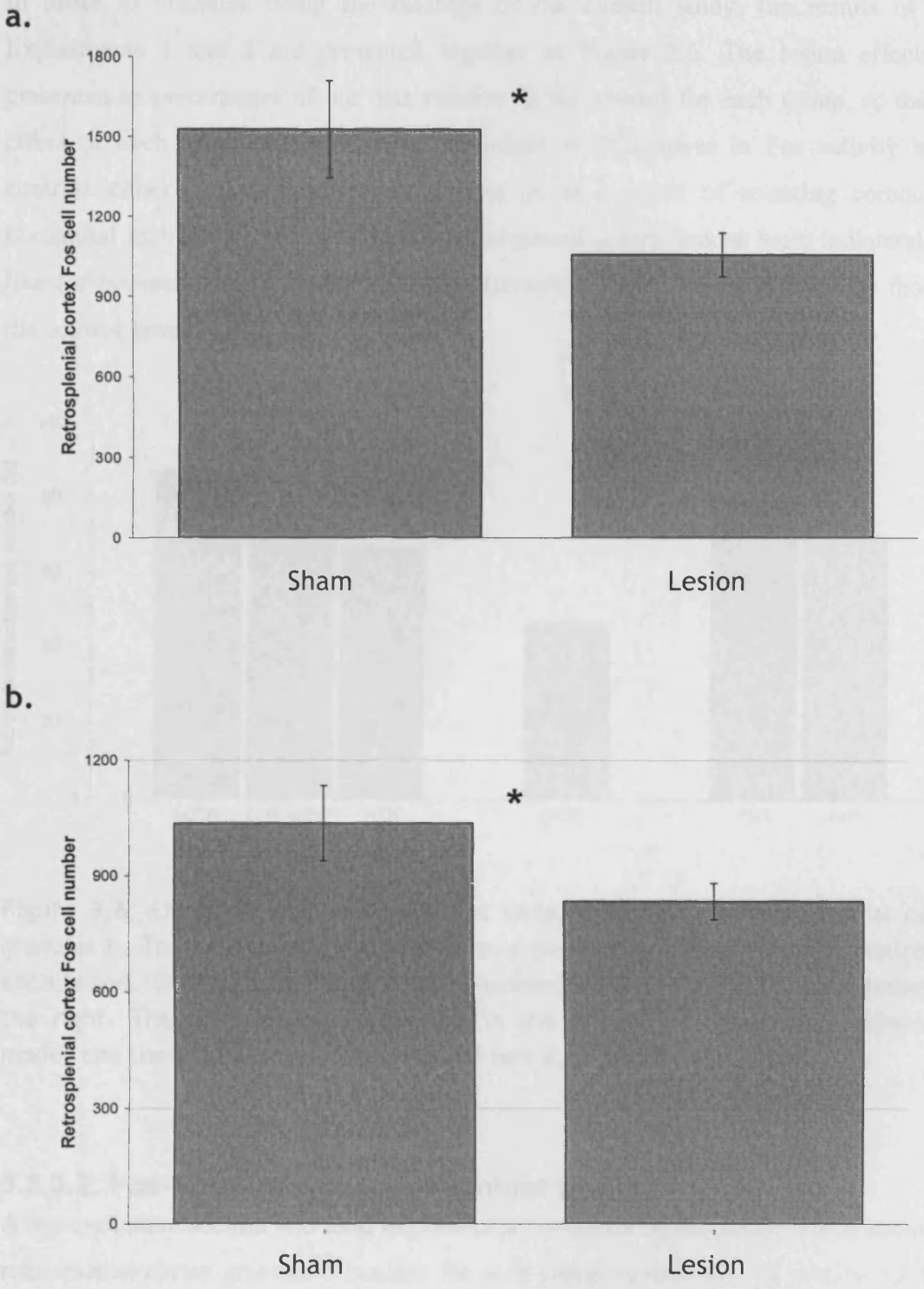

Figure 3.5: Effect of hippocampal lesions (a) and entorhinal cortex lesions on Fos immunoreactivity in retrosplenial cortex granular b. Error bars represent the standard error of the mean, * $p<0.05$.

In order to visualise better the findings of the current study, the results of both Experiments 1 and 2 are presented together in Figure 3.6. The lesion effects are presented as percentages of the data relative to the control for each group, so that the effect of each lesion can be seen independent of differences in Fos activity in the controls either due to baseline differences or as a result of counting coronal vs. horizontal sections. Note that although retrosplenial cortex lesions were unilateral, just like for between-groups comparisons, the (unilateral) counts were divided by those of the control group.

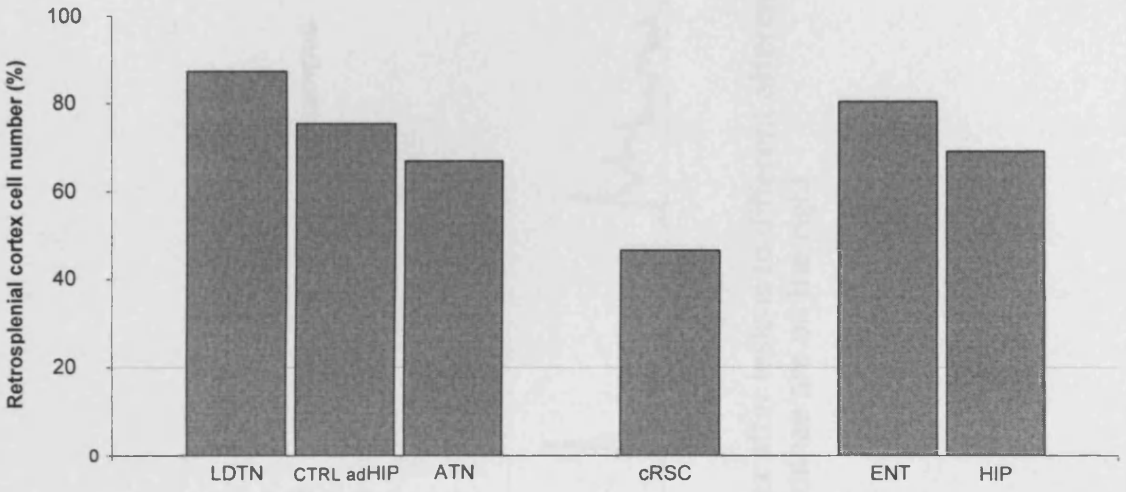

Figure 3.6: Effect of each lesion on Fos immunoreactivity in retrosplenial cortex granular b. The cell count is presented as a percentage relative to the control for each lesion. The unilateral lesions are presented on the left and bilateral lesions on the right. The retrosplenial cortex lies in the middle, as unilateral lesions were made, and the values compared to normal rats (i.e. between-subjects).

3.3.3.2: Fos-positive cell count laminar profiles

A representative section was used to produce a horizontal mean profile of Fos activity in retrosplenial cortex granular b laminae for each group, as described in section 3.2.5. As shown in Figure 3.7, it is apparent from this qualitative analysis that the laminae of retrosplenial cortex granular b are not equally affected by the lesions. In comparison to deep laminae, superficial laminae appear to be more prone to exhibit Fos hypoactivity.

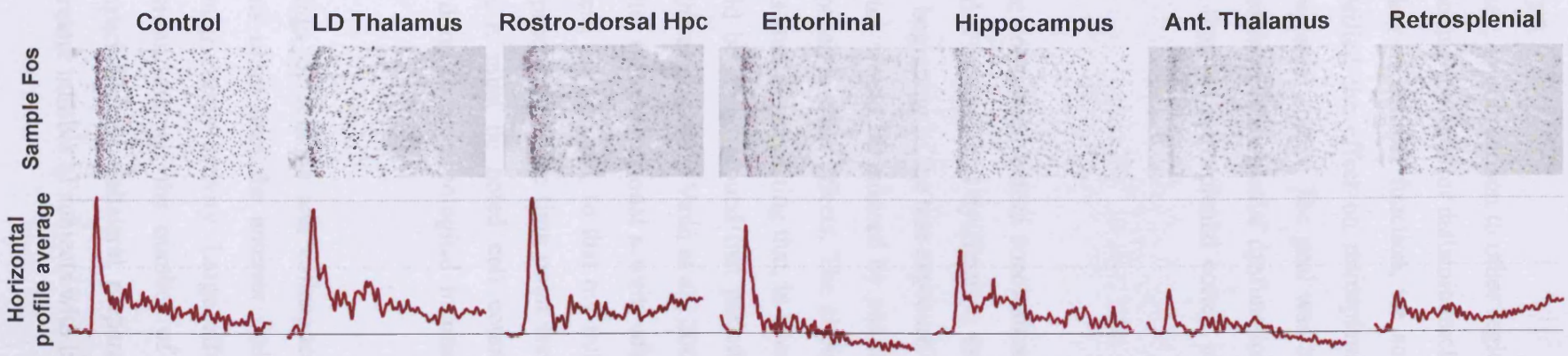

Figure 3.7: Profiles of Fos activity in retrosplenial cortex after lesions to different afferents. For each image and profile, the superficial laminae and on the left, and the deep laminae are on the right.

3.4: Discussion

The retrosplenial cortex, in comparison to other regions, appears highly sensitive to the loss of one of its afferents, the anterior thalamic nuclei (Jenkins et al., 2002). Using Fos expression as a marker of cellular function, we sought to verify the breadth of this vulnerability. We verified the effect on retrosplenial function of damage to several afferents of the retrosplenial cortex. The goal was to reveal possible candidate regions where damage can result in retrosplenial dysfunction in the absence of cell death. The present study found that the retrosplenial cortex is selectively vulnerable to afferent damage.

Some issues must be considered before conclusions can be drawn from our data. We operationally defined a retrosplenial dysfunction as a dysregulation of Fos production 90 minutes after the beginning of the test exposure. It was expected that the activity of the retrosplenial cortex would be induced by placing the rats in a novel environment, thereby preventing possible floor effects. The choice of the post-exposure period was informed by previous studies suggesting that, in several brain regions, Fos levels peaked and differences could be found around that period after novel environment exposure (Papa et al., 1993; Zhu et al., 1997; Vann et al., 2000; Struthers et al., 2005). However, it remains a possibility that the regional activity after exposure to a novel environment may follow a different time course, so that my null findings could reflect the relative insensitivity of the procedure at the time point tested, rather than an absolute lack of effect. Furthermore, it must be noted cell counts, either of Nissl or Fos-positive material, were not done in a stereological manner, and so 'counts' do not refer to absolute cell counts.

Based on the findings of Jenkins and colleagues (2004), we sought to verify the potential of afferents other than the anterior thalamic nuclei to produce substantial effects on retrosplenial cortex activity. Large effects were expected for the anterior thalamic nuclei lesions, and so the number of subjects used was minimised by optimising the comparisons via unilateral preparations. Where the effects were not certain, we used a greater number of subjects with bilateral lesions.

Large effects were found in both Experiments 1 and 2, even using relatively low numbers of rats in groups with unilateral lesions. In order to interpret the non-significant

effect of the interaction between surgical treatment and lesion target on retrosplenial cortex Fos immunoreactivity, it is important to consider the power of the analyses in the current study. It should be noted that while the power of the analyses of the main effects in both experiments in the current study was high ($\geq$ 0.8), that of the analyses of the interaction between the effects of surgical treatment and the target region was low (0.05 and 0.24 in Experiments 1 and 2, respectively). Thus, the power of the interaction analyses may have been insufficiently high to detect a significant effect, so precluding a conclusive finding for the analyses of the relative effects of each lesion on retrosplenial cortex Fos production. Further studies may be necessary to verify the relative effect of damage to each site on retrosplenial cortex Fos immunoreactivity.

In spite of a lack of power for interaction analyses, our results provided evidence that not all afferent damage impacts retrosplenial function in the same way. Anterior thalamic, hippocampal and entorhinal cortex but not laterodorsal thalamic nuclei damage clearly impair retrosplenial cortex function as visualised by Fos activity. Furthermore, the profiles of Fos activity according to retrosplenial cortex laminae varied with the lesion sites (see Figure 3.7). It appears that the effects of lesions in the anterior thalamic nuclei and the hippocampus are qualitatively the strongest, outside of damage to the retrosplenial cortex itself. The finding that the retrosplenial cortex is differentially vulnerable to damage to its afferents replicates and extends the observations of Jenkins and colleagues (2004). Our findings also further support the argument that covert pathology in the retrosplenial cortex could amplify the impact of neurological damage (Jenkins et al., 2004). That is, even in the apparent absence of alterations in cell counts in the retrosplenial cortex, the function of this region can be disturbed (present study, Garden et al., 2006), potentially permanently (Jenkins et al., 2004). According to standard interpretations, neurological insults yield detrimental effects on cognition as a result of local damage. However, these effects on cognition may also be partly due to retrosplenial cortex dysfunction. Our results thus address the debate surrounding the concept of cryptic pathology (Bachevalier and Meunier, 1996; Squire and Zola, 1996) by providing supporting evidence for dysregulation in 'intact' sites distal to a lesion.

Every site targeted for damage in our study is reciprocally connected with the retrosplenial cortex (Vogt, 1981b; van Groen and Wyss, 1990a, b; van Groen and Wyss, 1990c; van Groen and Wyss, 1992a; van Groen and Wyss, 1995; Insausti et al., 1997; van Groen et al., 1999; van Groen and Wyss, 2003; Wiltgen et al., 2004). Some of the

regions tested are also connected to each other (e.g. HIP to ATN to RSC)), so in theory it is also possible that indirect effects could occur. These regions may interact, each potentially mediating different aspects of related tasks. In the current study, damage to certain afferents led to a more extreme disruption of retrosplenial cortex cellular function than others. It is thus apparent that the level of interaction of these regions in a system mediating memory functions and spatial abilities is not homogeneous. However, the fact that the anterior thalamic nuclei, the hippocampus, and the entorhinal cortex seem capable of driving the retrosplenial cortex is consistent with electrophysiological tests of their influence on retrosplenial cortex neuronal firing. There is evidence suggesting that while the retrosplenial cortex may be able to independently generate a theta rhythm (Talk et al., 2004) and to modulate that of the hippocampus (Destrade and Ott, 1982), its functions may be critically modulated by the anterior thalamic nuclei (Kubota and Gabriel, 1995; Smith et al., 2002), the hippocampus (Talk et al., 2004), and the entorhinal cortex (Freeman et al., 1997).

While damage in the adHIP group was relatively negligible in scale compared to that in the HIP group, it should be noted that the rostral retrosplenial cortex granular b, studied here, receives projections from the hippocampus that mainly originate in its septal pole (Wyss and van Groen, 1992). The same region, namely the septal pole of the hippocampus, was involved in the adHIP lesions. The finding that even very modest damage in the adHIP area can result in an appreciable deficit in retrosplenial cortex Fos activity is consistent with the topography of the projections from the hippocampus.

The effect of entorhinal damage on retrosplenial function accords with the finding that, in baboons, entorhinal lesions can lead to long-term hypometabolism in a few regions, including the posterior cingulate cortex (Meguro et al., 1999). Our findings extend those of a metabolic dysregulation by Meguro and colleagues (1999) by showing that entorhinal cortex damage also leads to retrosplenial cortex immediate-early gene hypoactivity in the rat. While entorhinal cortex damage produced a significant deficit in retrosplenial cortex function, the impact of the damage appeared to be less than that after anterior thalamic nuclei damage and equal or milder than that of the limited hippocampal damage in the adHIP control group (see Figure 3.6). In fact, there is conflicting evidence over the existence of entorhinal cortex projections to this subregion of the retrosplenial cortex (Swanson and Kohler, 1986; Wyss and van Groen, 1992; Insausti et al., 1997). However, even when the results of anterograde tracing

experiments have been positive, projections to granular b retrosplenial cortex arising from the entorhinal cortex were strong caudally and only weak rostrally (Insausti et al., 1997). It is interesting to note that entorhinal cortex lesions produced a significant reduction in retrosplenial cortex granular b Fos activity, in spite of the limited extent its projections to that area.

Based on this anatomical evidence, it is altogether possible that entorhinal cortex damage produced an effect on retrosplenial cortex function that differs according to the rostro-caudal level. Such an effect could explain the finding in the current study of an overall weak effect of entorhinal cortex since counts were taken throughout the whole rostro-caudal extent of granular b retrosplenial cortex. Overall counts may have dampened a strong effect say, if a reduction was exhibited in caudal retrosplenial cortex, but only accompanied by a weaker reduction or no reduction of Fos in rostral retrosplenial cortex granular b. Alternatively, the Fos hypoactivity as a result of entorhinal cortex lesions may be equivalent throughout the extent of granular b retrosplenial cortex, as a result of propagating activity from intrinsic connections (e.g. van Groen and Wyss, 2003). Further analyses will be necessary to verify this issue.

It thus appears that entorhinal cortex lesions may have produced retrosplenial cortex cellular dysfunction in spite of very light, if any, direct projections to the area studied (see Table 3.1). It is possible that the reduction of Fos activity in rostral retrosplenial cortex may occur as an indirect consequence of entorhinal cortex damage via intrinsic granular b retrosplenial connections (e.g. van Groen and Wyss, 2003). Alternatively, this hypoactivity may be effected through another brain region that is directly connected to both the entorhinal cortex and granular b retrosplenial cortex. For example, the entorhinal cortex has strong projections with dysgranular retrosplenial cortex (Wyss and van Groen, 1992; Insausti et al., 1997), itself reciprocally connected to granular b retrosplenial cortex (van Groen and Wyss, 2003). It is possible that damage to granular b retrosplenial cortex afferents that results in Fos hypoactivity may also act via an indirect route through this third region, adding to the Fos hypo-activity in granular b retrosplenial cortex resulting from direct connections anywhere throughout its rostro-caudal extent. As such, this possibility evokes the hypothesis that distal damage may also indirectly mediate retrosplenial cortex dysfunction. Lesion effects mediated through such an indirect route may, again, be afferent-specific, as damage to the laterodorsal nucleus, which exhibits even stronger connections with dysgranular than

does granular b retrosplenial cortex (Sripanidkulchai and Wyss, 1986; van Groen and Wyss, 1992a; van Groen and Wyss, 1992b), failed to produce a significant reduction in Fos activity in granular b retrosplenial cortex. Entorhinal cortex lesions appear to produce a pattern of Fos hypoactivity that is more similar to that produced by hippocampal than anterior thalamic nuclei lesions, i.e. hypoactivity in both superficial and deep laminae (data not presented). Thus, another possible route through which dysregulation may be induced could be via the hippocampal formation.

The relatively minor effect of laterodorsal thalamic nuclei lesions is intriguing. Both anterior thalamic and laterodorsal thalamic nuclei have projections to retrosplenial cortex granular b, and damage to the laterodorsal nucleus of the thalamus, like the anterior thalamic nuclei, has been found to yield spatial memory deficits. Lesions that combined damage to anterior thalamic nuclei and laterodorsal thalamic nuclei produced substantial deficits on tasks dependent on spatial memory (Wilton et al., 2001), and importantly, inactivation restricted to the laterodorsal thalamic nuclei yielded deficits in a spatial working task in a radial-arm maze (Mizumori et al., 1994). More selective lesions, largely confined within the laterodorsal thalamic nuclei, produced much milder deficits that were overcome with further training when rats were tested in a water maze task where the platform changed position every session (van Groen et al., 2002). Several task-related differences may account for the different impact of laterodorsal thalamic nuclei damage in the studies mentioned above, but, based on our findings, one possibility is that deficits were stronger in the behavioural task that also depended on retrosplenial cortex function.

While no effect of the RSC lesion was apparent based on the results of Nissl counts (see Figure 3.3), it is apparent that contralateral lesions sometimes resulted in bilateral effects, as can be seen in Nissl-stained material in Figure 3.8. Superficial Nissl-stained cells in Figure 3.8a but not b were selectively affected by the contralateral damage. A representative image of Fos immunoreactivity throughout the extent of retrosplenial cortex contralateral to the damage is shown in Figure 3.8c. The reduction in Fos appears to occur even if the superficial band of cells remain intact. The integrity of contralateral Nissl-stained cells is not consistent, even within subjects, making a systematic analysis difficult. While removal of contralateral afferents by cutting the callosal connections produced minimal degeneration (Vogt, 1981b), it is possible that in our study, excitotoxic lesions may have had an effect on the integrity of contralateral cells,

especially in laminae II-III. It is also possible that the much longer duration of the post-operative period in our study may have uncovered a protracted phase of degeneration. The reason for this finding is not clear and future work will verify the integrity of the tissue by comparing the results of Nissl stains with other methods specific for cell degeneration. The effects of cutting the callosal connections could also be compared to those of a unilateral retrosplenial cortex lesion.

Within a hemisphere, neurons in lamina V send dendrites superficially. These arborise in lamina II and reach lamina I. These dendrites can share the same dendritic bundles as those emanating from neurons in lamina II (Vogt, 1981b; Wyss et al., 1990). It is therefore possible that the deeper neurons affect the activity of neurons in lamina II. Additionally, the contralateral projections terminate mostly in deep laminae, and the projections from cells in lamina II project directly contralaterally, unlike cells in laminae III and V that project to a broader portion of the rostro-caudal extent of the contralateral retrosplenial cortex (Vogt, 1981b; Wyss et al., 1990; van Groen and Wyss, 2003). It is possible that altered neural activity of cells in lamina V may have a detrimental impact on adjacent superficial cells, and that the dysregulation of the latter could also affect contralateral superficial retrosplenial cortex function. Thus, altered neural activity in deep retrosplenial cortex may have consequences both intrahemispherically and, indirectly, interhemispherically. Figure 3.8d may provide evidence for such a cascade of events. However, if the results in Figure 3.8d were replicated and it was confirmed that dysfunction could propagate across hemispheres after retrosplenial cortex damage, such an effect would appear not to be generalised. This is because after unilateral anterior thalamic nuclei lesions, superficial retrosplenial cortex dysfunction is only observed ipsilaterally, not across both hemispheres. In terms of the effects of contralateral retrosplenial lesions, further work will be needed to obtain lesions without any lamina II-III effect on Nissl-stained material. Importantly though, the mechanism underlying the dysfunction after contralateral retrosplenial cortex lesions may be qualitatively different from that resulting from anterior thalamic nuclei damage, and may also differ from that after hippocampal and entorhinal damage.

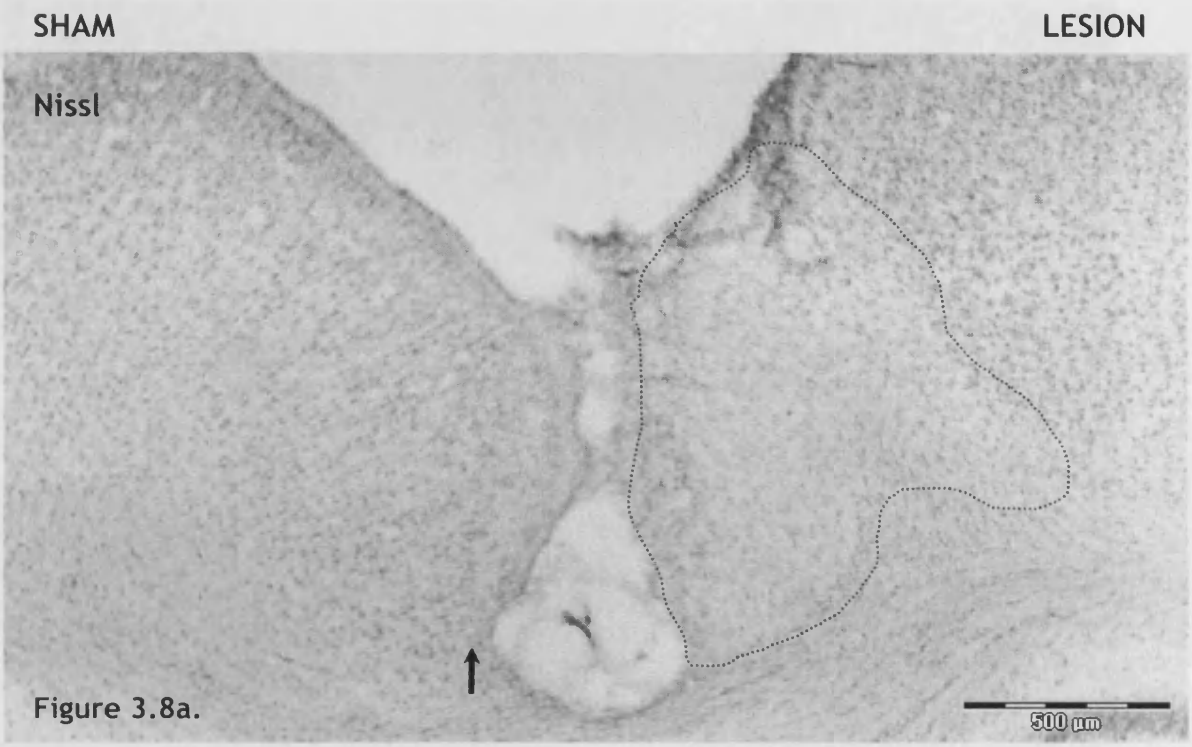

Figure 3.8a.

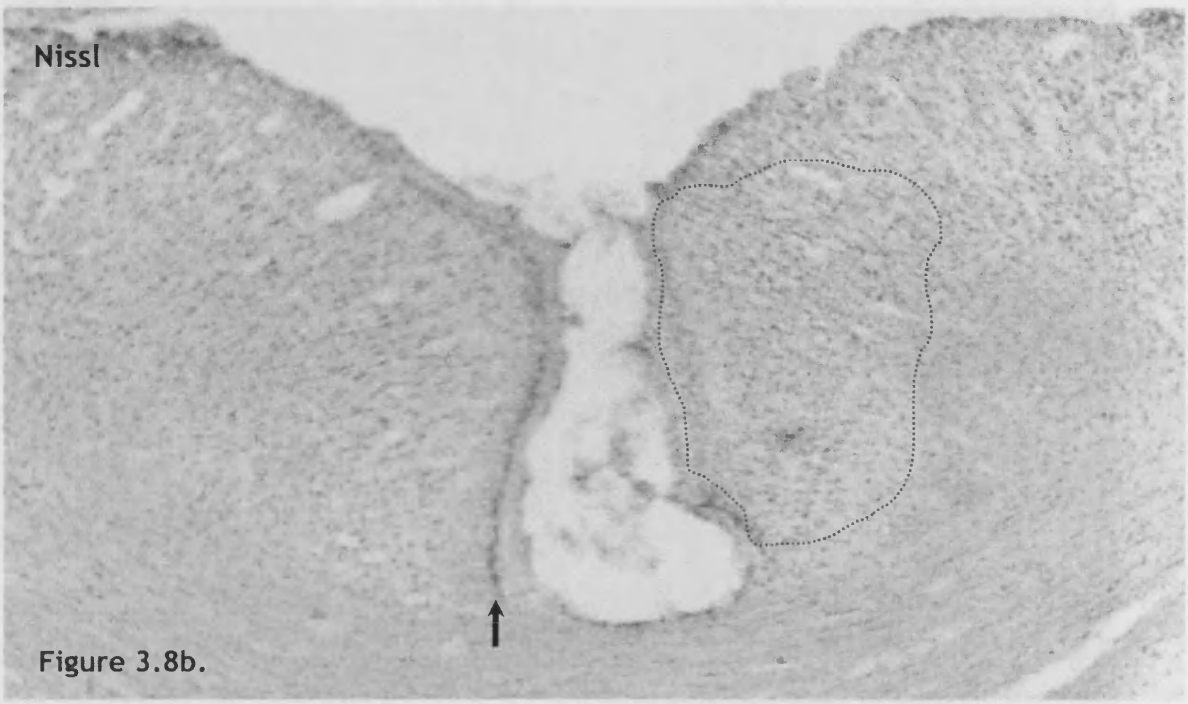

Figure 3.8b.

Figure 3.8a,b: Example of the effect of unilateral retrosplenial cortex lesions. Both images of Nissl-stained retrosplenial cortex tissue are from the same subject. The arrows indicate the location of lamina II cells.

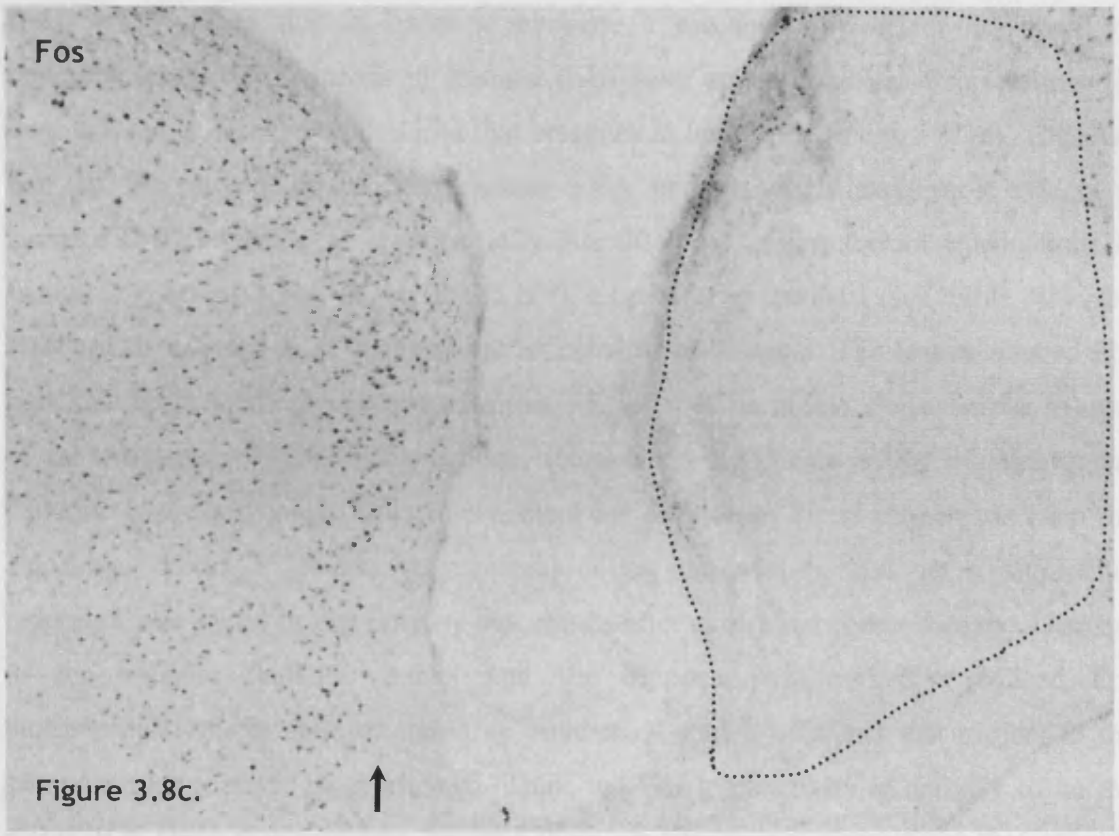

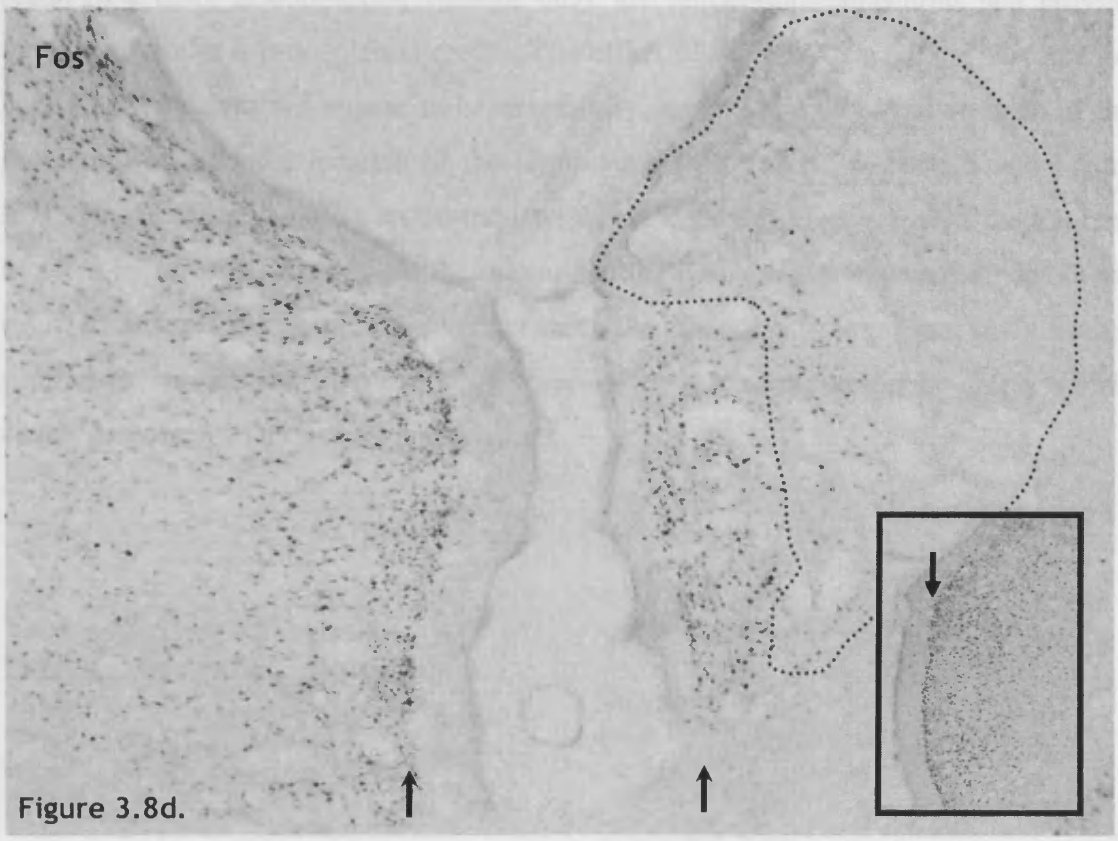

Figure 3.8c,d: Example of the effect of unilateral retrosplenial cortex lesions. Images are taken from one subject in c (same as a,b) and from another one in d. Images in a,b are of Nissl and c,d are of Fos staining. In d, the lesion is incomplete on that particular plane for this subject. It is worth noting how this deep lesion has resulted in a superficial reduction in Fos immediately adjacent, in addition to a contralateral reduction. Inset in d is a picture from a normal rat. The arrows indicate the location of lamina II cells that are normally strongly Fos-immuno-positive.

It is worth noting that in order to evaluate a disconnection effect, it should be remembered that the neurons in laminae II-III have apical dendrites that terminate in lamina I, and a descending dendrite that branches in lamina IV (Vogt, 1981a). Thus, the fact that the retrosplenial cortex granular b Fos hypoactivity appears most evident in laminae II-III could be at least partially due to a loss of input from terminations in lamina I. Whereas ATN, LD, HIP and ENT all project to lamina I (see Table 3.1) , the effect of damage in these regions was revealed to be unequal. The lesion-induced Fos hypoactivity is seen only for some lesions, i.e. for specific inputs. For example, in spite of the existence of direct connections, there is no significant effect of laterodorsal thalamic nucleus damage. Conversely, there are only weak direct projections from the entorhinal cortex to rostral retrosplenial cortex granular b, and yet a significant reduction was found in Fos-positive cell counts after entorhinal cortex damage. Damage to the anterior thalamic nuclei and the hippocampus markedly reduced Fos immunoreactivity in spite of the large number of spared afferents that project to the same laminae that are most affected. Thus, the Fos hypoactivity is unlikely to be the result of a mere disconnection because there are remaining connections that provide input to granular b retrosplenial cortex. The effect of afferent damage on retrosplenial cortex activity does not appear to be necessarily directly related to the strength of the projection or even the location of the termination (see Table 3.1A and B and Figure 3.7). The fact that the IEG lesion-induced effect does not always match the laminae targeted by afferents strengthens the notion that the retrosplenial hypoactivity is not the result of a direct disconnection. In conclusion, the findings of the present study further support the notion that the effects of selective brain damage could be amplified via covert pathology in the retrosplenial cortex.

Table 3.1A: The location and the approximate strength of the terminations of projections to retrosplenial cortex granular b (Rgb), according to laminae. * strong projections only in caudal granular b retrosplenial cortex (van Groen and Wyss, 1990a, b; van Groen and Wyss, 1990c; van Groen and Wyss, 1992a; Wyss and van Groen, 1992; van Groen and Wyss, 1995, 2003). On the right, examples are depicted of the effects of lesions on Fos immuno-reactivity in the retrosplenial cortex.

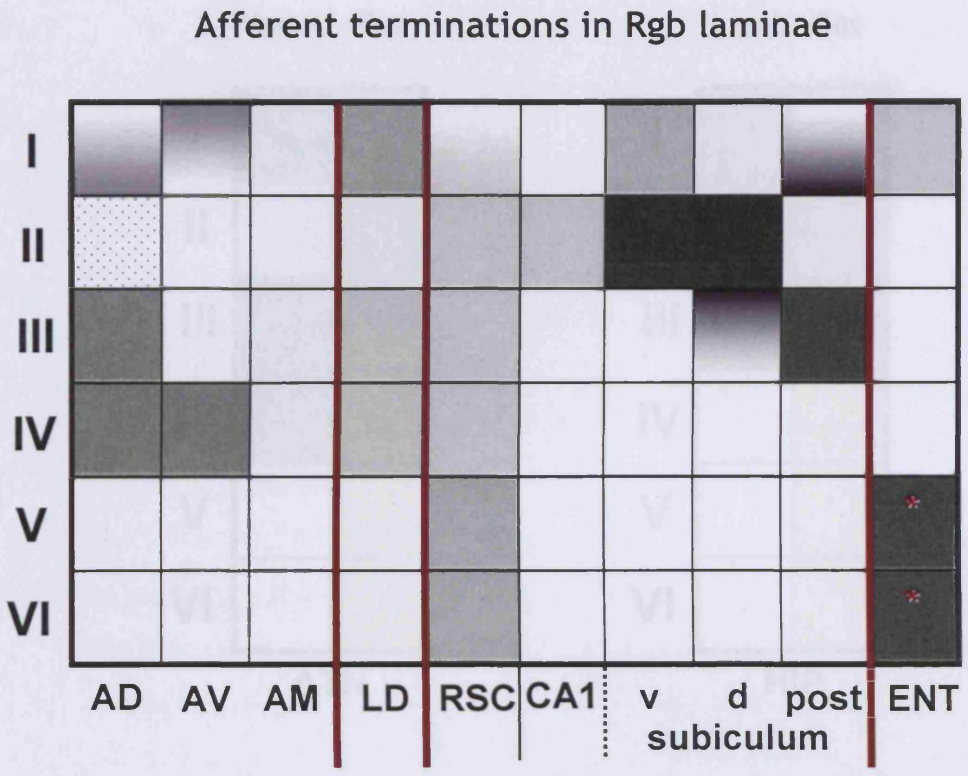

Table 3.1B: Illustration of the effects of anterior thalamic nuclei and hippocampal lesions on Fos immuno-reactivity in the retrosplenial cortex. Notice the mismatch between the patterns of Fos reduction (darkest equals most reduced) and the patterns of terminations from the relevant regions. Left = terminations in granular b retrosplenial cortex; right Fos activity after lesions.

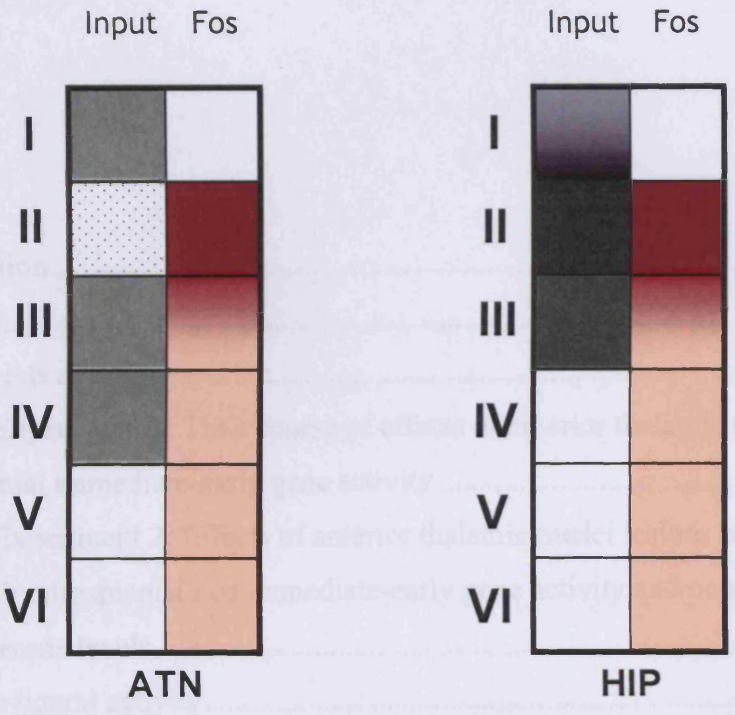

Chapter 4

Effects of anterior thalamic nuclei lesions on retrosplenial cortex immediate-early gene activity: Time course, cell characteristics, and association with corticosterone levels.

4.1: Introduction

The anterior thalamic nuclei (ATN) and the retrosplenial cortex are reciprocally connected (Vogt et al., 1981; van Groen et al., 1993). Damage to these regions induces similar learning deficits in rats. For example, deficits in allocentric spatial memory and object-in-place discrimination are found to be a common product of both anterior thalamic nuclei (Aggleton et al., 1996; Warburton et al., 2000; Wilton et al., 2001; Mair et al., 2003) and retrosplenial cortex (Vann and Aggleton, 2002; Parron and Save, 2004; van Groen et al., 2004; Cain et al., 2006). Furthermore, both regions are closely associated with amnesic syndromes in humans (Reed et al., 1999; Aupée et al., 2001; Maguire, 2001a; Maguire, 2001b; Reed et al., 2003; Svoboda et al., 2006). Interest in these two areas stems not only from direct evidence that they work together to support memory (Sutherland, 1993), but also from the ways in which they might jointly contribute to neurological disorders characterised by memory deficits. In Alzheimer's disease, for example, pathology commences at an early stage not in retrosplenial cortex but in the entorhinal cortex and the anterior thalamic nuclei (Braak and Braak, 1991a, b), yet it is retrosplenial cortex that is typically the first to show metabolic decreases (Minoshima, 1997; Nestor et al., 2003; Buckner, 2004). In light of this mismatch between overt pathology and metabolic alterations, one possibility to explain the early metabolic disturbance is that anterior thalamic pathology alters retrosplenial cortex function. In accord with this notion, Clarke and colleagues (1994) found that an anterior thalamic infarct resulted in retrosplenial hypometabolism.

Previous studies in the rat revealed that anterior thalamic nuclei lesions produce transynaptic molecular alterations in retrosplenial cortex. Large unilateral thalamic lesions in rats decrease levels of metabolic enzymes and of various presynaptic receptors in granular retrosplenial cortex (van Groen et al., 1993). The retrosplenial cortex in the rat has been found to be particularly susceptible to anterior thalamic damage (Jenkins et al., 2002). More recently, it was found that selective anterior thalamic lesions cause a dramatic loss of the protein products of the immediate early genes (IEGs) c-*fos* and *zif268* in superficial granular retrosplenial cortex (Jenkins et al., 2004). After anterior thalamic lesions, as many as 90% of the cells can stop producing Fos (Jenkins et al., 2004). This change may be an example of 'covert pathology' (i.e. a functional lesion where there is no overt pathology). This is because in contrast to the traditional view of diaschisis (cf. Luauté and Luauté, 2005), the effects seem permanent

(Jenkins et al., 2004), and there is no evidence of cell death in retrosplenial cortex (Vogt et al., 1981; Jenkins et al., 2004).

In the previous chapter, I described the findings of experiments designed to investigate the vulnerability of the retrosplenial cortex by evaluating the effects of damage to regions that project to it. The current chapter focuses on the effects of one of these regions, the anterior thalamic nuclei. The first experiment presented here sought to reveal the time course of the anterior thalamic nuclei lesion-induced reduction in Fos and Zif268 production in the retrosplenial cortex. In Experiment 1, within-subject comparisons were made after unilateral anterior thalamic nuclei lesions. These comparisons were from tissue from the hemisphere ipsilateral to the lesion ('Lesion') to the hemisphere contralateral to the lesion ('Intact'). In order to characterise further the onset of the effects, comparisons were made at several time points up to the earliest one that was evaluated by Jenkins and colleagues (Jenkins et al., 2004). The time points for tissue sampling were one, two, four and eight weeks after the surgeries. No earlier time points were chosen to minimise the potential confound arising from the acute effects of the surgery and the anaesthetic on IEG activity (Jeffery et al., 1990; Takayama et al., 1994; Hamaya et al., 2000). An additional goal of the study was to confirm the thalamic lesion-induced Fos hypoactivity in a different strain of rats to ensure that the finding was not particular to a specific strain.

Next, I sought to pinpoint more precisely the effects of anterior thalamic nuclei damage. In Experiment 2, focusing only on the activity patterns of the Fos IEG, immuno-positive cell characteristics were quantified in superficial and deep laminae of subregions (granular b and dysgranular) of the rostral retrosplenial cortex in rats with bilateral anterior thalamic nuclei lesions. In this second experiment, the scope of investigation was also widened by addressing the issue of dysfunction via distal lesions using a different measure, i.e. by evaluating the possibility that the anterior thalamic nuclei lesions could alter endocrine levels in a way that would affect retrosplenial cortex function. Corticosterone is a neuroactive hormone that is known to play a critical modulatory role in behaviour, cognitive abilities, and neuroplasticity (e.g. reviews by Lupien and McEwen, 1997; Belanoff et al., 2001; Sapolsky, 2003). Corticosterone can both potentiate and depress plasticity and memory, depending on the timing and the behavioural context; it is known that persistent activity of this hormone can reduce hippocampal neuroplasticity and produce memory impairments (e.g. reviews by Lupien

and McEwen, 1997; Belanoff et al., 2001; Sapolsky, 2003). Anterior thalamic nuclei lesions have been reported to affect the levels of circulating corticosterone (Suarez et al., 1987), but as yet no information is available on the effect that this particular alteration in endocrine response may have on the brain. It was therefore decided to test the potential association of the systemic levels of the hormone corticosterone and of Fos activity in the retrosplenial cortex. The present study thus increased the breadth of previous examinations of the effects of anterior thalamic nuclei lesions, and informs us about the nature and the onset of the retrosplenial cortex dysfunction.

4.2: Methods

Rats were housed in pairs under diurnal light conditions (14 h light/10 h dark) and after their arrival a period of at least a week was allowed before the rats received surgery. The rats were given unrestricted access to food and water in their home cages. All experiments were carried out in accordance with UK Animals (Scientific Procedures) Act, 1986 and associated guidelines.

4.2.1: Subjects and surgery

4.2.1.1: Experiment 1: Time course of effects of anterior thalamic nuclei lesion on retrosplenial immediate-early gene activity

The subjects were 26 male pigmented rats (Lister Hooded strain) weighing between 250 and 300g at the time of surgery. The rats were randomly assigned to four groups of different post-operative recovery periods (1 week, n=7); 2 weeks, n=7; 4 weeks, n=6; 8 weeks, n=6).

The rats were first anaesthetised with an intraperitoneal injection of pentobarbitone sodium (Sagatal, Rhône Mérieux, 80 mg/kg), and then placed in a stereotaxic frame (Kopf Instruments, CA) using atraumatic earbars, and with the incisor bar at +5.0. A craniotomy was made over the injection sites. Excitotoxic lesions were produced by injecting into two sites 0.22 µl of N-methyl-D-aspartate (NMDA; Sigma Chemicals UK; 0.12 M in phosphate buffered saline (PBS), pH 7.4) using a 1 µl syringe (Hamilton, Switzerland) that was attached to a moveable arm mounted on the stereotaxic frame. The stereotaxic coordinates relative to bregma were as follows: anterio-posterior, -0.2;

medio-lateral, ±1.0 and 1.8 from the midline, depending on the target hemisphere; dorso-ventral, -6.7 and -6.0 from dura for the medial and lateral injections, respectively. At the end of surgical procedure, the scalp incision was sutured, antibiotic powder (Aureomycin, Fort Dodge Animal Health, Southampton, UK) was subsequently applied topically and all rats also received a 5 ml subcutaneous injection of glucose saline. The rats were then placed in a recovery box maintained at 40°C. Paracetamol was dissolved in the rats' drinking water, and the rats were observed daily until recovery. Rats were administered the respiratory stimulant Millophylline (0.02 ml, s.c., Arnolds Veterinary Products, Shropshire, UK) as needed.

4.2.1.2: Experiment 2: Effects of anterior thalamic nuclei lesions on laminar granular b retrosplenial Fos immediate-early gene activity and on peripheral corticosterone levels

The subjects were 22 male pigmented rats (Dark Agouti strain) weighing between 224 and 264 g at the time of surgery. Rats received bilateral (n=16) or sham (n=6) lesions of the anterior thalamic nuclei. The procedures were the same as described above, but since bilateral lesions were made in a different strain, the anaesthetic dose, the infusion site volumes and their coordinates differed. The rats were anaesthetised with an intraperitoneal injection of 75mg/kg pentobarbitone sodium (Sagatal, Rhône Mérieux). Excitotoxic lesions were produced by injecting 0.20 µl of NMDA. The stereotaxic coordinates relative to bregma were as follows: anterio-posterior, -0.5; medio-lateral, ±1.0 and 1.7 from the midline; dorso-ventral, -6.3 and -5.7 from dura for the medial and lateral injections, respectively.

4.2.2: Behavioural activity

For experiments 1 and 2, the rats were exposed to a novel environment to induce immediate-early gene activation. They were placed for 15 minutes in a novel room, after which they were returned to their home cages. The groups of rats in Experiment 1 were tested as separate groups rather than in an inter-mixed fashion. The semi-random order in which the groups were tested was as follows: 8, 1, 4, then 2 week group.

Alterations in locomotor activity have been reported in rats with bilateral (Jenkins et al., 2004) but not unilateral anterior thalamic nuclei lesions (Jenkins et al., 2002). For this reason, a measure of locomotor activity was obtained in Experiment 2, where the rats had bilateral lesions. Measures were taken to characterise the reaction of the rats to the exposure to a novel environment. In the new environment, the rats were placed in activity test cages (Paul Fray Ltd, Cambridge, UK). These cages measured 56×39×19 cm, and were fitted with two photo-beams positioned 18 cm from opposite sides of the cage, 20 cm apart. The activity cage beam-break cross-over measure was used as an index of behavioural activity. The activity period was broken down into five three-minute bins.

4.2.3: Histology

Ninety minutes after the onset of this exposure to a novel context, the animals were irreversibly anaesthetised with sodium pentobarbital (140 mg/kg, Euthatal, Rhone Merieux, UK) and perfused transcardially with 0.1 M PBS followed by 4% paraformaldehyde in 0.1 M PBS. The brains were removed and post-fixed in 4% paraformaldehyde for four hours and then transferred to 25% sucrose overnight. Sections were cut coronally at 40 μm on a freezing microtome. Adjacent series were collected in 0.1 M PBS for Nissl staining and in 0.1 M PBS containing 0.2% Triton X-100 (PBST) for immunohistochemical visualisation of Fos protein.

4.2.4: Immunohistochemistry

Endogenous peroxidase activity was blocked by washing the sections with 0.3 % hydrogen peroxide in PBST for ten minutes, and then four times with PBST alone for the same duration. Sections were incubated at 4°C for 48 hours in PBST with rabbit polyclonal antibody for Fos (1:5000, Ab-5, Oncogene Science) and Zif268 (1:3000, C-19, Santa Cruz). Sections were then rinsed for ten minutes in PBST, four times. Next they were incubated in biotinylated secondary antibody, and then avidin-biotinylated horseradish peroxidase complex in PBST (Elite Kit, Vector Laboratories). Sections were next rinsed in Tris non-saline buffer (pH 7.4). Finally, immunoreactivity was visualised with diaminobenzidine (DAB Substrate Kit, Vector Laboratories) chromogen

incubation. Sections were then mounted on gelatinised slides. These slides and another series of cresyl violet stained tissue were dehydrated through a series of alcohol gradients and coverslipped.

4.2.5: Corticosterone assay

Enzyme immunoassay (EIA) for corticosterone content was performed using the IDS OCTEIA Corticosterone Kit (Immunodiagnostic Systems Ltd., Bolden, UK). Blood was obtained from the heart and centrifuged to separate the plasma. The plasma was frozen until the analysis. At the time of assay, the plasma was thawed to room temperature. Controls and samples were dilute by a factor of 10 with PBS containing horse serum. Protein and preservative were then added in duplicate to the polystyrene microplate coated with polyclonal rabbit anti-corticosterone antibody. The calibration curve was obtained by loading in duplicate calibrators (0-186 ng/ml) in the same plate. The samples were then incubated with corticosterone horseradish peroxidase-labelled overnight at 2-8°C. The wells were then washed three times with PBS. The colour was revealed by adding the enzyme substrate, tetramethylbenzidine (TMB) and incubating the plate at room temperature for 30 minutes before adding hydrochloric acid to stop the reaction. The absorbances were read at 450 nm using a microplate plate reader, the colour intensity developed being inversely proportional to the concentration of corticosterone. The percent binding (B/Bo%) of each calibrator, control and unknown sample was calculated as follows: B/Bo% = (mean absorbance) x 100 (mean absorbance for '0' calibrator). A calibration curve was prepared by plotting B/Bo% on the ordinate against concentration of corticosterone on the abscissa. The values were read from the curve in ng/ml.

4.2.6: Image capture and data analyses

Sections were viewed on a Leica DMRB microscope, photographed using an Olympus DP70 camera, and transferred to a computer. Counts of the stained nuclei were carried out using the program analySIS^D (Olympus, UK). The threshold was set automatically, at the same level for all sections from a same processing batch, based on overall illumination across both hemispheres. Counts were made in a frame area of 1768 x 1331 μm, using 5x magnification. The camera was positioned so that counts were taken across all layers of retrosplenial granular cortex b. Counts were typically taken

from three consecutive sections from both hemispheres of the retrosplenial cortex (approximately between -2.56 and 3.14 from bregma), and these counts were averaged to produce a mean. The regions of interest used are depicted in Figure 4.1. The SPSS 14.0 (Chicago) statistical package was used for all analyses.

For Experiment 1, mixed-design analyses of variance (ANOVA) were conducted to compare cell counts between the two retrosplenial cortex hemispheres after anterior thalamic nuclei lesions. A two-way ANOVA with surgical treatment and time point was carried out on the Nissl-stained cell counts. A three-way ANOVA was conducted, involving surgical treatment, IEG, and time point was carried out on the IEG-positive cell counts. The homogeneity of variances was verified using Levene's test of equality of variances for each ANOVA.

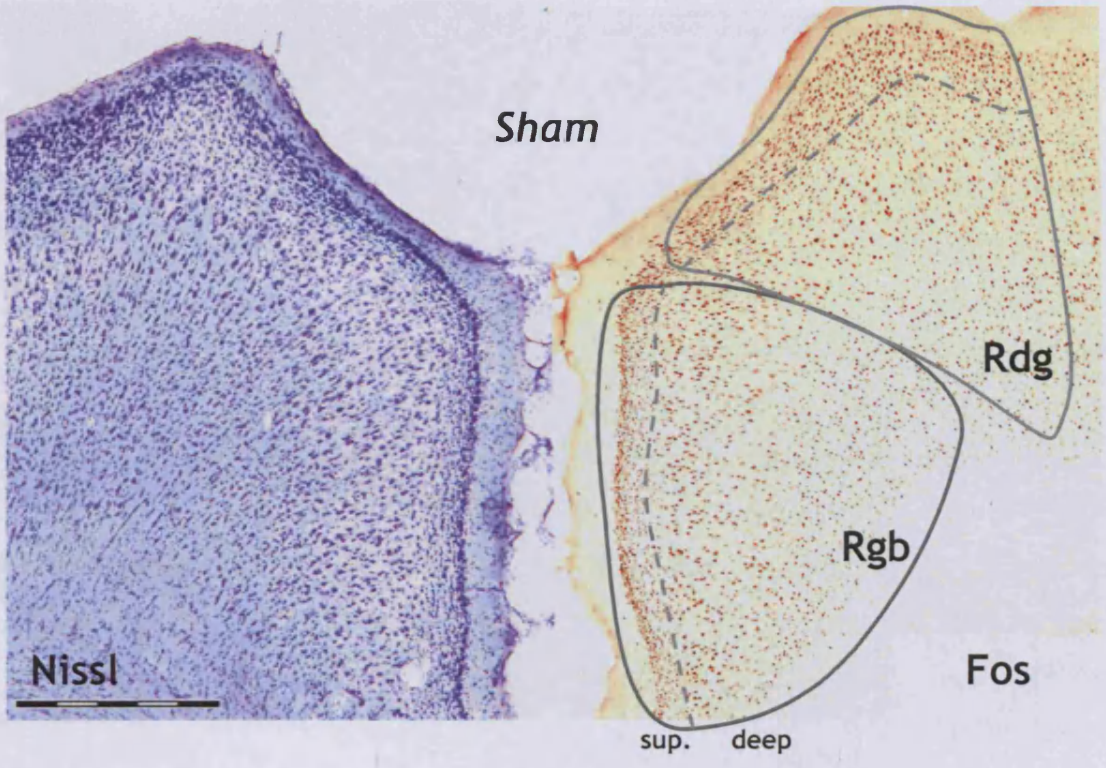

Figure 4.1: Regions of interest for Experiment 1 and 2; shown here is a normal brain. In Experiment 1, counts were obtained from all laminae in granular b retrosplenial cortex (Rgb), whereas in Experiment 2, separate counts were obtained for superficial (I-III) and deep (IV-VI) laminae in Rgb and dysgranular retrosplenial cortex (Rdg).Scale bar = 500 µm.

For Experiment 2, in order to evaluate the effect of lesions on counts of Nissl-stained, one-sample t-tests were used on Lesion data normalised to that of Sham subjects. In addition to cell counts, data on cell parameters were also obtained. Fos-positive cell area and sphericity (where 1= circle) were quantified using the program analySIS^D (Olympus, UK). A three-factor mixed-design ANOVA was first used for data analyses, with one between-groups factor (surgical treatment, Sham and Lesion) and two within-subjects factors (rostral retrosplenial cortex subregion, granular b (Rgb) and dysgranular (Rdg); and laminae, superficial and deep). The completed model included surgical treatment, retrosplenial cortex subregion and retrosplenial cortex laminae main effects. The dependent variables separately tested were the Fos-positive cell counts and the sphericity measure of those cells, as well as their area. A univariate analysis was used to test the effect of anterior thalamic nuclei lesions on corticosterone levels. In order to characterise further the relationship between the different factors tested, i.e. the relationship of Fos activity between retrosplenial cortex subregions, retrosplenial cortex subregion laminae, and in relation to behavioural activity, corticosterone, and weight, correlational analyses were conducted. Bivariate correlations were calculated using the Pearson product-moment correlation coefficient. Coefficients of determination were calculated by obtaining the square of the *r* values.

4.3: Results

4.3.1: Experiment 1

4.3.1.1: Histology

4.3.1.1.1: Nissl stains

4.3.1.1.1.1: Lesion analyses

An error during the immunohistochemical procedures precluded the analysis of one of the IEGs (Fos) for the tissue of the subjects in the four-week group. Thus, analyses for both IEGs were only performed on the three other time points (one-, two-, and eight-week recovery periods). The extent of the lesions was determined by verifying damage on Nissl-stained tissue in addition to tissue reacted for NeuN protein visualisation (see an example in Figure 4.2).

Figure 4.3 depicts the largest and the smallest lesions in Experiment 1. For the group in the first time point (1 week), one exhibited only minor anterior thalamic nuclei damage and was excluded. All remaining rats (n=6) showed substantial neuronal loss in the anterodorsal (AD) and anteroventral nuclei AV), except one case that had sparing in the latter. Some anteromedial nucleus (AM) sparing was found in four cases. All rats exhibited some laterodorsal thalamic nucleus (LD) damage, two rats showed some fimbria damage, and one showed some minor CA3 damage. For the second time point (2 week), two cases exhibited only partial damage of all three ATN, and were excluded. The remaining rats (n=5) displayed a complete unilateral loss of AD. Three cases showed some sparing of AV. Only two cases exhibited cell loss in AM. All rats exhibited some damage to rostral LD and only two showed some fimbria damage. Two cases in the third time point (8 weeks) exhibited no neuronal loss in AM and were excluded. The remaining four rats had substantial AD neuronal loss, one case showing some sparing of ventrolateral AV, and two some caudal AM sparing. All rats in this group also had some rostral LD damage.

Figure 4.2: An example of the benefit of using NeuN visualisation to assist in delineating the extent of anterior thalamic nuclei lesions.

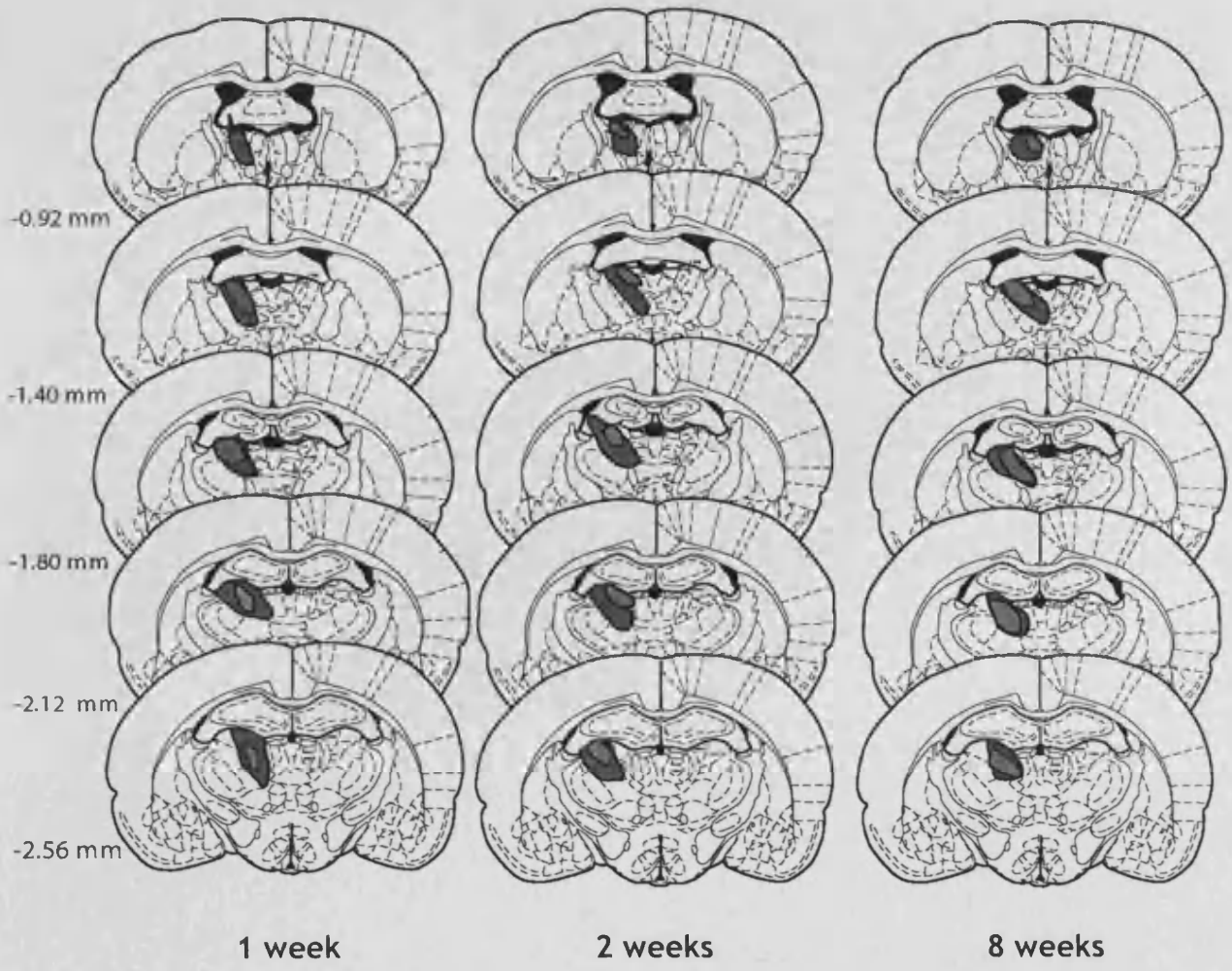

Figure 4.3: Extent of the damage produced by lesions centred on the anterior thalamic nuclei. The smallest and largest lesions are filled in dark and light colour, respectively. The numbers refer to the distance of the section from bregma (mm).

4.3.1.1.1.2: Quantification of Nissl-stained material

As shown in Figure 4.4, no overall differences were found in Nissl-stained material in retrosplenial cortex as a result of the lesions. In order to evaluate the effect of anterior thalamic nuclei lesions on retrosplenial cortex integrity, a mixed factorial design analysis of variance (ANOVA) was conducted, where surgical treatment was a within-subjects factor and time point was a between-subjects factor. The results of the ANOVA revealed that there was no statistically significant main effect of surgical treatment [$F(1,11) = 0.36$, $p=0.56$], nor any interaction between the effects of the surgical treatment and the time points [$F(2,11) = 0.58$, $p=0.58$]. However, there was a statistically significant effect of time point [$F(2,11) = 25.11$, $p<0.001$], with a very large effect size

(eta squared=0.82). Post hoc comparisons using the Bonferroni test indicated that Nissl counts were significantly greater for the first time point (M=5618.4, SD=309.7) compared to both the second (M=3806.1, SD=252.9, p=0.003) and the third time point (M=2534.5, SD=309.7, p<0.001). The third time point was also significantly lower than the second one (p=0.026).

Retrosplenial cortex Nissl counts across time points after ATN lesions.

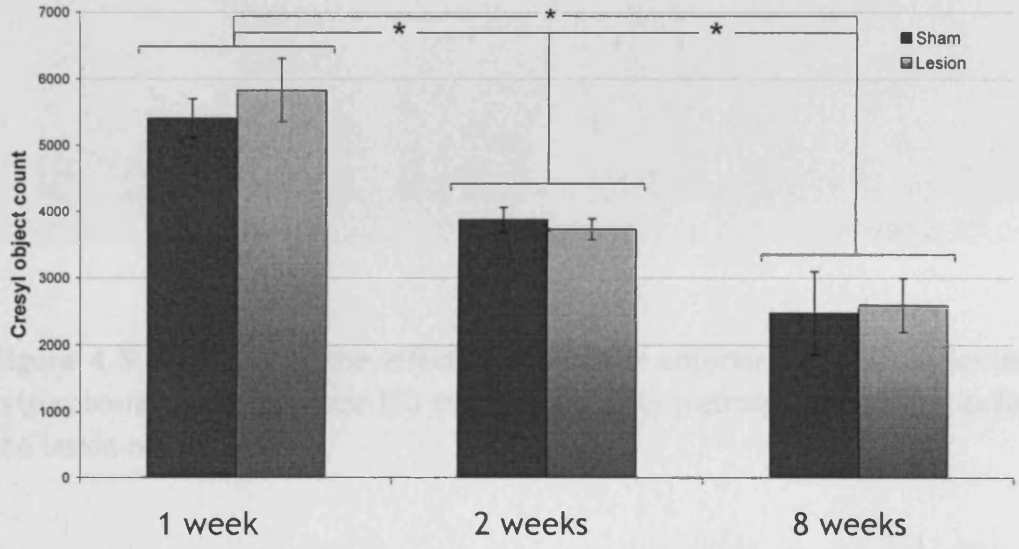

Figure 4.4: Relative to their respective controls, counts of Nissl-stained material revealed no differences between hemispheres as a result of the anterior thalamic nuclei lesion. There were, however, differences across time points with Nissl counts reducing significantly with time. Error bars represent the standard error of the mean. * p<0.05.

4.3.1.1.2: Immunohistochemistry

In order to evaluate the effect of anterior thalamic nuclei lesions on retrosplenial cortex IEG activity, a mixed-design, three-way analysis of variance (ANOVA) was conducted, with time (three between-subjects levels, one, two and eight weeks), surgical treatment (two within-subjects levels, 'Intact' and Lesion), and IEG protein (two within-subjects levels, Fos and Zif268). A sample of the immunohistochemical results is presented in Figure 4.5.

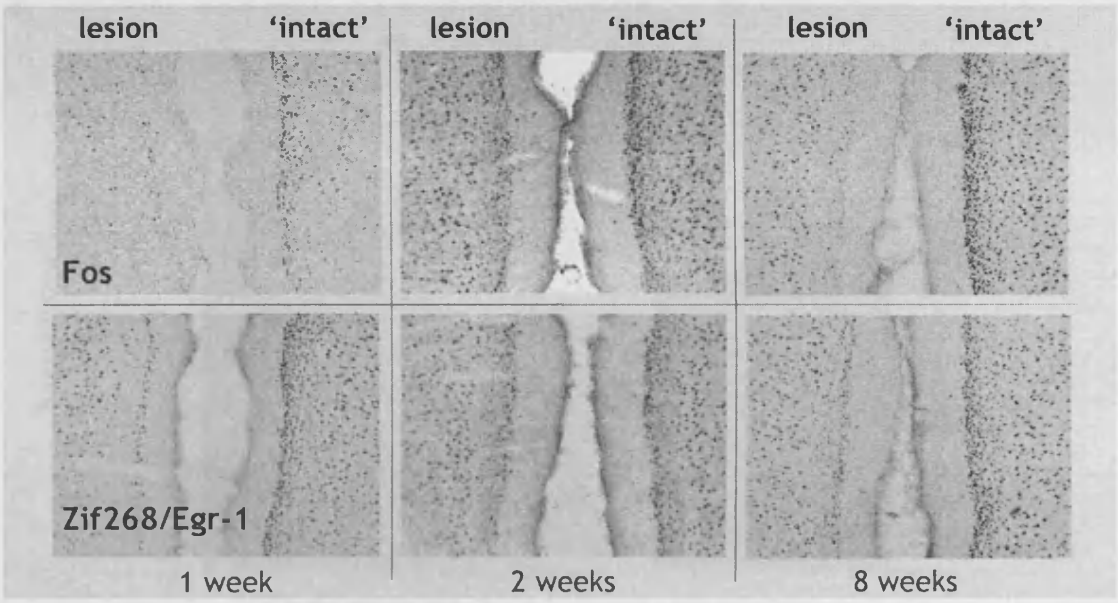

Figure 4.5: A sample of the effects of unilateral anterior thalamic nuclei lesions on retrosplenial cortex granular IEG immunoreactivity (retrosplenial cortex ipsilateral to the lesion on the left).

The results of the ANOVA revealed that there was no significant main effect of IEG protein [F (1,11) = 0.25, p=0.63], but the interaction of the main effects of surgical treatment and of protein was significant [F (1,11) = 5.42, p=0.04], i.e. anterior thalamic nuclei lesions produced a larger reduction in Fos than Zif268 production (see Figure 4.6b). Pairwise comparisons (Bonferroni adjusted for multiple comparisons) revealed a significant effect of the anterior thalamic nuclei lesions on both Fos and Zif268 activity in the retrosplenial cortex, as shown in Figure 4.6b. For Fos, cells counts were reduced in the lesion side (M=389.6, SD=30.4) compared to the sham side (M=561.9, SD=29.5, p<0.001), as they were for Zif268 (respectively M=405.8, SD=32.5, and M=520.8, SD=37.6, p=0.003).

a.

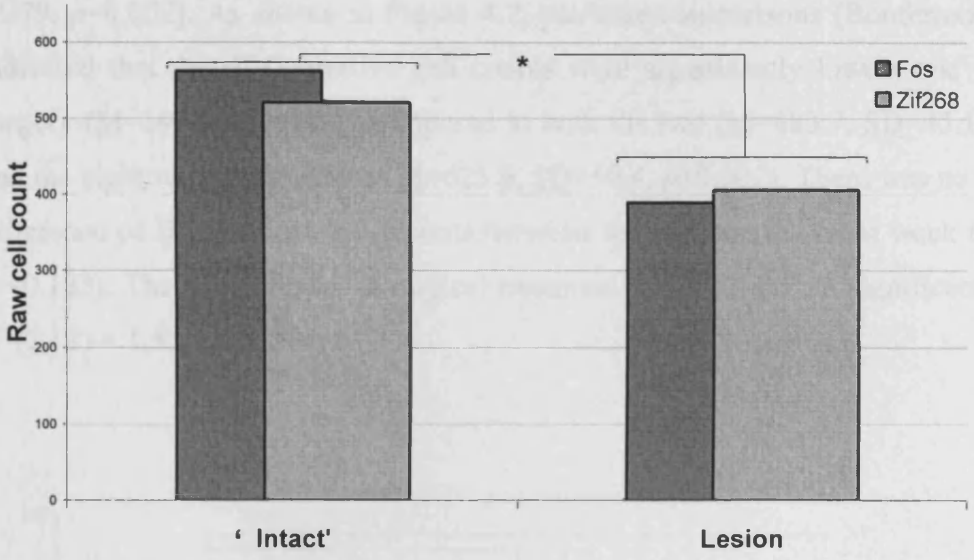

b.

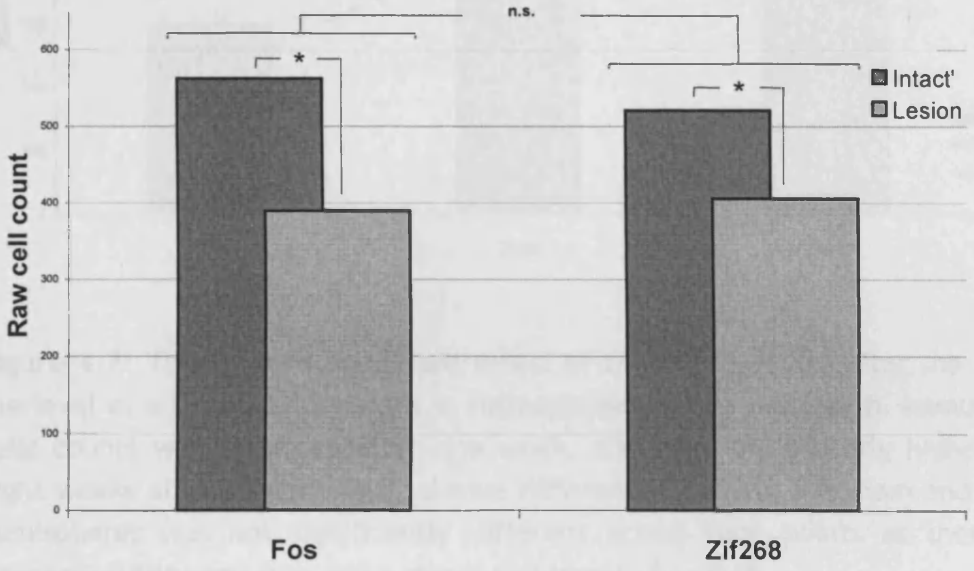

Figure 4.6: a) The effect of the surgical treatment was significant, as anterior thalamic nuclei lesions reduced overall IEG activity in the retrosplenial cortex. b) While there was no main effect of IEG protein, there was a significant interaction of the effects of surgical treatment and of IEG protein activity, anterior thalamic nuclei lesions resulting in a greater reduction of Fos than Zif268 expression. The effect of anterior thalamic nuclei lesions was significant for both Fos and Zif268. * $p < 0.05$.

There was a significant main effect of time on IEG-positive cell activity [F (2,11) = 11.79, p=0.002]. As shown in Figure 4.7, pairwise comparisons (Bonferroni adjusted) indicated that that IEG-positive cell counts were significantly lowest one week after surgery (M=299.9, SD=45.1) compared to both the two (M=483.7, SD=45.1, p=0.045) and the eight week time points (M=625.0, SD=50.4, p=0.002). There was no significant difference of IEG-positive cell counts between the two and the eight week time points (p=0.183). The main effects of surgical treatment and time did not significantly interact [F (2,11) = 1.53, p=0.259].

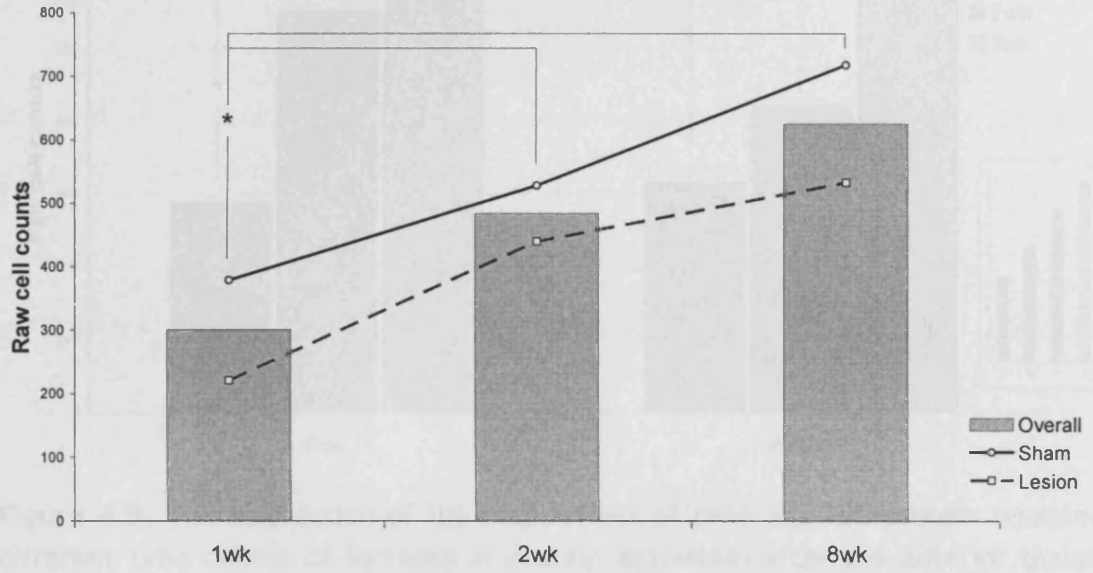

Figure 4.7: There was a significant effect of time of recovery after the surgery on the level of all IEG-positive cells in retrosplenial cortex granular b. Immunoreactive cells counts were reduced after one week, and were significantly higher two and eight weeks after surgery. The relative difference between the sham and the lesion hemispheres was not significantly different across time points as there was no interaction between time and surgical treatment. * p< 0.05.

There was a significant interaction between the main effects of time and protein [F (2,11) = 5.84, p=0.019]. Pairwise comparisons (Bonferroni adjusted for multiple comparisons) revealed a difference in the time course of the cell activity between Fos and Zif268 after the surgical treatment. As shown in Figure 4.8a, Fos overall cells counts were significantly lowest after one week (M=286.9, SD=46.6) in comparison

with the cells counts after two (M=548.6, SD=46.6, p=0.007) and eight weeks (M=591.8, SD=, 52.1, p=0.003). There was no significant difference in cell counts between two and eight weeks (p=1.00). In contrast, as shown in Figure 4.8b, Zif268 overall cells counts were not significantly different between one (M=312.9, SD=52.5) and two weeks (M=418.8, SD=52.5, (p=0.554). Zif268 activity was highest after eight weeks (M=658.2, SD=58.7), significantly different from both the one week (p=0.003) and the two week time points (p=0.034).

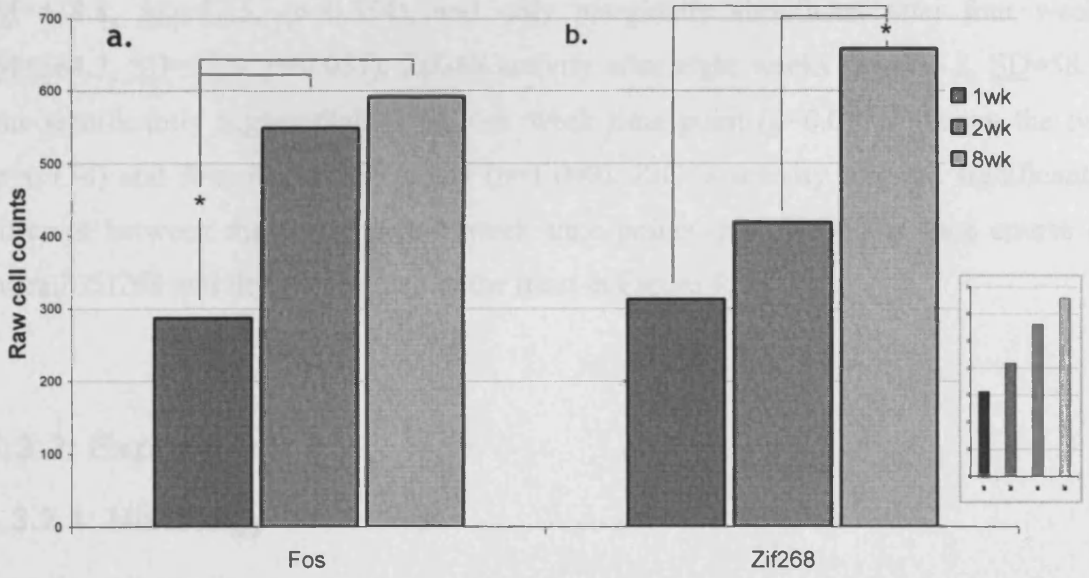

Figure 4.8: The interaction of the main effect of time and IEG protein revealed a different time course of increase in protein activation after the anterior thalamic nuclei lesions. On the left, it is shown that overall Fos activity was significantly lowest one week after surgery and quickly increased at two weeks and appeared to start to stabilise at that level. For Zif268, the activity levels were stable initially and increased significantly after eight weeks. Inset is the overall time course of Zif268 activity, including the additional four week time point. * p< 0.05.

The three-way interaction between surgical treatment, time point, and both IEG proteins was not significant [F (2,11) = 2.37, p=0.139]. As shown in Figure 4.6a, a statistically significant main effect of the anterior thalamic nuclei lesions was found [F (1,11) = 37.35, p<0.001].

The additional data available for Zif268 was used to separately test the time course of Zif268 activity across the four time points after the anterior thalamic nuclei lesions. It should be noted that the lesions in this particular group were similar to the other groups

(not shown). Including the four week time point in the analyses of Zif268 activity did not change the patterns previously observed with the analyses of only three of the time points. There was again a significant interaction of the surgical treatment [F (1,16) = 19.94, $p<0.0001$], and no significant interaction of the lesions or of the recovery time [F (3,16) = 1.23, $p=0.333$]. The effect of time after the anterior thalamic nuclei lesions was significant [F (3,16) = 5.49, $p=0.009$.

Pairwise comparisons (Bonferroni adjusted) revealed that the increase in Zif268 overall cells counts was not significantly different from one (M=312.9, SD=52.5) to two weeks (M=418.8, SD=52.5, ($p=0.554$), and only marginally significant after four weeks (M=564.2, SD=57.6, $p=0.057$). Zif268 activity after eight weeks (M=658.2, SD=58.7) was significantly higher than at the one week time point ($p=0.013$), but not the two ($p=0.134$) and four week time points ($p=1.000$). Zif268 activity was not significantly different between the two and four week time points ($p=0.648$). The time course of overall Zif268 activity is presented in the inset in Figure 4.8b.

4.3.2: Experiment 2

4.3.2.1: Histology

4.3.2.1.1: Nissl stains

4.3.2.1.1.1: Lesion analyses

Figure 4.9 depicts the largest and the smallest lesions in Experiment 2. Three subjects were excluded from the Lesion group because of incomplete lesions, which spared most of AM and AV unilaterally in one case, the other two exhibiting partial bilateral damage in AM, AV, and AD.

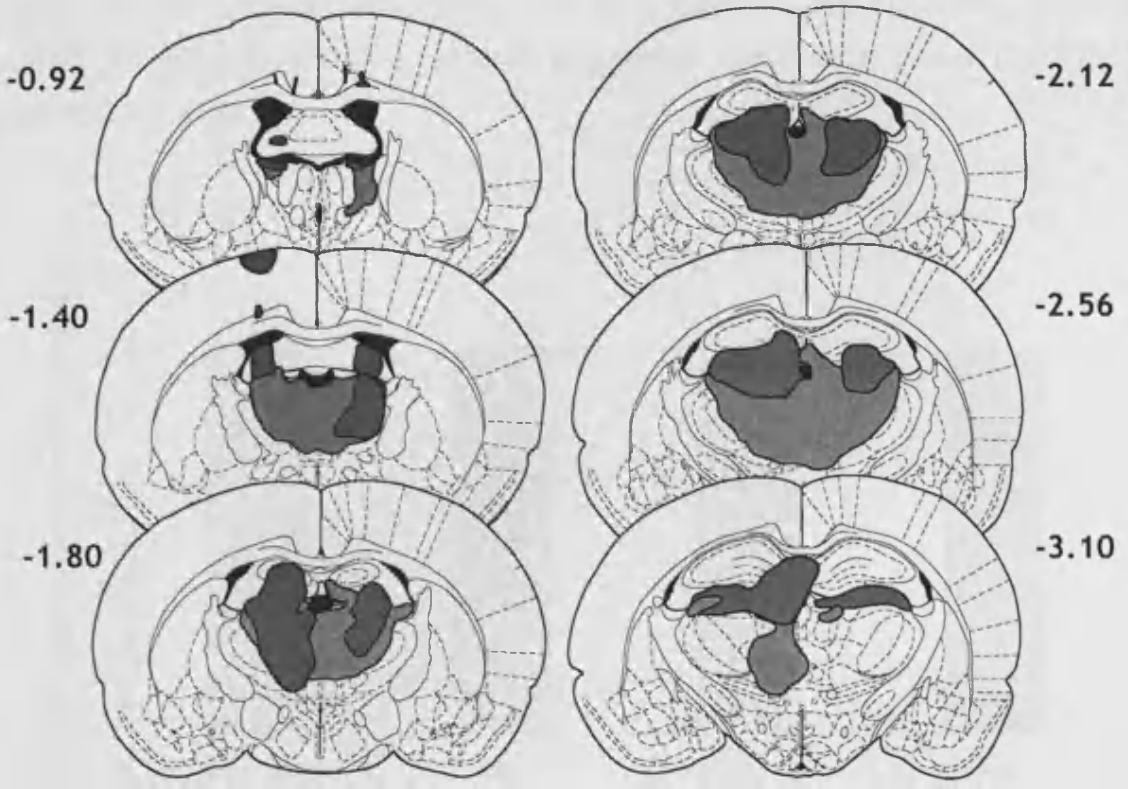

Figure 4.9: Extent of the damage produced by bilateral lesions centred on the anterior thalamic nuclei. The smallest and largest lesions are filled in dark and light colour, respectively. The numbers refer to the distance of the section from bregma (mm).

Typical lesions in the remaining rats (n=13), included all of AD, most if not all of AV, and generally spared some of AM (see Figure 4.9 for the smallest and largest extent of the lesions). The AV nucleus exhibited some minor sparing bilaterally in two cases and only unilaterally in another two cases. A complete lesion of the AM nucleus was apparent only in three cases. Damage was found in the most rostral portion of LD in all cases. There was an incursion of the damage into the overlying CA3 in all but three cases, and into the dentate gyrus in all cases. The injection tracts left visible fimbria fornix damage in all but two cases. Minor damage to the reticular thalamus adjacent to the anterior thalamic nuclei was also observed in all cases.

4.3.2.1.1.2: Nissl- stained material quantification

The mean of the group data for Nissl counts in the Lesion condition were normalised to the mean of the data from the Sham condition (100 = equivalent). As shown in Figure 4.10, one-sample t-tests to 100 revealed that Nissl counts in Lesion subjects did not significantly differ from Sham in either superficial (M=102.5, SD=7.1, p=0.275), or

deep granular b retrosplenial cortex (M=102.3, SD=10.3, p=0.472), and superficial (M=97.56, SD=9.5, p=0.416), or deep dysgranular retrosplenial cortex (M=100.37, SD=9.8, p=0.902).

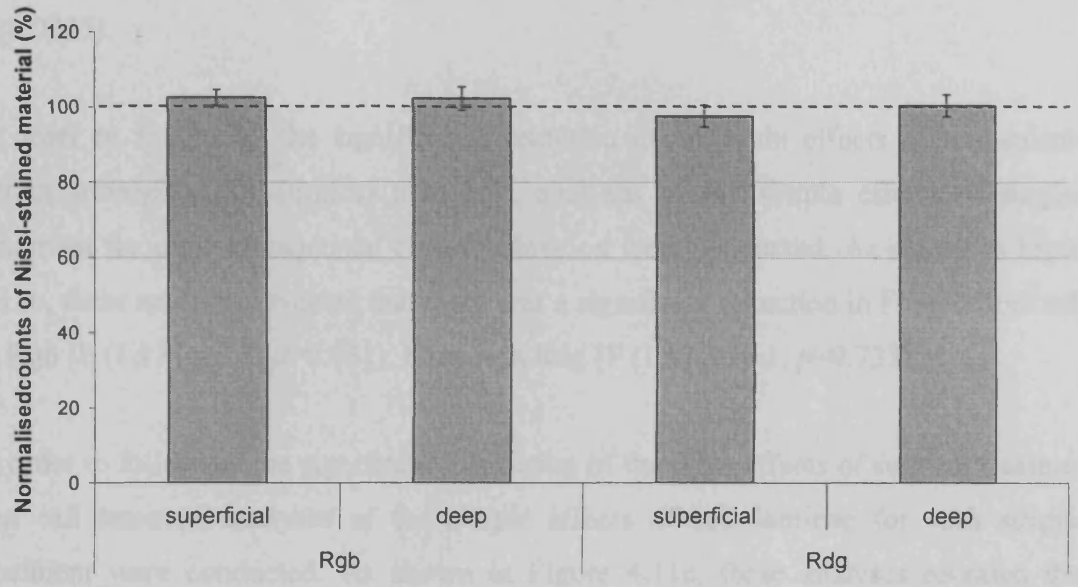

Figure 4.10: Counts of Nissl-stained material normalised to their controls revealed no statistically significant differences as a result of the anterior thalamic nuclei lesions. Error bars represent the standard error of the mean.

4.3.2.1.2: Immunohistochemistry

4.3.2.1.2.1: Fos-positive cell counts

A mixed-design ANOVA was conducted, with surgical treatment as a between-subjects factor, with rostral retrosplenial cortex subregion as a within-subjects factor, and cell laminae as another within-subjects factor. As shown in Figure 4.11, the main effect of surgical treatment was not significant [F (1,17) = 2.4, p=0.139], but the main effects of retrosplenial cortex subregion [F (1,17) = 33.7, p<0.0005] and of cell laminae [F (1,17) = 27.6, p<0.0005] were significant. There were significant interactions between the effects of retrosplenial cortex subregion and of cell laminae [F (1,17) = 7.9, p=0.012], the effects of surgical treatment and of retrosplenial cortex subregion [F (1,17) = 13.3, p=0.002], as well as of the effects of surgical treatment and of cell laminae [F (1,17) = 4.7, p=0.045]. A three-way interaction of retrosplenial cortex subregion, cell laminae, and surgical treatment was also significant [F (1,17) = 5.8, p=0.028].

In order to follow up the significant interaction of the main effects of retrosplenial cortex subregion and cell laminae, analyses of the simple effects of cell laminae for each retrosplenial cortex subregion were conducted. As shown in Figure 4.11a, these analyses revealed that Fos activity was significantly lower in superficial compared to deep cell laminae in both Rgb [$F(1,17) = 17.0$, $p=0.001$) and Rdg [$F(1,17) = 61.7$, $p<0.0005$).

In order to follow up the significant interaction of the main effects of retrosplenial cortex subregion and surgical treatment, analyses of the simple effects of surgical treatment for each retrosplenial cortex subregion were conducted. As shown in Figure 4.11b, these analyses revealed that there was a significant reduction in Fos-positive cells in Rgb [$F(1,17) = 5.5$, $p=0.031$), but not in Rdg [$F(1,17) = 0.1$, $p=0.733$).

In order to follow up the significant interaction of the main effects of surgical treatment and cell laminae, analyses of the simple effects of cell laminae for each surgical treatment were conducted. As shown in Figure 4.11c, these analyses revealed that, relative to deep cell laminae, there was a significantly lower number of Fos-positive cells in superficial laminae in Lesion subjects [$F(1,17) = 43.6$, $p<0.0005$], but not in Sham subjects [$F(1,17) = 3.5$, $p=0.080$].

a.

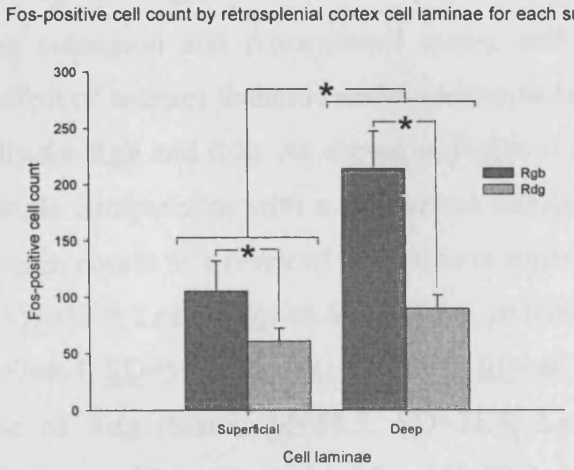

b.

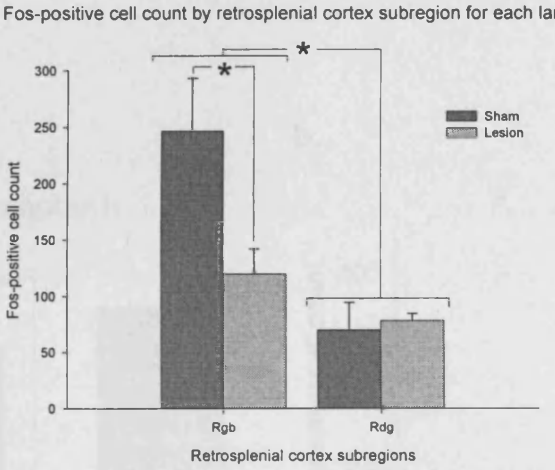

c.

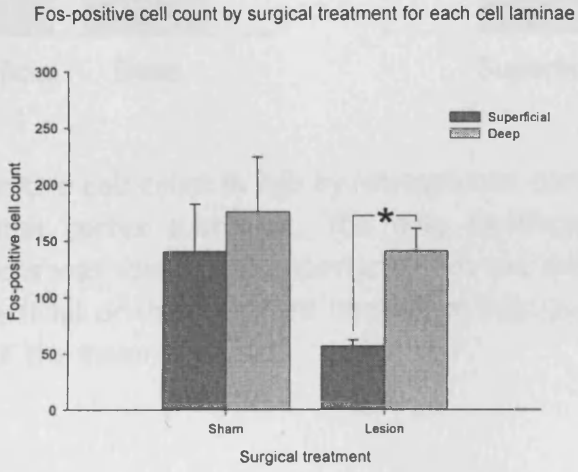

Figure 4.11: Significant main effects on Fos-positive cell counts of retrosplenial cortex cell laminae (a), and rostral retrosplenial cortex subregion (b), but not surgical treatment (c). There was a significant interaction of cell laminae and retrosplenial cortex subregion (a), retrosplenial cortex subregion and surgical treatment (b), surgical treatment and cell laminae (c). Error bars represent the standard error of the mean. *p< 0.05.

In order to follow up the significant three-way interaction of surgical treatment, retrosplenial cortex subregion and retrosplenial cortex cell laminae, analyses were conducted on the effect of anterior thalamic nuclei lesions in superficial and in deep cell laminae individually for Rgb and Rdg. As shown in Figure 4.12, pairwise comparisons (corrected for multiple comparisons with a Bonferroni adjustment) revealed that there was only a reduction in counts as a result of the lesion in superficial cell laminae of Rgb (Sham, M=226.8, SD=33.9; Lesion, M=48.8, SD=23.0, $p<0.0005$) but not deep laminae of Rgb (Sham, M=266.4, SD=59.3; Lesion, M=189.9, SD=40.3, $p=0.301$), nor in either superficial laminae of Rdg (Sham, M=54.3, SD=21.4; Lesion, M=64.5, SD=14.5, $p=0.698$) or deep laminae of Rdg (Sham, M=85.1, SD=22.2; Lesion, M=93.0, SD=15.1, $p=0.773$).

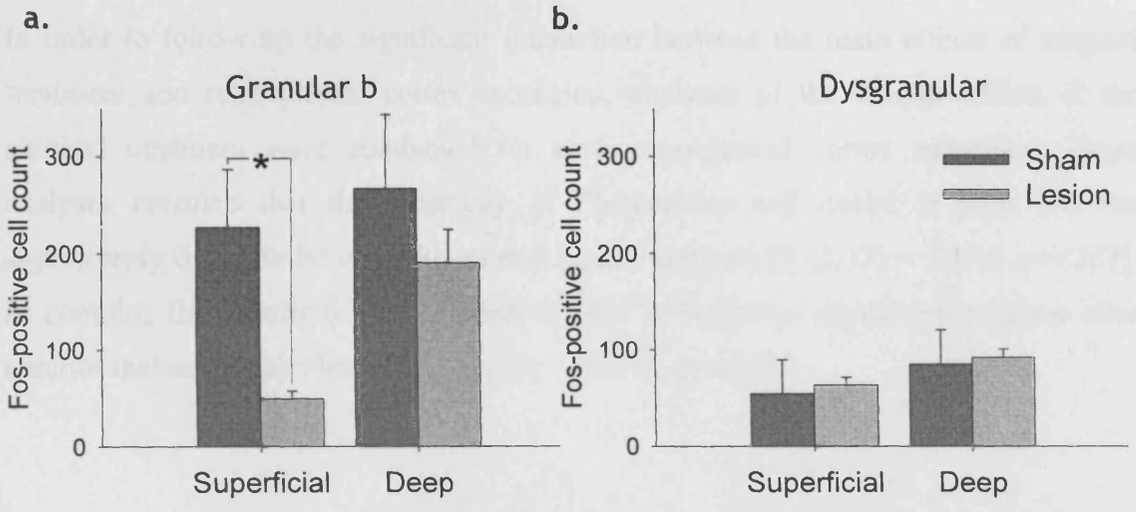

Figure 4.12: Fos-positive cell count in Rgb by retrosplenial cortex laminae separately for each retrosplenial cortex subregion. The only significant effect of anterior thalamic nuclei lesions was seen in the superficial, not the deep cell laminae in Rgb (a), nor either superficial or the deep cell laminae in Rdg (b). Error bars represent the standard error of the mean. * $p<0.05$.

4.3.2.1.2.2: Fos-positive cell mean sphericity

The statistical analyses conducted for the mean sphericity of Fos-positive cells were the same as for the cell counts. A mixed factorial ANOVA was conducted, where rostral retrosplenial cortex subregion and cell laminae were within-subjects factors, and surgical treatment was a between-subjects factor. As shown in Figure 4.13, the results of the ANOVA revealed that there were significant main effects of cell laminae [F (1,17) =

15.30, p=0.001], as sphericity was greater in superficial than deep cell laminae, and of surgical treatment [F (1,17) = 8.40, p=0.010], as the anterior thalamic nuclei lesions resulted in the activation of Fos-expressing cells of greater sphericity. There was, however, no significant main effect of retrosplenial cortex subregion [F (1,17) = 1.67, p=0.210].

The interaction between the effects of surgical treatment and of retrosplenial cortex subregion was significant [F (1,17) = 6.74, p=0.019]. However, the interaction between the effects of surgical treatment and of cell laminae was nonsignificant [F (1,17) = 0.80, p=0.384], and neither was that of the effects of retrosplenial cortex subregion and of cell laminae [F (1,17) = 3.64, p=0.074]. There was no significant three-way interaction of the effects on Fos-positive cell sphericity [F (1,17) = 0.01, p=0.917].

In order to follow up the significant interaction between the main effects of surgical treatment and retrosplenial cortex subregion, analyses of the simple effects of the surgical treatment were conducted for each retrosplenial cortex subregion. These analyses revealed that the sphericity of Fos-positive cell nuclei in Rgb was not significantly different between Sham and Lesion subjects [F (1,17) = 1.374, p=0.257]. In contrast, the sphericity of Fos-positive cells in Rdg was significantly higher after anterior thalamic nuclei lesions ([F (1,17) = 13.075, p=0.002].

a.

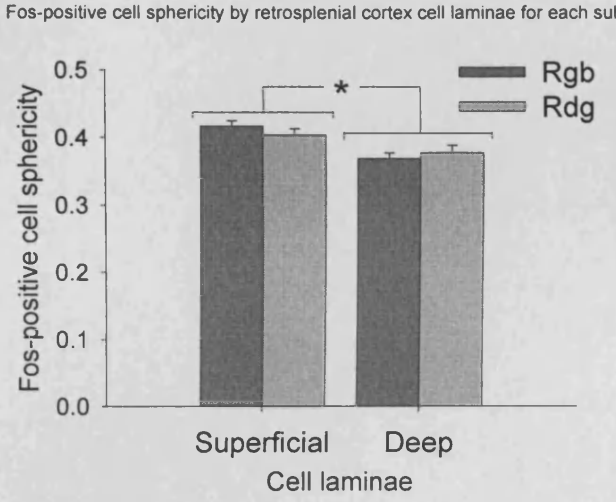

b.

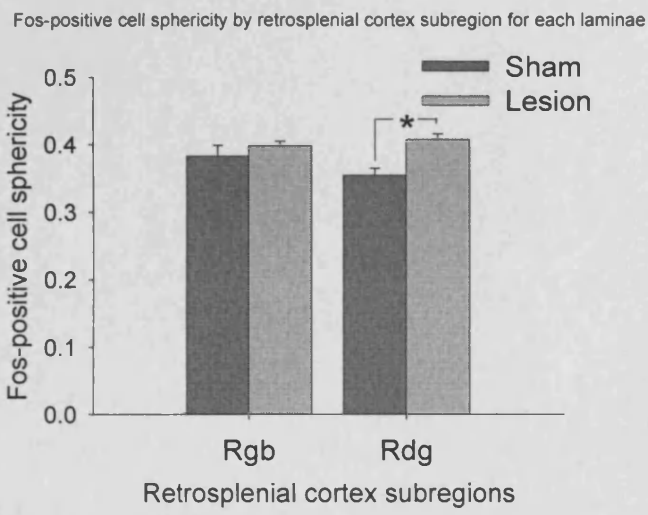

c.

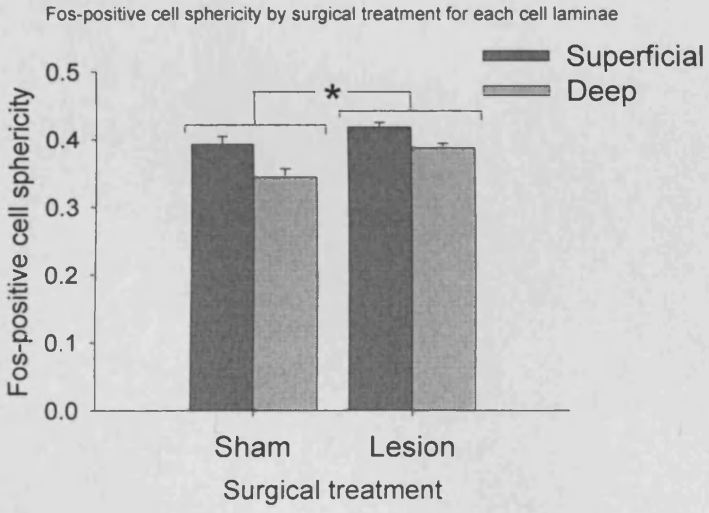

Figure 4.13: Significant main effect on Fos-positive cell sphericity of retrosplenial cortex cell laminae (a), and surgical treatment (c), but not rostral retrosplenial cortex subregion (b). There was only a significant interaction of the effects of retrosplenial cortex subregion and surgical treatment, whereby the anterior thalamic nuclei lesions resulted in a sphericity increase in Rdg, but not Rgb (b). Error bars represent the standard error of the mean. *p< 0.05.

4.3.2.1.2.3: Fos-positive cell mean area

As shown in Figure 4.14, there were no significant effects of any of the factors on Fos-positive cell area. The main effects of retrosplenial cortex subregion [F (1,17) = 0.653, p=0.430], and of cell laminae [F (1,17) = 0.020, p=0.889], the interaction between the main effects of surgical treatment and of retrosplenial cortex subregion [F (1,17) = 0.243, p=0.629], the interaction between the effects of surgical treatment and of cell laminae [F (1,17) = 0.086, p=0.772], the interaction between the effects of retrosplenial cortex subregion and of cell laminae [F (1,17) = 0.520, p=0.481], and three-way interaction [F (1,17) = 0.382, p=0.544] were all nonsignificant. The analyses of Fos-positive cell mean area revealed that any effects were small and would have required more statistical power to be detected. A summary of the analyses on Fos-positive cells is presented in Figure 4.15. Analyses of the Fos-positive cell mean area were thus insufficiently sensitive to detect any potential effects of the anterior thalamic lesions.

a.

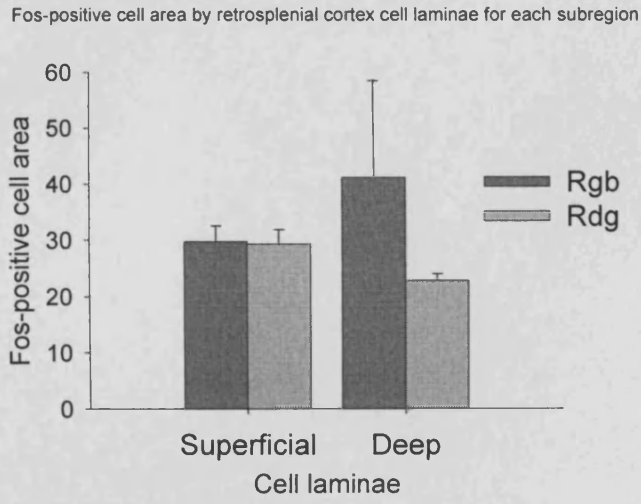

b.

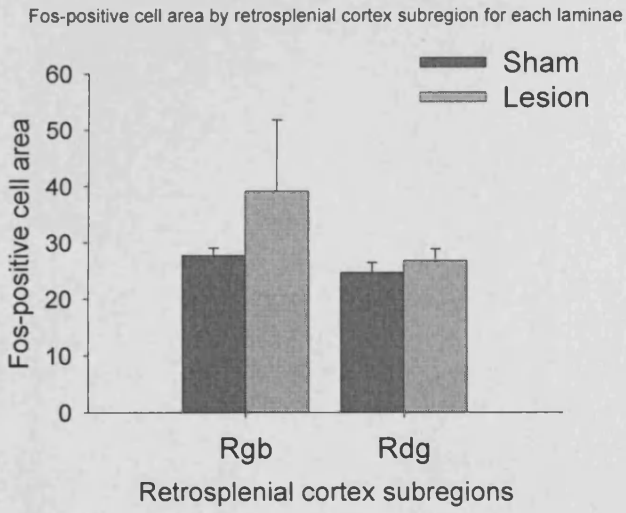

c.

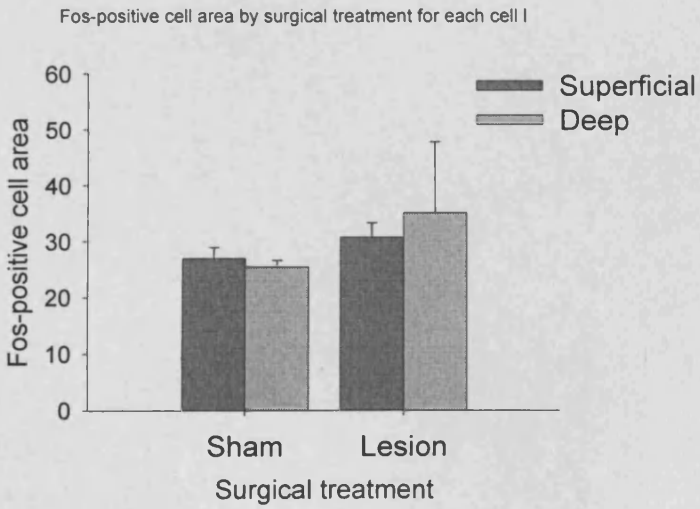

Figure 4.14: There were no significant main effects on Fos-positive cell area of retrosplenial cortex of cell laminae (a), rostral retrosplenial cortex subregion (b), and surgical treatment (c), nor of any of the interaction of the effects of these factors. Error bars represent the standard error of the mean.

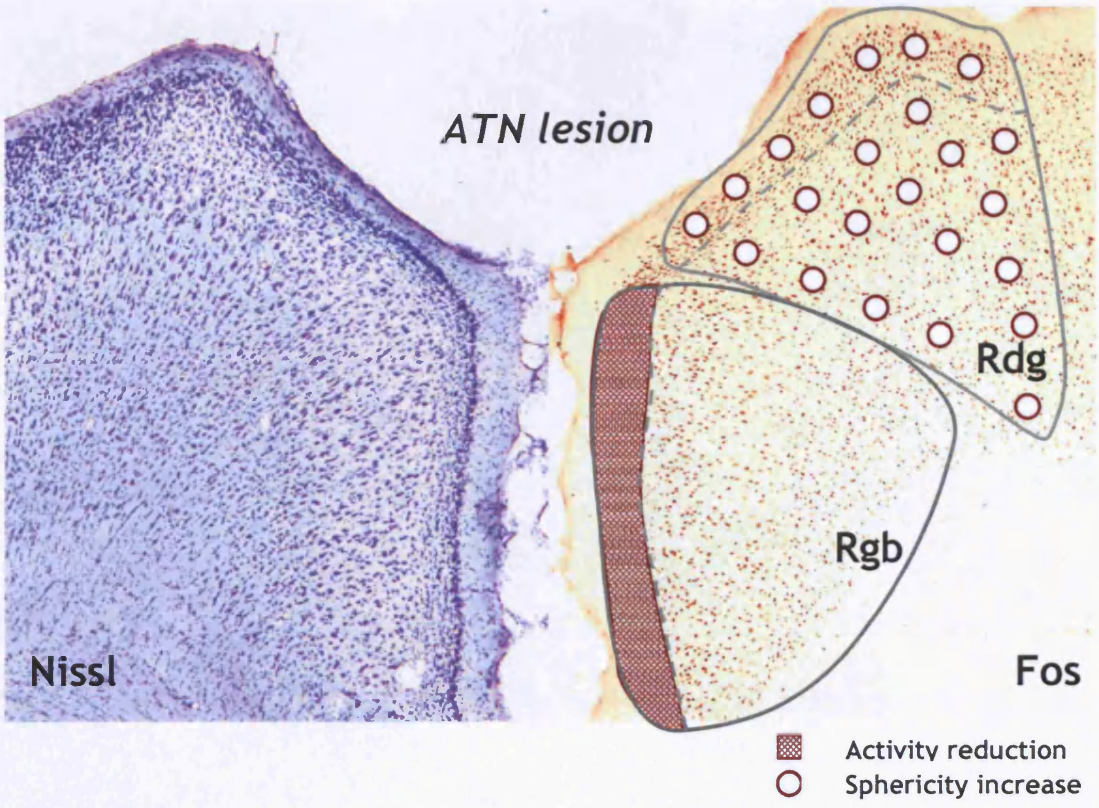

Figure 4.15: Summary of the effects of anterior thalamic nuclei lesions in rostral retrosplenial cortex on the expression of the Fos IEG. There were no apparent Nissl changes, but Fos-positive cell numbers were reduced in superficial Rgb, and the population of cells expressing Fos in Rdg displayed an increase in sphericity.

4.3.2.2: Corticosterone results

As shown in Figure 4.16, the main effect of surgical treatment on corticosterone levels was nonsignificant [$F(1,17) = 0.31$, p=0.582].

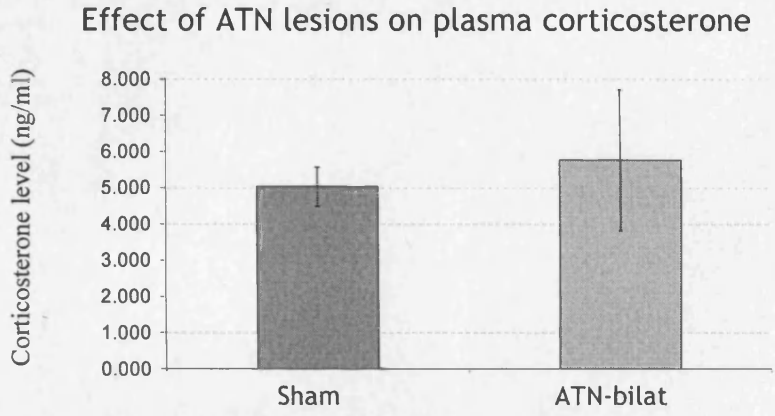

Figure 4.16: There was a nonsignificant effect of the anterior thalamic nuclei lesions on corticosterone levels. Error bars represent the standard error of the mean. * $p<0.05$.

4.3.2.3: Activity cage behavioural results

A mixed-design ANOVA was conducted on the data obtained from the behavioural activity boxes, with surgical treatment as a between-subjects factor and time bin as a within-subjects factor. As seen in Figure 4.17, the ANOVA revealed a significant main effect of time [$F(4,11) = 13.8$, $p<0.0005$], nonsignificant effect of the anterior thalamic nuclei lesions [$F(1,14) = 1.068$, $p=0.319$], but a significant interaction of the main effects of time and of surgical treatment [$F(4,17) = 4.0$, $p=0.030$].

Within-subjects contrasts analysis revealed that the effect of time on behavioural activity was significantly quadratic for Sham subjects [$F(1,3) = 77.7$, $p=0.003$], but linear for Lesion subjects [$F(1,11) = 11.5$, $p=0.006$].

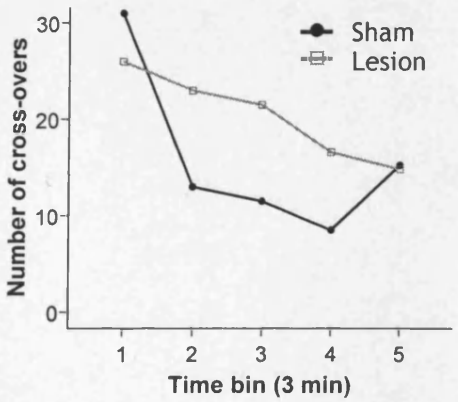

Figure 4.17: Cross-over means in activity box as a measure of behavioural activity. There was a significant effect of time, but not of anterior thalamic nuclei lesions. The interaction of these main effects was, however, significant.

4.3.2.4 Correlation analyses

The relationships between behavioural, hormonal, and cellular activity, and animal weight were investigated using Pearson product-moment correlation coefficients, separately for Sham and Lesion groups (cf. Tables 4.1 and 4.2, respectively). This complementary analysis was particularly salient for factors for which small effects—not amenable to detection by previous ANOVAs given the size of our samples, may prove of physiological and behavioural significance. The weight of the animals was included because a trend was observed for Lesion subjects to weigh less than Sham subjects.

4.3.2.4.1 Sham subjects

In Sham subjects, there was a strong, positive correlation between all retrosplenial cortex subregions and cell laminae studied. Fos-positive cell numbers in $Rgb_{(sup)}$ were positively correlated to cell counts in $Rgb_{(deep)}$ [r= 0.97, n=6, p<0.01], $Rdg_{(sup)}$ [r= 0.89, n=6, p<0.05], $Rdg_{(deep)}$ [r= 0.90, n=6, p<0.05]. Fos-positive cell numbers in $Rgb_{(deep)}$ were positively correlated with cell numbers in $Rdg_{(sup)}$ [r= 0.96, n=6, p<0.01], $Rdg_{(deep)}$ [r= 0.96, n=6, p<0.01], and finally, $Rdg_{(sup)}$ Fos-positive cell numbers were also positively correlated with $Rdg_{(deep)}$ [r= 1.00, n=6, p<0.01]. Calculating the coefficients of determination revealed that the retrosplenial cortex subregions and cell laminae share an impressive percentage of their variance. It appears that dysgranular cortex superficial and deep cell laminae share most of their variance (99.4%), followed by granular b retrosplenial cortex superficial and deep cell laminae (93.3%), granular b retrosplenial cortex deep and dysgranular retrosplenial cortex superficial cell laminae (91.8%), granular b retrosplenial cortex deep and dysgranular retrosplenial cortex deep cell laminae (91.6%), and finally granular b retrosplenial cortex superficial cell laminae and dysgranular retrosplenial cortex deep cell laminae (80.3%), and granular b retrosplenial cortex superficial cell laminae and dysgranular retrosplenial cortex superficial cell laminae (79.2%). In other words, Fos production within and between the rostral retrosplenial cortex subregions is very intimately inter-related.

An inverse relationship was found between Fos-positive cell counts in both granular b and dysgranular retrosplenial cortex and the sphericity of Fos-positive cells found in deep cell laminae. Cell counts in $Rgb_{(sup)}$ were strongly, negatively correlated with cell sphericity in $Rdg_{(deep)}$ [r= -0.81, n=6, p<0.05], whereas cell counts in $Rdg_{(sup)}$ and $Rdg_{(deep)}$ were strongly, negatively correlated with cell sphericity in $Rgb_{(deep)}$

[respectively, r= -0.82, n=6, p<0.05; r= -0.83, n=6, p<0.05]. In other words, except for $Rgb_{(deep)}$, higher Fos-positive cells counts in one retrosplenial cortex subregion were associated with lower sphericity of Fos-positive cells in the deep laminae of the other retrosplenial cortex subregion. Sphericity of Fos-positive cells was also strongly, positively correlated between $Rgb_{(deep)}$ and $Rdg_{(deep)}$ [r= 0.90, n=6, p<0.05]. Interestingly, there was a strong, positive correlation between corticosterone level and $Rgb_{(sup)}$ Fos-positive cell sphericity [r= 0.86, n=6, p<0.05].

4.3.2.4.2 Lesion subjects

In Lesion subjects, almost all associations found were different to those found for Sham subjects. Correlations between Fos-positive cell numbers between granular b and dysgranular retrosplenial cortex and their cell laminae were no longer as strong. Only a strong, positive correlation remained between Fos-positive cell numbers in $Rgb_{(sup)}$ and $Rgb_{(deep)}$ [r= 0.91, n=13, p<0.01], and between $Rdg_{(sup)}$ and $Rdg_{(deep)}$ [r= 0.83, n=13, p<0.01]. Lesion-specific correlations were also found. A strong, negative correlation was now found between animal weight and $Rgb_{(deep)}$ Fos-positive cell sphericity [r= -0.66, n=13, p<0.05]. In contrast to Sham subjects, no association was found between $Rgb_{(sup)}$ Fos-positive cell sphericity or any other retrosplenial cortex parameter tested in Lesion subjects. However, a marginally significant strong, positive correlation was found between corticosterone levels and weight.[r= 0.54, n=13, p=0.057].

The number of Fos-positive cells in $Rgb_{(sup)}$ was strongly, positively correlated with Fos-positive cell area in $Rgb_{(sup)}$ [r= 0.62, n=13, p<0.05] and $Rdg_{(sup)}$ [r= 0.62, n=13, p<0.05]. The number of Fos-positive cells in $Rgb_{(deep)}$ was strongly, positively correlated with cell area in $Rdg_{(sup)}$ [r= 0.60, n=13, p<0.05]. Fos-positive cell area in $Rgb_{(sup)}$ was also strongly, positively correlated with cell area in $Rdg_{(sup)}$ [r= 0.61, n=13, p<0.05]. Fos-positive cell area in $Rdg_{(sup)}$ and in $Rdg_{(deep)}$ were strongly, positively correlated with cell sphericity in $Rdg_{(deep)}$ [respectively, r= 0.56, n=13, p<0.05; r= 0.56, n=13, p<0.05]. In contrast to the correlation of sphericity between deep cell laminae in sham subjects, sphericity of Fos-positive cells in Lesion subjects was strongly, positively correlated between $Rgb_{(sup)}$ and $Rdg_{(sup)}$ [r= 0.70, n=13, p<0.01].

Table 4.1

Pearson product-moment correlations for separately for Sham subjects, between measures of Fos activity, corticosterone levels, and animal weight.

Measures for **Sham subjects**			Cort	Weight	LocAct	Cell count				Cell area				Cell sphericity			
						granular b		dysgranular		granular b		dysgranular		granular b		dysgranular	
						superior	deep	superior	Deep	superior	deep	superior	deep	superior	deep	superior	deep
Corticosterone																	
Weight			-.398														
Locomotor Activity			.402	.577													
Count	gran	sup	-.146	.743	.931												
		deep	-.257	.614	.290	**.966****											
	dysg	sup	-.393	.558	-.893	**.890***	**.958****										
		deep	-.387	.580	-.856	**.896***	**.957****	**.997****									
Area	gran	sup	.694	-.351	-.236	-.357	-.459	-.477	-.430								
		deep	.615	.257	.893	.105	-.108	-.351	-.321	.459							
	dysg	sup	-.119	-.161	.124	.058	.163	.020	-.028	-.630	-.023						
		deep	.334	-.734	-.750	-.293	-.150	-.112	-.098	.514	-.201	-.035					
Sphericity	gran	sup	**.861***	-.385	.581	-.483	-.639	-.754	-.737	.789	.701	-.254	.177				
		deep	.004	-.526	-.329	-.795	-.762	**-.822***	**-.828***	.093	.142	.398	.172	.343			
	dysg	sup	-.231	-.282	-.420	-.161	-.027	-.139	-.149	-.283	-.020	.766	.339	-.208	.645		
		deep	.035	-.683	-.161	**-.813***	-.735	-.751	-.787	-.101	-.098	.527	.145	.259	**.897***	.538	

N=6 (4 for Act). Cort=Corticosterone; Act=Activity box total cross-over mean measure; gran=granular b retrosplenial cortex; dysg=dysgranular retrosplenial cortex. * $p<0.05$; ** $p<0.01$

Table 4.2

Pearson product-moment correlations for separately for Lesion subjects, between measures of Fos activity, corticosterone levels, and animal weight.

Measures for Lesion subjects			Cort	Weight	LocAct	Cell count				Cell area				Cell sphericity			
						granular b		dysgranular		granular b		dysgranular		granular b		dysgranular	
						superior	deep	superior	Deep	superior	deep	superior	deep	superior	deep	superior	deep
Corticosterone																	
Weight			.540¤														
Locomotor Activity			.299	.366													
Count	gran	sup	.054	.006	.221												
		deep	-.014	-.013	.354	.908**											
	dysg	sup	-.187	-.009	.006	.150	.362										
		deep	-.151	.091	.376	.306	.445	.830**									
Area	gran	sup	.404	.039	.522	.616*	.497	.147	.413								
		deep	.474	.199	.315	-.210	-.151	-.058	-.134	-.042							
	dysg	sup	.069	.015	.242	.622*	.599*	.377	.384	.610*	-.074						
		deep	.158	-.042	.046	.355	.218	.134	.060	.398	.261	.401					
Sphericity	gran	sup	.007	.039	-.170	-.096	-.091	-.241	-.417	-.355	.473	-.111	-.040				
		deep	-.181	-.659*	-.215	-.030	-.148	-.360	-.336	.224	-.337	-.059	.159	-.098			
	dysg	sup	.262	.148	-.294	-.055	-.203	-.217	-.379	-.073	.324	.020	.456	.701**	.123		
		deep	.234	-.219	-.190	.034	-.033	.266	.058	.383	-.014	.555*	.558*	-.382	.299	.100	

N=13 (12 for Act). Cort=Corticosterone; Act=Activity box total cross-over mean measure; gran=granular b retrosplenial cortex; dysg=dysgranular retrosplenial cortex. * $p<0.05$; ** $p<0.01$, ¤ = marginally significant ($p=0.057$)

═══: Significant correlations in Sham subjects.

4.4: Discussion

The effects of the anterior thalamic nuclei lesions in Lister Hooded rats were found to be similar to that in Dark Agouti rats (Jenkins et al., 2004) and, thus, it was confirmed that the retrosplenial hypo-immunoreactivity after anterior thalamic nuclei lesions is not strain specific. Jenkins and colleagues (2004) observed the effects of anterior thalamic nuclei lesions on the retrosplenial cortex six to twelve weeks and ten months after anterior thalamic lesions. The effects leading up to this point were as yet unknown. The results of the Experiment 1 in the current study extend those of Jenkins and colleagues (2004) by providing evidence that the relative hypo-immunoreactivity of IEGs on the lesion side appears as early as one week after the anterior thalamic nuclei lesions, and the relative size of the effect does not significantly change with time between one and eight weeks.

An unexpected finding of Experiment 1 was the effect of time on counts of both Nissl-stained material and IEG-positive cells. Counts of Niss-stained material were not different between the Lesion and 'Intact' hemispheres, but they significantly decreased with time. In contrast, while the evaluation of IEG activity in the retrosplenial cortex in Experiment 1 revealed lower IEG levels on the Lesion side at all time points, IEG levels in both hemispheres increased across time, a significant rise being observed from week 1 to 2 but not 2 from to 8 weeks as numbers appeared to be stabilising. It is important to note that the groups of rats were not processed in a chronological order (i.e. 8, 1, 4, then 2 week group). It is possible that the differences in absolute numbers could be due to differences in batches of chemical reagents, or even due to the effect of differences in the ambient temperature on the efficacy of these reagents. However, such an influence would have had to affect Nissl staining and IEG immunohisotchemistry in opposite fashion, as Nissl counts decreased but IEG counts increased with time.

Alternatively, it may also be possible that the effects of time could be the reflection of a bilateral effect on Nissl and Fos activity following the unilateral anterior thalamic nuclei lesions. In order to verify the possibility of a bilateral effect, it would be useful to compare the data from rats with unilateral lesions to data from rats without damage in any hemisphere, to verify the extent to which the 'Intact' tissue is actually normal. As shown next, data from section 3.3 can be used to evaluate this possibility. In that

particular experiment, the effects of unilateral anterior thalamic nuclei, laterodorsal thalamic nuclei, antero-dorsal hippocampus and retrosplenial cortex lesions were investigated. Comparisons for the rats with retrosplenial cortex lesions necessitated the use of another group of rats to compare the activity in the contralateral retrosplenial cortex. The rats used for the control group were obtained from the same cohort, thus were of the same age and underwent the same experiences, except for the anesthesia and surgery.

The post-operative delays before sampling for these particular lesions were closest to the last time point. Bearing this fact in mind, the comparison between 'intact' and normal tissue may be more informative for Fos than for Nissl, since in the latter case, a putative increase in gliosis may have already abated. The data for the Nissl-counts and Fos-positive cell counts in the 'intact' hemispheres of rats with anterior thalamic nuclei, laterodorsal thalamic nuclei and antero-dorsal hippocampal lesions were pooled, and compared to data obtained for the normal rats that were used as a control group for the unilateral retrosplenial cortex lesions. As shown in Figure 4.18a, a univariate analysis of variance revealed that there were no significant differences in counts of Nissl-stained material between normal and 'intact' retrosplenial cortex tissue [$F(1,18) = 0.529$, $p=0.476$].

In terms of Fos activity, Levene's Test for Equality of Variances revealed that the variance was not equal between the groups. Since the assumption of equality of variances was violated, the alpha level was set to a more conservative 0.01 to determine the significance, as suggested by Tabachnik and Fidell (1996, p. 80). As shown in Figure 4.18b, a univariate analysis of variance revealed that the values of Fos activity in the 'intact' hemispheres were significantly lower than in the normal rats [$F(1,20) = 5.2$, $p=0.037$]. This result suggested that the 'intact' retrosplenial cortex tissue did not produce as much Fos as normal tissue.

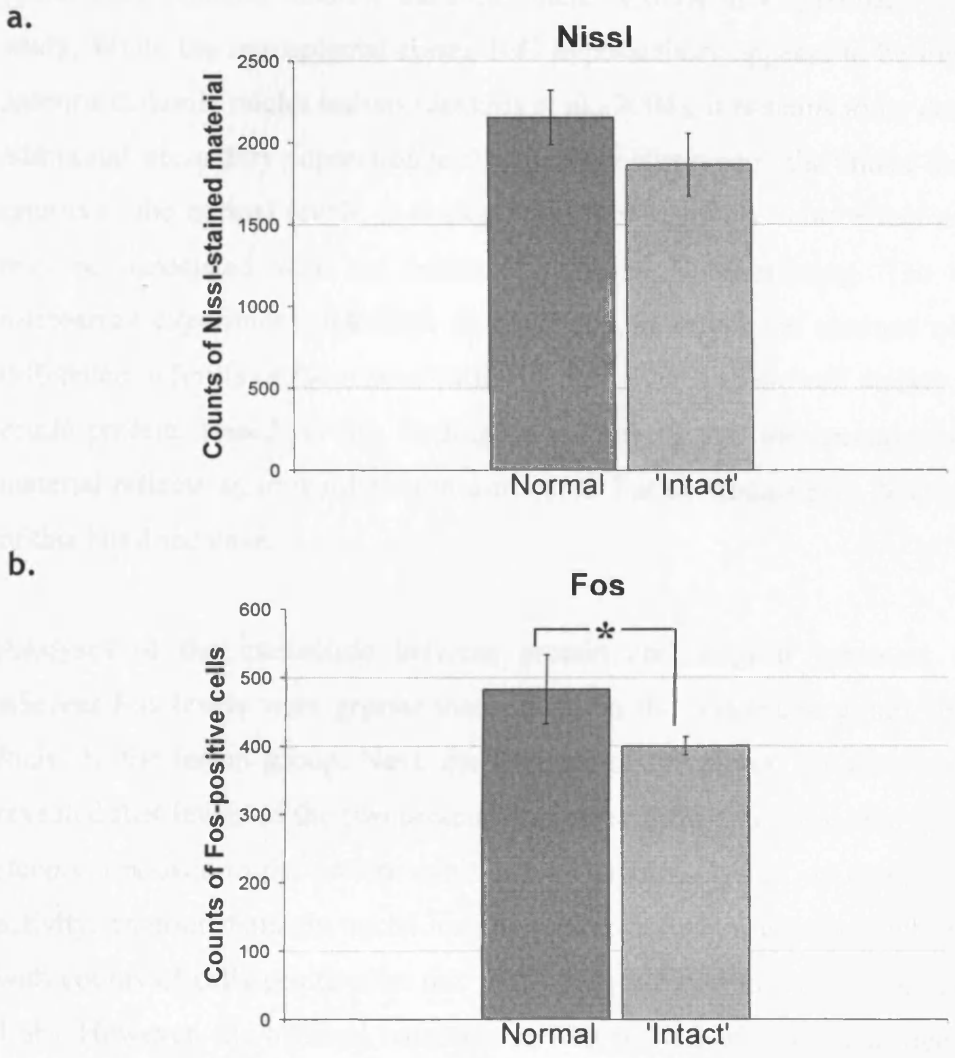

Figure 4.18: a) There was no difference in counts of Nissl-stained material between normal and 'intact' retrosplenial cortex tissue. b) There was a significant reduction in Fos-positive cell counts in the 'intact' retrosplenial cortex hemisphere of rats with anterior thalamic nuclei, laterodorsal thalamic nuclei lesions or antero-dorsal hippocampal lesions, compared to normal rats. Error bars represent the standard error of the mean. * $p < 0.01$.

It is possible that that the pattern of IEG activity reflects a refractory period after the surgery. The finding that Fos activity is decreased even in the 'intact' hemisphere accords with evidence from electrophysiological studies. Using slices from rats with unilateral anterior thalamic nuclei lesions, it was found that the retrosplenial cortex in the 'intact' hemisphere exhibited a slightly reduced ability for the induction of long-term potentiation (D. Garden, unpublished observations). It is plausible that the increase in Nissl-stained material may be temporary, as no differences on this parameter were

found after bilateral anterior thalamic nuclei lesions in Experiment 2 of the current study. While the retrosplenial cortex IEG hypo-activity appears to be long-lasting after anterior thalamic nuclei lesions (Jenkins et al., 2004), it remains to be determined if the additional, secondary depression in IEG activity observed in the 'Intact' hemisphere ever returns to the normal levels. It is likely that this relatively acute effect on IEG activity may be associated with the increase found in Nissl staining. The results of the microarray experiment described in chapter 5, revealed the absence of a significant difference in levels of the transcript for the astrocyte-specific cell marker glial fibrillary acidic protein. Based on this finding, it is unlikely that the increase in Nissl-stained material reflects an upregulation in astrocytes. Future studies may determine the nature of this Nissl increase.

Analyses of the interaction between protein and surgical treatment revealed that, whereas Fos levels were greater than Zif268 in the non-lesion group, the reverse was found in the lesion group. Next, the analysis of the protein by time point interaction revealed that levels of the two proteins increased differently, Fos first quickly then less steeply, opposite to the pattern exhibited by Zif268. Overall, in comparison to Zif268 activity, anterior thalamic nuclei lesions appear to have a greater acute impact on Fos, with counts of cells positive for this IEG being reduced to a greater extent (see Figure 4.6b). However, the bilateral reduction in IEG activity after surgical treatment appears to last longer for Zif268 than for Fos activity. This temporal characterisation of retrosplenial cortex IEG function after anterior thalamic damage suggests a protracted "recovery" period, which is unequal for the IEGs studied. Future work may investigate whether the Nissl-staining augmentation and the increase in Fos are related to some structural activity and synapse alterations and re-innervations in reaction to the lesions. Such restorative phenomena are known to occur in the dentate gyrus after entorhinal cortex lesions, where the fast rate of recovery of the number of synaptic junctions declines dramatically after 30 days (Daitz and Powell, 1954; Matthews et al., 1976b, a). It will be necessary to compare the levels of Nissl-stained material in other regions to verify selectivity of this effect.

A number of factors could explain the differential effects found in this study on Fos and Zif268 activity. One of these is the fact that these IEGs are involved in different cellular processes. While there can exist an overlap in the timing of expression of Fos and Zif268 and in their responsiveness to stimuli (Herdegen and Leah, 1998; Zangenehpour

and Chaudhuri, 2002), as shown in Figure 4.19, there is an incomplete overlap in the conditions and pathways that result in the induction of these IEGs, and this is due to the fact that the promoter elements on their respective promoter regions are different (cf. review by Herdegen and Leah, 1998). Thus, Fos and Zif268 do not provide redundant information. For example, based on the fact that Fos is involved in the negative feedback of its own activity, Chaudhuri (1997) suggested that Fos activity may be more sensitive to acute changes in cellular activity, whereas Zif268 may better reflect ongoing activity. Zif268 production, in contrast to Fos, can exhibit a positive feedback (Herdegen and Leah, 1998). If we take this view to include both increases and decreases in Fos activity, then, accordingly, the early depression in Fos activity may be an immediate but relatively short-lived result of the effect of the lesion, signalling the onset of alterations in retrosplenial cortex cellular activity patterns—even in the 'Intact' hemisphere. Zif268 activity may then be a reflection of the reduced level of retrosplenial cortex activity, in *both* hemispheres, which slowly resumes after the insult at a similar rate in both hemispheres. This general, or unspecific surgery-related depression in IEG activity may occur in parallel with the more important reduction that occurs selectively in retrosplenial cortex that is ipsilateral to the lesion.

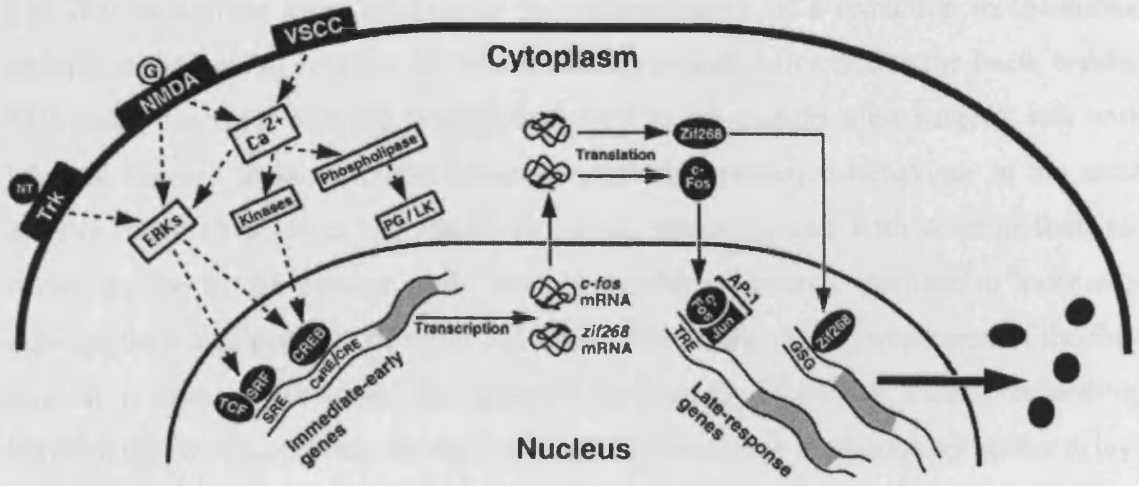

Figure 4.19: Some overlap between the pathways activating Fos and Zif268 induction (taken from Chaudhuri, 1997).

Further research is needed to determine whether Zif268 is less sensitive to the anterior thalamic nuclei lesions, or if the smaller effect on this IEG compared to Fos reflects the fact that Fos is normally only expressed in a subset of Zif268-positive cells. It is important to note that Fos levels are low under basal conditions, enabling sensitive

detection of increased signal activity, whereas in contrast, Zif268 levels are high, facilitating the detection of reductions in activity (Hughes et al., 1992). The finding of a differential time course in the increase of the two IEGs after the anterior thalamic nuclei lesions may potentially simply be due to the different basal levels of each IEG. Again, further analyses will require the addition of control areas to verify the regional specificity of the effect of time on IEG and Nissl-stained cell counts.

The results of Experiment 2 revealed that the bilateral anterior thalamic nuclei lesions resulted in a Fos-positive cell count decline selectively in the superficial cell laminae of granular b retrosplenial cortex, replicating the results of Jenkins and colleagues (2004). The vulnerability of this particular area is also consistent with results presented in the previous chapter, and other work that showed that, after unilateral anterior thalamic lesions, reductions were found in ligand binding to adrenergic (reduction in cell laminae I and III), cholinergic and serotonergic (both reduced in cell laminae I-III) receptors in retrosplenial cortex (van Groen et al., 1993). The reductions in ligand binding were deemed to be due to reductions in pre-synaptic retrosplenial receptors (van Groen et al., 1993).

The IEG reductions were unlikely to be a consequence of a reduction in locomotor activity as the Lesion subjects did not exhibit an overall difference in the beam breaks. This result contrasts with the finding that, nine to ten months after surgery, rats with bilateral anterior thalamic nuclei lesions exhibited hyperactive behaviour in the same activity cages (Jenkins et al., 2004). However, while the rats with anterior thalamic nuclei lesions in the current study did not exhibit an overall increase in locomotor activity, they did appear to be more active than the shams over a proportion of the time bins. It is thus possible that the apparent differences in overall locomotor activity between the two studies may be attributable to differences in methodology and/or delays after the surgeries. In the present experiment, the rats were placed for fifteen minutes in the activity cages, not thirty minutes (Jenkins et al., 2004). Similarly, the delay after the surgeries was of one, not nine to ten months (Jenkins et al., 2004), and as such, it may also be possible that a developing hyperactivity effect would become more robust with time.

Analyses of the sphericity metric in sham subjects revealed that, overall, this parameter distinguished between the superficial and deep cell laminae, but not between granular b

and dysgranular retrosplenial cortex. This observation was supplemented by the finding, through the correlation analyses, that the sphericity of cells in the deep laminae of both retrosplenial cortex subregions is similar, suggesting comparable cell populations in these two areas. Combined, these findings provided a form of validation of the sphericity parameter, because it has been reported that populations of cells of different shapes exist in these laminae (Vogt and Peters, 1981). While pyramidal cells occur everywhere in the retrosplenial cortex, mainly of medium size, some large, multipolar cells are also found in deep cell laminae (Vogt and Peters, 1981). The superficial cell laminae of granular b and dysgranular retrosplenial cortex visibly have less in common (Vogt and Peters, 1981). Small multipolar cells are found in superficial cell laminae in both regions, and bitufted cells (with elongated somata) can be found in superficial dysgranular cell laminae. The majority of cells in superficial granular b retrosplenial cortex are fusiform and small pyramidal cells. Some large stellate (with round somata) and small and medium pyramids are also found there (Vogt and Peters, 1981).

Cells may be somewhat larger in dysgranular than granular be retrosplenial cortex (Vogt and Peters, 1981; van Groen and Wyss, 1992; Jones et al., 2005), but this observation appears not to affect overall trends in cell nuclei shape as measured in this study. The subtle overall difference in the shape of superficial cell nuclei between superficial and deep laminae as well as between superficial laminae of both retrosplenial cortex subregions was salient enough to be detected with the correlation analyses, which only revealed a correlation of cell sphericity between the deep cell laminae of the two retrosplenial cortex subregions.

The results of Experiment 2 also provided additional insight into the anterior thalamic nuclei lesion-induced dysfunction of retrosplenial cortex. In addition to replicating the selective Fos hypo-immunoreactivy in the superficial laminae of granular b retrosplenial cortex reported by Jenkins and colleagues (2004), the results of Experiment 2 also highlighed a change in shape of the population of cells expressing Fos in dysgranular, but not granular b, retrosplenial cortex. While in Lesion subjects the reductions of Fos activity were apparent only in superficial granular b retrosplenial cortex, the analyses of sphericity revealed an increase in this parameter throughout the cell laminae of dysgranular retrosplenial cortex, suggesting that in this area, cell population changes were occurring, without affecting the overall number of Fos-positive cells. The occurrence of a spatial discrepancy between Fos hypoactivity and nuclei shape

differences in the present study was unexpected, and revealed that lesion-induced changes in cell function may also be present in dysgranular cortex, even before Fos production is reduced there Jenkins and colleagues (2004, cf. prolonged post-operative delay).

The correlation analyses revealed that the numbers of Fos-positive cells in dysgranular retrosplenial cortex appear to be associated with the shape of the cells that are Fos-positive in deep granular b retrosplenial cortex. Conversely, the number of Fos-positive cells in superficial granular b retrosplenial cortex appears to be intimately associated with the shape of the activated population in the deep dysgranular subregion. The connections between granular b and dysgranular retrosplenial cortex are from deep granular b to superficial dysgranular retrosplenial cortex (Sripanidkulchai and Wyss, 1987; van Groen and Wyss, 1992), and from dysgranular to all of granular b, most strongly cell laminae I, IV and V (van Groen and Wyss, 1992), but also to cell laminae II, III, and VI (Jones et al., 2005). In light of these connections, the findings of the current study are in accord with Fos-mediating projections from deep Rgb to superficial Rdg, and from deep Rdg to superficial Rgb. The associations were strong, in spite of the fact that the connections from granular b are more sparse than the reciprocal connections from dysgranular retrosplenial cortex (van Groen and Wyss, 2003). Given the correlations found here between sphericity and Fos expression in the adjacent region, it is possible that the activity of homogeneous cell populations (i.e. of a particular cell type) may be especially involved in the communication between these two regions.

Importantly, the correlation analyses further revealed that a number of associations were disturbed by the anterior thalamic nuclei lesions. In Lesion subjects, most of the correlations found in Sham subjects disappeared, and were replaced by others. In comparison to the patterns exhibited by the Sham subjects, the Lesion subjects only retained the correlations between superficial and deep cell laminae in both Rgb and Rdg. It was apparent that the Lesion subjects exhibited an uncoupling between the levels of Fos-expressing cells in Rgb and Rdg. In light of this particular finding and that of the double dissociation found between the effects of the anterior thalamic nuclei lesions on Rgb but not Rdg Fos-positive cell counts, and on Rdg but not Rgb Fos-positive cell sphericity, it is possible that the granular b retrosplenial cortex Fos hypoactivity is not just accompanied by cellular alterations in superficial Rgb, but that

some may also be present in dysgranular retrosplenial cortex. It remains unclear whether alterations in Rdg in cell nuclei shape, or in changes in the cell populations that are expressing Fos, result in the Rgb Fos reduction, or vice versa. The former direction of causality would suggest that it is possible that the reductions in IEG activity seen in Rgb after certain lesions may be at least partially mediated by altered function in Rdg. This account could also help explain the effects of entorhinal cortex lesions on granular b retrosplenial cortex Fos activity, as this region may not be strongly connected with rostral Rgb but rather with Rdg (Wyss and van Groen, 1992; Insausti et al., 1997).

The cells that are present in those Rgb cell laminae that are barren of Fos after the afferent damage are mainly fusiform and small pyramidal neurons (Vogt and Peters, 1981). Assuming that the sphericity metric used in Experiment 2 was sensitive enough to detect differences between the Fos-positive nuclei of fusiform and small pyramidal cells, the absence of an effect of the lesions on sphericity in the superficial cell laminae of Rgb in the ANOVA analyses would suggest that the hypoactivity of Fos is displayed indiscriminately by both of these cell types, assumed similar population numbers for both of these cell types.

In the superficial Rgb cell laminae of Lesion rats, a strong, positive association between the number of Fos-positive cells and their nucleus area was apparent, suggesting that, as numbers are reduced, so is the area of the remaining cells. It could be that the larger cell types may be most affected by the anterior thalamic nuclei lesions. According to this view, the fusiform cells, as well as the large multipolar and medium pyramidal cells that constitute a minority, would be most adversely affected by anterior thalamic nuclei damage. A selective effect of anterior thalamic nuclei damage on larger cells (i.e. multipolar and fusiform) could result in an increase in sphericity, again assuming the sufficient sensitivity of the sphericity metric. Alternatively, and maybe more likely, it is possible that indiscriminate atrophy of Rgb cells was associated with reduced Fos activity.

There is converging evidence that could support the idea that the activity of fusiform cells may be altered as a result of anterior thalamic nuclei lesions. The results of the microarray experiment (see Table 5.1) revealed that the relative levels of *Adenylate cyclase activating polypeptide 1* (Adcyap1) differ between retrosplenial cortex hemispheres as a result of the unilateral anterior thalamic nuclei lesion. Adcyap1

localisation is particularly dense in lamina II (Hashimoto et al., 1996), and this neuropeptide binds VIP receptors (reviewed in Harmar and Lutz, 1994). It has been proposed that VIP binding may be associated with fusiform cells (Vogt and Peters, 1981). Thus, as a result of anterior thalamic nuclei damage, elevated Adcyap1 levels may reflect an alteration in the function of the fusiform cells, unique to Rgb (Vogt, 1993).

The results of Experiment 2 provided evidence for the potential appearance of an endocrine dysregulation as a result of the anterior thalamic nuclei lesions. It should first be noted that at least two confounds exist regarding the sampling of corticosterone in the current experiment, and these may have selectively minimised the effects of the manipulations. First, corticosterone levels display a circadian rhythm, lower levels exhibited in the morning, rising later in the afternoon to peak in the evening, and the effect of stressors on the elevation of corticosterone is stronger when the baseline is low (e.g. Buijs et al., 1997), i.e. in the morning. Corticosterone was sampled in a two-hour window for all rats in Experiment 2, between 16h and 18h.

Whereas the choice of this window may have been adequate for the minimisation of disruptive activity that could affect Fos induction, as disturbance is minimal at this time in the laboratory, the amplification of corticosterone may not have been optimal, because the baseline was high. Second, and maybe most importantly, open field exposure that is accompanied by strong c-*fos* induction in the retrosplenial cortex results in a strong corticosterone elevation that returns to baseline levels around 120 minutes following the initiation of the stimulus (Emmert and Herman, 1999). In order to maximise the detection of Fos protein, a period of 90 minutes was allowed after the initiation of the novel room exposure. While beneficial to the detection of effects on Fos expression, this delay was obviously suboptimal for corticosterone. In spite of these issues, significant effects were found through the correlation analyses.

Increases in corticosterone levels are well known to be triggered by the relatively mild stress of an exposure to a novel environment (e.g. Pfister, 1979; Katz et al., 1981). It appears that, in the current study, this response was not affected by the anterior thalamic nuclei lesions. The results of the microarray study in Chapter 5 revealed a number of potential hormonal pathways that were affected in the retrosplenial cortex by the anterior thalamic nuclei lesions. In the microarray experiment, some transcripts found to

display altered expression are known to be involved in glucocorticoid activity. These transcripts include Adcyap1, and *hydroxysteroid dehydrogenase 11 beta, type 1* (HSD11β1). The mRNA transcripts for these enzymes are distributed throughout all retrosplenial cortex cell laminae. As stated above, Adcyap1 localisation is particularly dense in lamina II (Hashimoto et al., 1996), while HSD11β1 is very dense throughout all cell laminae (Roland et al., 1995). In conjunction with the findings of the microarray experiment (see Chapter 5), the findings of the present study yield several possible lines of investigation. Adcyap1 plays a role in the modulation of the hypothalamo-pituitary–adrenal axis (Vaudry et al., 2000), and HSD11β1 is an enzyme that converts cortisone into active corticosterone (equivalent to cortisol in humans). There appears to be a complex interplay of the conjoint activity of ATN, retrosplenial cortex and mammillary bodies in their effects on peripheral corticosterone levels in different states of stress, as revealed by electrophysiological stimulation and lesion studies in rats (Suarez et al., 1987; Suarez and Perassi, 1988, 1990; Suarez and Perassi, 1997). Clinically, stimulation of the anterior thalamic nuclei can produce alterations in cortisol levels that are observable at the plasma level (Upton et al., 1987). The alteration found in HSD11β1 could either produce an increase in corticosterone or be the result of homeostatic mechanisms in response to low corticosterone. Corticosterone activity is known to have potent modulatory effects on behaviour and cognition, and neuroplasticity (e.g. reviewed by Lupien and McEwen, 1997; Belanoff et al., 2001; Sapolsky, 2003). Adcyap1 and HSD11β1 activities have also been found to produce effects on behaviour and memory (e.g. Sacchetti et al., 2001; Seckl and Walker, 2004). Corticosterone is also known to play a role in energy management, through its interaction with insulin, for example (cf. review by Dallman et al., 1993) , and antagonistically controls neuronal glucose metabolism (Belanoff et al., 2001). In turn, HSD11β1 itself is known to be associated with insulin activity and resistance (Seckl and Walker, 2004; Westerbacka et al., 2006).

In the current study, bearing in mind the confounds due to timing, no difference was found in corticosterone levels as a result of the anterior thalamic nuclei lesions, yet associations were still found between the levels of this hormone and Fos activity. While the sphericity of Fos-positive cells superficial Rgb of Sham subjects was proportional to corticosterone levels, this association was absent in Lesion subjects. Additionally, a marginally significant, yet strong, positive association was found between weight and corticosterone levels in the latter. Furthermore, the weight of the Lesion subjects was

strongly, positively associated with the shape of Fos-positive cells in deep Rgb cell laminae. Given the changes in associations of corticosterone levels and subject parameters in the Lesion group, it could be that while the corticosterone surge may be intact, it is the subsequent physiological response to this surge that may have been affected by the lesions. The corticosterone findings may allude to an alteration in hormonal sensitivity resulting from anterior thalamic nuclei lesions.

In conclusion, the results of the current study extended current knowledge about the effects of anterior thalamic nuclei lesions by revealing the early occurrence of the IEG hypo-activity, uncovering changes in dysgranular retrosplenial cortex in addition to those already known in granular b retrosplenial cortex, and finally, finding evidence of hormonal dysregulation. These results provide many directions for future work aimed at uncovering the role of the retrosplenial cortex, the anterior thalamic nuclei and associated brain structures in behavioural and cognitive disorders.

Chapter 5

Using microarray techniques to target the impact of anterior thalamic nuclei lesions in rats upon retrosplenial cortex function:

Why might anterior thalamic damage cause covert pathology in the retrosplenial cortex?

5A.1: Introduction

Evidence presented in the previous chapters addressed several aspects of the nature of the retrosplenial cortex vulnerability to distal damage. In Chapter 3, the incidence of retrosplenial cortex dysfunction was verified after damage to a number of afferent regions, in order to verify further the generalisability of the vulnerability of this region to distal neurological insult. In Chapter 4, the course of onset of the IEG hypo-immunoreactivity was characterised further, and local changes that resulted from anterior thalamic nuclei lesions were identified in granular and dysgranular retrosplenial cortex. In the current chapter, I sought to identify underlying subcellular programs that could explain the retrosplenial cortex dysfunction.

Immediate-early gene (IEG) immunoreactivity in rats with anterior thalamic nuclei lesions is markedly depressed when assayed after behavioural treatment or in rats taken from their home cage (Chapters 3 and 4, Jenkins et al., 2002). In the retrosplenial cortex, the protein products of the IEGs Fos and Zif268 display a striking reduction in expression, which is stable, and unaccompanied by neuronal degeneration (Chapters 3 and 4, Jenkins et al., 2004). In addition to depressed IEG production in granular b retrosplenial cortex, it is also known that unilateral anterior thalamic nuclei lesions result in reductions in ligand binding to adrenergic (reduction in laminae I and III), cholinergic and serotonergic (both reduced in laminae I-III) receptors (van Groen et al., 1993). These reductions in ligand binding were deemed to be due to reductions in pre-synaptic retrosplenial receptors (van Groen et al., 1993).

Our aim was to analyse the response of retrosplenial cortex to anterior thalamic lesions using a technique that would allow a broad assay of molecular functions. In light of the observations that the retrosplenial cortex after anterior thalamic nuclei lesions exhibits neuroplasticity deficits (Garden et al., 2006), in the apparent absence of neuronal death, it remains unclear what the IEG changes reflect about cellular function. For example, are specific cellular pathways affected, or are widespread alterations produced? In order to examine the nature of the anterior thalamic nuclei lesion-induced retrosplenial cortex hypoactivity, we conducted a broader gene expression analysis to evaluate the extent of retrosplenial cortex dysregulation. We decided to examine the extent of this hypoactivity

by assessing gene expression via a microarray analysis. This approach not only made it possible to determine if IEGs in addition to c-*fos* and *Zif268* were appreciably altered, but also to detect the existence of much more pervasive disruptions and identify especially disrupted molecular pathways.

5A.2: Methods

5A.2.1: Subjects

A total of 49 Dark Agouti male rats (Harlan, UK) were housed in pairs under a standard laboratory lighting regime (L:D, 13:11, lights on at 07.00) with *ad libitum* access to food and water. Each animal was habituated to handling. The weight of the animals was monitored (212-248 g at the time of surgery), and controlled food restriction applied to those animals that were over the target weight for the surgery. All experiments were performed in accordance with the UK Animals (Scientific Procedures) Act (1986) and associated guidelines.

5A.2.2: Surgery

As mentioned in Chapter 4, the connections from the anterior thalamic nuclei to the retrosplenial cortex are ipsilateral (Tomitaka et al., 2000; Wang et al., 2001). For this reason, unilateral anterior thalamic nuclei lesions were produced, so permitting a reduction in animal numbers while minimising variability between samples.

Animals were anaesthetised with an intraperitoneal injection of pentobarbitone sodium (Sagatal; 75mg/kg), their head shaven, and then placed in a stereotaxic frame (David Kopf Instruments, CA). The scalp was cut and retracted to expose the skull. Over the target region, a rectangular-shaped craniotomy was performed by using a hand-held drill, thus revealing the dura, which was then opened over the injection sites. Excitotoxic lesions were produced by injecting into two sites 0.18-0.20 μL of N-methyl-D-aspartate (NMDA; Sigma Chemicals UK; 0.12 M in phosphate buffered saline (PBS), pH 7,2) using a 1 μL syringe (Hamilton, Switzerland). The stereotaxic coordinates for the sites were as follows: anterio-posterior, compromise of inter-aural +4.9 and bregma -0.5; medio-lateral, ±1,0 and 1.7

from the midline, depending on the target hemisphere; dorso-ventral, -6.3 and -5.7 from dura for the medial and lateral injections, respectively. The incisor bar was set at +5.0. Each microinjection was made gradually over a 4 min period, after which the needle was left *in situ* for an additional 4 min before being retracted. Next, the wound was cleaned and the skin was sutured, and an antibiotic powder (Aureomycin, Fort Dodge Animal Health, Southampton, UK) was applied. All rats also received a 5 ml subcutaneous injection of glucose saline, paracetamol dissolved in their drinking water, and were observed daily until recovery. Rats were administered the respiratory stimulant Millophylline (0.02 mL, s.c., Arnolds Veterinary Products, Shropshire, UK) as needed. A period of four weeks preceded tissue sampling.

5A.2.3: Microdissection of tissue

Five days preceding the tissue extraction, the animals were separated and individually housed. They were habituated daily for 3 hours to their designated place in a separate room that was used exclusively for the purposes of this experiment. Twenty-four hours prior to tissue extraction, the animals were taken from the holding room and placed in this test room, under the same feeding regimen and light cycle. The next day, the animals were individually placed for 20 minutes in a novel cage in a novel environment. It was expected that any floor effects of transcript expression might be eliminated. The rats were then returned to the test room. The process was staggered to allow each animal to be dealt with separately.

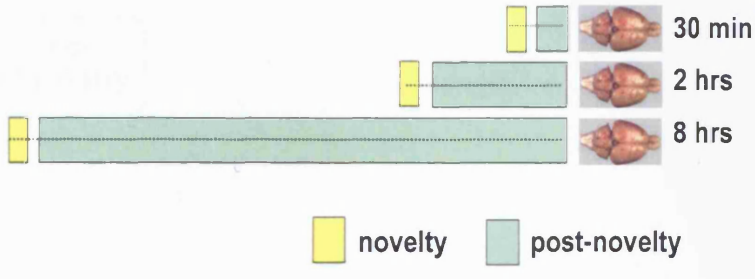

Figure 5A.1: Course of action on the final day. On the last day, the animals were individually placed for 20 minutes in a novel cage in a novel environment. The rats were then returned to the test room for the period dictated by their group (either 10 min, 1h40min or 7h40min).

Tissue from animals with unilateral anterior thalamic lesions was sampled at three time points following exposure to a novel environment (30 min, 2 and 8hrs from onset of exposure, see Figure 5A.1). Each cell consisted of the pooled unilateral tissue from two animals at each time point (i.e. 2 animals per cell per treatment per time point). This was replicated once, for a total of 12 animals. Furthermore, in order to increase the likelihood of finding numerically small but potentially biologically significant expression changes, a small tissue volume was sampled, thereby reducing cell heterogeneity. Discrete samples of granular retrosplenial cortex were punched out from a 2 mm coronal slice with a 19 gauge punch (see Figure 5A.3), using techniques already validated for array analysis (Holter et al., 2001).

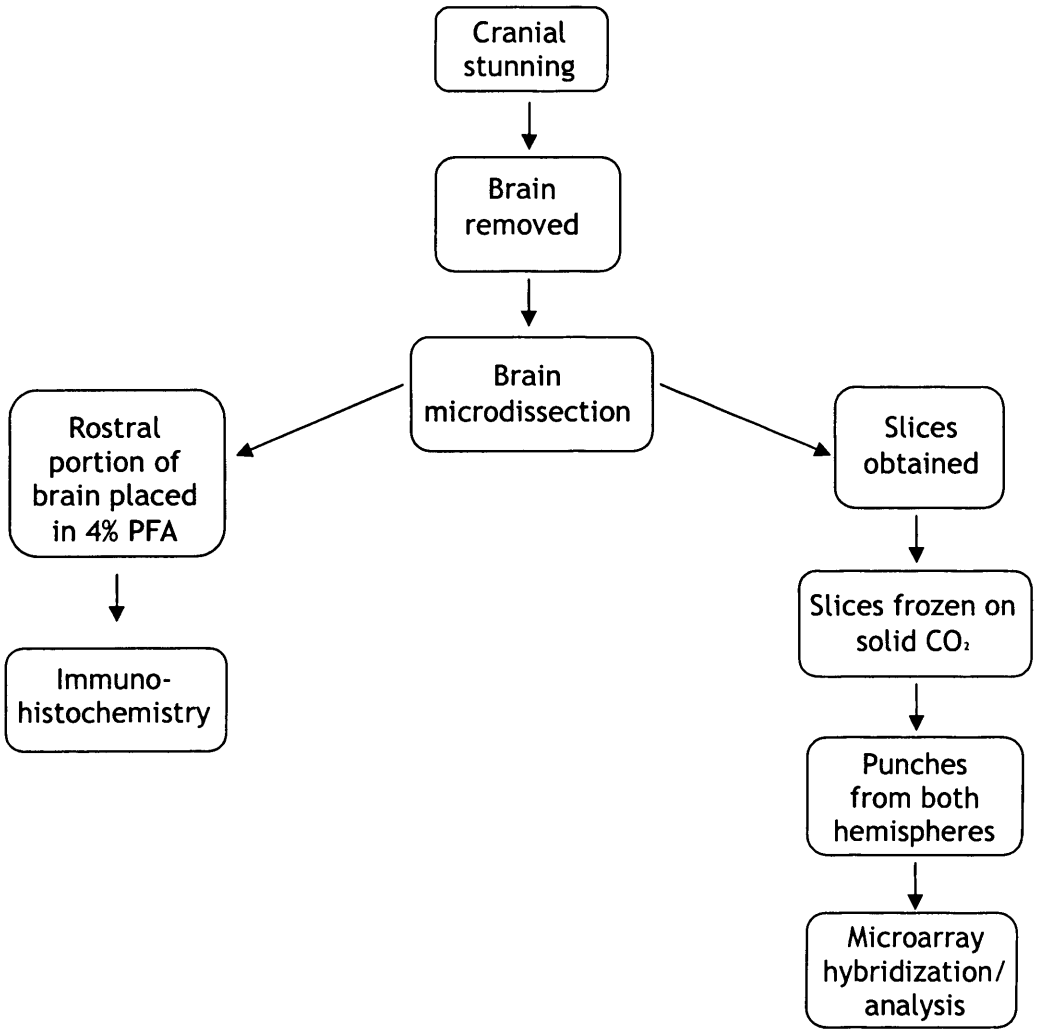

Figure 5A.2: Schema of steps involved in tissue sampling.

Rats were killed between 17h and 20h by stunning followed immediately by cervical dislocation (see Figure 5A.2 for experimental steps from that point). The scalp was removed, and next an opening was created in the skull, fully exposing the top of the brain by inserting one tip of scissors into spinal hollow, cutting along the fused bone, and removing the flap. Curved forceps were used to severe the olfactory nerves and excise the brain. Following removal from the skull, the brain was rinsed in cold, DEPC-treated 0.1 M phosphate-buffered saline (PBS), dried briefly by touching the ventral surface on tissue paper, and placed, dorsal surface up, in a rat brain matrix (specific for rats weighing 175-300g).

The dissection lasted at most two minutes and was then performed with reference to a standard brain atlas (Paxinos and Watson, 1997). New single-sided razor blades were used to produce tissue sections. Three colour-coded blades were used concurrently, positioned in slots 10, 11, and 12 (thus 10, 11, and 12 mm from rostral end). Each was gently positioned with a back-and-forth sawing motion. These were carefully lifted together from the matrix, slices held in between. DEPC-PBS was added and the blades were held apart, ensuring that the caudal side of the slices was exposed. Dissection landmarks were briefly confirmed, aided by a quick examination of the rostral and caudal portions of the brain. The optimal slice was thus chosen; the remaining slice and the caudal portion of the brain were discarded. In order to conduct histological procedures, the rostral portion was placed overnight 4 % paraformaldehyde in PBS solution for fixation, and next again overnight in 25% sucrose in PBS.

Drops of PBS were added and the selected brain slice was manipulated such that the hemispheres were well apart. The slice was frozen under microscope by applying the under-side of the razor blade onto a solid CO_2 pellet for a period of approximately 5-10 sec., such that the section is not rendered brittle and liable to fracture by punching. Punches were obtained from both sides of the brain using a blunted 19 gauge needle (freshly cleaned every time). A punch in each hemisphere was taken at a point above the corpus callosum and as close to the midline as possible. The punches for each hemisphere were then each ejected into separate 1.5 ml plastic Eppendorf tubes (from previously unopened bag to minimise contamination) using a 1ml syringe attached to the punch needle, and the tube

was immediately placed on dry ice. The punches were stored at -70°C until immunohistological confirmation of the lesions, after which the punches from 2 rats per group were pooled prior to RNA extraction.

a.

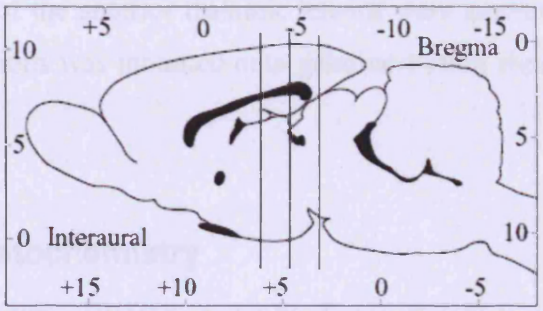

b.

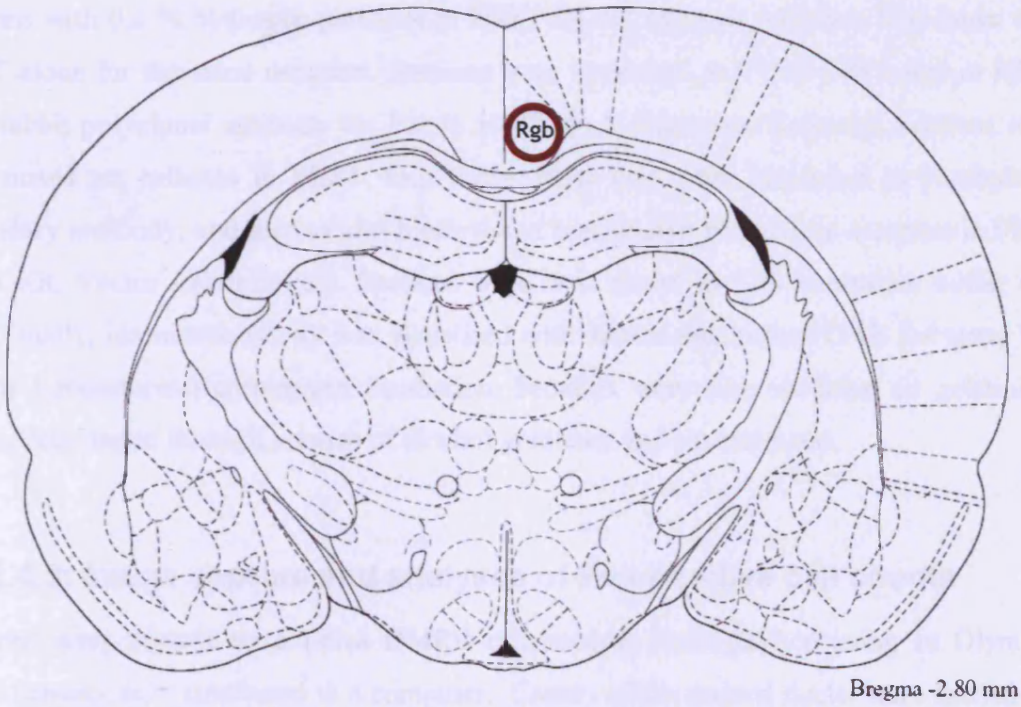

Figure 5A.3: Location of the tissue punch along the rostro-caudal axis (a), and on a coronal plane (adapted from Paxinos and Watson, 1997).

5A.2.4: Histology

The portion of the brain rostral to the first brain slice was kept for histological analysis. Three series of adjacent series of coronal sections were obtained at 40 μm on a cryostat.

5A.2.4.1: Lesion analysis

The size and specificity of the anterior thalamic lesions were assessed by traditional Nissl staining. A series of sections was mounted onto gelatine-coated slides, stained with cresyl violet.

5A.2.4.2: Immunohistochemistry

Two series of sections were collected in 0.2 % Triton-X-100 in 0.1 M PBS at pH 7,4 (PBST). For each replicate, material from all conditions was concurrently processed to reduce staining variability. Endogenous peroxidase activity was blocked by washing the sections with 0.3 % hydrogen peroxide in PBST for ten minutes, and then four times with PBST alone for the same duration. Sections were incubated at 4°C for 48 hours in PBST with rabbit polyclonal antibody for Fos (1:5000, Ab-5, Oncogene Science). Sections were then rinsed ten minutes in PBST, four times. Next they were incubated in biotinylated secondary antibody, and then avidin-biotinylated horseradish peroxidase complex in PBST (Elite Kit, Vector Laboratories). Sections were next rinsed in Tris non-saline buffer (pH 7.4). Finally, immunoreactivity was visualised with diaminobenzidine (DAB Substrate Kit, Vector Laboratories) chromogen incubation. Sections were then mounted on gelatinised slides, dehydrated through a series of alcohol gradients and coverslipped.

5A.2.4.3: Image capture and analyses of Fos-positive cell counts

Sections were viewed on a Leica DMRB microscope, photographed using an Olympus DP70 camera, and transferred to a computer. Counts of the stained nuclei were carried out using the program analySIS^D (Olympus, UK). The threshold was set automatically, at the same level for all sections from a same processing batch, based on overall illumination across both hemispheres. Counts were made in a frame area of 1768 x 1331 μm, using 5x magnification. The camera was positioned so that counts were taken across all layers of

retrosplenial granular cortex b. Counts were typically taken from three consecutive sections from both hemispheres of the retrosplenial cortex (approximately between -2.56 and 3.14 from bregma), and these counts were averaged to produce a mean. The SPSS 14.0 (Chicago) statistical package was used for all analyses.

The analyses of Fos-positive cell numbers were complemented by a qualitative analysis of the patterns of the effects of the lesions according to retrosplenial cortex laminae. For this purpose, the horizontal mean profile function of analySIS^D (Olympus, UK) was used. A representative section was chosen from each lesion group in order to produce laminar profiles of Fos activity. For each section, an area of equal size was selected in granular b retrosplenial cortex. A measure of the intensity of each pixel was made on a single horizontal plane, across all laminae (i.e. across the width of the image). Horizontal line profiles were made across the vertical axis, and averaged for that area, thus producing a mean profile of the Fos activity in granular b retrosplenial cortex. The areas chosen contained laminae that appeared as parallel as possible, thus optimising the averaging of the horizontal profiles by keeping the laminae aligned.

5A.2.4.4: RNA extraction and microarray hybridization

RNA was extracted as described previously (Chomczynski and Sacchi, 1987). This was performed from pooled tissue by Dr.D.Carter (cf. Humphries et al., 2002). Briefly, the sample was homogenised in the denaturing solution (guanidinium isothiocyanate/mercaptoethanol) and then sodium acetate, phenol, and chloroform-iso-amyl alcohol mixture were added and the solution shaken vigorously. After a 10 minute incubation on ice, samples were centrifuged for 10 minutes at 14000 rpm at 4°C. At this point the RNA was present in the aqueous phase. This phase was removed and mixed with ethanol and placed at -20°C for an hour for the RNA to precipitate. This solution was centrifuged again for 10 minutes and the resulting pellet was dissolved in the denaturing solution and then precipitated with ethanol at -20°C for 1 hour. After further centrifuging the pellet was washed in 95% Ethanol, dried and dissolved in DEPC-treated water. Yields of total cellular RNA extracted from the pooled punches in each sample ranged from 1.40 – 2.52 μg. A 3 μl aliquot (approx. 0.6 μg) of each sample was supplied to the Wales Gene Park Affymetrix GeneChip Expression Profiling Service, Department of Pathology,

UWCM. Before further processing, each RNA sample was quality controlled using Agilent RNA6000 chips. Following this check, 100ng of each sample was used to amplify biotinylated cRNA targets using Affymetrix GeneChip protocols and reagents. The biotinylated cRNA (target) was probed with rat genome 230A GeneChips. Hybridization and washing was performed using a GeneChip fluidics station 400 (Affymetrix). After scanning the microarrays, initial data processing was conducted with Microarray Suite 5.0 (Affymetrix). The average signal intensity of each array was scaled to 100. This procedure normalizes the raw data and corrects for technical variation between the arrays (eg. differences in hybridization conditions).

5A.2.4.5: Analyses of microarray data

5A.2.4.5.1: Data screening

Microarray expression analyses were conducted using GeneSpring™ software 6.1 (Silicon Genetics, Redwood City, CA) to characterise in granular retrosplenial tissue the genetic programs that are altered by anterior thalamic lesions. The hybridisation intensity was normalised per chip to the 50th percentile (.01 cutoff value), and per gene to the median. After log transformations of the data, the hybridisation histograms appeared to be similar and normally distributed, and thus no set was removed (see Appendix A). All samples were also highly correlated (>.90, .25 weighing coefficient). Data filtering was applied using parameters recommended by Silicon Genetics. Genes labelled "absent" are expressed at a low level and their signal may be very susceptible to noise. Genes that were labelled as "absent" in all samples were removed. Filtering was also applied on signal strength relative to control.

This filtering of the data left 9075 of the original 15923 transcripts. In order to obtain good reliability, we conducted analyses of variance using the cross-gene error model, where "precision calculations for all samples are based on the combined within-sample and between-sample variation" (GeneSpring™ User Manual, Cross-gene error model, section 4-47, p.95) and combined with variation from control strength (Rocke-Lorenzato model), obtained from values produced by the scanning software for the signal precision of each transcript (cf. GeneSpring ™ User Manual for additional information). Application of the

cross-gene error model used by GeneSpring™ generally yields more conservative results that are based on variance of each gene for all replicates rather than signal strength compared to control.

5A.2.4.5.2: Treatment profiling

Analyses of variance can extract interactions in gene expression, yet the nature of the analysis precludes small changes from being significant even if they are robust. Furthermore, this type of analysis is generally based on (static) fold changes that are dependent upon the setting of an almost arbitrary value for the fold change. While producing a reasonable list of differentially expressed transcripts, this fold change analysis bears no biological merit. Since for some transcripts it may be expected that only a small fold-change is biologically meaningful, it is possible that significant findings may be precluded by an analysis of fold changes (Murphy, 2002; Pavlidis, 2003). Instead of fold change analyses, more statistically-driven approaches can be used.

For example, the Class Prediction function of GeneSpring™ compares the expression of genes between treatments, irrespective of the levels of the other conditions. In effect, the levels of the time condition were treated as replicates and small but robust gene changes were singled out. This analysis allowed us to create a transcriptome profile of the retrosplenial cortex in the two surgical conditions (i.e. 'Intact' and Lesion hemispheres).

The samples were evaluated for their overall expression profile. Genes were assayed as potential class predictors, and those genes whose relative expression level correctly predicted class membership were identified. This type of analysis allows the additional identification of genes that exhibit much more subtle changes than could otherwise be detected by fold-change analyses. Briefly, the class prediction function uses Fisher's exact test to assign a *p*-value for the possibility of transcripts being located by chance closer to either of the classes (according to hypergeometric distribution), on either side of a decision cutoff value. This value is created by producing for each transcript the ratio of the p-values from each class. The cutoff is user-defined. We chose a cutoff value of 0.2, meaning that the magnitude of the difference between the p-values must be five or more. This forms the basis for the prediction strength value, according to which the transcripts are then ranked. The number of best predictors is user-determined; we chose 2 % of the total number of

transcripts assayed. The class prediction analysis yielded a set of genes that always correctly identified surgical treatment membership.

5A.2.4.5.3: Expression pattern cluster analysis

A Quality Threshold Cluster analysis was conducted on this class prediction list. The parameters used in this case were minimum cluster size 5; minimum similarity 0.9; similarity measure Pearson Correlation.

5A.2.4.5.4: Gene annotation

For this and further analyses, nucleotide-nucleotide searches were conducted on the sequences of all ESTs (Expressed Sequence Tags) using the Basic Local Alignment Search Tool (BLAST), a sequence similarity search program (http://www.ncbi.nlm.nih.gov/BLAST/). Transcripts that were labelled by GeneSpring™ as "similar to" a known gene were also thus confirmed. In essence, the unidentified mRNA transcript sequences were compared to known ones, thus producing a similarity score. A positive identity was inferred when high similarity ratings were produced, where the possibility that a similar nucleotide sequence match would be found by chance was low (i.e. the E-value was close to zero). Genes were annotated using gene ontology information from the Rat Genome Database (www.rgd.mcw.edu), Genecards (www.genecards.org) and literature searches on Pubmed (www.ncbi.nlm.nih.gov/entrez/). They were classified according to the Kyoto Encyclopedia of Genes and Genomes scheme (http://www.genome.jp/kegg/).

5A.3: Results

5A.3.1: Histology

Animals that were included for analysis exhibited the most complete anterodorsal and anteroventral thalamic nuclei damage. Additionally, only those animals with the most discrete lesions were included in our analyses (Figure 5A.4). The number of acceptable lesions was reduced by removing the lowest ranked in order to maintain the same number of animals per condition. Consequently, tissue from 12 subjects was processed for the

microarray analysis. The smallest lesion reveals some anterior ventral nucleus sparing throughout, though mainly in the rostral part of the nucleus with less sparing further caudally. Complete loss of the anterior dorsal nucleus was seen with little damage seen in the anterior medial nucleus or the lateral dorsal nucleus. The largest lesion removed all of the anterior ventral and anterior dorsal nuclei. There was damage in the anterior medial nucleus but it was not completely removed. Limited damage was observed in immediately adjacent dentate gyrus (n=8), and also in fornix (n=7, needle track). There was some damage in the dorsal portion of the lateral dorsal nucleus in all cases.

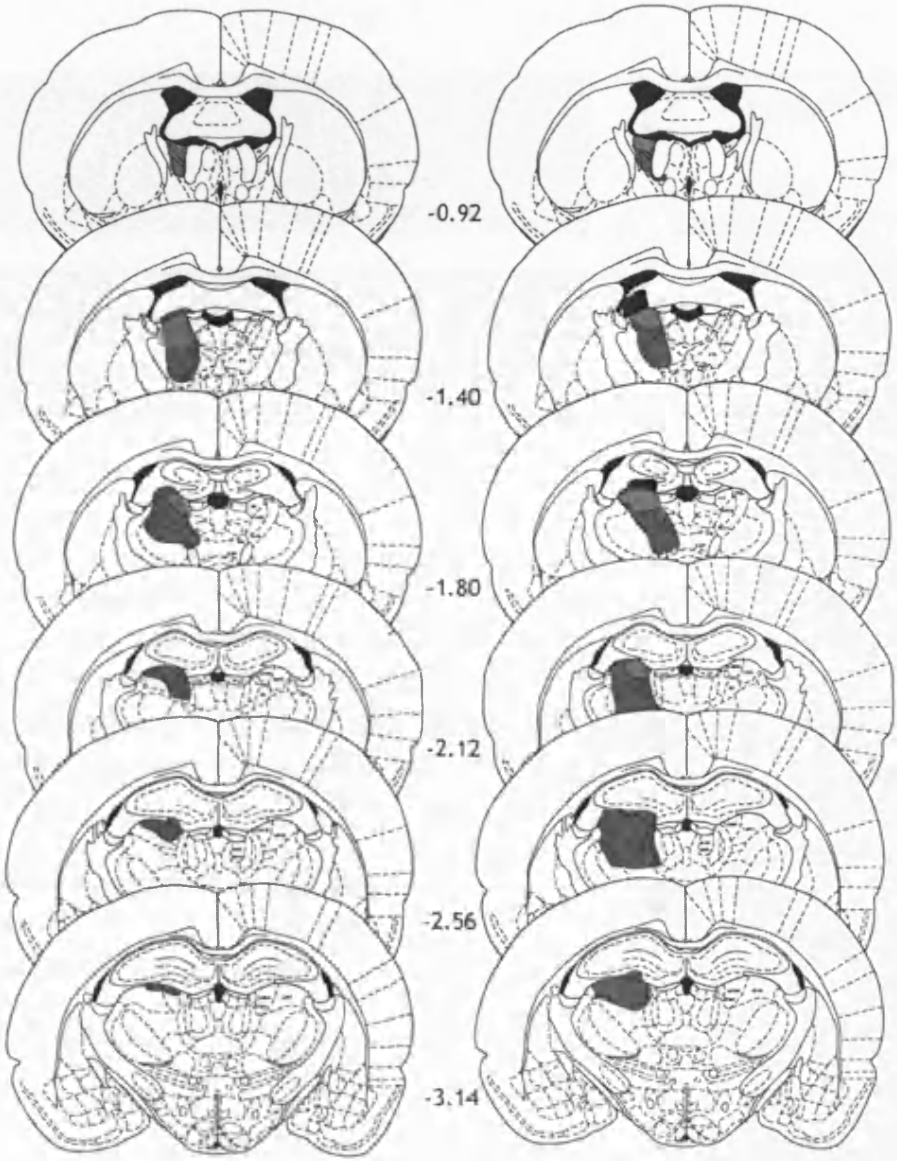

Figure 5A.4: Extent of the anterior thalamic nuclei lesions for each replicate (light = smallest amount of damage; dark = largest). The numbers refer to the distance from bregma.

5A.3.2: Immunohistochemistry

The results again replicated those reported by Jenkins and colleagues (2004), as well as those presented in Chapters 3 and 4. Immuno-histochemistry for c-Fos revealed a striking attenuation of protein expression in the superficial layers of retrosplenial cortex. A two-sample t-test (one-tailed) confirmed the significant reduction of Fos immunoreactivity between the 'Intact' and the Lesion hemisphere ($t=9.4$, $p<0.05$), as shown in Figure 5A.5, with an example of the observed Fos reduction.

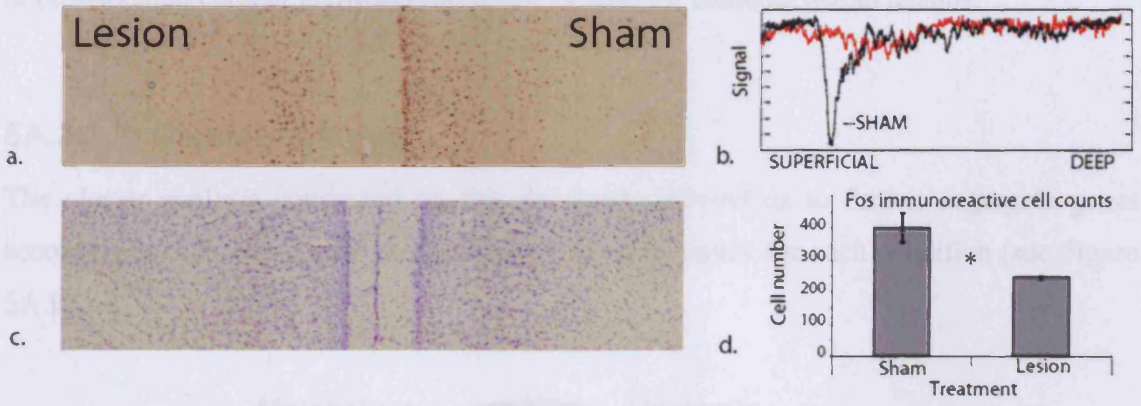

Figure 5A.5: a) Visualisation of the dramatic Fos reduction in the superficial laminae of granular b retrosplenial cortex after anterior thalamic nuclei lesions. b) Mean horizontal intensity profiles comparing the intensity of Fos in a. c) Nissl stain (note the normal appearance of the side ipsilateral to the lesion). d) There was a significant difference in Fos-positive cell counts between the 'Intact' and the Lesion hemisphere. Error bars represent the standard error of the mean. *p<0.05.

5A.3.3: Microarray analyses

5A.3.3.1: Treatment profiling

Predictive patterning allows the segregation of the transcripts according to the different levels of a variable, only according to robust differential expression levels. Pooling the Surgical treatment conditions and producing class predictions for Time was unreliable as this yielded numerous group prediction errors. As such the results of this analysis are not presented. In contrast, pooling across time points and using the class prediction tool for the

Surgical treatment variable yielded no prediction errors. These were made on 2 % of the list consisting of all genes other than those flagged absent in all samples, filtered for control signal strength. The class prediction analysis yielded a set of genes for which relative expression levels were consistent for data across all time points and both replicates (cf. Table 5A.1). For example, the expression of a specific transcript was always significantly greater in one level of the Surgical treatment, for all time points and across both replicates.

Classification of the genes according to biological functions (see Figures 5A.6, and 5A.7) and according to cellular compartments (see Figure 5A.8) revealed the pervasive alterations in retrosplenial cellular pathways produced by anterior thalamic nuclei lesions.

5A.3.3.2: Cluster analysis

The cluster analysis conducted on this list again allowed us to further segregate genes according to their expression patterns across the time points for each condition (see Figure 5A.9).

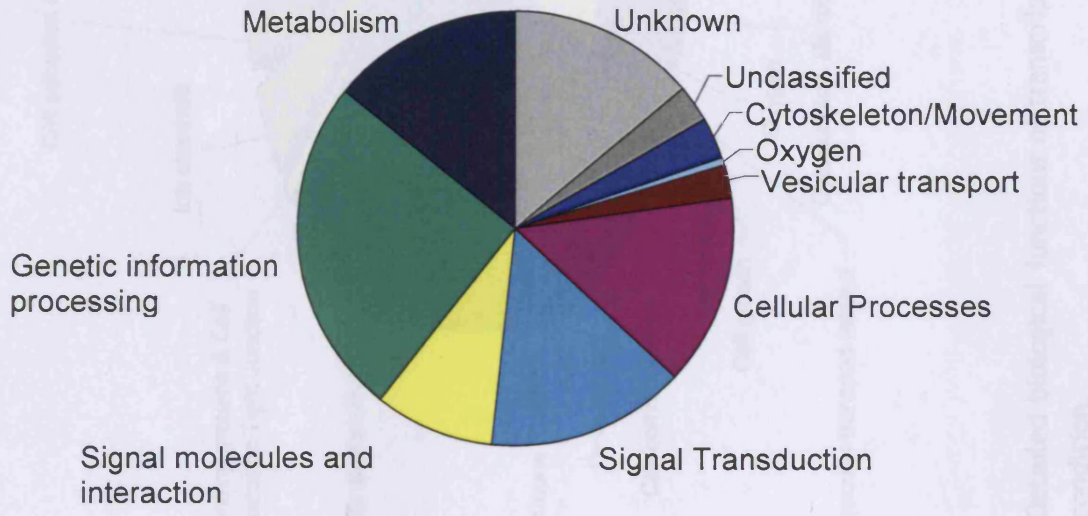

Figure 5A.6: Biological functions of transcripts that exhibited altered expression levels found to be predictive of experimental condition.

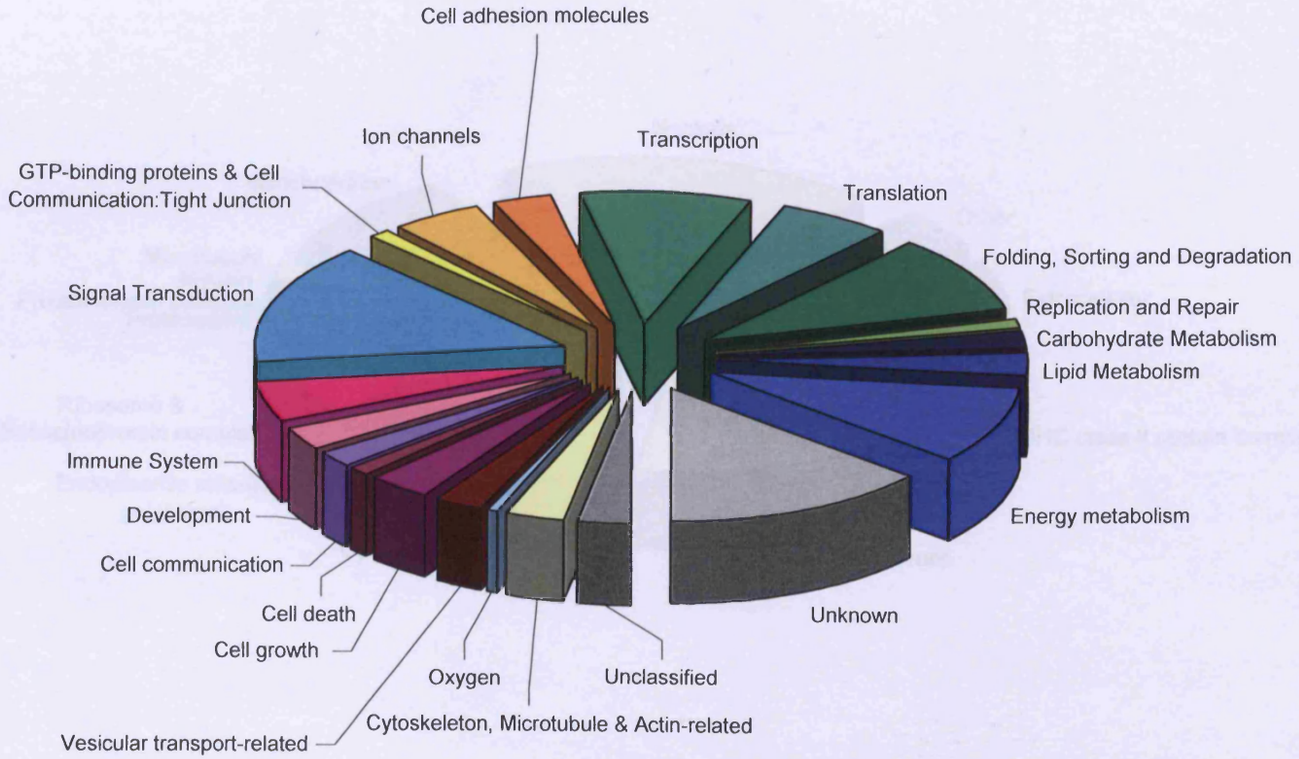

Figure 5A.7: Detailed biological functions of transcripts that exhibited altered expression levels found to be predictive of experimental condition.

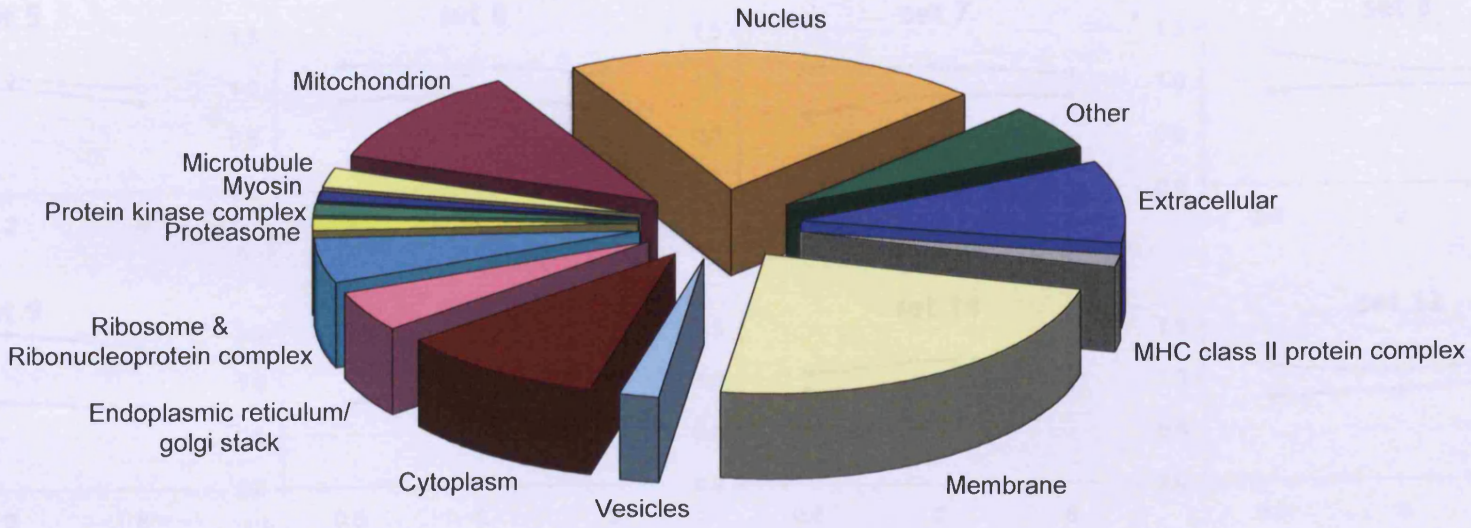

Figure 5A.8: Cellular compartments of transcripts that exhibited altered expression levels found to be predictive of experimental condition.

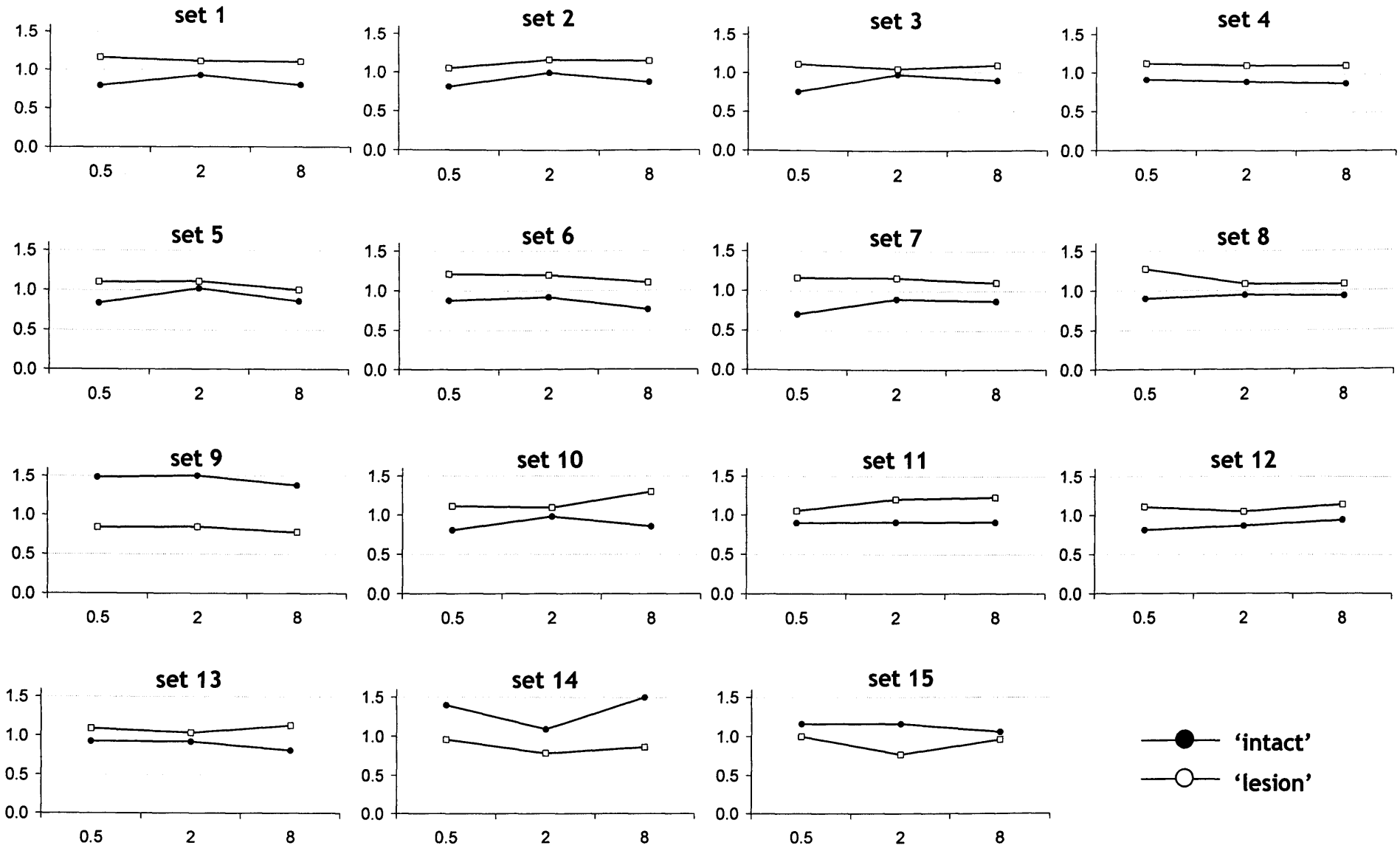

Figure 5A.10: Cluster analysis of transcripts that exhibited altered expression levels found to be predictive of the experimental condition. 76 transcripts remained unclassified. Y-axis= Normalised intensity (log scale); X-axis= Time(h).

Table 5A.1: List of genes that were found to be consistently at different levels in the 'Intact' and the Lesion retrosplenial cortex hemispheres, grouped by expression pattern sets. *For EST similarity, the value on the left is the similarity score, and the value on the right is the E-value. (S = Sham, L = Lesion)

Cluster	Direction	Function Classification	Name	Synonym	EST similarity, if applicable *	Genbank
1	L>S	**Immune system**	(Chapman et al., 1996)	Gig 18, Tssn1	1203 0.0	BE108162
		unclassified	Secretory carrier embrane protein 1 (Scamp1)			BM386698
		unclassified	Protein phosphatase 1, regulatory (inhibitor) subunit 1c (Ppp1r1c)		801 0.0	AA943808
		unclassified	Disabled homolog 2 (Drosophila) interacting protein (Dab2ip)	DIP1/2		AF236130
		unclassified	Protein kinase, cAMP dependent regulatory, type 1 beta (Prkar1b) R1beta			BG375376
		GTP-binding proteins/Cell Comm>TightJunctio n	RAB11 family interacting protein 5 (RAB11FIP5)	Gamma-SNAP-associated factor 1 (GAF1), pp75, RIP11, KIAA0857, DKFZP434H018, D6Ertd32e	505 6e-140	BI296378
		Ion channels	Potassium voltage-gated channel, delayed rectifier, subfamily S, 1 (kcns1)	Voltage-gated potassium channel subunit Kv9.1		NM_053954
		Transcription	Bromodomain containing 8 (Brd8)	Small acidic protein (Smap), thyroid receptor coactivating protein, p120		AI549477
		Transcription	Kruppel-like factor 5 (intestinal) (Klf5)	IKLF, BTEB-2		NM_053394
		Translation	Ribosomal 60S protein l15 (Rpi15)	EC45, RPYL10		AA800007
		Folding, Sorting and Degradation	Heat shock 70kD protein 1-like (Hspa1l)	LOC361797; Heat shock protein 70-3 (HSP70 - 3); HSP70-HOM; Major histocompatibility component complex 4-1 (C4-1)	561 8e-157	BG381414
		Folding, Sorting and Degradation	Mitochondria associated granulocyte macrophage CSF signaling molecule (Magmas)	CGI-136, TIM16		BG379323
		Replication and repair	Replication protein A3 (Rpa3)		720 0.0	BM383451
		Carbohydrate metabolism	Malate dehydrogenase, mitochondrial (Mdh2)	Mor1		NM_031151
		ATP synthesis	ATP synthase, H+ transporting, mitochondrial F1 complex, O subunit (Atp5o)			D13127
		Nitrogen metabolism	glutamate-ammonia ligase (Glul)	Glutamine synthase		AW528806
		Metabolism of cofactors and vitamins	Uroporphyrinogen decarboxylase (Urod)	hemE		Y00350
2	L>S	**Cell growth**	Kelch domain containing 3 (Klhdc3)/ Protein	Peas for klhdc3	(confirmed)	AA894104

			phosphatase 2a regulatory b56-delta subunit (Ppp2r5d)/Male-enhanced antigen-1 (Mea1), [OVERLAPPING GENES]		662 0.0	
		Development	Neuritin 1 (Nrn1)	Nrn		NM_053346
		unclassified	Synaptotagmin 5 (Syt5)			NM_019350
		unclassified	Calcium/calmodulin-dependent protein kinase (CaM kinase) II gamma (Camk2g)			NM_133605
		unclassified	N-ethylmaleimide sensitive fusion protein attachment protein alpha (Napa)	SNAPA		NM_080585
		GTP-binding proteins/Cell Comm>TightJunctio n	Rab3B protein			NM_031091
		Transcription	Nuclear factor I/X (Nfix)	CTF, NF1A		BF420722
		Transcription	Single stranded DNA binding protein 3 (SSBP3)	SSDP, CSDP; FLJ10355		NM_053358
		Translation	DEAD (aspartate-glutamate-alanine-aspartate) box polypeptide 25 (Ddx25)	GRTH		NM_031630
		Translation	Deoxyhypusine synthase (DHS/Dhps/Dys1)			AA892493
		Folding, Sorting and Degradation	Down syndrome critical region homolog 2 (H. sapiens (Dscr2)	C21LRP, LRPC21, PAC1	803 0.0	BF407158
		Folding, Sorting and Degradation	F-box only protein 6b (Fbxo6b)	FBX6, FBG2,FBS2		AF393484
		Lipid Metabolism	Monoglyceride lipase (Mgll)			AI713204
		Oxidative phosphorylation	NADH dehydrogenase (Ndufa8)		1029 0.0	BI280270
		Unclassified	Small nuclear ribonucleoprotein associated protein N, upstream reading frame (SNURF)		60.0 9e-06	AI171982
		Unknown	SID1 transmembrane family, member 2 (sidt2)	CGI-40	942 0.0 (predicted); 474 1e-130	AI579643
3	L>S	**unclassified**	Phosphatidylinositol transfer protein (Pitpn)	VIB1A (Homo sapiens: PITPNA (Homologs)		NM_017231
		MAPK signaling	PTPL1-associated RhoGAP1 (Parg1)		490 3e-135	AI407483
		WNT signaling pathway	Groucho protein (GRG1)	DGPWD, Transducin-like enhancer of split 1 (Tle1)		BG380534
		Calcium signaling	5-HT2C receptor (5-HT2cR)	Htr1c	509 3e-141	BF285539
		Ion channels	Potassium voltage gated channel, shaker related subfamily, member 4 (kcna4)	KV1.4		NM_012971
		Cell adhesion molecules	Olfactomedin 3 (Olfm3)	Optimedin form B, NOE3		AF442822
		Transcription	Polymerase (RNA) III a (155kd) RPC155	BC053071; MGC62420	733 0.0	BI274108
		Translation	40S ribosomal protein S14 (RPS14)			NM_022672
		Translation	Mitochondrial ribosomal protein L4 isoform 2 (Mrpl4)	CGI-28		BI275903

		Folding, Sorting and Degradation	Ubiquitin specific protease 3 (Usp3)			AI411205
		Folding, Sorting and Degradation	Cyclophilin B (Ppib)			
		Oxidative phosphorylation	NADH dehydrogenase, mitochondrial 24-kDa subunit (Ndufv2)			M22756
		Vesicular transport-related	Adaptor-related protein complex 2, mu 1 subunit (Ap2m1)	Clathrin coat assembly protein AP50; clathrin-associated/assembly/adaptor protein, medium 1 (CLAPM1)		NM_053837
4	L>S	**unclassified**	Protein phosphatase 1, regulatory (inhibitor) subunit 1A (Ppp1r1a)			NM_022676
		unclassified	Exostosin 1 (Ext1)			BM384468
		MAPK signaling	Regulator of G-protein signaling 4 (Rgs4)	RGP4		U27767
		Ion channels	GABA A receptor delta (Gabrd)			NM_017289
		Ion channels	Sodium channel, voltage-gated, type I, beta polypeptide (Scn1b)	GEFSP1		NM_017288
		Cell adhesion molecules	Syndecan-1 (Sdc1)	Syndecan 1 (Synd1), CD138 antigen, HSPG, Syndeca, CD138		NM_013026
		Folding, Sorting and Degradation	Proteasome (prosome, macropain) 26s non-ATPase subunit 3 (Psmd3)	26S Proteasome subunit p58, Psd3, AntP91a, Tstap91a, D11Bwg1349e		BI285842
		Lipid Metabolism	hypothetical protein MGC11324, Hypothetical phospholipid and glycerol acyltransferase		398 9e-108	AI599365
		ATP synthesis	ATPase, vacuolar, 14 kD (Atp6s14)	Atp6v1f, VATF, VMA7		NM_053884
		Unclassified	Host cell factor C1 regulator 1 (XPO1-dependent; HCFC1R1)	HPIP, FLJ20568, MGC70711		AA944494
5	L>S	**Development**	Plexin b2 (Plxnb2)			BG380275
		Immune System	CD83			AI412355
		MAPK signaling	Adrenergic receptor kinase, beta 1 (Adrbk1)	BARK1, GRK2		AI716801
		MAPK signaling	Mitogen-activated protein kinase 6 (Mapk6)	ERK3		NM_031622
		Transcription	nuclear receptor subfamily 4, group A, member 1 (NR4A1)	Nur77/NGFIB downstream protein 2		BI282332
		Translation	Ribosomal protein L23a (Rpl23a)	60S ribosomal protein L23a	(confirmed) 1003 0.0	AI172199
		Lipid Metabolism	Phosphatidic acid phosphatase type 2B (PPAP2B)	Endoplasmic reticulum transmembrane protein (Dri 42), Phosphatidic acid phosphohydrolase, Vascular endothelial growth factor and type I collagen inducible		Y07783
		Lipid Metabolism	Fatty acid Coenzyme A ligase, long chain 6 (Facl6)			NM_130739
		Unknown	KIAA1086		728 0.0	BI294610
6	L>S	**Cell growth**	Cyclin D2 (CCND2)	KIAK0002, MGC102758		BG380633
		Cell growth	PKC-delta binding protein (Prkcdbp)		NM_134449	

		Transcription	U2(RNU2) small nuclear RNA auxillary factor 1-like 1 (U2AF1L1) [located in an intron of the Murr1 gene]	SP2, U2afi-rsi, U2AF1RS1, U2AFBPL		BF404554
		Translation	Staufen			NM_053436
		Folding, Sorting and Degradation	Proteasome [20S] (prosome,macropain) inhibitor subunit 1 (Psmf1)	PI31, MGC18784		BF561377
		Oxidative phosphorylation	NADH dehydrogenase (Ndufb6)			AI104528
		Cytoskeleton, microtubule and actin-related	Neurofilament, heavy polypeptide (Nefh)	Nfh		AF031879
7	L>S	**Cell communication**	Tubulin alpha 4 chain (alpha-tubulin 4)			BI284599
		Calcium signaling	Adenylate cyclase activating polypeptide 1 (Adcyap1)	PACAP		NM_016989
		Cell adhesion molecules	Limbic system-associated membrane protein (Lsamp)	LAMP-1, CD107a, LGP120		U31554
		Translation	Eukaryotic initiation factor 5 (eIF-5)			BE107346
		Folding, Sorting and Degradation	similar to similar to Protein C20orf22 homolog		908 0.0	BI284608
		Folding, Sorting and Degradation	Signal recognition particle 68kDa (Srp68)	MGC38208		BI296671
		Unknown	leucine rich repeat containing 57 (Lrrc57)		389 7e-105	BE101274
8	L>S	**MAPK signaling**	MAPKK Mitogen-activated protein kinase kinase 1 interacting protein 1 (MAP2K1IP1)	Mek binding partner 1 (Mp1), Mabp		AA817829
		Ion channels	Potassium voltage gated channel, Shaw-related subfamily, member 1 (kcnc1)	KV3.1; KV4		NM_012856
		Transcription	Splicing factor 3a, subunit 3 (Sf3a3)	SAP 61, SF3A60	1065 0.0	BM391739
		Oxidative phosphorylation	Cytochrome C oxidase- subunit Via polypeptide 1 (Cox6a1)			BI282326
		Amino acid metabolism	Asparagine synthetase (Asns)	Asparagine synthetase, Cell cycle control protein TS11, Glutamine- dependent asparagine synthetase		U07202
		Cytoskeleton, microtubule and actin-related	Microtubule-associated protein 2 (MAP2)	Mtap2		X74211
9	S>L	**Cell growth**	Mdm4, transformed 3T3 cell double minute 1, p53 binding protein (mouse) (mdm1)			BE099784
		Immune System	CD74	INVG34, LN2		NM_013069
		unclassified	transmembrane emp24 protein transport domain containing 4 (tmed4)	HNLF	204 2e-49	AI235294
		unclassified	Solute carrier organic anion transporter family, member 2B1 (SLCO2B1)	Solute carrier family 21 (organic anion transporter), member 9 (Slc21a9)		AF169410
		Transcription	Putative homeodomain transcription factor 2 (Phtf2)		295 8e-77	AI410924
		Folding, Sorting and Degradation	DEAH (Asp-Glu-Ala-His) box polypeptide 40 (DHX40)	ARG147, DDX40, PAD		AI178155
10	L>S	**Cell growth**	Retinoblastoma binding protein 5 (RBBP-5)	RBQ 3	396 3e-107	AA946518

		unclassified	G protein-coupled receptor 162 (GPR162)	Gene rich cluster, A gene (Grca); A-2		BM386619
		Ion channels	Calcium channel, voltage-dependent T-type, alpha 1I subunit (CACNA1I), transcript variant 2	Cav3.3	287 1e-74	BE105417
		Lipid Metabolism	CDP-diacylglycerol synthase (phosphatidate cytidylyltransferase) 1 (Cds1)			NM_031242
		Metabolism of cofactors and vitamins	coenzyme Q9 homolog		1068 0.0	AI232494
		Unknown	similar to and predicted: chromosome 20 open reading frame 116 (LOC296162)		601 6e-169	AI638949
11	L>S	**Development**	Nasal embryonic LHRH [luteinizing hormone-releasing hormone] factor (Nelf)	Jacob protein alternatively spliced isoform delta1 (jac gene)		AJ293698
		unclassified	Calcium/calmodulin-dependent protein kinase kinase 1, alpha (Camkk1)			NM_031662
		Ion channels	Transient receptor potential cation channel, subfamily V, member 5 (TRPV5)	Epithelial calcium channel 1 (Ecac1)		NM_053787
		Transcription	THAP domain containing 4 (Thap4)	CGI-36, PP238		BI275281
		Folding, Sorting and Degradation	Matrix metalloproteinase 24 (Mmp24)	Mt5-mmp	188 1e-44	BF285924
		Metabolism of cofactors and vitamins	Pantothenate kinase 4 (Pank4)			NM_133531
12	L>S	**Cytoskeleton, microtubule and actin-related**	Actin alpha-1 (Acta1)			NM_019212
		Vesicular transport-related	Frequenin homolg (Drosophila)	Neuronal calcium sensor 1 (NCS-1)		NM_024366
		Vesicular transport-related	Exocyst complex component 7 (Exoc7)	EXO70		BM388722
		Unknown	transmembrane protein 93; Vanilloid receptor subtype 1 (H. sapiens)	MGC2963	944 0.0; 507 1e-140	BI285673
		Unknown	Homo Sapiens Chromosome 9 open reading frame 25 (C9orf25)	FLJ39031, bA573M23.5	272 6e-70	BI298306
13	L>S	**Cell growth**	Nuclear distribution gene C homolog (Aspergillus; Nudc)	c15, Silg92		NM_017271
		Transcription	DNA-directed RNA polymerase II 7.6 kda polypeptide L (POL2RL)	RBP-10	476 3e-161	AA924509
		Unclassified	Selenoprotein M (Selm)	SepM, A230103K18, 1500040L08Rik		BI282694
		Unknown	Gene rich cluster C10 (Grcc10)	C10, C12orf57		BI282112
		Unknown	RGD1564450_predicted	LOC294291	793 0.0	AW915035
14	S>L	**Cell growth**	Reprimo (candidate mediator of the tp53-dependent G2 arrest)		672 0.0	BG381258
		Immune System	LOC171412	E-3 epididymal fluid protein, 2D6 glycoprotein; Defb22,		AF329091
		Folding, Sorting and Degradation	Apobec-1 complementation factor (Acf)	ACF64		NM_133400
		Unknown	Calpain10 (capn10); BDNF exon 5		176 6e-41; 172 1e-39	BI296532

		Unknown	EST			BI291373
15	S>L	**Transcription**	Neurogenic differentiation 1 (NeuroD1)	BETA2, BHF-1, Neurod		AI639109
		Oxidative phosphorylation	Cytochrome oxidase 6b1 (Cox6b1)		739 0.0	AI230604
		Metabolism	Kynurenine 3-monooxygenase (KMO)	Kynurenine 3-hydroxylase		NM_021593
		Vesicular transport-related	EH-domain containing 2 (Ehd-2)	MGEPS, PAst2, MGC25606, MGC38650		BE110691
		Unknown	Family with sequence similarity 26, member B	LOC294019, Hypothetical protein FLJ12133, 2810048G17Rik	1120 0.0	BM391099
unclassified	L>S	**Cell death**	Death associated protein 3 (DAP-3)	Mitochondrial 28S ribosomal protein S29 (MRP-S29)	831 0.0	BI285645
	L>S	**Cell death**	Tnf receptor-asociated factor 7 (Traf7)	MGC7807, RFWD 1	(confirmed) 682 0.0	BI287266
	S>L	**Cell communication**	PREDICTED: Mus musculus angiomotin-like 1, transcript variant 5 (Amotl1), mRNA	JEAP	678 0.0	BI277433
	S>L	**Cell communication**	Zyxin (Zyx)	HED-2		AA943537
	S>L	**Development**	Netrin 1			NM_053731
	L>S	**Development**	Dihydropyrimidinase-like 4 (Dpysl4)	rCRMP-3		BF413467
	S>L	**Development**	Enah/Vasp-like (Evl)	RNB6		BF404078
	S>L	**Immune System**	Major histocompatibility complex clas II DM beta (Hla-dmb)			AI171966
	S>L	**Immune System**	RT1 class histocompatibility antigen, B-1 beta chain precursor (RT1.B beta 1)			AI715202
	S>L	**Immune System**	Rat MHC class II RT1.u-D-alpha chain mRNA, 3' end (RT1-Da)			Y00480
	S>L	**Immune System**	Trispanning orphan (Tore)	CRIT (complement C2 receptor inhibitory trispanning)*		NM_022679
	S>L	**Immune System**	Mannan-binding lectin serine protease 1 (Masp1)	Complement-activating component of Ra-reactive factor precursor (CRARF1)		BE111083
	L>S	**Immune System**	PX-19	PX-19-like protein homolog, H. sapiens); Preli, CGI-106		BI279855
	L>S	**unclassified**	Amiloride binding protein 1 (Abp1)			NM_022935
	L>S	**unclassified**	Mitogen activated protein kinase kinase 2 (Map2k2)			D14592
	S>L	**MAPK signaling**	*predicted similar to A-kinase anchor protein 13 isoform 2 isoform 11 [mus musculus] 428 9e-117 *Homo sapiens A kinase (PRKA) anchor protein 13 (AKAP13), transcript variant 2 180 3e-42		428 9e-117 180 3e-42	AI599048
	S>L	**MAPK signaling**	Membrane-spanning 4-domains, subfamily A, member 6B (Ms4a6b) [homolog of Homo sapiens Ms4a6b]	CD20L3 [Homo sapiens]		BI294706
	S>L	**MAPK signaling**	similar to G protein-coupled receptor 146 (Gpr146)	similar to G protein-coupled receptor PGR8	369 7e-99	AI170446
	L>S	**MAPK signaling**	G protein-coupled receptor kinase-interactor 1 (Git1)	Cat-1		NM_031814
	L>S	**WNT signaling pathway**	Frizzled homolog 2 (D. melanogaster; Fzd2)	Fz2		L02530

	S>L	**Calcium signaling**	Adrenergic receptor, beta 3 (Adrb3)			NM_013108
	L>S	**Ion channels**	Potassium voltage-gated channel, shaker-related subfamily, beta member 2 (Kcnab2)	KVbeta2.1; KVbeta2.2		BE097195
	S>L	**Ion channels**	Potassium inwardly-rectifying channel, subfamily J, member 6 (kcnj6)	KCNJ7; GIRK2; GIRK3.2; KIR3.2		AB073756
	S>L	**Ion channels**	Sodium channel, voltage-gated, type VII, alpha polypeptide (SCN7a)	Sodium channel, voltage gated type 6 alpha polypeptide (scn6a); Na-G		BF285019
	L>S	**Cell adhesion molecules**	immunoglobulin superfamily, member 4B (IGSF4B)	Membrane glycoprotein: nectin-like protein 1 (necl1)/TSLC1-like 1 (Tsll1)/brain immunoglobulin receptor precursor (BlgR)	(confirmed) 729 0.0	BG378062
	L>S	**Cell adhesion molecules**	Cartilage acidic protein 1 (Crtac1)	Acidic secreted protein 1 (ASPIC1), Chondrocyte expressed protein 68 kDa (CEP-68), CRTAC1-B, W307		NM_134401
	L>S	**Cell adhesion molecules**	Vitronectin (Vtn)			NM_019156
	L>S	**Transcription**	SWI/SNF-related matrix-associated actin-dependent regulator of chromatin c, member 2 (SMARCC2)	Rsc8, BAF170, CRACC2		BF396079
	L>S	**Transcription**	RuvB-like protein 1 (Ruvbl1)	ECP54; NMP238; TIP49a (TATA binding protein interacting protein 49 kDa); Pontin52		AB002406
	L>S	**Transcription**	Smad3 (Mad homolog 3, D. melanogaster)			BF552908
	S>L	**Transcription**	Retinoid X receptor gamma (RXRγ)	NR2B3		BE118450
	S>L	**Transcription**	Nuclear factor of activated T cells 5 (T cell transcription factor NFAT5)	Tonicity-responsive enhancer binding protein (TONEBP)	287 2e-74	BM384203
	S>L	**Transcription**	Neuronal activity regulated pentraxin protein II (NPTX2)	NARP	1051 0.0	AI228623
	L>S	**Translation**	hypothetical Eukaryotic initiation factor 1A (eIF-1A)/S1 domain IF1 type profile/Nucleic acid-binding OB-fold containing protein	1158 0.0	2010003J03 Rik, LOC293673, MGC11102	BF420639
	L>S	**Translation**	Ribosomal protein L3 (Rpl3)	TARBP-B		AA892367
	L>S	**Translation**	Ubiquitin A-52 residue ribosomal protein fusion product 1 (Uba52)			NM_031687
	L>S	**Translation**	Speckle-type POZ protein (Spop)	TEF2	476 2e-131	BF283504
	L>S	**Folding, Sorting and Degradation**	Matrix metalloproteinase 9 (Mmp9)	Gelatinase b (GELB), Macrophage gelatinase, Type V collagenase, 92kD type IV collagenase, CLG4B		NM_031055
	L>S	**Folding, Sorting and Degradation**	Dnaj (Hsp40 homolog, subfamily C, member 8 (Dnajc8)	SPF31, HSPC331		AI227785
	L>S	**Folding, Sorting and Degradation**	FK506 binding protein 3 (FKBP3)	FKBP25, PPIase, Rotomase		AA891798
	L>S	**Folding, Sorting and Degradation**	Ubiquilin 1, transcript variant 1 (ubqln1)	DA41, DSK2, PLIC-1, XDRP1		BI279735
	L>S	**Folding, Sorting and Degradation**	ADP-ribosylarginine hydrolase (Adprh)			M86341
	L>S	**Folding, Sorting and Degradation**	Syntaxin binding protein 1 (stxbp1)			U06069
	L>S	**Replication and repair**	Replication factor C (activator 1) 2 (Rfc2)			BF283113

	L>S	**Carbohydrate metabolism**	Phosphomannomutase 2		222 7e-55	AI411161
	L>S	**Carbohydrate metabolism**	Solute carrier family 3, member 1 (Slc3a1)	Amino acid transporter 1 (Atr1); Neutral and basic amino acid transport protein rBAT (B(0,+)-type amino acid transport protein (NBAT); CSNU, D2H		NM_017216
	S>L	**Carbohydrate metabolism**	Glycoprotein galactosyltransferase alpha 1, 3 (Ggta1)			AI178222
	S>L	**Lipid Metabolism**	Prostaglandin-endoperoxide synthase 1 (Ptgs1)	Cyclooxygenase 1 (COX1), COX3		NM_017043
	L>S	**Oxidative phosphorylation**	Cytochrome c1 (Cyc1)			BI277021
	L>S	**Oxidative phosphorylation**	Cytochrome c1, non heme 7.2 kDa protein	Ubiquinol-cytochrome C reductase complex (UCRC), HSPC119, HSPC151	278 1e-71	AI007981
	L>S	**Oxidative phosphorylation**	Succinate dehydrogenase complex (Sdhc), subunit b/c		1405 0.0	AI009817
	L>S	**Nitrogen metabolism**	Carbonic anhydrase 4 (Ca4)			NM_019174
	L>S	**Amino acid metabolism**	Liver glutaminase	Gls2, L-glutaminase, L-glutamine amidohydrolase, phosphate-activated/-dependent glutaminase		J05499
	L>S	**Glycan Biosynthesis and Metabolism**	Hyaluronoglucosaminidase 2 (Hyal2)	LUCA-2		AF034218
	L>S	**Cytoskeleton, microtubule and actin-related**	Myosin-1e (Myo1e)	Myo1c		BI275813
	S>L	**Cytoskeleton, microtubule and actin-related**	Myosin-IXA(Myo9a)	Myr7	801 0.0	AW917818
	S>L	**Cytoskeleton, microtubule and actin-related**	Kif6 (Kinesin family member 6)	Kinesin-related protein 3 (Krp3)		AY035403
	L>S	**Oxygen-related**	Hemoglobin alpha-1 (Hba1)	Hbam, CD31		AI179404
	L>S	**Vesicular transport-related**	Low density lipoprotein receptor-related protein 3 (LRP3)			NM_053541
	L>S	**Unclassified**	VGF nerve growth factor inducible			NM_030997
	L>S	**Unclassified**	Hypothetical HAD-like structure containing protein		139 1e-29	BG380656
	S>L	**Unclassified**	PREDICTED Rattus norvegicus ATPase inhibitor (Atpi); Urinary protein 2/3 precursor (RUP-2/3)		1003 0.0; 902 0.0	AA893518
	L>S	**Unknown**	PREDICTED: Rattus norvegicus similar to D3Mm3e (LOC500226)		1021 0.0	AI178206
	L>S	**Unknown**	weakly similar to Proline-rich protein MP-2 precursor		486 4e-134	AI236927
	L>S	**Unknown**	LOC362671			AI409584
	L>S	**Unknown**	LOC317191	UNQ8193, GC0XP083030		AW254686
	L>S	**Unknown**	LOC294291	MGC57858, GC06M034261, GC06M034215		AW915035

	L>S	**Unknown**	EST			BE108374
	L>S	**Unknown**	EST			BF391141
	L>S	**Unknown**	clone RP24-75K5 from chromosome 5			BF401709
	L>S	**Unknown**	Similar to hypothetical protein FLJ14466 (LOC304496)			BG378798
	L>S	**Unknown**	KIAA0683 gene product		293 3e-76	BI279598
	S>L	**Unknown**	1700021K19Rik, 5330403K09	Hypothetical protein KIAA0226; Similar to D. melanogaster gene encoded in P1 clone DS00642		BE113144
	S>L	**Unknown**	Chromosome 22 open reading frame 23 (C22ORF23)	LOC315126; EVG1; FLJ32787	301 1e-78	BI286421
	S>L	**Unknown**	LIM domain containing 2, LIMD2	MGC10986	1356 0.0	BI294855
	S>L	**Unknown**	EST			BI300513
	S>L	**Unknown**	Hypothetical protein 6330514E13 OR RNI-like structure containing protein		307 2e-80	AA964675
	L>S	**Unknown**	Fibronectin type III domain containing 5 (Fndc5)	LOC260327	599 4e-168	AI172165
	S>L	**Unknown**	Zinc finger, FYVE domain containing 21 (zfyve21)	zinc finger, FYVE domain containing 21 (predicted) (Zfyve21_predicted)	1322 0.0 (predicted); 244 3e-61	BI283114

5A.3.3.2: Pathway analyses

For the list of genes found by the class prediction analyses, automated gene classifications using GeneSpring™ identified pathways that exhibited significantly altered transcript levels between the 'Intact' and 'Lesion' retrosplenial cortex tissue. This automated analysis was only possible for transcripts where information was available in the databases used by the software. These pathways included alkaloid biosynthesis II; arginine and praline metabolism, beta-alanine, glycine, serine and threonine, histidine, phenylalanine, tryptophan, and tyrosine metabolism (amiloride-binding protein 1); amyotrophic lateral sclerosis (Nefh); ATP synthesis and oxidative phosphorylation (Atp5o, Atp6s14); MAPK signalling pathway (Map2k2); ribosomal pathways (Rpl3, Rps14, Rpl15, Uba52); and WNT signalling (Ruvbl1). These pathway analyses using software-generated analyses remain incomplete as very few transcripts were already annotated and thus taken into account for these automated analyses. Information for the un-annotated transcripts was subsequently obtained from other sources, as described in section 5A.2.4.5.3. Information will be presented about additional pathways that appeared to be altered by the anterior thalamic nuclei lesions in section 5A.4.1.

It is important to re-emphasize that genes that exhibited an absent signal in all conditions were removed. Genes with absent flags are expressed at a low level and their signal may be very susceptible to noise. However, it is possible that for some of these genes the signal is not affected by noise, thus producing false negatives. This is particularly plausible for the treatment profiling analyses. If changes are consistent across all time points, it seems unlikely that this would happen by chance. In other words, changes may be robust even if the signal is deemed to be absent. For this reason, it could prove fruitful to verify a subset of these transcripts by RT-PCR (reverse transcriptase polymerase chain reaction). These transcripts may include for example calcitonin receptor; leucine-rich protein induced by beta-amyloid (Lib); MGC72638/AI412117 (serine protease inhibitor, Kunitz type 2); Proteasome subunit b9 (Psmb9); interferon gamma (Ifng); presenilin2 (Psen2); calsenilin (Csen); beta-synuclein (sncb); amyloid beta (A4) precursor protein-binding, family A,(APBA1); APBA3; Nos2/iNos/Nos2; Nos3; transglutaminase 1 (Tgm1); sialyltransferase 8 A (siat8a); siat8b.

5A.4: Discussion

Results from our work suggest widespread consequences of anterior thalamic lesions on retrosplenial cortex. Therefore, the decrease in Fos protein expression observed previously (Chapters 3 and 4, Jenkins et al., 2004) is accompanied by pervasive changes in cellular gene expression.

Using GeneSpring™, we have filtered for signal strength, removed absent flags and conducted statistical analyses, measures that should have minimised the degree of false positives. However, and importantly, it remains that for closely similar samples, many false negatives might be produced, even where small differences (i.e. smaller than fold-change value) are robust.

Approximately three quarters of genes were found to be at greater expression levels in the Lesion condition of retrosplenial cortex (159 vs. 45 for predictive patterning). Genetic functions of translation, DNA replication and repair appeared to be at higher levels solely in the Lesion condition, whereas those of transcription, folding, sorting and degradation were at mixed levels between the two surgical conditions.

Beyond fold-change analyses, predictive treatment analysis delineated genetic programs that were consistently altered at the three time points studied. The relative expression level of these genes could predict treatment in any condition of either duplicate. Amongst the pervasive changes observed, gene ontology queries revealed that the largest functional alterations were found in genetic information processing, signal transduction and metabolism, as well as diverse cellular processes.

5A.4.1: Functional analyses

5A.4.1.1: Cell signalling

Cell signalling appears to be grossly affected by the surgical treatment. Diverse neurotransmitter receptors, in addition to several sodium and potassium ion channels, display robust, consistent differences between the surgical treatment conditions (e.g. adrenergic, serotonergic, and gabaergic pathways, cf. Table 5A.1).

5A.4.1.2: Metabolism

Interestingly, whereas no glutamate receptors were found to be differentially regulated, several transcripts suggest a disturbance in glutamate functions. Enzymes involved in the metabolism of glutamate itself and of molecules involved in glutamate function were found to be affected as a result of the anterior thalamic nuclei lesion. Higher levels in the Lesion condition of glutamine synthetase, glutaminase, and asparagine synthetase suggest an alteration in glutamate metabolism and homeostasis, including glutamate-glutamine cycling. As shown in Figures 5A.10 and 5A.11, glutamate is converted to glutamine by glutamine synthetase, a glial-specific enzyme (Norenberg and Martinez-Hernandez, 1979), and as such, the disparity between the surgical conditions may reflect differences in glutamate signaling and in neuron-glia interaction (cf. Hertz and Zielke, 2004; Patel et al., 2005). Given the fact that glutamate is a GABA precursor, it could be expected that levels of GABAergic synthesis would also be altered, but there is no such indication in our results. However, higher expression of GABA subunit delta transcripts and of ubiquilin (a mediator of GABA receptor subunit composition, cf. Bedford et al., 2001), suggests that trafficking, although not synthesis of GABA may be altered.

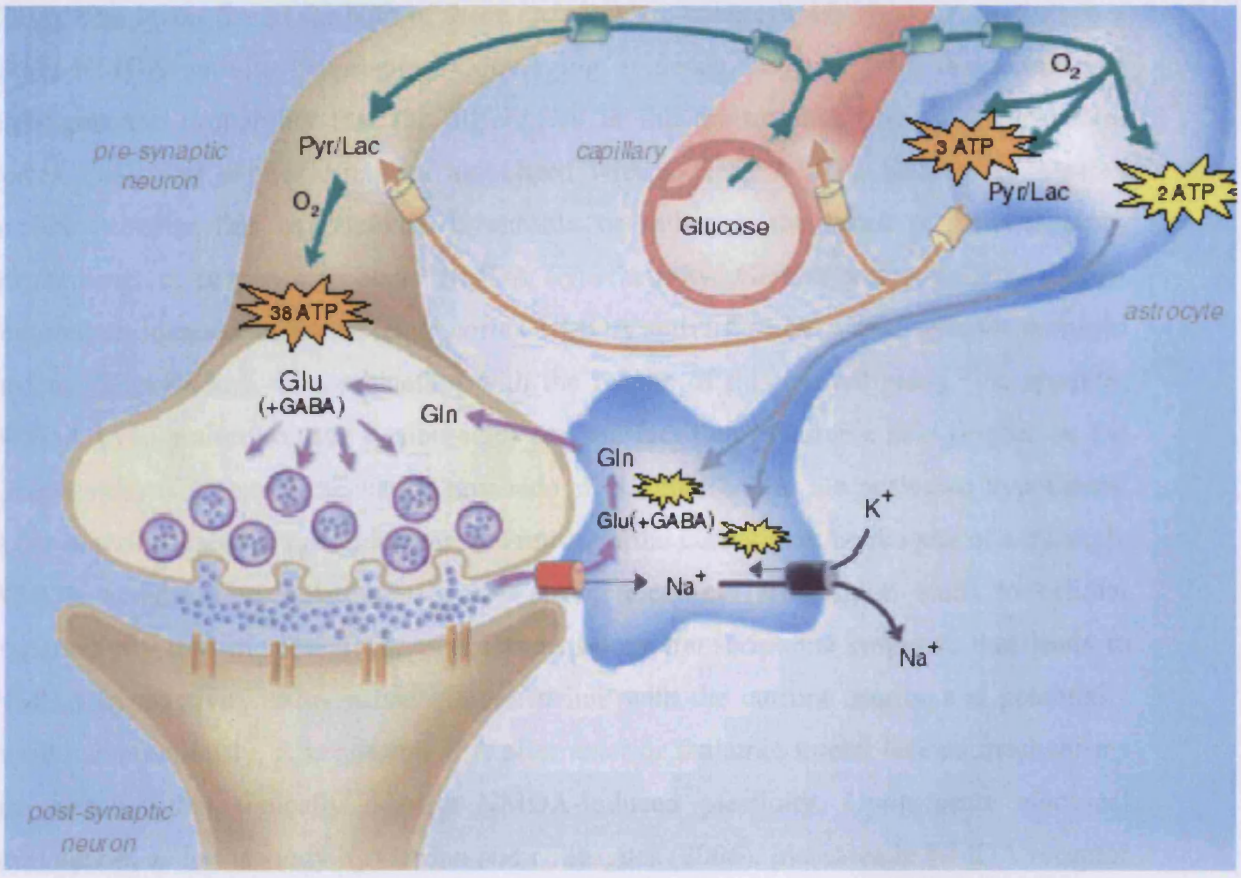

Figure 5A.10: Coupling between synaptic activity and glucose metabolism via interaction of neurons and astrocytes (taken from Hyder et al., 2006). Gln= glutamine, Glu=glutamate.

Further evidence of perturbations in glutamate function arises from apparent alterations in kynurenine metabolism. In our study, the balance of kynurenine metabolism appears to be different in the two surgical conditions, based on the fact that the transcripts for cyclooxygenase 1 (COX1) and kynurenine 3-monooxygenase (KMO), two enzymes associated with the metabolites of this pathway, are found to be at higher levels on the lesion side. The endpoints of kynurenine metabolism are kynurenic acid and quinolinic acid (Moroni, 1999). Kynurenic acid, a neuroprotective molecule, and quinolinic acid are respectively antagonists and agonists of NMDA receptor subtypes. Reduced levels of KMO produce an increase in kynurenic acid (Carpenedo et al., 2002; Erhardt and Engberg, 2002). COX1 has been reported to be associated with NMDA activity and the modulation of kynurenic acid levels. NMDA activation increases levels of this enzyme (Pepicelli et al., 2005), and similarly, COX1 reduction increases kynurenic acid levels (Schwieler et al.,

2005). The levels found for both of these enzymes are coherent, and this again points to a likely NMDA activity disturbance. Converging evidence from our microarray analyses highlights the probability that the differences in the transcriptome of the retrosplenial cortex ipsilateral to the lesion are associated with reduced NMDA activity. It remains unclear whether this hypoactivity is chronic or rather is the result of compensatory mechanisms in response to acute NMDA hyperactivity. Garden and colleagues (2006) reported an increase in retrosplenial cortex NMDA activity *in vitro* after anterior thalamic lesions. This finding, in combination with the results of this current study (i.e. apparent NMDA hypo-activity on the Lesion side) and the fact that kynurenic acid (higher on the Lesion side) is a neuroprotectant (Carpenedo et al., 2002), lead me posit two hypotheses. After anterior thalamic nuclei lesions, the retrosplenial cortex may be the site of a dynamic NMDA activity dysregulation, whereby strong electrical stimulation leads to cellular hyperactivity that in turn produces a compensatory transcriptome response that leads to NMDA hypoactivity. Alternatively, more in line with the current results, and potentially more parsimoniously, it is possible that after anterior thalamic nuclei lesions mechanisms are effected that tonically depress NMDA-induced plasticity. Upon acute electrical stimulation, as in the study by Garden and colleagues (2006), increases in NMDA receptor activity may attempt to compensate for the deficient cellular signal integration. Further work will be necessary to test these hypotheses. An additional effect that may underscore NMDA activity disturbances will be discussed later (cf. c-*fos* mRNA and Fos protein discrepancy, section 5A.4.1.7).

The proposed NMDA hypoactivity is coherent with the activity levels of other metabolic enzymes. NMDA receptor antagonism leads to increases in glutamine synthetase and in extended tricarboxylic acid cycling (Brenner et al., 2005). On the Lesion side, the enhanced expression of gene transcripts for malate dehydrogenase and succinate dehydrogenase suggests increased activity of the tricarboxylic acid cycle. Altogether, while this evaluation of the molecular activity patterns exhibited by both conditions points heavily towards a NMDA signalling dysregulation, I should also point out the potential alterations in other neurotransmitters. Given the fact that GABA is metabolised from glutamine (see Figure 5A.11), it is also plausible that GABA signalling is altered, as indicated by the greater abundance of transcripts for the GABA(A) delta receptor on the Lesion side. GABAergic signalling may play an important role in the apparent hypoactivity of the granular b

retrosplenial cortex, potentially being associated with the apparent reduction in NMDA activity. Additionally, as shown in Table 5A.1, serotonergic and adrenergic signalling also appears to be altered.

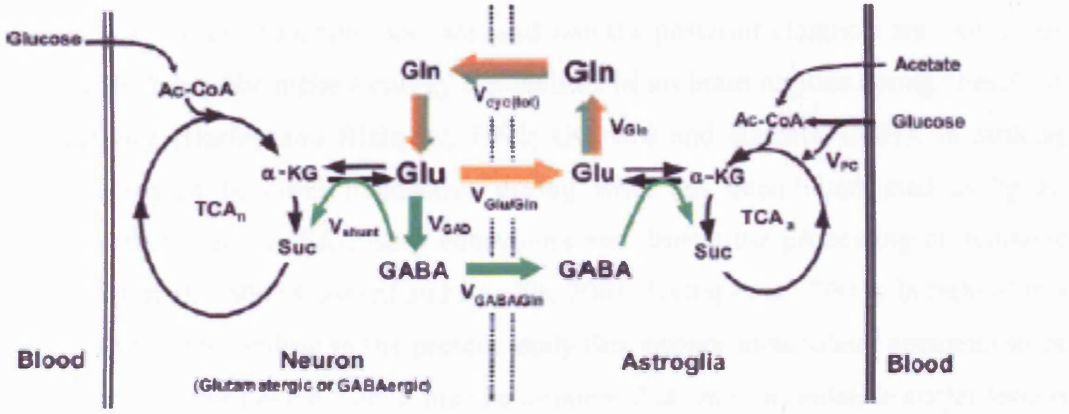

Figure 5A.11: Metabolism of glutamate and GABA in neurons and astroglia (taken from Patel et al., 2005).

5A.4.1.2.1: Energy metabolism alterations and potential oxidative stress

Mitochondria appear to have been affected by the surgical treatment, consistently at the three time points sampled. Pervasive alterations were found in the function of this organelle, transcripts exhibiting altered expression patterns in most mitochondrial compartments. Enzymes and other components of energy metabolism pathways were found to be differentially regulated, almost exclusively higher in the Lesion condition (cf. Table 5A.1). Coenzyme Q9 was also found to be elevated in the Lesion relative to the Sham condition, and it also is correlated with the presence of reactive oxygen species (Lass et al., 1997). Energy metabolism in itself can have an effect on neuroplasticity (Vaynman et al., 2006). Changes in transcripts reported to play a role in neuroplasticity will be discussed later.

In addition to these changes in energy metabolism, we also found changes suggestive of blood and oxygen activity disturbances. In the Lesion condition, we found elevated levels of genes that are known to be associated with haemoglobin oxygen transport (Hba1, Urod). Additionally, the aforementioned COX1 change may be associated with oxygenation and energy as COX1 knockout mice exhibit reduced blood flow (Iadecola et al., 2001).

The retrosplenial cortex in humans and rats (and also the posterior cingulate and precuneus in the former) exhibits the highest energy expenditure of all brain regions during "basal" or "resting" activity (Harley and Bielajew, 1992; Gusnard and Raichle, 2001). In striking contrast, this region becomes hypoactive during what has been interpreted as "goal-directed", or other than "self-focused" behaviours and during the processing of semantic tasks (Shulman et al., 1997; Gusnard and Raichle, 2001; Lustig et al., 2003). In light of this observation and of the finding in the present study that energy metabolism appeared to be relatively higher on the Lesion side, it may be possible that anterior thalamic nuclei lesions could not simply lead to retrosplenial cortex hypo-function, but rather to inappropriate function, where it could potentially be active in inappropriate instances. In other words, the retrosplenial could be dysfunctional by displaying incorrect activity patterns rather than just being inactive.

Mitochondria play an important role in oxidative phosphorylation, and also the glutamine-glutamate cycle, and their altered activity levels may be related to the disturbance in this system. Alternatively, the observed mitochondrial alterations may be a function of oxidative stress. Reactive oxygen species are mainly derived from the mitochondrion. Numerous mitochondrial genes find their expression levels to be higher on the Lesion than the Sham side. This clearly suggests the presence of altered metabolism function in retrosplenial cortex, a consequence of anterior thalamic lesions. A striking finding is the relative upregulation of the transcript for the mitochondrial ribosome Death-associated protein 3. This molecule is reported to be involved in fragmentation of mitochondria and also positive mediation of apoptosis (Kimchi, 1999; Koc et al., 2001; Mukamel and Kimchi, 2004).

In addition to the mitochondrial alterations, other oxidative mechanisms appear to be more active on the lesion side of the retrosplenial cortex. Oxidation due to metal-related

functions could be involved, and we found several transcripts that could be involved in such activity. Murr1 has recently been linked to copper metabolism, more precisely copper excretion. Murr1 has been negatively correlated with cytoplasm copper content (Burstein et al., 2004). Similarly, mutation of this gene has been reported to be associated with copper toxicosis (Tao et al., 2003). Another candidate for metabolic disruption is pantothenate kinase 4. Pantothenate kinase is necessary for the production of coenzyme A, itself very important for, amongst others, metabolic functions. Pantothenate kinase plays a role in the regulation of iron pathways; mutation of this gene has also been associated with iron deposition and neurodegeneration (Thomas and Jankovic, 2004). Urod, a gene involved in the heme biosynthesis pathway is also found at higher levels on the Lesion side. Auclair and colleagues (2006) have reported that mild iron deficiency-induced anaemia resulted in increases in Urod. Selenoprotein M, also higher in the Lesion condition, is another gene suggesting that there may be trace metal level alterations. Selenium is thought to have anti-oxidant properties and in a recent review it was emphasized that altered levels of this trace metal were found in several neurodegenerative disorders (Chen and Berry, 2003). This gene has also been found to be differentially regulated between mice overexpressing human presenilin-2 and their wild-type littermates (Hwang et al., 2005). Trace metals have been found to be increased in neurodegenerative disorders, and it is believed by some that at the core of Alzheimer-like neurodegeneration lies mitochondrial alterations and oxidative stress processes (Roloff and Platt, 1999).

5A.4.1.3: Neuroplasticity

Transcripts that have been shown to play a role in neuroplasticity are found in greater abundance on the Lesion side. For example, several genes found to be differentially regulated in this study have also been reported to be involved in enhanced NMDA receptor activity (Adcyap1), and long term potentiation (LTP; Adcyap1, Camk2g, NCS-1, LRP3, PPP1r1a), or long term depression (LTD; Map2k2, Prkar1b). Additionally, RXRγ levels were found to be highest in retrosplenial cortex contralateral to the lesion. This gene has been reported to be involved in LTD, but not LTP (Chiang et al., 1998). MHC class genes have been reported to be involved in neuroplasticity. Null MHC class I transgenic mice are reported to exhibit a LTD failure (Huh et al., 2000).

Neuroplasticity alterations at the molecular level would be coherent with recent findings of electrophysiological plasticity deficits in retrosplenial cortex after anterior thalamic nuclei lesions. Briefly, recent work by Garden and colleagues (2006) evaluated the effect of anterior thalamic nuclei lesions on single unit recordings in retrosplenial cortex. Recordings were taken in retrosplenial cortex layer II pyramidal neurons after stimulation in layer II or V. In unilateral preparations, LTD could be induced in both layers in the Sham but not layer II in the Lesion hemisphere. This electrophysiological finding provides further evidence for the unresponsiveness of superficial layers in the retrosplenial cortex after anterior thalamic nuclei lesions.

5A.4.1.4: Inflammation and immune-related responses

The presence of genes involved in immunity or inflammation in our study (e.g. CD74, CD83, Cysltl, Hla-dmb, LOC171412, Maspl, Ppib, RTl.B beta 1, RTl-Da, Tore) may be related to denervation, oxidative stress, or dysregulation of these functions. The majority of these genes were found to be increased on the sham side. Different research groups have reported an increase in genes associated with immune responses, including major histocompatibility complex (MHC) genes, after denervation. For example, in deafferented tissue in the hippocampus after disconnection from entorhinal connections (Ying et al., 2004) and after medial forebrain bundle transection (Cho et al., 2006). Both anterograde and retrograde effects of denervation may be at play (e.g. Block et al., 2005).

5A.4.1.5: Re-innervation, cell proliferation and possible aberrant connections

Differential activation of several transcripts may reflect the activity in retrosplenial of events that could be involved in the remodelling of the dendrites and axonal sprouting of retrosplenial cortex neurons following denervation (e.g. MAP2, Nelf, Netrinl, Neuritinl, Plexinb2, Neurofilament heavy polypeptide, Myosin Ie and IXa, and LSAMP).

Reprimo is associated with cell cycle arrest. It is relatively higher on the Sham side. Likewise, so is *NFAT5*. This transcription factor is required for the optimisation of cell proliferation. Conversely, *cyclinD2*, *klf5*, *rbbp-5*, *staufen*, *neuroD1*, *Fbxo6b* and *adcyapl*

are amongst those transcripts that are found at a higher level on the Lesion side; they are associated with cell proliferation, differentiation and some also with neuritic processes. It is likely that these are related to reorganisation resulting from the denervation. There is, however, another explanation that can account for the expression of genes that are known to be involved in proliferation. Cell cycle re-entry is a phenomenon observed in some neurodegenerative disorders such as Alzheimer's disease. Disturbance of mitogenic pathways leads to increases in cell differentiation and proliferation proteins, as well as cytoskeletal and mitochondrial proteins (Arendt, 2000). It has become appreciated more recently that pathways activated during development can also be active in the adult organism. During this period, these mechanisms are believed to be involved in plasticity processes (Levenson and Sweatt, 2005; Schmetsdorf et al., 2005).

It remains to be determined whether the expression patterns discussed above are the result of cell proliferation processes following the deafferentation of the Lesion side, a pathological return to an earlier cellular developmental stage (i.e. cell-cycle re-entry), or even the reflection of pathology on the Sham side. However, there clearly is a striking difference in proliferative potential between both sides, even though recovery processes, including an *increase* in Fos protein, are thought to peak 3-10 days after injury return to baseline before one month (Nieto-Sampedro et al., 1982; Buytaert et al., 2001; Mingorance et al., 2005).

Any resulting aberrant connections that could be produced by new neurites may add to the dysfunction that could be caused by metabolic alterations. These could generate and also propagate disruptive activity and further compromise retrosplenial function and that of its efferents, as seen in the hippocampal formation after kainic acid treatment (e.g. Tauck and Nadler, 1985).

5A.4.1.6: Immediate-early genes and brain injury

Fos is the protein product of the immediate-early gene c-*fos*. It plays a central role in the regulation of gene activity induced by excitatory stimulation. Like c-*fos*, *zif268* (also known as Egr-1, krox24, Tis8, NGFI-A) is also an IEG that is involved in regulation of genes by excitatory stimuli (Chaudhuri, 1997; Herdegen and Leah, 1998; Hughes et al., 1999; Tischmeyer and Grimm, 1999; Platenik et al., 2000; Bozon et al., 2002; Hoffman and Lyo, 2002; Wu et al., 2004). Its expression pattern is also similar to that of c-*fos* (Zangenehpour and Chaudhuri, 2002).

The relationship between brain injury and these two IEGs is different. Axotomy is associated with more selective and persistent expression of immediate-early genes. After axotomy, c-Jun and weakly zif268, but not c-fos, are expressed in the axotomised neurons (Hughes et al., 1999). The induction of c-Jun is prolonged, it has been observed up to 100 days later (Brecht et al., 1995). This effect can be observed in neurons that neither regenerate nor undergo apoptosis. Transient c-Jun expression has been reported in neurons until they re-connect or undergo apoptosis. In a review of the literature, Hughes and colleagues (Hughes et al., 1999) suggest that apart from c-Jun, and to a lesser extent JunD, other IEGs do not play a role in axotomised neurons. These associations between certain immediate-early genes and injury appear to be in stark contrast to what is observed in our study. Here Zif268 is downregulated in the Sham treatment and *zif268* mRNA does not appear to be altered, nor are *c-jun* and *junD*. These expression patterns are not in accord with those expected for death-associated mechanisms and this is supported by the failure to observe cell death as visualised with a traditional Nissl stain.

More puzzling at first sight are the expression levels of Fos and *c-fos*. *c-fos* exhibits a higher expression level in the Lesion treatment, in striking opposition to the reduced expression that is observed at the protein level. While both prolonged *c-fos* and transient Fos expression have been associated with impending cell death in more natural contexts (e.g. (e.g Gonzalez-Martin et al., 1992; Smeyne et al., 1993), failure in our study to observe *c-Jun* alterations suggests that the increase in c-*fos* expression is not a reflection of cell death programs. The discrepancy of our findings between levels of c-*fos* mRNA and Fos protein will be further discussed below.

Whereas cell death mechanisms appear not to be involved, evidence from other studies concur with our findings of a metabolic alteration distal to the lesion site. In general, cellular activity is either at control levels or at least transiently increased after toxin infusion. Metabolic assay after entorhinal lesion revealed a 10-40% reduction in glucose utilisation, which in the dentate gyrus persisted up to three months—the last time point assessed (Beck et al., 1996). Similarly, widespread effects on nitric oxide synthase and Fos hypoactivity have been found after entorhinal (Liu et al., 2003) and perirhinal lesions (Glenn et al., 2005), respectively. Our results are in accord with such findings of a metabolic disturbance as well as hypo-reactivity of the IEG Fos with distal lesions.

5A.4.1.7: Dissociation between c-*fos* and Fos

The pattern of c-fos mRNA expression across time appears consistent with a previous report also examining the expression of this IEG across similar time points after 20-minute exposure to a (novel) open field (Kerr et al., 1996). However, the current experiment revealed a discrepancy between c-*fos* mRNA and Fos protein. While Fos protein expression is markedly reduced in retrosplenial tissue from the Lesion hemisphere (Jenkins et al., 2004), c-*fos* mRNA is actually found in greater abundance in this side, as revealed by both the microarray and QPCR analyses. Levels of mRNA decrease over the time in both conditions, but are constantly at a higher level on the lesion side compared to the sham side. This suggests activity-regulated transcription in both conditions. Other than the discrepancy between mRNA and protein on the Lesion side, a dissociation is also present on the Sham side. In the Sham condition, the pattern across time appears to be linear for mRNA and nonlinear for protein. Assuming no transcript modifications, this precludes a role for transcription in the patterns observed.

The only difference in protein levels appears to be in the superficial layer of the Lesion condition. The reduction in Fos protein is especially evident in the superficial layers of the retrosplenial cortex, where the protein appears to non-responsive, whilst in contrast the deeper layers exhibit an expression pattern that is not different from the Sham condition. Thus, any difference in mRNA may be attributable to changes occurring in the superficial layers.

The induction of discrepant levels of mRNA and protein is a phenomenon that has been observed in various paradigms. It is seen in hippocampal slice work (Taubenfeld et al., 2002), after toxin exposure (Collombet et al., 2006), and in ischemia studies (Liu et al., 2001; Liu, 2003). Several mechanisms are plausible, and these include regulation of mechanisms at epigenetic, transcription, translation, post-translational or protease levels.

It is important to bear in mind that the c-*fos* gene is negatively regulated. This negative feedback mechansim has been oberved under various guises, for example by the direct reduction of transcription by elevated protein levels. Examples of potential mechanisms include c-*fos* transrepression and superinduction, found by some (Chen and Allfrey, 1987; Rahmsdorf et al., 1987; Sassone-Corsi et al., 1988; Gutman et al., 1991; Edwards and Mahadevan, 1992) but not other researchers (Lee et al., 1988; Lin et al., 1992; Chen et al., 1995), or also by the sequestration of co-activators of the gene promoter elements (Cahill, 1997). It is plausible that the mechanisms responsible for the apparent uncoupling of c-*fos* mRNA and protein may be the product of dysregulated autoregulatory transrepression. Based on the results of the microarray analyses, various mechanisms will be further discussed below.

5A.4.1.7.1: Epigenetic and transcription mechanisms

The expression of the c-*fos* gene can be dictated by histone modifications, including acetylation (cf. review by Sng et al., 2004). Acetylation as a mechanism involved in the observed difference in transcription is plausible, and may be mediated by Ruvbl1, a gene playing a role in the histone acetyltransferase complex, which is also found at higher levels in Lesion condition tissue. Alternatively, the observed difference may be the product of mRNA splicing changes (assuming the primary antibody and the sequence used for the microarray hybridisation are not splice-specific). The unspliced form of c-*fos* mRNA cannot be translated because it includes an intron with a stop codon (Shur, 2005). Inhibition of protein phosphatases increases the level of the unspliced form of c-*fos* mRNA (Feng et al., 2001). Further tests could verify the relevance of the observed difference in our study of spliceosome-related genes (Sf3a3 and U2AF1L1) and of protein phosphatase inhibitor subunits A and C for the role of c-*fos* splicing in the observed mRNA/protein discrepancy.

Additionally, effects that could lead to protein differences include the consequences of oxidative processes. Researchers studying ischemia have reported that as a result of oxidative processes following reperfusion, there is a transient yet important increase in the proportion of faulty transcripts produced. mRNA has been found to be capable of being transcribed despite an oxidative DNA lesion, but the faulty c-*fos* mRNA produced does not yield Fos protein, and subsequently cannot heterodimerize with Jun to activate the AP-1 transcription factor and its target genes (Liu et al., 2001; Liu, 2003). Evidence for DNA problems may be suggested by the increased expression on the Lesion side of replication factors A3 and C2, both reported to be involved in DNA mismatch repair (Kolodner and Marsischky, 1999). It is plausible that the increase in mRNA levels in the Lesion condition may be the product of extended transcription or maybe reduced transcription attenuation.

5A.4.1.7.2: Reduced or faulty translation with antigen changes

Alternatively, another mechanism has been proposed to explain a reduction in protein levels where the problems occur at the level of the protein, not the mRNA. An effect at the translational level could simply be reduced translation, or the result of faulty translation, therefore yielding a protein product in a form that is no longer recognised by the antibody used. In terms of translation, transcripts related to this function are again all found to be at a higher level in the Lesion condition (cf. Table 5A.1). We cannot ascertain though whether these are induced because of higher translation or in attempt to boost attenuated translation. Regarding the possibility of faulty translation, there are precedents. For example, after ischemia protein aggregation has been observed, resulting in irreversible inhibition of protein synthesis in that cell population (e.g. Liu et al., 2005). This protein aggregation occurs because of problems with protein quality control after depletion of ATP associated with ischemia. The protein synthesis and degradation machinery aggregate, resulting in molecular dysfunction. Protein synthesis inhibition after ischemia is considered a hallmark of delayed neuronal death. Additionally, after ischemia metabolic levels and ionic homeostasis recover in the affected cells, until they eventually die. Given the failure to observe neuronal cell death and the existence of metabolic dysregulation in our study, it seems doubtful that irreversible protein synthesis inhibition is the reason for the observed effects. However, a hypothetical loss of antigenicity remains plausible.

5A.4.1.7.3: Antigen changes

A loss of protein antigenicity has been reported after ischemia and toxin exposure (respectively Unal-Cevik et al., 2004; Collombet et al., 2006). The latter authors have contended that masking of the antigen sites was more likely than their alteration. They propose heat shock proteins as likely candidates responsible for this masking. Such an effect is again plausible in our study, where we find members of the heat shock protein family to be at higher levels in the Lesion condition (Dnajc8 and Hspa11). Members of this family are known to associate with denatured proteins (c.f. Sharp et al., 1999). This could suggest that after ATN lesions Fos protein is not being synthesised properly in retrosplenial cortex, or even is being produced but because it is aggregated, or even damaged, the antibody used for immunohistochemical analysis cannot bind to its epitope. A potential loss of antigenicity could be tested by verifying Fos levels using Western blots. Further post-translational mechanisms will be discussed later.

5A.4.1.7.4: Proteolysis

Alternatively, increased proteolytic pathways could be enhanced on the Lesion side, maximising Fos protein degradation and dramatically reducing the extent and duration of protein elevation. It has been shown that Fos can be degraded by the proteasome and the ubiquitin systems, and by lysosomes (cf. review by Jariel-Encontre et al., 1997). Members of these systems have all been found to be exclusively elevated in the Lesion condition. The proteasome is involved, in association with 26S ribosomal proteins (Wang et al., 1996) and for example, we found the psmd3 transcript, for a 26S ribosomal protein (but also psmf1, a 20S ribosomal protein, proteasome inhibitor). In association with the ubiquitin system, we found uba52, usp3, fbxo6b. Finally, lysosome-related genes were also found: hyal2 and potentially lsamp. It plausible that such mechanisms related to these systems are more active in the Lesion condition, but more research is necessary to verify this hypothesis.

5A.4.1.7.5: Potential implication of phosphorylation

In Lesion condition tissue, genes that are part of the protein kinase complex are found at higher levels (camk2g, camkk1, map2k2, mapk6, MAP2K1IP1, prkar1b, prkcdbp. There is also higher expression in that condition of Ppp1r1a and Ppp1r1c, protein phosphatase inhibitors.

Phosphorylation can modulate Fos expression on a number of levels, including its transcription, translation and degradation (Ofir et al., 1990; Atadja et al., 1994; Tsurumi et al., 1995; Takeuchi et al., 2001; Coronella-Wood et al., 2004) Tsurumi et al., 1995). However, evidence for the existence of differential post-translational modifications of Fos in tissue from the present study appears to be absent when assayed with a Western blot (Poirier et al., 2004).

5A.4.1.7.6: Potential role of NMDA receptors

NMDA receptor blockade has been reported to reduce Fos protein levels (Sharp et al., 1993; Hasegawa et al., 1998). Studying the effect of NMDA antagonism on Fos expression, Sharp and colleagues found that blockade of NMDA receptors specifically prevented induction of Fos-like protein but did not prevent induction of mRNA—the receptor blockade having no effect on overall protein synthesis. If NMDA receptors are needed for Fos induction, this suggests that their dysregulation could result in a deficit in Fos protein production. Lesions produced using NMDA are the consequence of excitoxic mechanisms, the cells firing until they die. Given the strong connections between the ATN and the retrosplenial cortex, it may be that retrosplenial cells suffer chronic, non-degenerative injury as a result of ATN lesions. In the current study, a role for NMDA receptors in the observed mRNA and protein uncoupling is further supported by the glutamate homeostasis alteration discussed previously.

NMDA receptor modulation is mediated by kinesin-related proteins that have a role in the movement of the receptors (e.g. Yuen et al., 2005). A variety of these proteins have a known role in neurotransmitter receptor movement. An example is *kif6/kinesin-related protein 3*, which was found to be at a higher level on the sham side. The finding that this and other microtubule and movement-related genes are found to be differentially expressed

after anterior thalamic nuclei damage, in conjunction with a potential NMDA hypoactivity, may be a reflection of NMDA receptor dysregulation. Further studies are needed to address this, but electrophysiological results appear to confirm a role for NMDA receptors in the deficient retrosplenial cortex plasticity after anterior thalamic nuclei lesions (Garden et al., 2006). Garden and colleagues found NMDA receptor activity to be greater in retrosplenial cortex ipsilateral to ATN lesions. In light of the reported disturbances in anterior thalamic nuclei and retrosplenial cortex in Alzheimer's Disease and schizophrenia, such a finding would be consistent with the proposal (Farber et al., 2002) for the role of NMDA receptor dysregulation in the dysfunction of both of these brain regions in both of these disorders.

Further studies are required to elucidate the observed c-*fos* protein and mRNA discrepancy. Different techniques will be necessary to tackle this problem. *In situ* hybridisation could reveal with precision the localisation of the alterations, and confirm the laminae affected. It is possible that superficial layers exhibit a reduction that is counterbalanced by overexpression in deeper layers. This is, however, unlikely based on the fact that deeper layers do not exhibit increased immunoreactivity. Analyses using Western blots would confirm or disconfirm the effect using this technology, informing us on the nature of the effect. The capacity of superficial layer cells in retrosplenial cortex to synthesise protein could be evaluated. For example, electrical stimulation could be used to induce Fos, in superficial retrosplenial layers (e.g. Knyihar-Csillik et al., 2005). Likewise, the presence of protein products of genes that are increased on the Lesion side could be verified.

5A.4.2: Conclusions

Anterior thalamic nuclei lesions induce widespread alterations in cellular function of the retrosplenial cortex. Future work could pursue the analysis of the effects of anterior thalamic lesions on retrosplenial cortex to determine whether it is possible that the observed transcriptome may in fact be a reflection of oxidative stress. Such studies could provide more evidence for a role of retrosplenial deafferentation in memory deficits and the instigation of Alzheimer-like neurodegenerative processes. Regulatory sequence analyses of the promoter sequences of the genes found to be differentially expressed in this study could pinpoint the role of one or a select group of transcription factors.

Overall, some of the recurrent associations of the altered transcripts are with functions of metabolism, genetic information processing, and signal transduction. Future studies are necessary to better understand the interaction of the anterior thalamic nuclei and of the retrosplenial cortex, and the role of these two regions that are critical to cognitive functions and to the development of Alzheimer's disease.

A better characterisation of this retrosplenial dysfunction would further our understanding of distal effects of insults to the brain, and may provide paths to diminish the sequelae in dysfunctional regions that do not exhibit overt pathology.

5B.1: Introduction

The high-throughput nature of microarray studies and the associated statistical analyses has prompted several commentators to recommend the use of replication and subsequently to append independent methods to substantiate any findings (e.g. Murphy, 2002; Nisenbaum, 2002). As a reminder, the design of the microarray experiment presented above consisted of two surgical conditions and three time conditions. The tissue from the two surgical conditions was obtained from the same subject, thus minimising unspecific gene expression variability due to factors other than the surgical treatment. Each "cell" consisted of the pooled tissue from two subjects, such that outliers were less likely to skew the results. The predictive patterning approach essentially treated each of the three time points as replicates. This analysis yielded a list of genes that exhibited a consistent relative expression level across each time point. Furthermore, the experiment was duplicated, and the data were analysed together, taking into account variation in gene expression between the duplicates. Thus, overall, transcripts that were deemed to be differentially different between the 'Intact' and the Lesion condition were identified on the basis of findings that were obtained six times, via the same technology.

The results of the microarray analyses described above were followed up by confirmatory experiments, which included both alternative technical means and independent tissue samples. A technological verification was conducted using material from the same subjects as the microarray experiment. Quantitative real-time RT-PCR was then used to test the expression levels of some candidate genes. The details and the results of this analysis have been presented by Shires (2006), and those data have been used to compare the expression levels previously found by microarray techniques (see Figure 5B.1). The results of the quantitative RT-PCR analyses overall validated the findings produced by the microarray analyses. The only exception appeared to occur at 30 min for *zyxin*. Thus, the validation by technological replication of the relative expression levels was congruent for 26 out of 27 conditions (i.e. 9 genes x 3 time points). It should be noted that c-*fos* was included because of the strong effect observed for the protein product of this gene.

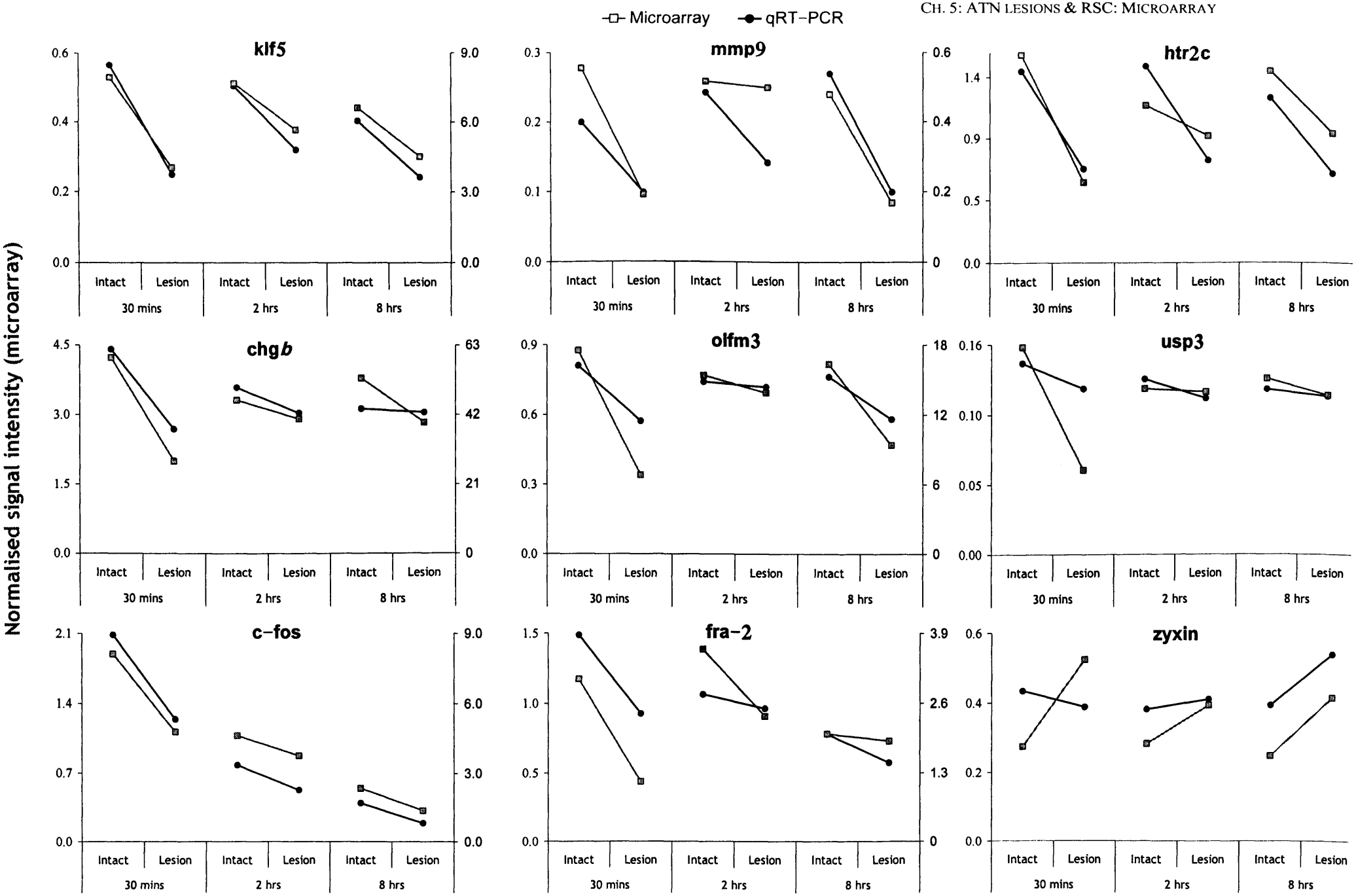

Figure 5B.1: Comparison of the expression levels of candidate genes obtained two different techniques. Each graph has two y-axes, one for the microarray results on the left, and another for the quantitative RT-PCR results on the right.

A second verification, *in situ* hybridisation, has been used to examine three candidate genes using. This approach provides much greater spatial resolution of the changes found in the retrosplenial cortex. Importantly, *in situ* hybridisation was used on independent tissue, thus providing both a technological validation and a biological replication. Results for the genes *htr2c*, *gabrd*, and c-*fos* are depicted in Figure 5B.2.

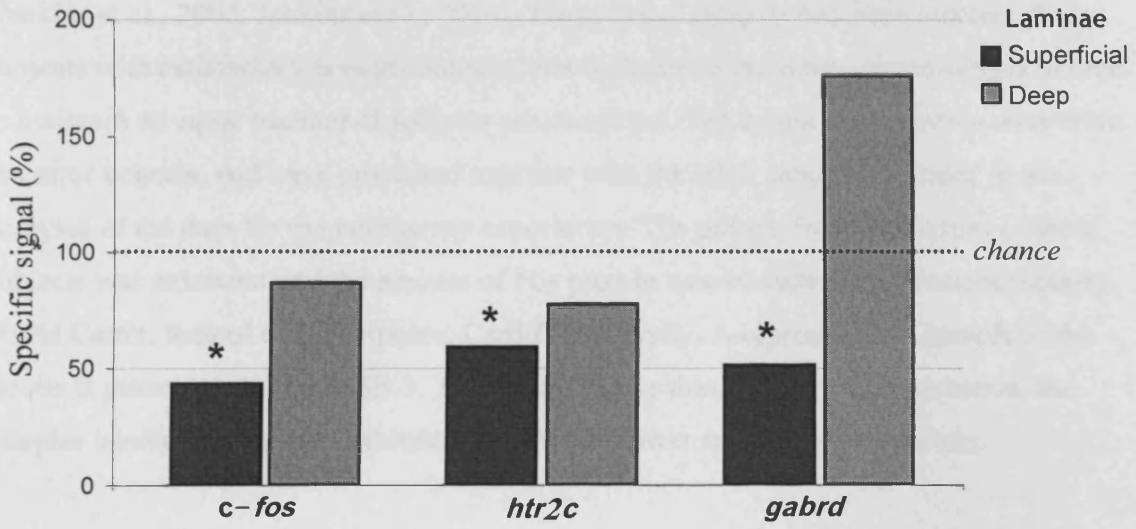

Figure 5B.2: The results of the *in situ hybridisation* experiment for c-*fos*, *htr2c*, and *gabrd* are presented as the specific signal found in the Lesion condition as a percentage of the 'Intact' condition. *≤ 0.05.

A paired-sample t-test (two-tailed) on the grain counts revealed significant reductions in the superficial laminae for *htr2c*, *gabrd*, and c-*fos* (respectively ($t=4.1$, $p<0.05$; $t=3.9$, $p=0.05$; and $t=2.4$, $p<0.05$). No significant differences are apparent in lamina V for either *htr2c*, *gabrd*, or c-*fos* (respectively ($t=0.7$, $p>0.05$; $t=-1.3$, $p>0.05$; and $t=0.9$, $p>0.05$).

The results of the *in situ hybridisation* experiment for *htr2c*, *gabrd*, and c-*fos* were inconsistent with the results of the microarray and the qRT-PCR analyses. Most obvious was the inconsistency in the c-Fos data as the microarray and qRT-PCR analyses showed

higher mRNA levels on the lesion side yet the *in situ* findings were the opposite i.e. lower mRNA on the lesion side. This inconsistency suggested a potential problem with the data.

In order to resolve this apparent contradiction, I took advantage of the remaining tissue samples that had not been used for the microarray analyses. The rationale was as follows: the identity of the surgical treatment condition of the samples could be ascertained by testing the amount of Fos protein, which was known to be reduced in the Lesion condition (Jenkins et al., 2002; Jenkins et al., 2004). These tissue samples had been obtained from subjects with satisfactory lesions, but were not included in the microarray analyses in order to maintain an equal number of subjects per condition. The subjects in question were from the same cohorts, and were processed together with the other subjects included in the analyses of the data for the microarray experiment. The protein from the tissues of these subjects was extracted and the amount of Fos protein was evaluated via Western blots by David Carter, School of Biosciences, Cardiff University. A representative sample of the results is presented in Figure 5B.3. This figure shows that, contrary to expectation, the samples labelled as "Intact" exhibited a relatively lower amount of Fos protein.

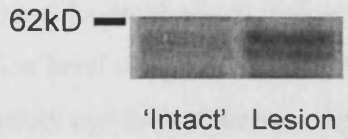

Figure 5B.3: Representative Western blot of Fos protein from a subject in the 30 min post-novel environment exposure group.

It thus became apparent that an inversion in the labels of the surgical conditions of the samples had probably occurred. Based on the following converging evidence, it was reasoned that a systematic error had yielded inverted results for the microarray and the qRT-PCR analyses—which stem from the same samples.

1) The inverted results of the Western blot;
2) The contradiction between both the microarray and the qRT-PCR results and the *in situ* results for c-*fos*, *htr2c* and *gabr*.

Thus it seems highly likely that a systematic error occurred in the manipulation or labelling of the tissue samples that were used both for the microarray and the qRT-PCR analyses. Because of the biological replication within the microarray experiment, and the fact that the three time points were treated essentially as replicates for the predictive patterning analyses, only consistent gene changes could have been detected. Unsystematic errors would have led to increased noise, but not a complete inversion of the findings across two methodologies.

In light of this information, which highlighted an inversion in the attributed condition of the samples obtained for the microarray and qPCR analyses, the results of the microarray experiment were rectified, and will be re-evaluated below. Taking into account a likely systematic inversion of the conditions in the microarray experiment, the ensuing rectification yielded more coherent results on two fronts. First, there now is no apparent discrepancy between the relative levels of the c-*fos* mRNA and protein levels, a more standard result. Second, the results, as discussed below, are now more consistent with the findings of Garden et al. (2006). These more coherent findings support the accuracy of the current interpretation of the microarray data, and the validity of the decision to re-visit the data and invert the findings. It must be emphasised that any inversion, if systematic, can only affect the relative expression level of the genes found to have been affected by the surgical treatment, not their identity nor their statistical significance. In other words, regardless of the inversion of the data, the exact same gene transcripts and the same cellular functions of these as a whole appear to be affected in the retrosplenial cortex following anterior thalamic nuclei lesions. The next section presents the results of the microarray experiment in their correct form, and is followed by a new discussion of these results. Only those results that now differ will be presented. The pie charts presented earlier with relation to the functions and the cellular compartments associated with the list of genes remain intact, and will thus not be presented. Table 5B.1 presents the rectified expression patterns of the list of genes, while Figure 5B.4 shows the same sets of genes grouped by expression patterns, but not with the opposite pattern for the 'Intact' and the Lesion conditions.

Table 5B.1: List of genes that were found to be consistently at different levels in the 'Intact' and the Lesion retrosplenial cortex hemispheres, grouped by expression pattern sets. *For EST similarity, the value on the left is the similarity score, and the value on the right is the E-value. (S = Sham, L = Lesion)

Cluster	Direction	Function Classification	Name	Synonym	EST similarity, if applicable *	Genbank
1	S>L	**Immune system**	Glucocorticoid induced transcript 1 (Glcci1)	Gig 18, Tssn1	1203 0.0	BE108162
		unclassified	Secretory carrier embrane protein 1 (Scamp1)			BM386698
		unclassified	Protein phosphatase 1, regulatory (inhibitor) subunit 1c (Ppp1r1c)		801 0.0	AA943808
		unclassified	Disabled homolog 2 (Drosophila) interacting protein (Dab2ip)	DIP1/2		AF236130
		unclassified	Protein kinase, cAMP dependent regulatory, type 1 beta (Prkar1b) R1beta			BG375376
		GTP-binding proteins/Cell Comm>TightJunctio n	RAB11 family interacting protein 5 (RAB11FIP5)	Gamma-SNAP-associated factor 1 (GAF1), pp75, RIP11, KIAA0857, DKFZP434H018, D6Ertd32e	505 6e-140	BI296378
		Ion channels	Potassium voltage-gated channel, delayed rectifier, subfamily S, 1 (kcns1)	Voltage-gated potassium channel subunit Kv9.1		NM_053954
		Transcription	Bromodomain containing 8 (Brd8)	Small acidic protein (Smap), thyroid receptor coactivating protein, p120		AI549477
		Transcription	Kruppel-like factor 5 (intestinal) (Klf5)	IKLF, BTEB-2		NM_053394
		Translation	Ribosomal 60S protein l15 (Rpl15)	EC45, RPYL10		AA800007
		Folding, Sorting and Degradation	Heat shock 70kD protein 1-like (Hspa1l)	LOC361797; Heat shock protein 70-3 (HSP70 - 3); HSP70-HOM; Major histocompatibility component complex 4-1 (C4-1)	561 8e-157	BG381414
		Folding, Sorting and Degradation	Mitochondria associated granulocyte macrophage CSF signaling molecule (Magmas)	CGI-136, TIM16		BG379323
		Replication and repair	Replication protein A3 (Rpa3)		720 0.0	BM383451
		Carbohydrate metabolism	Malate dehydrogenase, mitochondrial (Mdh2)	Mor1		NM_031151
		ATP synthesis	ATP synthase, H+ transporting, mitochondrial F1 complex, O subunit (Atp5o)			D13127
		Nitrogen metabolism	glutamate-ammonia ligase (Glul)	Glutamine synthase		AW528806
		Metabolism of cofactors and vitamins	Uroporphyrinogen decarboxylase (Urod)	hemE		Y00350
2	S>L	**Cell growth**	Kelch domain containing 3 (Klhdc3)/ Protein	Peas for klhdc3	(confirmed)	AA894104

			phosphatase 2a regulatory b56-delta subunit (Ppp2r5d)/Male-enhanced antigen-1 (Mea1), [OVERLAPPING GENES]		662 0.0	
		Development	Neuritin 1 (Nrn1)	Nrn		NM_053346
		unclassified	Synaptotagmin 5 (Syt5)			NM_019350
		unclassified	Calcium/calmodulin-dependent protein kinase (CaM kinase) II gamma (Camk2g)			NM_133605
		unclassified	N-ethylmaleimide sensitive fusion protein attachment protein alpha (Napa)	SNAPA		NM_080585
		GTP-binding proteins/Cell Comm>TightJunctio n	Rab3B protein			NM_031091
		Transcription	Nuclear factor I/X (Nfix)	CTF, NF1A		BF420722
		Transcription	Single stranded DNA binding protein 3 (SSBP3)	SSDP, CSDP; FLJ10355		NM_053358
		Translation	DEAD (aspartate-glutamate-alanine-aspartate) box polypeptide 25 (Ddx25)	GRTH		NM_031630
		Translation	Deoxyhypusine synthase (DHS/Dhps/Dys1)			AA892493
		Folding, Sorting and Degradation	Down syndrome critical region homolog 2 (H. sapiens (Dscr2)	C21LRP, LRPC21, PAC1	803 0.0	BF407158
		Folding, Sorting and Degradation	F-box only protein 6b (Fbxo6b)	FBX6, FBG2,FBS2		AF393484
		Lipid Metabolism	Monoglyceride lipase (Mgll)			AI713204
		Oxidative phosphorylation	NADH dehydrogenase (Ndufa8)		1029 0.0	BI280270
		Unclassified	Small nuclear ribonucleoprotein associated protein N, upstream reading frame (SNURF)		60.0 9e-06	AI171982
		Unknown	SID1 transmembrane family, member 2 (sidt2)	CGI-40	942 0.0 (predicted); 474 1e-130	AI579643
3	S>L	**unclassified**	Phosphatidylinositol transfer protein (Pitpn)	VIB1A (Homo sapiens: PITPNA (Homologs)		NM_017231
		MAPK signaling	PTPL1-associated RhoGAP1 (Parg1)		490 3e-135	AI407483
		WNT signaling pathway	Groucho protein (GRG1)	DGPWD, Transducin-like enhancer of split 1 (Tle1)		BG380534
		Calcium signaling	5-HT2C receptor (5-HT2cR)	Htr1c	509 3e-141	BF285539
		Ion channels	Potassium voltage gated channel, shaker related subfamily, member 4 (kcna4)	KV1.4		NM_012971
		Cell adhesion molecules	Olfactomedin 3 (Olfm3)	Optimedin form B, NOE3		AF442822
		Transcription	Polymerase (RNA) III a (155kd) RPC155	BC053071; MGC62420	733 0.0	BI274108
		Translation	40S ribosomal protein S14 (RPS14)			NM_022672
		Translation	Mitochondrial ribosomal protein L4 isoform 2 (Mrpl4)	CGI-28		BI275903

		Folding, Sorting and Degradation	Ubiquitin specific protease 3 (Usp3)			AI411205
		Folding, Sorting and Degradation	Cyclophilin B (Ppib)			
		Oxidative phosphorylation	NADH dehydrogenase, mitochondrial 24-kDa subunit (Ndufv2)			M22756
		Vesicular transport-related	Adaptor-related protein complex 2, *mu* 1 subunit (Ap2m1)	Clathrin coat assembly protein AP50; clathrin-associated/assembly/adaptor protein, medium 1 (CLAPM1)		NM_053837
4	S>L	**unclassified**	Protein phosphatase 1, regulatory (inhibitor) subunit 1A (Ppp1r1a)			NM_022676
		unclassified	Exostosin 1 (Ext1)			BM384468
		MAPK signaling	Regulator of G-protein signaling 4 (Rgs4)	RGP4		U27767
		Ion channels	GABA A receptor delta (Gabrd)			NM_017289
		Ion channels	Sodium channel, voltage-gated, type I, beta polypeptide (Scn1b)	GEFSP1		NM_017288
		Cell adhesion molecules	Syndecan-1 (Sdc1)	Syndecan 1 (Synd1), CD138 antigen, HSPG, Syndeca, CD138		NM_013026
		Folding, Sorting and Degradation	Proteasome (prosome, macropain) 26s non-ATPase subunit 3 (Psmd3)	26S Proteasome subunit p58, Psd3, AntP91a, Tstap91a, D11Bwg1349e		BI285842
		Lipid Metabolism	hypothetical protein MGC11324, Hypothetical phospholipid and glycerol acyltransferase		398 9e-108	AI599365
		ATP synthesis	ATPase, vacuolar, 14 kD (Atp6s14)	Atp6v1f, VATF, VMA7		NM_053884
		Unclassified	Host cell factor C1 regulator 1 (XPO1-dependent; HCFC1R1)	HPIP, FLJ20568, MGC70711		AA944494
5	S>L	**Development**	Plexin b2 (Plxnb2)			BG380275
		Immune System	CD83			AI412355
		MAPK signaling	Adrenergic receptor kinase, beta 1 (Adrbk1)	BARK1, GRK2		AI716801
		MAPK signaling	Mitogen-activated protein kinase 6 (Mapk6)	ERK3		NM_031622
		Transcription	nuclear receptor subfamily 4, group A, member 1 (NR4A1)	Nur77/NGFIB downstream protein 2		BI282332
		Translation	Ribosomal protein L23a (Rpl23a)	60S ribosomal protein L23a	(confirmed) 1003 0.0	AI172199
		Lipid Metabolism	Phosphatidic acid phosphatase type 2B (PPAP2B)	Endoplasmic reticulum transmembrane protein (Dri 42), Phosphatidic acid phosphohydrolase, Vascular endothelial growth factor and type I collagen inducible		Y07783
		Lipid Metabolism	Fatty acid Coenzyme A ligase, long chain 6 (Facl6)			NM_130739
		Unknown	KIAA1086		728 0.0	BI294610
6	S>L	**Cell growth**	Cyclin D2 (CCND2)	KIAK0002, MGC102758		BG380633
		Cell growth	PKC-delta binding protein (Prkcdbp)			NM_134449

		Transcription	U2(RNU2) small nuclear RNA auxillary factor 1-like 1 (U2AF1L1) [located in an intron of the Murr1 gene]	SP2, U2afi-rsi, U2AF1RS1, U2AFBPL		BF404554
		Translation	Staufen			NM_053436
		Folding, Sorting and Degradation	Proteasome [20S] (prosome,macropain) inhibitor subunit 1 (Psmf1)	PI31, MGC18784		BF561377
		Oxidative phosphorylation	NADH dehydrogenase (Ndufb6)			AI104528
		Cytoskeleton, microtubule and actin-related	Neurofilament, heavy polypeptide (Nefh)	Nfh		AF031879
7	S>L	**Cell communication**	Tubulin alpha 4 chain (alpha-tubulin 4)			BI284599
		Calcium signaling	Adenylate cyclase activating polypeptide 1 (Adcyap1)	PACAP		NM_016989
		Cell adhesion molecules	Limbic system-associated membrane protein (Lsamp)	LAMP-1, CD107a, LGP120		U31554
		Translation	Eukaryotic initiation factor 5 (eIF-5)			BE107346
		Folding, Sorting and Degradation	similar to similar to Protein C20orf22 homolog		908 0.0	BI284608
		Folding, Sorting and Degradation	Signal recognition particle 68kDa (Srp68)	MGC38208		BI296671
		Unknown	leucine rich repeat containing 57 (Lrrc57)		389 7e-105	BE101274
8	S>L	**MAPK signaling**	MAPKK Mitogen-activated protein kinase kinase 1 interacting protein 1 (MAP2K1IP1)	Mek binding partner 1 (Mp1), Mabp		AA817829
		Ion channels	Potassium voltage gated channel, Shaw-related subfamily, member 1 (kcnc1)	KV3.1; KV4		NM_012856
		Transcription	Splicing factor 3a, subunit 3 (Sf3a3)	SAP 61, SF3A60	1065 0.0	BM391739
		Oxidative phosphorylation	Cytochrome C oxidase- subunit Via polypeptide 1 (Cox6a1)			BI282326
		Amino acid metabolism	Asparagine synthetase (Asns)	Asparagine synthetase, Cell cycle control protein TS11, Glutamine- dependent asparagine synthetase		U07202
		Cytoskeleton, microtubule and actin-related	Microtubule-associated protein 2 (MAP2)	Mtap2		X74211
9	L>S	**Cell growth**	Mdm4, transformed 3T3 cell double minute 1, p53 binding protein (mouse) (mdm1)			BE099784
		Immune System	CD74	INVG34, LN2		NM_013069
		unclassified	transmembrane emp24 protein transport domain containing 4 (tmed4)	HNLF	204 2e-49	AI235294
		unclassified	Solute carrier organic anion transporter family, member 2B1 (SLCO2B1)	Solute carrier family 21 (organic anion transporter), member 9 (Slc21a9)		AF169410
		Transcription	Putative homeodomain transcription factor 2 (Phtf2)		295 8e-77	AI410924
		Folding, Sorting and Degradation	DEAH (Asp-Glu-Ala-His) box polypeptide 40 (DHX40)	ARG147, DDX40, PAD		AI178155
10	S>L	**Cell growth**	Retinoblastoma binding protein 5 (RBBP-5)	RBQ 3	396 3e-107	AA946518

		unclassified	G protein-coupled receptor 162 (GPR162)	Gene rich cluster, A gene (Grca); A-2		BM386619
		Ion channels	Calcium channel, voltage-dependent T-type, alpha 1I subunit (CACNA1I), transcript variant 2	Cav3.3	287 1e-74	BE105417
		Lipid Metabolism	CDP-diacylglycerol synthase (phosphatidate cytidylyltransferase) 1 (Cds1)			NM_031242
		Metabolism of cofactors and vitamins	coenzyme Q9 homolog		1068 0.0	AI232494
		Unknown	similar to and predicted: chromosome 20 open reading frame 116 (LOC296162)		601 6e-169	AI638949
11	S>L	**Development**	Nasal embryonic LHRH [luteinizing hormone-releasing hormone] factor (Nelf)	Jacob protein alternatively spliced isoform delta1 (jac gene)		AJ293698
		unclassified	Calcium/calmodulin-dependent protein kinase kinase 1, alpha (Camkk1)			NM_031662
		Ion channels	Transient receptor potential cation channel, subfamily V, member 5 (TRPV5)	Epithelial calcium channel 1 (Ecac1)		NM_053787
		Transcription	THAP domain containing 4 (Thap4)	CGI-36, PP238		BI275281
		Folding, Sorting and Degradation	Matrix metalloproteinase 24 (Mmp24)	Mt5-mmp	188 1e-44	BF285924
		Metabolism of cofactors and vitamins	Pantothenate kinase 4 (Pank4)			NM_133531
12	S>L	**Cytoskeleton, microtubule and actin-related**	Actin alpha-1 (Acta1)			NM_019212
		Vesicular transport-related	Frequenin homolg (Drosophila)	Neuronal calcium sensor 1 (NCS-1)		NM_024366
		Vesicular transport-related	Exocyst complex component 7 (Exoc7)	EXO70		BM388722
		Unknown	transmembrane protein 93; Vanilloid receptor subtype 1 (H. sapiens)	MGC2963	944 0.0; 507 1e-140	BI285673
		Unknown	Homo Sapiens Chromosome 9 open reading frame 25 (C9orf25)	FLJ39031, bA573M23.5	272 6e-70	BI298306
13	S>L	**Cell growth**	Nuclear distribution gene C homolog (Aspergillus; Nudc)	c15, Silg92		NM_017271
		Transcription	DNA-directed RNA polymerase II 7.6 kda polypeptide L (POL2RL)	RBP-10	476 3e-161	AA924509
		Unclassified	Selenoprotein M (Selm)	SepM, A230103K18, 1500040L08Rik		BI282694
		Unknown	Gene rich cluster C10 (Grcc10)	C10, C12orf57		BI282112
		Unknown	RGD1564450_predicted	LOC294291	793 0.0	AW915035
14	L>S	**Cell growth**	Reprimo (candidate mediator of the tp53-dependent G2 arrest)		672 0.0	BG381258
		Immune System	LOC171412	E-3 epididymal fluid protein, 2D6 glycoprotein; Defb22,		AF329091
		Folding, Sorting and Degradation	Apobec-1 complementation factor (Acf)	ACF64		NM_133400
		Unknown	Calpain10 (capn10); BDNF exon 5		176 6e-41; 172 1e-39	BI296532

		Unknown	EST			BI291373
15	L>S	**Transcription**	Neurogenic differentiation 1 (NeuroD1)	BETA2, BHF-1, Neurod		AI639109
		Oxidative phosphorylation	Cytochrome oxidase 6b1 (Cox6b1)		739 0.0	AI230604
		Metabolism	Kynurenine 3-monooxygenase (KMO)	Kynurenine 3-hydroxylase		NM_021593
		Vesicular transport-related	EH-domain containing 2 (Ehd-2)	MGEPS, PAst2, MGC25606, MGC38650		BE110691
		Unknown	Family with sequence similarity 26, member B	LOC294019, Hypothetical protein FLJ12133, 2810048G17Rik	1120 0.0	BM391099
unclassified	S>L	**Cell death**	Death associated protein 3 (DAP-3)	Mitochondrial 28S ribosomal protein S29 (MRP-S29)	831 0.0	BI285645
	S>L	**Cell death**	Tnf receptor-asociated factor 7 (Traf7)	MGC7807, RFWD 1	(confirmed) 682 0.0	BI287266
	L>S	**Cell communication**	*PREDICTED: Mus musculus angiomotin-like 1*, transcript variant 5 (Amotl1), mRNA	JEAP	678 0.0	BI277433
	L>S	**Cell communication**	Zyxin (Zyx)	HED-2		AA943537
	L>S	**Development**	Netrin 1			NM_053731
	S>L	**Development**	Dihydropyrimidinase-like 4 (Dpysl4)	rCRMP-3		BF413467
	L>S	**Development**	Enah/Vasp-like (Evl)	RNB6		BF404078
	L>S	**Immune System**	Major histocompatibility complex clas II DM beta (Hla-dmb)			AI171966
	L>S	**Immune System**	RT1 class histocompatibility antigen, B-1 beta chain precursor (RT1.B beta 1)			AI715202
	L>S	**Immune System**	Rat MHC class II RT1.u-D-alpha chain mRNA, 3' end (RT1-Da)			Y00480
	L>S	**Immune System**	Trispanning orphan (Tore)	CRIT (complement C2 receptor inhibitory trispanning)*		NM_022679
	L>S	**Immune System**	Mannan-binding lectin serine protease 1 (Masp1)	Complement-activating component of Ra-reactive factor precursor (CRARF1)		BE111083
	S>L	**Immune System**	PX-19	PX-19-like protein homolog, H. sapiens); Preli, CGI-106		BI279855
	S>L	**unclassified**	Amiloride binding protein 1 (Abp1)			NM_022935
	S>L	**unclassified**	Mitogen activated protein kinase kinase 2 (Map2k2)			D14592
	L>S	**MAPK signaling**	*predicted similar to A-kinase anchor protein 13 isoform 2 isoform 11 [mus musculus] 428 9e-117 *Homo sapiens A kinase (PRKA) anchor protein 13 (AKAP13), transcript variant 2 180 3e-42		428 9e-117 180 3e-42	AI599048
	L>S	**MAPK signaling**	Membrane-spanning 4-domains, subfamily A, member 6B (Ms4a6b) [homolog of Homo sapiens Ms4a6b]	CD20L3 [Homo sapiens]		BI294706
	L>S	**MAPK signaling**	similar to G protein-coupled receptor 146 (Gpr146)	similar to G protein-coupled receptor PGR8	369 7e-99	AI170446
	S>L	**MAPK signaling**	G protein-coupled receptor kinase-interactor 1 (Git1)	Cat-1		NM_031814
	S>L	**WNT signaling pathway**	Frizzled homolog 2 (D. melanogaster; Fzd2)	Fz2		L02530

	L>S	**Calcium signaling**	Adrenergic receptor, beta 3 (Adrb3)			NM_013108
	S>L	**Ion channels**	Potassium voltage-gated channel, shaker-related subfamily, beta member 2 (Kcnab2)	KVbeta2.1; KVbeta2.2		BE097195
	L>S	**Ion channels**	Potassium inwardly-rectifying channel, subfamily J, member 6 (kcnj6)	KCNJ7; GIRK2; GIRK3.2; KIR3.2		AB073756
	L>S	**Ion channels**	Sodium channel, voltage-gated, type VII, alpha polypeptide (SCN7a)	Sodium channel, voltage gated type 6 alpha polypeptide (scn6a); Na-G		BF285019
	S>L	**Cell adhesion molecules**	immunoglobulin superfamily, member 4B (IGSF4B)	Membrane glycoprotein: nectin-like protein 1 (necl1)/TSLC1-like 1 (Tsll1)/brain immunoglobulin receptor precursor (BIgR)	(confirmed) 729 0.0	BG378062
	S>L	**Cell adhesion molecules**	Cartilage acidic protein 1 (Crtac1)	Acidic secreted protein 1 (ASPIC1), Chondrocyte expressed protein 68 kDa (CEP-68), CRTAC1-B, W307		NM_134401
	S>L	**Cell adhesion molecules**	Vitronectin (Vtn)			NM_019156
	S>L	**Transcription**	SWI/SNF-related matrix-associated actin-dependent regulator of chromatin c, member 2 (SMARCC2)	Rsc8, BAF170, CRACC2		BF396079
	S>L	**Transcription**	RuvB-like protein 1 (Ruvbl1)	ECP54; NMP238; TIP49a (TATA binding protein interacting protein 49 kDa); Pontin52		AB002406
	S>L	**Transcription**	Smad3 (Mad homolog 3, D. melanogaster)			BF552908
	L>S	**Transcription**	Retinoid X receptor gamma (RXRγ)	NR2B3		BE118450
	L>S	**Transcription**	Nuclear factor of activated T cells 5 (T cell transcription factor NFAT5)	Tonicity-responsive enhancer binding protein (TONEBP)	287 2e-74	BM384203
	L>S	**Transcription**	Neuronal activity regulated pentraxin protein II (NPTX2)	NARP	1051 0.0	AI228623
	S>L	**Translation**	hypothetical Eukaryotic initiation factor 1A (eIF-1A)/S1 domain IF1 type profile/Nucleic acid-binding OB-fold containing protein	1158 0.0	2010003J03 Rik, LOC293673, MGC11102	BF420639
	S>L	**Translation**	Ribosomal protein L3 (Rpl3)	TARBP-B		AA892367
	S>L	**Translation**	Ubiquitin A-52 residue ribosomal protein fusion product 1 (Uba52)			NM_031687
	S>L	**Translation**	Speckle-type POZ protein (Spop)	TEF2	476 2e-131	BF283504
	S>L	**Folding, Sorting and Degradation**	Matrix metalloproteinase 9 (Mmp9)	Gelatinase b (GELB), Macrophage gelatinase, Type V collagenase, 92kD type IV collagenase, CLG4B		NM_031055
	S>L	**Folding, Sorting and Degradation**	Dnaj (Hsp40 homolog, subfamily C, member 8 (Dnajc8)	SPF31, HSPC331		AI227785
	S>L	**Folding, Sorting and Degradation**	FK506 binding protein 3 (FKBP3)	FKBP25, PPIase, Rotomase		AA891798
	S>L	**Folding, Sorting and Degradation**	Ubiquilin 1, transcript variant 1 (ubqln1)	DA41, DSK2, PLIC-1, XDRP1		BI279735
	S>L	**Folding, Sorting and Degradation**	ADP-ribosylarginine hydrolase (Adprh)			M86341
	S>L	**Folding, Sorting and Degradation**	Syntaxin binding protein 1 (stxbp1)			U06069
	S>L	**Replication and repair**	Replication factor C (activator 1) 2 (Rfc2)			BF283113

	S>L	**Carbohydrate metabolism**	Phosphomannomutase 2		222 7e-55	AI411161
	S>L	**Carbohydrate metabolism**	Solute carrier family 3, member 1 (Slc3a1)	Amino acid transporter 1 (Atr1); Neutral and basic amino acid transport protein rBAT (B(0,+)-type amino acid transport protein (NBAT); CSNU, D2H		NM_017216
	L>S	**Carbohydrate metabolism**	Glycoprotein galactosyltransferase alpha 1, 3 (Ggta1)			AI178222
	L>S	**Lipid Metabolism**	Prostaglandin-endoperoxide synthase 1 (Ptgs1)	Cyclooxygenase 1 (COX1), COX3		NM_017043
	S>L	**Oxidative phosphorylation**	Cytochrome c1 (Cyc1)			BI277021
	S>L	**Oxidative phosphorylation**	Cytochrome c1, non heme 7.2 kDa protein	Ubiquinol-cytochrome C reductase complex (UCRC), HSPC119, HSPC151	278 1e-71	AI007981
	S>L	**Oxidative phosphorylation**	Succinate dehydrogenase complex (Sdhc), subunit b/c		1405 0.0	AI009817
	S>L	**Nitrogen metabolism**	Carbonic anhydrase 4 (Ca4)			NM_019174
	S>L	**Amino acid metabolism**	Liver glutaminase	Gls2, L-glutaminase, L-glutamine amidohydrolase, phosphate-activated/-dependent glutaminase		J05499
	S>L	**Glycan Biosynthesis and Metabolism**	Hyaluronoglucosaminidase 2 (Hyal2)	LUCA-2		AF034218
	S>L	**Cytoskeleton, microtubule and actin-related**	Myosin-1e (Myo1e)	Myo1c		BI275813
	L>S	**Cytoskeleton, microtubule and actin-related**	Myosin-IXA(Myo9a)	Myr7	801 0.0	AW917818
	L>S	**Cytoskeleton, microtubule and actin-related**	Kif6 (Kinesin family member 6)	Kinesin-related protein 3 (Krp3)		AY035403
	S>L	**Oxygen-related**	Hemoglobin alpha-1 (Hba1)	Hbam, CD31		AI179404
	S>L	**Vesicular transport-related**	Low density lipoprotein receptor-related protein 3 (LRP3)			NM_053541
	S>L	**Unclassified**	VGF nerve growth factor inducible			NM_030997
	S>L	**Unclassified**	Hypothetical HAD-like structure containing protein		139 1e-29	BG380656
	L>S	**Unclassified**	PREDICTED Rattus norvegicus ATPase inhibitor (Atpi); Urinary protein 2/3 precursor (RUP-2/3)		1003 0.0; 902 0.0	AA893518
	S>L	**Unknown**	PREDICTED: Rattus norvegicus similar to D3Mm3e (LOC500226)		1021 0.0	AI178206
	S>L	**Unknown**	weakly similar to Proline-rich protein MP-2 precursor		486 4e-134	AI236927
	S>L	**Unknown**	LOC362671			AI409584
	S>L	**Unknown**	LOC317191	UNQ8193, GC0XP083030		AW254686
	S>L	**Unknown**	LOC294291	MGC57858, GC06M034261, GC06M034215		AW915035

	S>L	**Unknown**	EST			BE108374
	S>L	**Unknown**	EST			BF391141
	S>L	**Unknown**	clone RP24-75K5 from chromosome 5			BF401709
	S>L	**Unknown**	Similar to hypothetical protein FLJ14466 (LOC304496)			BG378798
	S>L	**Unknown**	KIAA0683 gene product		293 3e-76	BI279598
	L>S	**Unknown**	1700021K19Rik, 5330403K09	Hypothetical protein KIAA0226; Similar to D. melanogaster gene encoded in P1 clone DS00642		BE113144
	L>S	**Unknown**	Chromosome 22 open reading frame 23 (C22ORF23)	LOC315126; EVG1; FLJ32787	301 1e-78	BI286421
	L>S	**Unknown**	LIM domain containing 2, LIMD2	MGC10986	1356 0.0	BI294855
	L>S	**Unknown**	EST			BI300513
	L>S	**Unknown**	Hypothetical protein 6330514E13 OR RNI-like structure containing protein		307 2e-80	AA964675
	S>L	**Unknown**	Fibronectin type III domain containing 5 (Fndc5)	LOC260327	599 4e-168	AI172165
	L>S	**Unknown**	Zinc finger, FYVE domain containing 21 (zfyve21)	zinc finger, FYVE domain containing 21 (predicted) (Zfyve21_predicted)	1322 0.0 (predicted); 244 3e-61	BI283114

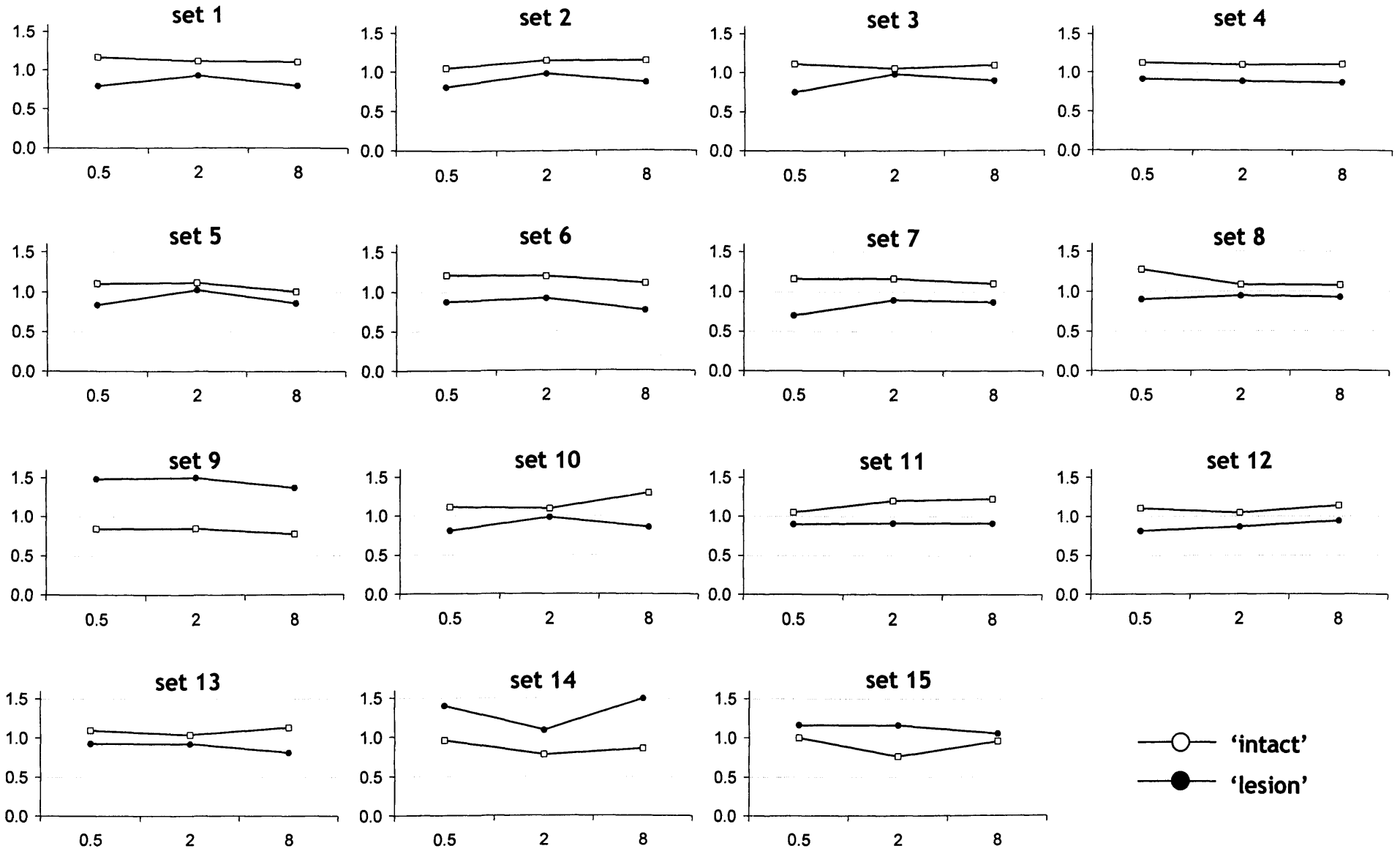

Figure 5B.4: Cluster analysis of transcripts that exhibited altered expression levels found to be predictive of the experimental condition. 76 transcripts remained unclassified. Y-axis= Normalised intensity (log scale); X-axis= Time(h).

5B.4: Discussion

Results from our work suggest widespread consequences of anterior thalamic lesions on retrosplenial cortex. Therefore, the decrease in Fos protein expression observed previously (Chapters 3 and 4, Jenkins et al., 2004) is accompanied by pervasive changes in cellular gene expression.

Using GeneSpring™, we have filtered for signal strength, removed absent flags and conducted statistical analyses, measures that should have minimised the degree of false positives. However, and importantly, it remains that for closely similar samples, many false negatives might be produced, even where small differences (i.e. smaller than fold-change value) are robust.

Approximately three quarters of genes were found to be at greater expression levels in the 'Intact' condition of retrosplenial cortex (159 vs. 45 for predictive patterning). Genetic functions in retrosplenial cortex seemed grossly affected by the anterior thalamic nuclei lesions. Translation, DNA replication and repair appeared to be reduced on the Lesion side, as transcripts associated with these functions were all at relatively lower levels in that condition. Meanwhile, those associated with transcription, folding, sorting and degradation were at mixed levels between the two surgical conditions.

Beyond fold-change analyses, predictive treatment analysis delineated genetic programs that were consistently altered at the three time points studied. The relative expression level of these genes could predict treatment in any condition of either duplicate. Amongst the pervasive changes observed, gene ontology queries revealed that the largest functional alterations were found in genetic information processing, signal transduction and metabolism, as well as other diverse cellular processes.

5.4.1: Functional analyses

5B.4.1.1: Cell signalling

Cell signalling appears to be grossly affected by the surgical treatment. Various neurotransmitter receptors, in addition to several sodium and potassium ion channels, display robust, consistent differences between the surgical treatment conditions (e.g. adrenergic, serotonergic, and gabaergic pathways, cf. Table 5B.1).

5B.4.1.2: Metabolism

Interestingly, whereas no glutamate receptors were found to be differentially regulated, several transcripts suggest a disturbance in glutamate functions. Enzymes involved in the metabolism of glutamate itself and of molecules involved in glutamate function were found to be affected as a result of the anterior thalamic nuclei lesion. Relatively lower levels in the Lesion condition of glutamine synthetase, glutaminase, and asparagine synthetase suggest an alteration in glutamate metabolism and homeostasis, including glutamate-glutamine cycling. As shown in Figures 5B.5 and 5B.6, glutamate is converted to glutamine by glutamine synthetase, a glial-specific enzyme (Norenberg and Martinez-Hernandez, 1979), and as such, the disparity between the surgical conditions may reflect differences in glutamate signaling and in neuron-glia interaction (cf. Hertz and Zielke, 2004; Patel et al., 2005). Given the fact that glutamate is a GABA precursor, it could be expected that levels of GABAergic synthesis would also be altered, but there is no such indication in our results. However, lower expression in the Lesion condition of GABA subunit delta transcripts and of ubiquilin (a mediator of GABA receptor subunit composition, cf. Bedford et al., 2001), suggests that trafficking, although not synthesis of GABA may be altered.

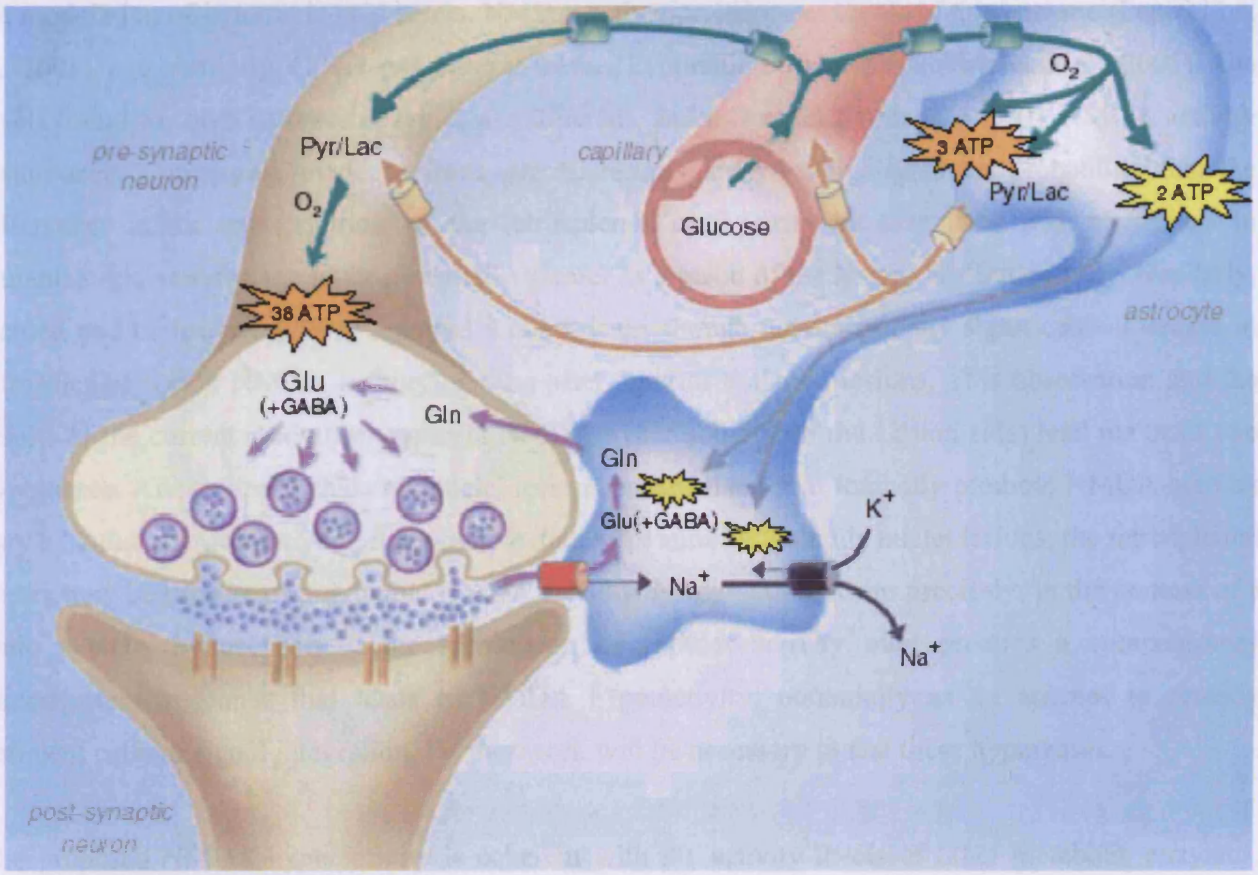

Figure 5B.5: Coupling between synaptic activity and glucose metabolism via interaction of neurons and astrocytes (taken from Hyder et al., 2006). Gln= glutamine, Glu=glutamate.

Further evidence of perturbations in glutamate function arises from apparent alterations in kynurenine metabolism. In our study, the balance of kynurenine metabolism appears to be different in the two surgical conditions, based on the fact that the transcripts for cyclooxygenase 1 (COX1) and kynurenine 3-monooxygenase (KMO), two enzymes associated with the metabolites of this pathway, are found to be at relatively higher levels on the Lesion side. The endpoints of kynurenine metabolism are kynurenic acid and quinolinic acid (Moroni, 1999). Kynurenic acid, a neuroprotective molecule (Carpenedo et al., 2002), and quinolinic acid are respectively antagonists and agonists of NMDA receptor subtypes. Reduced levels of KMO produce an increase in kynurenic acid (Carpenedo et al., 2002; Erhardt and Engberg, 2002). COX1 has been reported to be associated with NMDA activity and

the modulation of kynurenic acid levels. NMDA activation increases levels of this enzyme (Pepicelli et al., 2005), and similarly, COX1 reduction increases kynurenic acid levels (Schwieler et al., 2005). The levels found for both of these enzymes are coherent, and this again points to a likely NMDA activity disturbance. Converging evidence from our microarray analyses highlights the probability that the differences in the transcriptome of the retrosplenial cortex may be associated with alterations in glutamatergic activity, the latter potentially greater as a result of the lesion. NMDA activity. Similarly, Garden and colleagues (2006) reported a numerical—though not statistically significant—increase in retrosplenial cortex NMDA activity *in vitro* after anterior thalamic lesions. This observation and the results of the current study (i.e. apparent NMDA hyper-activity on the Lesion side) lead me posit two hypotheses. After anterior thalamic nuclei lesions, mechanisms that tonically promote NMDA activity may be induced. Alternatively, it is possible that, after anterior thalamic nuclei lesions, the retrosplenial cortex may be the site of a dynamic NMDA activity dysregulation. More precisely, in the context of a tonic NMDA hypoactivity, acute stimulation of cellular activity may produce a compensatory transcriptome response that leads to NMDA hyperactivity, potentially as an attempt to remedy deficient cellular signal integration. Further work will be necessary to test these hypotheses.

The proposed NMDA hyperactivity is coherent with the activity levels of other metabolic enzymes. NMDA receptor antagonism leads to increases in glutamine synthetase and in extended tricarboxylic acid cycling (Brenner et al., 2005). Accordingly, NMDA hyperactivity may be associated with a reduction in glutamine synthetase and in less tricarboxylic acid cycling. In the present experiment, lower expression on the Lesion side of gene transcripts for malate dehydrogenase and succinate dehydrogenase suggests a reduced activity of the tricarboxylic acid cycle. This is consistent with the finding of lower glutamine synthetase also on the Lesion side, and again suggestive of a relative elevation of NMDA activity in the retrosplenial cortex on the Lesion side. Altogether, while this evaluation of the molecular activity patterns exhibited by both conditions points heavily towards a NMDA signalling dysregulation, I should also point out the potential alterations in other neurotransmitters. Given the fact that GABA is metabolised from glutamine (see Figure 5B.6), it is also plausible to suppose that GABA signalling is altered, as indicated by the lower abundance of transcripts for the GABA(A) delta receptor on the Lesion side. GABAergic signalling may play an important role in the apparent dysregulation of the granular b retrosplenial cortex, and appears to be

associated with a deficit in long-term depression in this region *in vitro* after anterior thalamic nuclei lesions (Garden et al., 2006). Additionally, as shown in Table 5B.1, serotonergic (5HT2C) and adrenergic (Adrb3) signalling also appears to be lower on the lesion side, consistent with previous findings for 5HT1B, and opposite to Adrb2 (van Groen et al., 1993).

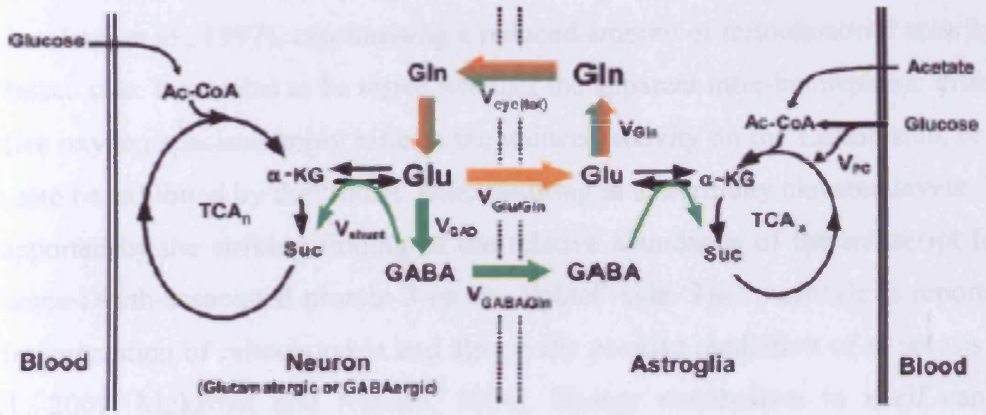

Figure 5B.6: Metabolism of glutamate and GABA in neurons and astroglia (taken from Patel et al., 2005).

5B.4.1.2.1: Alterations of energy metabolism and potential oxidative stress

Mitochondria appear to have been affected by the surgical treatment, consistently at the three time points sampled. Pervasive alterations were found in the function of this organelle, transcripts exhibiting altered expression patterns in most mitochondrial compartments. Enzymes and other components of energy metabolism pathways were found to be differentially regulated, almost exclusively lower in the Lesion condition (cf. Table 5B.1).

Mitochondria play an important role in oxidative phosphorylation, and also the glutamine-glutamate cycle, and their altered activity levels may be related to the disturbance in this system. Alternatively, the observed mitochondrial alterations may be a function of oxidative stress. Reactive oxygen species

are mainly derived from the mitochondrion. Numerous mitochondrial genes find their expression levels to be lower on the Lesion than the 'Intact' side. This clearly suggests the presence of altered metabolism function in retrosplenial cortex, a consequence of anterior thalamic lesions.

In addition to the mitochondrial alterations, other oxidative mechanisms appear to be more active on the 'Intact' side of the retrosplenial cortex. Coenzyme Q9 was also found to be lower in the Lesion relative to the 'Intact' condition. This enzyme is correlated with the presence of reactive oxygen species (Lass et al., 1997), emphasising a reduced amount of mitochondrial activity on the Lesion than the 'Intact' side. It remains to be tested whether the apparent inter-hemispheric difference in the level of reactive oxygen species simply reflects the reduced activity on the Lesion side, or if some dysfunction may also be exhibited by the 'Intact' side, resulting in abnormally elevated levels. The latter hypothesis is supported by the striking finding of the relative abundance of the transcript for the mitochondrial ribosome Death-associated protein 3 on the 'Intact' side. This molecule is reported to be involved in the fragmentation of mitochondria and also in the positive mediation of apoptosis (Kimchi, 1999; Koc et al., 2001; Mukamel and Kimchi, 2004). Energy metabolism in itself can have an effect on neuroplasticity (Vaynman et al., 2006), and the observed alterations in mechanisms related to the former may prove to be involved in the plasticity changes reported by Garden and colleagues (2006). Changes in gene transcripts reported to play a role in neuroplasticity will be discussed later.

Another source of oxidative mechanisms may be metal-related, and several transcripts that could be involved in such activity were found at relatively lower levels on the Lesion side. Murr1 has recently been linked to copper metabolism, more precisely copper excretion, as it has been negatively correlated with cytoplasm copper content (Burstein et al., 2004). Similarly, mutation of this gene has been reported to be associated with copper toxicosis (Tao et al., 2003). Another candidate for metabolic disruption is pantothenate kinase 4. Pantothenate kinase is necessary for the production of coenzyme A, itself very important for, amongst others, metabolic functions. Pantothenate kinase plays a role in the regulation of iron pathways; mutation of this gene has also been associated with iron deposition and neurodegeneration (Thomas and Jankovic, 2004). Urod, a gene involved in the heme biosynthesis pathway is also found at lower levels on the Lesion side. Auclair and colleagues (2006) have reported that mild iron deficiency-induced anaemia resulted in increases in Urod. Selenoprotein M, also lower

in the Lesion condition, is another gene suggesting that there may be trace metal level alterations. Selenium is thought to have anti-oxidant properties and in a recent review it was emphasized that altered levels of this trace metal were found in several neurodegenerative disorders (Chen and Berry, 2003). This gene has also been found to be expressed at lower levels in mice overexpressing human presenilin-2 in comparison to their wild-type littermates (Hwang et al., 2005). Trace metals have been found to be differentially regulated in neurodegenerative disorders, and it is believed by some that at the core of Alzheimer-like neurodegeneration lies mitochondrial alterations and oxidative stress processes (Roloff and Platt, 1999).

In addition to these changes in energy metabolism and oxidative processes, we also found changes suggestive of blood and oxygen activity disturbances. In the Lesion condition, we found lower levels of genes that are known to be associated with haemoglobin oxygen transport (Hba1, Urod). Additionally, the aforementioned COX1 change may be associated with this probable alteration in oxygenation and energy as COX1 knockout mice exhibit reduced blood flow (Iadecola et al., 2001).

The retrosplenial cortex in humans and rats (and also the posterior cingulate and precuneus in the former) exhibits the highest energy expenditure of all brain regions during "basal" or "resting" activity (Harley and Bielajew, 1992; Gusnard and Raichle, 2001). In striking contrast, this region becomes hypoactive during what has been interpreted as "goal-directed", or other than "self-focused" behaviours and during the processing of semantic tasks (Shulman et al., 1997; Gusnard and Raichle, 2001; Lustig et al., 2003). In the present study, energy metabolism appeared to be lower on the Lesion side. In the context of aforementioned observations, no inferences can be made about the functional state of the retrosplenial cortex on the Lesion side, other than that it is abnormal.

5B.4.1.3: Neuroplasticity

The expression of transcripts that have been shown to play a role in neuroplasticity is lower on the Lesion side. For example, several genes found to be differentially regulated in this study have also been reported to be involved in enhanced NMDA receptor activity (Adcyap1), and long term potentiation (LTP; Adcyap1, Camk2g, NCS-1, LRP3, PPP1r1a), or long term depression (LTD;

Map2k2, Prkar1b). In contrast, RXRγ levels were found to be highest in retrosplenial cortex ipsilateral to the lesion. This gene has been reported to be involved in LTD, but not LTP (Chiang et al., 1998).

Neuroplasticity alterations at the molecular level would be coherent with recent findings of electrophysiological plasticity deficits in retrosplenial cortex after anterior thalamic nuclei lesions. Briefly, recent work by Garden and colleagues (2006) evaluated the effect of anterior thalamic nuclei lesions on single unit recordings in retrosplenial cortex. Recordings were taken in retrosplenial cortex layer II pyramidal neurons after stimulation in layer II or V. In unilateral preparations, LTD could be induced in both layers in the Sham but not layer II in the Lesion hemisphere. This electrophysiological finding provides further evidence for the unresponsiveness of superficial layers in the retrosplenial cortex after anterior thalamic nuclei lesions.

5B.4.1.4: Inflammation and immune-related responses

The presence of genes involved in immunity or inflammation in our study (e.g. CD74, CD83, Cyslt1, Hla-dmb, LOC171412, Masp1, Ppib, RT1.B beta 1, RT1-Da, Tore) may be related to denervation, oxidative stress, or dysregulation of these functions. The majority of these genes were found to be increased on the Lesion side. Different research groups have reported an increase in genes associated with immune responses, including major histocompatibility complex (MHC) genes, after denervation. For example, in deafferented tissue in the hippocampus after disconnection from entorhinal connections (Ying et al., 2004) and after medial forebrain bundle transection (Cho et al., 2006). Both anterograde and retrograde effects of denervation may be at play (e.g. Block et al., 2005).

5B.4.1.5: Re-innervation, cell proliferation and possible aberrant connections

Differential activation of several transcripts may reflect the activity in retrosplenial of events that could be involved in the remodelling of the dendrites and axonal sprouting of retrosplenial cortex neurons following denervation (e.g. MAP2, Nelf, Netrin1, Neuritin1, Plexinb2, Neurofilament heavy polypeptide, Myosin Ie and IXa, and LSAMP).

Reprimo is associated with cell cycle arrest. It is relatively higher on the Lesion side. Likewise, so is *NFAT5*. This transcription factor is required for the optimisation of cell proliferation. Conversely, *cyclinD2*, *klf5*, *rbbp-5*, *staufen*, *neuroD1*, *Fbxo6b* and *adcyap1* are amongst those transcripts that are found at a relatively lower level on the Lesion side; they are associated with cell proliferation, differentiation and some also with neuritic processes. It is most likely that these actions are related to normal physiological functions, which may be affected on the Lesion side.

It remains to be determined whether the expression patterns discussed above are the result of processes following the deafferentation of the Lesion side, or even the reflection of increased activity or pathology on the 'Intact' side. However, there clearly is a striking difference in proliferative potential between both sides, even though recovery processes, including an *increase* in Fos protein, are thought to peak 3-10 days after injury return to baseline before one month (Nieto-Sampedro et al., 1982; Buytaert et al., 2001; Mingorance et al., 2005).

Any resulting aberrant connections that could be produced by new neurites may add to the dysfunction that could be caused by metabolic alterations. These could generate and also propagate disruptive activity and further compromise retrosplenial function and that of its efferents, as seen in the hippocampal formation after kainic acid treatment (e.g. Tauck and Nadler, 1985).

5B.4.1.6: Immediate-early genes and brain injury

Fos is the protein product of the immediate-early gene c-*fos*. It plays a central role in the regulation of gene activity induced by excitatory stimulation. Like c-*fos*, *zif268* (also known as Egr-1, krox24, Tis8, NGFI-A) is also an IEG that is involved in regulation of genes by excitatory stimuli (Chaudhuri, 1997; Herdegen and Leah, 1998; Hughes et al., 1999; Tischmeyer and Grimm, 1999; Platenik et al., 2000; Bozon et al., 2002; Hoffman and Lyo, 2002; Wu et al., 2004). Its expression pattern is also similar to that of c-*fos* (Zangenehpour and Chaudhuri, 2002).

The relationship between brain injury and these two IEGs is different. Axotomy is associated with more selective and persistent expression of immediate-early genes. After axotomy, c-Jun and weakly

zif268, but not c-fos, are expressed in the axotomised neurons (Hughes et al., 1999). The induction of c-Jun is prolonged, it has been observed up to 100 days later (Brecht et al., 1995). This effect can be observed in neurons that neither regenerate nor undergo apoptosis. Transient c-Jun expression has been reported in neurons until they re-connect or undergo apoptosis. In a review of the literature, Hughes and colleagues (Hughes et al., 1999) suggest that apart from c-Jun, and to a lesser extent JunD, other IEGs do not play a role in axotomised neurons. These associations between certain immediate-early genes and injury appear to be in stark contrast to what is observed in our study. Here *zif268* mRNA levels do not appear to be significantly altered, nor are those of *c-jun* and *junD*. These expression patterns are not in accord with those expected for death-associated mechanisms and this is supported by the failure to observe cell death as visualised with a traditional Nissl stain.

Whereas cell death mechanisms appear not to be involved, evidence from other studies concur with our findings of a cellular alterations distal to a lesion. In general, cellular activity is either at control levels or transiently increased after toxin infusion. Metabolic assay after entorhinal lesions revealed a 10-40% reduction in glucose utilisation, which in the dentate gyrus persisted up to three months—the last time point assessed (Beck et al., 1996). Similarly, widespread nitric oxide synthase and Fos hypoactivity have been found after entorhinal lesions (Liu et al., 2003) and perirhinal lesions (Glenn et al., 2005), respectively. Our results are in accord with such findings of distal disturbances and suggest that after the acute effect of a lesion, metabolic hypoactivity is associated with hypo-reactivity of IEGs.

5B.4.2: Conclusions

Anterior thalamic nuclei lesions induce widespread alterations in cellular function of the retrosplenial cortex. Future work could pursue the analysis of the effects of anterior thalamic lesions on retrosplenial cortex to determine whether it is possible that the observed transcriptome may in fact be a reflection of oxidative stress. Such studies could provide more evidence for a role of retrosplenial deafferentation in memory deficits and the instigation of Alzheimer-like neurodegenerative processes. Regulatory sequence analyses of the promoter regions of the genes found to be differentially expressed in this study could pinpoint the role of one or a select group of transcription factors.

Overall, some of the recurrent associations of the altered transcripts are with functions of metabolism, genetic information processing, and signal transduction. Future studies are necessary to better understand the interaction of the anterior thalamic nuclei and of the retrosplenial cortex, and the role of these two regions that are critical to cognitive functions and to the development of Alzheimer's disease.

A better characterisation of this retrosplenial dysfunction would further our understanding of distal effects of insults to the brain, and may provide paths to diminish the sequelae in dysfunctional regions that do not exhibit overt pathology.

Appendix 5A

Histogram representation of the normalised intensity (log scale) profiles of all the samples.

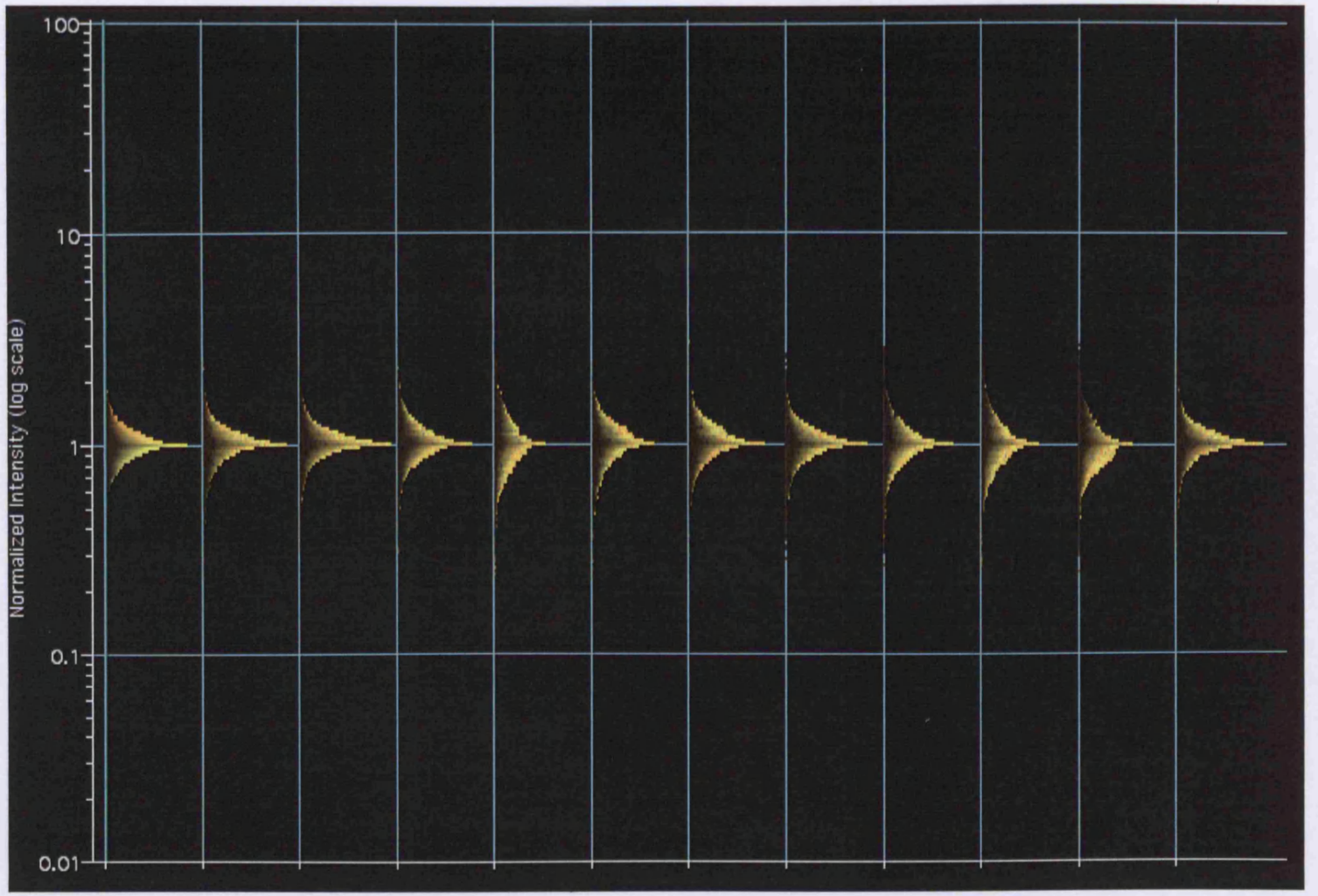

Chapter 6

General discussion

Summary of findings

Since the seminal report of Scoville and Milner (1957), the hippocampal formation and the entorhinal cortex have been an important research focus for their role in memory abilities. In more recent literature the role of other brain regions has come to be appreciated. Importantly, there is a spreading impetus to consider the networks of brain regions that may underlie various cognitive abilities (e.g. Horel, 1978; Tulving and Markowitsch, 1997; Aggleton and Brown, 1999; Sporns et al., 2004), and that this network activity is dynamic, rather than static (e.g. Friston et al., 1993; McIntosh, 1999; Ranganath, 2005; Krause et al., 2006). Patients who suffer from amnesia that particularly affects episodic memory have often been reported to exhibit dysfunction in structures forming the Papez/limbic circuit, or extended "hippocampal system" (hippocampus–fornix–mamillary body–anterior thalamic nuclei–cingulate cortex–entorhinal cortex–hippocampus), evidence that is corroborated by the animal literature (e.g. Steckler et al., 1998; Aggleton and Brown, 1999).

In contrast to models such as the "medial temporal memory system" proposed by Squire and Zola-Morgan (1991), some recent models have proposed that the structures included in this system are not all interdependent as presumed, that memory impairment is not simply proportional to the amount of damage of tissues, and that some functional dissociations may exist between the regions involved in the so-called medial temporal lobe memory system. One such alternative view (Aggleton and Brown, 1999) proposed a re-appraisal of this MTL system. In addition to proposing an extension to this MTL system to include diencephalic structures, Aggleton and Brown (1999) argued that much greater independence exists between these structures, so that qualitatively different forms of memory are handled by different subsets of components.

In the course of this thesis, I have provided evidence in Chapter 2 to show that in the performance of a task dependent on spatial memory, multiple brain regions exhibited a relationship with memory. Importantly, the regions displayed associations with different memory components, and these associations appeared to be dynamic as they changed according to the experience and the performance level of the subjects.

Structural equation modelling analyses revealed that, in spite of apparently similar levels of activity between different training levels, and even between different

experimental conditions, different networks of brain regions were active for each condition. The structural modelling analyses yielded quantitative estimations of the influence that each region exerted within the network tested. In doing so, empirical data on network dynamics was produced, which could be of potential use for computational modelling investigations. The structural modelling analyses revealed that, for the regions tested, network activity appeared to be best at describing the paths of activity in the prolonged training group. A salient feature of the regional network activity for the Trained subjects was an apparent disengagement of the dentate gyrus with prolonged training. A time-limited role of subregions of the hippocampus was apparent with prolonged training, emphasising the need to consider the individual contributions not just of brain regions within an extended hippocampal system, but also of hippocampal subregions. This finding emphasises functional specialisation within the hippocampus, in a way that may be coherent with recent views (cf. reviews by McClelland and Goddard, 1996; Rolls and Kesner, 2006).

In spite of the changing relationships between each of the brain regions with training or even according to experimental condition, it emerged that the activity in the retrosplenial cortex appeared to correlate best with the activity of the other regions (compare the $\mathbf{R^2}$ values for each region in Figures 2.9 to 2.16). This is in line with the proposed role of the retrosplenial cortex in information integration (van Groen and Wyss, 2003). It was also apparent that the activity of the retrosplenial cortex is strongly influenced by the CA1 region. The influence of cortical regions appeared to change according to condition, and differentially according to the route. It was revealed that the putative shift from hippocampal to neocortical responsibility for memory in long-term memory (Teyler and DiScenna, 1985; Squire et al., 2004; Wiltgen et al., 2004; but not Moscovitch et al., 2005) is not necessarily instantiated as acquisition progresses.

Tests were conducted in order to verify the vulnerability of granular b retrosplenial cortex to distal damage. It was revealed that, in addition to anterior thalamic nuclei damage, granular b retrosplenial cortex can exhibit hypo-active immediate-early gene expression as a result of entorhinal cortex and of both large and restricted hippocampal damage. However, laterodorsal thalamic nucleus damage is not sufficient to produce granular b retrosplenial cortex hypo-activity. Next, the observation of the time course of the occurrence of the retrosplenial cortex dysfunction was tested, bringing the time of

onset forward from the previously tested two months to a shorter post-surgical delay of only one week.

The effects of anterior thalamic nuclei lesions on retrosplenial cortex IEG-positive cell counts were consistent for each experiment in Chapters 3, 4, and 5, and also agreed with previous results (Jenkins et al., 2004). The analyses of Fos-positive cell characteristics, made on rats with bilateral anterior thalamic nuclei lesions, revealed that changes in retrosplenial cortex tissue were apparent even where Fos-positive cell counts were normal. That is, these analyses of Fos-positive cell characteristics revealed that the superficial area of granular b retrosplenial cortex was not the only site in the retrosplenial cortex that exhibited alterations as a result of anterior thalamic nuclei lesions. It was discovered that the dysgranular division of the retrosplenial cortex was also affected, though not in quantity of Fos-positive cells, but rather in the sphericity of the active population. It remains to be verified whether this sphericity change can be associated with a particular cell type.

Finally, the breadth of the changes suffered by granular b retrosplenial cortex was evaluated by conducting a microarray analysis (see Chapter 5). The results of this experiment revealed that it was not only Fos that was affected by the anterior thalamic nuclei lesions. On the contrary, alterations in mRNA transcript expression were found throughout a variety of cellular pathways and compartments. The findings suggested widespread alterations in cellular function, which appeared to be especially related to energetic and metabolic function, but also included proteasome, neurotransmitter and extracellular matrix activity, to name a few (see Figure 6.1). Next, I will attempt to integrate the findings of this thesis to explain Fos hypo-activity as a result of distal lesions, using anterior thalamic damage as a template (see also Figure 6.2). The effects posited may provide a framework for future analyses of the vulnerability of the retrosplenial cortex with distal neurological insult.

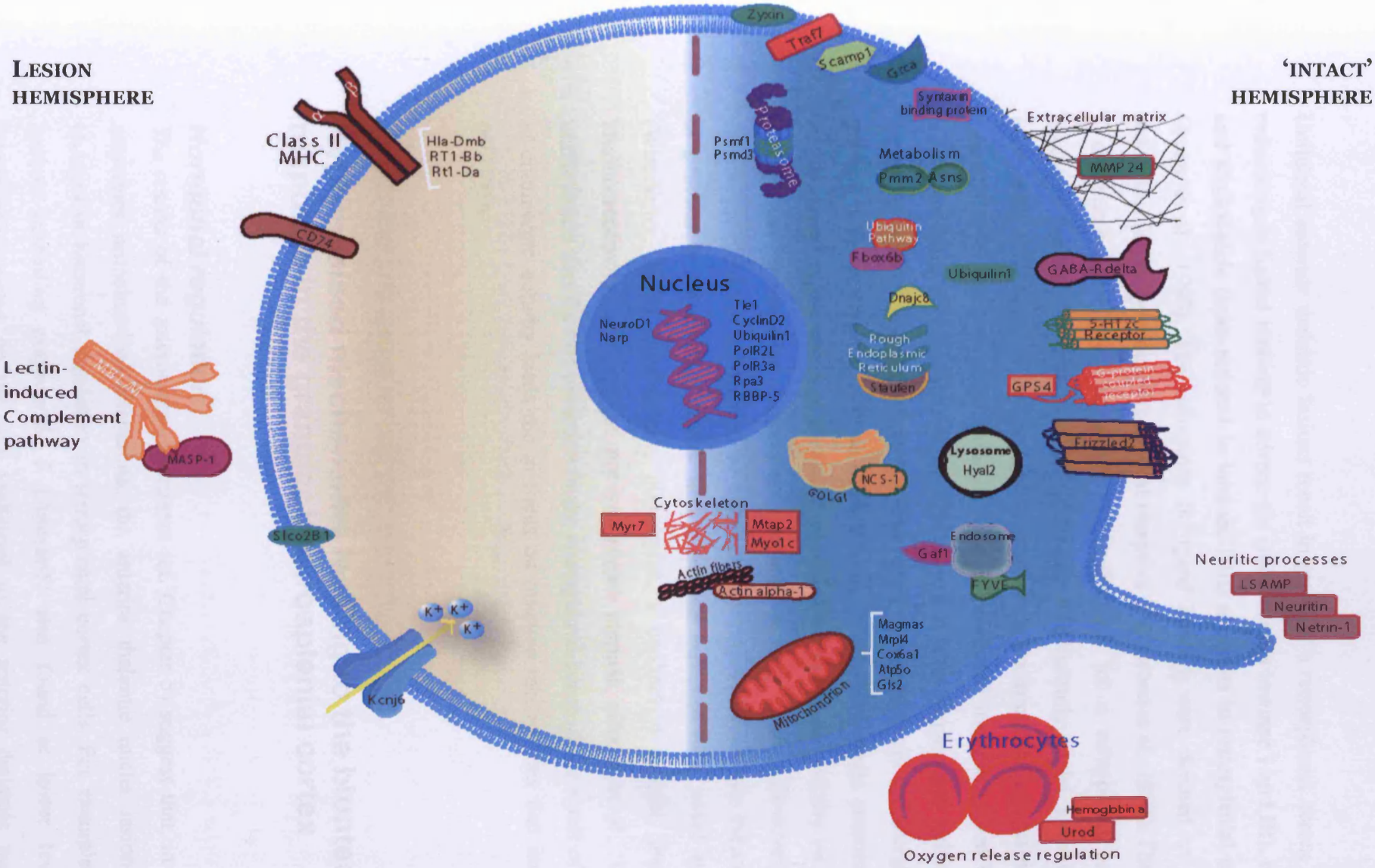

Figure 6.1: The microarray analyses revealed an overall reduction in transcript activity on the Lesion side, where examples of the effects observed include elevations in mitochondrial, nuclear, proteasomal, ribosomal, membrane receptor, and extracellular activity. In contrast, one of the functions most obviously elevated on the Lesion relative to the 'Intact' side was immunity.

Unilateral anterior thalamic lesions result in granular b retrosplenial cortex displaying reductions in ligand binding to adrenergic (reduction in laminae I and III), cholinergic and serotonergic (both reduced in laminae I-III) receptors in retrosplenial cortex (van Groen et al., 1993). The reductions in ligand binding were deemed to be due to reductions in pre-synaptic retrosplenial receptors (van Groen et al., 1993). The results of a microarray experiment suggested that transcripts for a subtype of serotonergic receptors were reduced as a result of the anterior thalamic nuclei lesions, and that adrenergic, GABAergic, as well as glutamatergic communication pathways were altered. No differences were found in cholinergic-related transcripts (see Table 5.1). Basal forebrain cholinergic mechanisms play a role in exploration behaviours and locomotor activity and lesions in this area result in reductions in cholinergic terminal staining in the retrosplenial cortex (Torres et al., 1994). Cholinergic neurotransmission in the ventral tegmental area mediates the effect of locomotor activity on granular b retrosplenial cortex Fos expression (Ikemoto et al., 2003). However, systemic cholinergic blockade appeared to be only partially responsible for the induction of Fos in granular b retrosplenial cortex as a result of exposure to a novel environment (Wirtshafter, 2005). Furthermore, pilocarpine, a cholinergic agonist, increases Fos immunoreactivity in deep but not superficial laminae (Bucci et al., 1998). The unlikelihood that the Fos reduction in the retrosplenial cortex is the result of alterations in cholinergic activity leads me to focus on putative mechanisms that include other pathways.

Hypothesised mechanisms leading to the blunted Fos response in the granular b retrosplenial cortex

Hormonal regulation

The results of the microarray experiment (cf. Chapter 5) suggest that, in addition to important mitochondrial alterations, the anterior thalamic nuclei lesions produced changes in hormonal regulation in retrosplenial cortex cells. For example, *Adenylate cyclase activating polypeptide 1* (Adcyap1) was found at lower levels in the retrosplenial cortex on the side ipsilateral to the anterior thalamic nuclei lesion.

Adcyap1 plays a role in the modulation of the hypothalamo-pituitary–adrenal axis (Vaudry et al., 2000), and its localisation is particularly dense in lamina II of retrosplenial cortex granular b (Hashimoto et al., 1996). Interestingly, this neuropeptide binds VIP receptors (reviewed in Harmar and Lutz, 1994), which have been proposed to be associated with fusiform cells (Vogt and Peters, 1981), unique to Rgb (Vogt, 1993).

The transcript for *retinoic X-receptor gamma* (RXRγ), also found to be at different levels between the hemispheres, selectively plays a role in regulation of thyroid-stimulating hormone. Brd8, co-activator of a RXRγ heterodimer, was also found to be differentially regulated as a result of the anterior thalamic nuclei lesions. Additionally, the transcript for *regulator of G protein signalling-4* (RGS4) was found at lower levels in retrosplenial cortex ipsilateral to anterior thalamic nuclei lesion (see Table 5.1). The RGS family negatively modulate G protein signalling (Druey et al., 1996; Berman and Gilman, 1998; De Vries et al., 2000; Ross and Wilkie, 2000; Hollinger and Hepler, 2002; Neubig and Siderovski, 2002). RGS2 knock-out mice display behaviours interpreted as increased anxiety (Oliveira-dos-Santos et al., 2000), and of particular relevance to this thesis, RGS4 is modulated by stress and corticosterone (Ni et al., 1999).

The results of the microarray experiment revealed that levels of *11beta-hydroxysteroid dehydrogenase type 1* (Hsd11b1) were different between the two hemispheres in two of the three time points (data not shown). The Hsd11b1 gene is involved in converting corticosterone to its active form, which can have consequences on metabolism and cognition (cf. Seckl and Walker, 2004). It has been shown that the mRNA for the Hsd11b1 enzyme is heavily distributed in the retrosplenial cortex (Roland et al., 1995). In the microarray experiment, Hsd11b1 and Fos protein levels appear to be proportional to each other across the three time points in the superficial laminae of retrosplenial tissue that was contralateral to the lesion (i.e. 'Intact' condition). Meanwhile, in the Lesion condition, where Fos is consistently low, the levels of Hsd11b1 were lower on the Lesion than the 'Intact' hemisphere at 30 min and 8 hours after the introduction into the novel environment, and exhibited a much less dynamic pattern (data not shown). The implications of an altered level of this molecule have widespread implications for learning, memory and behaviour in general (cf. review by Seckl and Walker, 2004).

Strikingly, results presented in Chapter 4 suggested that retrosplenial cortex neurons in the superficial laminae of the granular subdivision are significantly associated with corticosterone levels in the Sham group, but not in the Lesion group. This finding suggests that a dynamic equilibrium of hormonal activity and retrosplenial cortex response may be disrupted by the anterior thalamic nuclei lesions. Corticosteroid levels have been shown to be associated with retrosplenial Fos activity (Abraham and Kovacs, 2000; Park et al., 2003; Fevurly and Spencer, 2004) and the manipulation of this hormone can modulate the pattern of Fos expression (e.g. Kovács, Földes, & Sawchenko, 2000), without resulting in retrosplenial cortex morphological changes or degeneration (Cerqueira et al., 2005b; Cerqueira et al., 2005a). It is plausible that the anterior thalamic nuclei lesions result in dramatic Fos hypo-reactivity in the superficial laminae of granular retrosplenial cortex via the action of glucocorticoids. Anterior thalamic nuclei lesions result in apparent population changes in Fos-positive cells in dysgranular cortex and in the dissociation of granular from dysgranular retrosplenial cortex Fos activity (see Chapter 4). It remains to be tested whether these effects are directly related to corticosterone response alterations.

GABAergic regulation

An decrease in transcript abundance of the GABA(A) receptor subunit δ was found after anterior thalamic nuclei lesions (see Table 5.1). GABA(A) receptor binding is known to be high in superficial but weak in deep cell laminae of granular b retrosplenial cortex (Unnerstall et al., 1981; Gonzalo-Ruiz et al., 1996). More specifically, subunit δ of the GABA(A) receptor is found selectively in lamina II of granular b retrosplenial cortex, albeit maybe at low levels in normal rats (Shivers et al., 1989; Wisden et al., 1992; Peng et al., 2002). It was posited that postsynaptic GABA(A) receptor binding may be associated with somatodendritic membranes, except in lamina I where it may be associated with apical dendritic tufts (see discussion in Vogt, 1993).

The properties of the GABA(A) receptor subunit δ suggest that alterations in the abundance of this particular subunit may be associated with changes in cell excitability. For example, neuronal activity reduction was reported to reduce the abundance of the delta subunit in frontal cortex (Kim et al., 2000), while seizure induction increased its abundance in retrosplenial cortex (Penschuck et al., 1997). Additionally, knockout mice lacking the delta subunit exhibit a greater seizure potential and faster decay of inhibitory

postsynaptic potentials (Spigelman et al., 2002). The electrophysiological properties of neurons where this particular GABA(A) receptor subunit is active also include a slower recovery of current amplitude and slower desensitisation to continuous GABA stimulation (Saxena and Macdonald, 1994). These observations highlight the dynamic nature of GABA(A) receptor composition and evoke the potent role of the GABA(A) receptor delta subunit in modulating cell excitation.

It has been proposed that different populations of GABA(A) receptors exist. They are synaptic and extrasynaptic, and they respectively regulate phasic and tonic inhibition (cf. review by Mody, 2001). The delta subunit was reported to be almost exclusively extrasynaptic (Sun et al., 2004). Clustering of the extrasynaptic GABA(A) receptors has been shown to impact tonic inhibitory conductance (Petrini et al., 2004). Such clustering of the GABA(A) receptors is dependent upon activity of Ubiquilin1 (Bedford et al., 2001), the transcript of which is also found to be less abundant on the side ipsilateral to the lesion (see Table 5.1).

Mediation of corticosterone effects via GABA(A) receptor subunit δ

The apparent alteration in retrosplenial cortex of GABA(A) receptor subunit composition may be associated with the observed dissociation between corticosterone and Fos signalling in rats with anterior thalamic nuclei lesions (see Chapter 4). Adrenalectomy, chronic stress, and acute social stress can produce different regional alterations in the composition GABA(A) receptor subunits in the brain (Kang et al., 1991; Orchinik et al., 1994, 1995). Neuroactive steroids upregulate the expression of GABA(A) receptor subunit δ (Orchinik et al., 1995; Shen et al., 2005), which mediates the observed steroid-induced reduction in cell excitation (Stell et al., 2003). Conversely, GABA(A) receptor subunit δ knock-out mice display an attenuated sensitivity to neuroactive steroids (e.g. Mihalek et al., 1999; Spigelman et al., 2002). The effect of acute administration of neuroactive steroids on anxiety is also prevented by manipulating levels of GABA(A) receptor subunit δ (Mihalek et al., 1999; Shen et al., 2005).

Potential mediation of corticosterone effect on Fos by GABA(A) receptor subunit δ

The observations presented above may suggest a plausible chain of events that would result in retrosplenial cortex Fos hypo-activity after anterior thalamic nuclei lesions. It is proposed that anterior thalamic nuclei lesions lead to a chronic dysregulation in corticosterone response and homeostasis in the retrosplenial cortex. The altered local corticosterone response reduces the tonic inhibition of pyramidal (including fusiform) cells in lamina II of retrosplenial cortex by downregulating the levels of somatodendritic GABA(A) receptor subunit δ. Ubiquilin1 activity mediates the current disinhibition that is produced, and which leads to deficient somatodendritic signal integration. The stimulus-transcription coupling that would otherwise have occurred is precluded, and the induction of Fos in the superficial laminae of granular retrosplenial cortex is diminished. As the reduced tonic inhibition in lamina II stops incoming information from being transmitted correctly, it may prevent the propagation of the oscillatory activity that can be generated in deep granular a retrosplenial cortex laminae with afferent stimulation (Yoshimura et al., 2005) from propagating to efferent regions and, as such, the retrosplenial cortex fails to successfully instill coherence in the active network.

This explanation would suggest that the general alteration in retrosplenial genetic response, and the electrophysiological dysregulation reported by Garden and colleagues (2006), may be mediated by endocrine factors. Further work is required to determine the potential relationship between the activities of the GABA(A) receptor δ subunit, corticosterone, and of Fos-positive cells in granular b retrosplenial cortex.

An additional link in the causal chain of effects from distal insult to retrosplenial cortex Fos hypo-activity may lie in the role of β-adrenergic receptors on corticosterone activity. While it has previously been reported that unilateral anterior thalamic nuclei lesions result in reductions in ligand binding to beta-2 adrenergic receptors (van Groen et al., 1993), the microarray experiment revealed that *adrenergic receptor beta 3* (Adrb3) levels were higher on the Lesion than the 'Intact' side, yet no changes were found for *Adrb2*. Opposite patterns for these receptor subtypes is not necessarily contradictory as these have been found to play different roles (cf. review by Gibbs and Summers, 2002). Furthermore, *adrenergic receptor kinase, beta 1* (Adrbk1) and *G protein-coupled receptor kinase-interactor 1* (Git1) were both found at lower levels in

Lesion than the 'Intact' side. The levels of these transcripts are in accord with an augmentation in adrenergic activity as a result of the anterior thalamic nuclei lesions because Adrbk1 and Git1 together play a role in the inactivation of beta-adrenergic receptors (e.g. Premont et al., 1998). It has been reported that beta- but not alpha-adrenergic activity can increase corticosterone levels in hippocampal, amygdaloid and hypothalamic areas (Dietl, 1987), and that adrenergic and glucocorticoid mechanisms interact to produce dose- and time-dependent effects on memory (reviewed by McGaugh et al., 1996). Therefore, it is possible that beta-adrenergic activation is an early step in the proposed chain of events that lead to Fos hypo-activity in the retrosplenial cortex after anterior thalamic nuclei lesions.

Further interest in the role of Adrb3 lies in its effects on cellular metabolism. The results of the microarray experiment highlighted a down-regulation of transcript levels in Lesion tissue that pervaded most if not all of the mitochondrial complexes (see Table 5.1). Low glucose levels can increase mitochondrial activity and the production of reactive oxygen species (Mattson and Liu, 2002). The activity of Adrb3 can increase glucose uptake by astrocytes (cf. review by Gibbs and Summers, 2002). Therefore, the activation of Adrb3 in retrosplenial cortex on the Lesion side may be part of a mechanism to increase astrocytic glucose, and boost mitochondrial activity. The occurrence of astrocytic energy processes may play a causal role in the potential alteration in astrocyte-neuron communication and glutamate activity discussed in section 5.4.1.2.

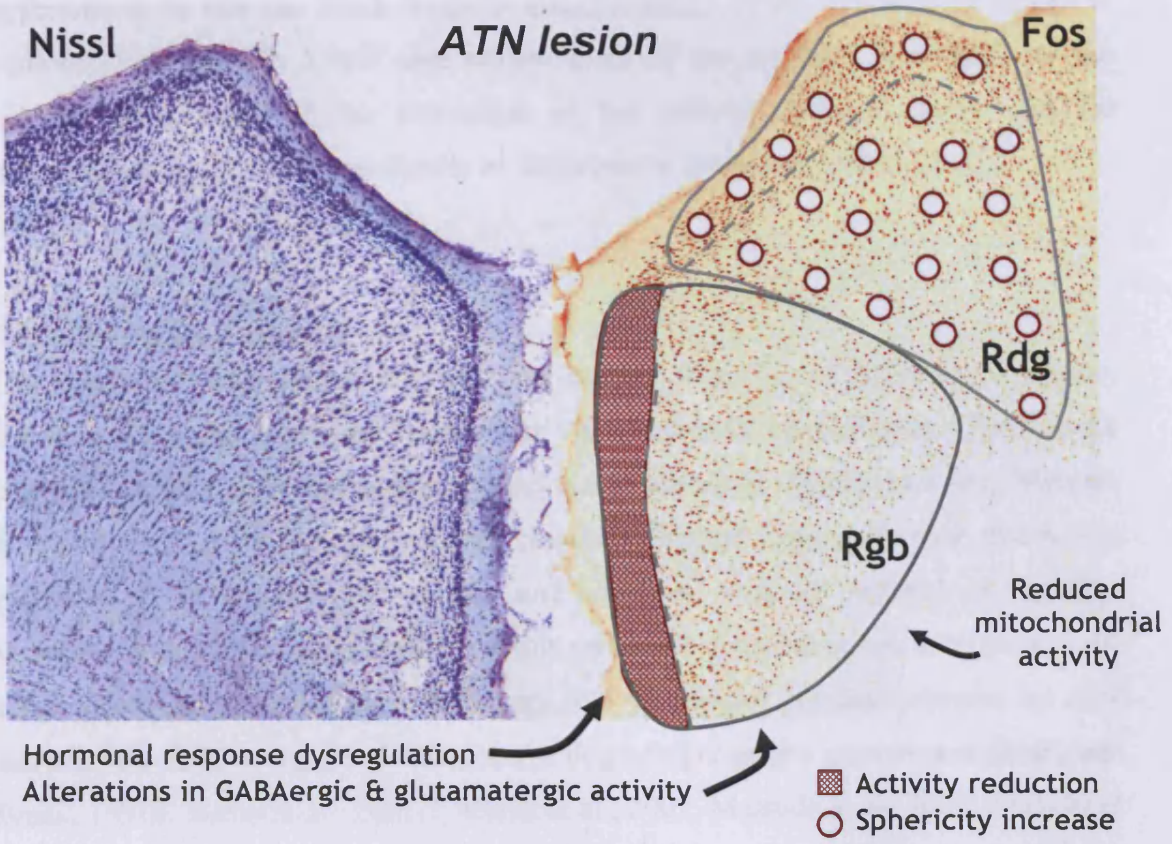

Figure 6.2: Overview of some of the effects of anterior thalamic nuclei lesions on retrosplenial cortex function.

Clinical significance of the findings

Widespread evidence exists of retrosplenial cortex dysregulation in disorders that involve memory impairment. These disorders include Alzheimer's disease (Desgranges et al., 1998; Nestor et al., 2003), vascular dementia (Martinez-Bisbal et al., 2004), Wernicke-Korsakoff syndrome (Aupée et al., 2001; Reed et al., 2003), hypoxia-induced amnesia (Reed et al., 1999; Aupée et al., 2001), hypo-thyroidism (Krausz et al., 2004), epilepsy (Archer et al., 2003), and schizophrenia (Mitelman et al., 2003; Laurens et al., 2005; Newell et al., 2005). Furthermore, damage that is mainly focused on the retrosplenial cortex due to haemorrhage or infarct has been found to result in amnesia (Maguire, 2001), amnesia accompanied by temporal order judgment impairment (Valenstein et al., 1987; Bowers et al., 1988), amnesia with topographic disorientation (Yasuda et al., 1997) and topographic disorientation without episodic memory impairment (Takahashi et al., 1997). There is also evidence that ageing and

hypertension in rats can result in gross disorganisation of the dendrites of lamina II neurons (Wyss, 1992). I will next review some of the evidence that highlights the potential importance of the interaction of the anterior thalamic nuclei and the retrosplenial cortex, more specifically in Alzheimer's disease and schizophrenia.

Alzheimer's disease

Our results are of potential relevance for early dysfunction in Alzheimer's disease. Interestingly, the progression of Alzheimer's disease exhibits a discrepancy between the course of atrophy and overt pathology, and that of metabolic disturbances (e.g. Matsuda et al., 2002). In early AD, the posterior cingulate displays hypometabolism that is then pervasive to all stages of the disease and correlated with the severity of cognitive impairment (e.g. Minoshima, 1997), yet this metabolic disturbance has been found to be either unaccompanied by overt pathology and by atrophy, or accompanied by mild atrophy that itself is not correlated with the degree of cognitive impairment (Braak and Braak, 1991b; Baron et al., 2001; Chételat et al., 2002; Matsuda et al., 2002; Chételat et al., 2003). Memory deficits and dementia have been found to be correlated with posterior cingulate but not hippocampal or medial temporal lobe metabolism and neurotransmitter changes, and with hippocampal but not posterior cingulate atrophy (Kantarci et al., 2000; Salmon et al., 2000; Chételat et al., 2003; Martinez-Bisbal et al., 2004).

The metabolic reduction and neurotransmitter change in the posterior cingulate cortex have been deemed by some to be of predictive and early diagnostic value. It can be observed in patients with very early in Alzheimer's disease, it is the earliest and strongest found in AD-converting patients diagnosed with Mild Cognitive Impairment (MCI)—a subtype of which present with intermediate pathology, and can be a prodrome of Alzheimer's disease (Herholz, 2003; Nestor et al., 2003; Gauthier et al., 2006; Petersen et al., 2006), and even before symptom apparition in some patients that progress to a diagnosis of AD (Minoshima, 1997; Kogure et al., 2000; Matsuda, 2001; Desgranges et al., 2002; Devous, 2002; Huang et al., 2002; Drzezga et al., 2003). It has been reported that more specifically within the posterior cingulate gyrus, it is the retrosplenial cortex that is the most consistent site of hypometabolism (Nestor et al., 2003). It is important to emphasize that this hypoactivity appears to precede that

exhibited by prefrontal and medial temporal regions (Matsuda, 2001; Huang et al., 2002; Drzezga et al., 2003).

It has been proposed that the posterior cingulate hypometabolism in AD is the result of a reduction in projecting fibres from the rhinal cortex (Meguro et al., 1999; Matsuda et al., 2002) or of hippocampal atrophy (Chételat et al., 2003). In addition to the potential loss of input due to afferent pathology, there is further evidence to support a reduction in connectivity in AD. The integrity of white matter fibre tracts seems compromised in AD. In relation to the retrosplenial cortex, there are contradictory findings of white matter integrity in the cingulum bundles, reductions have been found in some (Rose et al., 2000; Takahashi et al., 2002; Medina et al., 2006) but not all studies (Naggara et al., 2006; Xie et al., 2006). Particularly striking is the report that the only additional decrease in white matter integrity reduction in AD from MCI is in the posterior cingulum bundle and posterior cingulate sub-gyral region (Medina et al., 2006). There are reasons to believe that both the anterior thalamic nuclei and the hippocampus are regions that become disconnected in AD. Patients diagnosed with Alzheimer's Disease exhibit reduced connectivity between the posterior cingulate and the hippocampus (Greicius et al., 2004; Wang et al., 2006). In the case of the anterior thalamic nuclei, the evidence is less conclusive, maybe because of the greater difficulty entailed in evaluating this area and its projections. For example, white matter integrity was compromised in the internal capsule, which contains thalamo-cortical and cortico-thalamic connections, in some studies (Medina et al., 2006; Xie et al., 2006) but not others (Bozzali et al., 2002; Duan et al., 2006; Naggara et al., 2006). Overall, recent findings support the role of the retrosplenial cortex in the aetiology of AD cognitive symptoms. Whereas the impact of entorhinal cortex pathology is appreciated and is used as a model of AD in rats (e.g. Meguro et al., 1999), our findings support the additional importance of subcortical regions, such as the anterior thalamic nuclei and the hippocampus.

In conclusion, our findings further support the notion that the effects of selective brain damage could be amplified via covert pathology in the retrosplenial cortex. In light of the aetiology of Alzheimer's disease and of the discrepancy between the loci of pathology and the site of initial metabolic disturbances, we concur with the notion that some of the alterations in brain function in this disorder may be the result of a disconnection of certain brain regions (Meguro et al., 1999; Matsuda et al., 2002;

Chételat et al., 2003). We further stress that in additional to hippocampal and entorhinal cortex, the functional disturbances of retrosplenial cortex in Alzheimer's disease may stem from diencephalic sources, more specifically the anterior thalamic nuclei. The course of pathology in the anterior thalamic nuclei (Braak and Braak, 1991a), in conjunction with the emerging diagnostic value of retrosplenial cortex dysfunction suggest that the interaction of these regions may be crucial for cognitive abilities and its disruption may underlie the conversion of patients to a diagnosis of possible Alzheimer's disease. The consideration of such an amplification phenomenon would broaden our understanding of clinical conditions such as Alzheimer's disease and diencephalic amnesia.

Schizophrenia

Finally, further interest for the study of the anterior thalamus-retrosplenial relationship comes from recent research investigating schizophrenia. Similarly to AD (Coleman and Yao, 2003), schizophrenia is also seen by some as a disease of the synapse (Mirnics et al., 2001). Patients with schizophrenia that have never been medicated exhibit reductions in thalamic glucose metabolism, as seen with PET (Buchsbaum et al., 1996). Reductions in thalamic volumes with schizophrenia have also been observed using MRI even early in the manifestation of the disease symptoms (Ettinger et al., 2001; Lang et al., 2006) or in never-medicated patients (Buchsbaum et al., 1996; Gilbert et al., 2001), and this pattern has been confirmed by meta-analyses of studies of chronic schizophrenia (Konick and Friedman, 2001). More precisely, reductions have also been found in the anterior thalamic nuclei (Buchsbaum et al., 1996; Hazlett et al., 1999; McIntosh et al., 2004), although not consistently (e.g. Byne et al., 2002). Reductions in anterior thalamic nuclei cell numbers have also been found with stereological measurements (Young et al., 2000). Furthermore, reductions in thalamic connectivity have been suggested by reports of reduced white matter integrity in various fibre tracts, including in the anterior limb of the internal capsule (Suzuki et al., 2002; Zhou et al., 2003; Hulshoff Pol et al., 2004; Lang et al., 2006)

The retrosplenial cortex also appears to be dysfunctional in schizophrenia. For example, the posterior cingulate cortex of patients with schizophrenia exhibits receptor binding alterations (Newell et al., 2005; Newell et al., in press) and metabolite alterations suggestive of neuronal dysfunctions (Shimizu et al., in press). Cingulum bundle integrity appears to be affected in schizophrenia (Suzuki et al., 2002), and the

retrosplenial cortex has been reported to be smaller in poor-outcome subtype schizophrenia (Mitelman et al., 2003, 2005a). Additionally, the correlation that is found in normal subjects for white matter between the thalamus and the posterior cingulate is absent in patients with schizophrenia (Mitelman et al., 2005b). Such a reduction in inter-regional correlations in schizophrenia was also found between the gray matter volume of the posterior cingulate and of the hippocampus (Woodruff et al., 1997). Finally, patients with schizophrenia display a dysfunction in the orienting response to novel stimuli, which is accompanied by hypo-activity of the retrosplenial cortex (Laurens et al., 2005).

Patients afflicted with this neuropsychological disorder often exhibit memory deficits (Clare et al., 1993). In relation to this observation, it has been reported that the antipsychotic clozapine can improve cognitive deficits (including memory) in schizophrenia significantly better than haloperidol (e.g. Potkin et al., 2001). It is of interest to note that pharmacological studies in animal models have shown that the only brain region that shows consistent metabolic effects with the antipsychotics clozapine and haloperidol is the anterior thalamus (Cochran et al., 2002). Furthermore, while the administration of either of these antipsychotics results in glucose metabolism reduction in the anterior thalamus, only with clozapine are reductions also observed in the retrosplenial cortex, the anterior cingulate cortex, and in the mammillary bodies. Similarly, within the Papez circuit, greater IEG activation (e.g. c-*fos* and *zif268*) was observed after clozapine rather than haloperidol (Cochran et al., 2002). Additionally, clozapine, but not haloperidol, can reduce the NMDA antagonist-induced changes in neuropeptide activity seen in the retrosplenial cortex of rats (Arif et al., 2006). Together, these observations may suggest that antipsychotics that can produce a greater improvement in the cognitive abilities of patients with schizophrenia also have a greater effect on retrosplenial cortex function. Given these observations, it is possible that the findings presented in this thesis may be also of relevance for schizophrenia.

The studies that I presented provided additional information to extend our understanding of the neural processes of spatial memory in the rat, widely believed to depend on brain structures homologous to those that are also required for the performance of spatial memory abilities in humans. I evaluated the activity occurring in brain areas during the acquisition of a spatial memory task. The methodology used broadened our understanding of memory processes by improving knowledge about the

circuit dynamics involved in the performance of this task, as well as suggesting potential regional sites of plasticity that could be associated with particular memory components of the task. An important finding was the observation that increased success in the performance of a task reliant upon spatial memory was associated with the concerted activity of a network of regions that appear to each play different but complementary roles.

The retrosplenial cortex emerged as a node that, in the network tested, exhibited the highest correlative activity with the rest of the regions. It was further revealed that the retrosplenial cortex is vulnerable to damage in several regions that are connected to it. The results of the different technical approaches allowed the appraisal of the nature of the retrosplenial cortex vulnerability to distal damage. These experiments yielded an insight into the time course of the retrosplenial cortex dysfunction, its selective vulnerability to distal damage according to the target of the damage, as well the identification of precise molecular functions that could be affected.